University of Southampton

Faculty of Medicine

Human Development and Health

Novel insights into endometrial architecture and function in reproductive health and disease

by

Jennifer Pearson-Farr

Thesis for the degree of Doctor of Philosophy

October 2020

University of Southampton

<u>Abstract</u>

Faculty of Medicine

Human Development and Health

Thesis for the degree of Doctor of Philosophy

Novel insights into endometrial architecture and function in reproductive
health and disease

by

Jennifer Pearson-Farr

Successful embryo implantation is a trade-off between a receptive endometrium and a
good quality embryo. Endometrial glands are important for successful pregnancy, creating
a favourable uterine environment for the implanting embryo. The 3D structure and gene
expression profile of endometrial glands during endometrial receptivity are yet to be
determined. The European Society of Human Reproduction and Embryology guidelines
suggest recurrent pregnancy loss occurs in approximately 2% of women. While the
pathogenesis of recurrent pregnancy loss remains unclear, it has been associated with
reduced endometrial gland secretions and altered endometrial receptivity.

In this thesis, multi-modal 3D imaging and RNA sequencing are applied to the
endometrium from control women and women with recurrent pregnancy loss, to identify
3D structural alterations and a gene expression profile of endometrial glands during the
implantation window. This thesis takes a multi-scale approach to investigating
endometrial glands. Beginning with the relationship between endometrial glands and
endometrial stromal cells in whole endometrium, investigating endometrial glands only,
and finally glandular ciliated cell components.

This thesis used 3D imaging to further our understanding of the spatial relationships
between stromal cells and endometrial glands and their relationship to recurrent
pregnancy loss. Quantitative 3D distance maps demonstrated for the first time that
endometrial cells from women who experience recurrent pregnancy loss have altered 3D
spatial relationships compared to controls. This 3D spatial information may help

understand the underlying biology and the changes that are observed in disease states. Endometrial function may underlie a range of fertility disorders and these 3D imaging approaches could ultimately lead to more informative diagnostic testing and new treatments.

3D imaging provided insight into glandular structure and was combined with high-speed video to quantify endometrial gland cilia movements. This study made a number of observations that would not have been obvious from 2D imaging. One of these was that microvesicles appear to be forming on the tips of glandular microvilli. Secretion of glandular microvesicles into the uterine lumen may help mediate a favourable uterine environment during embryo implantation. The microvillus surface of the glandular lumen was interspersed with ciliated cells. The role of glandular cilia is not clear but it is hypothesised that they may facilitate the movement of microvesicles to the uterine lumen. The cilia beat pattern observed in endometrial glands from controls and women with recurrent pregnancy loss however, was uncoordinated. High-speed video could be developed in the future and provide a fast diagnostic of glandular cilia function.

This thesis used 3D imaging and RNA sequencing to further our understanding of the gene expression profile of endometrial glands and glandular beta-tubulin from women with recurrent pregnancy loss. Differentially expressed genes were identified in endometrial glands from women with recurrent pregnancy loss compared to controls and beta-tubulin enrichment in glandular ciliated cells was established. Combined 3D imaging and gene expression analysis also demonstrated that beta-tubulin isoforms were altered on a gene transcript level and a protein level in endometrial glands from women with recurrent pregnancy loss. Combining 3D imaging and gene expression data allows gene expression changes to be located in endometrial tissue. Teasing out beta-tubulin changes in the glandular ciliated epithelium could lead to specific endometrial gland biomarkers of a recurrent pregnancy loss phenotype.

This multi-scale and multi-modal approach has established a four dimensional view of endometrial glands during the window of implantation. Alterations in the endometrial gland architecture and their spatial relationship to the endometrial stroma could be associated with recurrent pregnancy loss. This new approach can be applied to other patient groups who suffer from unsuccessful pregnancy, such as infertility and recurrent implantation failure, and in future, contribute to the development of diagnostics.

Table of Contents

Table of Tables

Table of Figures

List of Accompanying Materials

Video 4.1: https://youtu.be/IGO8GrcQS7Y

Video 4.2: https://youtu.be/GmeepETM8Wk

Video 4.3: https://youtu.be/4NMWunVLyRM

Video 4.4: https://youtu.be/ggf1aNXNZDI

Video 4.5: https://youtu.be/cMLHr3W9RSE

Video 4.6: https://youtu.be/Gv1GHwnSstw

Video 5.1: https://youtu.be/3yWLBziNG6U

Video 5.2: https://youtu.be/lqhPW6uTmQs

Research Thesis: Declaration of Authorship

Print name: Jennifer Pearson-Farr

Title of thesis: Novel insights into endometrial architecture and function in reproductive health and disease

I declare that this thesis and the work presented in it are my own and has been generated by me as the result of my own original research.

I confirm that:

1. This work was done wholly or mainly while in candidature for a research degree at this University;
2. Where any part of this thesis has previously been submitted for a degree or any other qualification at this University or any other institution, this has been clearly stated;
3. Where I have consulted the published work of others, this is always clearly attributed;
4. Where I have quoted from the work of others, the source is always given. With the exception of such quotations, this thesis is entirely my own work;
5. I have acknowledged all main sources of help;
6. Where the thesis is based on work done by myself jointly with others, I have made clear exactly what was done by others and what I have contributed myself;
7. None of this work has been published before submission

Signature: …………………………….Date: ....

Acknowledgements

I wouldn't have been able to complete this thesis without the support and guidance of many important people.

Firstly, I would like to thank my supervisor Professor Ying Cheong. Thank you for imparting your knowledge of the endometrium upon me, and for all of your help encouragement and patience during my PhD. I love your out the box ideas and I look forward to continuing to work with you.

I would also like to thank my supervisors Dr Jane Cleal and Professor Rohan Lewis, thank you for sharing your knowledge and expertise with me and encouraging me to seek opportunities for development.

Thank you to the patients of Princess Anne Hospital for allowing this research to take place, through the selfless act of donating their endometrial samples. Also to the clinicians at Princess Anne Hospital, for allowing me to collect endometrial samples.

Thank you to friends and family, especially Dr Emma Lofthouse and Dr Brogan Ashley.

Definitions and Abbreviations

Abbreviation	Definition
AMH	Anti-mullerian hormone
B&H	Benjamini & Hochberg
BMI	Body mass index
BSA	Bovine serum albumin
CBF	Cilia beat frequency
cDNA	Complementary DNA
Cp	Crossing point
DAPI	4',6-diamidino-2-phenylindole
DIO2	Iodothyronine Deiodinase 2
DMEM	Dulbecco's modified Eagle's medium
dNTP	Deoxynucleotide Triphosphates
Drop-seq	Droplet generating single cell sequencing
EMMPRIN	Extracellular matrix metalloproteinase inducer
ENPP	Ectonucleotide Pyrophosphatase/Phosphodiesterase
ERA	Endometrial receptivity array
ESHRE	The European Society of Human Reproduction and Embryology
FDR	False discovery rate
FITC	Fluorescein Isothiocyanate
FOXA2	Forkhead box protein A2
FOXJ1	Forkhead box protein J1
FSH	Follicle stimulating hormone
HEK293	Human embryonic kidney 293 cells
HLA	Human leukocyte antigen
IFT	Intraflagellar transport
IL	Interleukin
ILC	Innate lymphoid cell family
IVF	*In-vitro* fertilisation
KIR	Killer-cell immunoglobulin-like receptors
LGR5	Leucine-rich repeat-containing G-protein coupled receptor 5
LH	Luteinising hormone
LIF	Leukaemia inhibitory factor
MHC	Major histocompatibility complex
MmLV RT	Moloney Murine Leukaemia Virus Reverse Transcriptase

mRNA	Messenger RNA
MUC1	Mucin-1
NEC	No enzyme control
NKG2	Natural killer group 2 receptors
NTC	No template control
PBS	Phosphate buffered saline
PCD	Primary cilia dyskinesia
PE	Phycoerythrin
PerCP	Peridinin Chlorophyll Proetin Complex
PFA	Paraformaldehyde
pNK	Peripheral natural killer
qPCR	Quantitative polymerase chain reaction
RFX	Regulatory factor X
RIN	RNA Integrity Number
RIPA	Radioimmunoprecipitation assay buffer
RPL	Recurrent pregnancy loss
RSPH4A	Radial spoke head 4 homolog A
SBFSEM	Serial block face scanning electron microscopy
SCARA5	Scavenger Reporter Class A Member 5
SDI	Spatial distribution index
SDS-PAGE	Sodium dodecyl sulphate -polyacrylamide gel electrophoresis
SEM	Scanning electron microscopy
SOX9	SRY-box 9
SPP1	Secreted phosphoprotein
SSEA-1	Stage-specific embryonic antigen-1
TBST	Tris buffered saline plus tween20
TDE	2,2' Thiodiethanol
TEM	Transmission electron microscopy
TGF-β	Transforming growth factor beta
TNF	Tumour necrosis factor
TTL	Tubulin tyrosine ligase
UGKO	Ovine uterine gland knockout
uNK	Uterine natural killer

Chapter 1   General Introduction

1.1 The clinical problem – recurrent pregnancy loss

Recurrent pregnancy loss is distressing for couples and often diagnosed as unexplained. Successful pregnancy requires the endometrium, the mucosal lining of the uterus, to be remodelled into a receptive state allowing a conceptus to implant and be supported in its early development. The underlying biology of the endometrium in women with recurrent pregnancy loss is not fully understood.

An oocyte is fertilised in the fallopian tube before travelling to the uterine cavity for implantation into the endometrium. The human non-pregnant endometrium is a dynamic tissue that undergoes growth, differentiation and regression periods throughout the menstrual cycle in response to hormonal regulation. During the mid-luteal phase of the menstrual cycle (days 21 – 24), post ovulation, the endometrium becomes receptive to an implanting conceptus, termed the window of implantation.

Unsuccessful pregnancy can occur before or after the implantation process. Clinically, they manifest as recurrent implantation failure or early pregnancy loss. Recurrent implantation failure includes women who have difficulty with embryo implantation, often following multiple rounds of *in-vitro* fertilisation (IVF) of a good quality embryo. Early pregnancy loss, is defined as the loss of a clinical pregnancy before gestation week 20, otherwise known as the loss of an embryo or fetus < 400 g if the gestational age is unknown (Zegers-Hochschild et al., 2009). Ectopic, molar and biochemical pregnancies are not included, highlighted in The European Society of Human Reproduction and Embryology (ESHRE) recurrent pregnancy loss guidelines (ESHRE Early Pregnancy Guideline Development Group, 2017). A pregnancy loss can also be classified as an embryonic loss before 10 gestational weeks and a fetal loss after 10 gestational weeks (Kolte et al., 2015).

Recurrent pregnancy loss, defined as two or more consecutive pregnancy losses, occurs in 2% of women (Ford & Schust, 2009). There are discrepancies however, between countries and healthcare providers as to when to introduce a clinical investigation for recurrent pregnancy loss patients (Kutteh, 2015). The American Society for Reproductive Medicine Practise Committee defined recurrent pregnancy loss as "two or more failed consecutive pregnancies", however, the Royal College of Obstetricians and Gynaecologists defined recurrent miscarriage as "the loss of three or more consecutive pregnancies"

(Royal College Obstetricians and Gynaecologists, 2011; The Practice Committe of the American Society for Reproductive, 2012). Recurrent pregnancy loss research is required to provide patients with more evidence-based clinical interventions and therapeutics (ESHRE Early Pregnancy Guideline Development Group, 2017; Odendaal et al., 2019).

The most common outcome of a recurrent pregnancy loss clinical investigation are chromosomal abnormalities followed by an immune disorder or an anatomical abnormality (ESHRE Early Pregnancy Guideline Development Group, 2017; Simpson, 2007). For the majority of couples however, the designated cause is 'unexplained'. The risk of unexplained recurrent pregnancy loss has been shown to increase with lifestyle factors such as maternal obesity (Lo et al., 2012). The risk of recurrent pregnancy loss is also understood to increase with maternal age (Lund et al., 2012).

Recurrent pregnancy loss has been associated with an endometrium that is over receptive or demonstrating an out of phase window of implantation (Macklon & Brosens, 2014; Salker et al., 2012). There is no consensus to the gene expression profile of the endometrium during the window of implantation in women with recurrent pregnancy loss nor its 3D architecture. The endometrium is also a heterogeneous tissue, consisting of different epithelial and stromal cell types with different functions (Lucas et al., 2020). This thesis investigates the association between different endometrial cell types and recurrent pregnancy loss.

1.2 Healthy endometrium and implantation

1.2.1 The endometrium

The endometrium is the mucosal lining of the uterus, forming the first point of attachment for an implanting blastocyst (Figure 1.1) (Spencer et al., 2012). Before implantation, an oocyte is fertilised outside the ovary in the fallopian tube, forming a zygote. The zygote undergoes cell division to form the blastocyst of two distinct cell lineages, the outer trophectoderm that will develop into the placenta and the inner cell mass that will develop into the fetus (Cockburn & Rossant, 2010).

The endometrium consists of two functional layers, the lower stratum basalis and the upper stratum functionalis (Figure 1.2). The stratum functionalis and the uterine cavity are separated by the luminal epithelial surface, where endometrial glands start as invaginations and radiate towards the basalis layer. The stratum basalis consists of two zones, one including loose stroma and endometrial gland bodies, while the other including the termination regions of endometrial glands and endometrial progenitor cells (Padykula, 1991). Beneath the endometrium is the myometrium, a layer of uterine smooth muscle.

In summary, the endometrium is a heterogeneous tissue consisting of the stratum basalis and the stratum functionalis. The stratum functionalis is the focus of this study, which sheds and re-grows monthly in a cyclic manner.
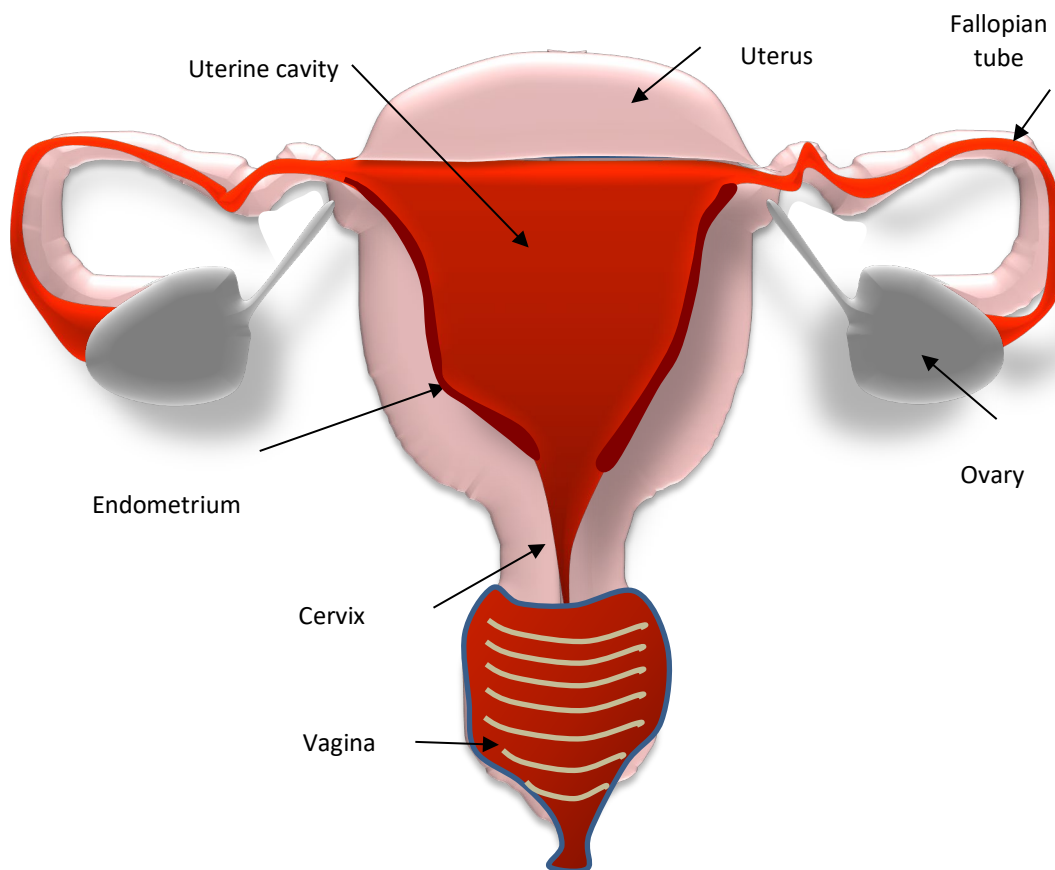
Figure 1.1 *The endometrium is the innermost mucosal lining of the uterine cavity, which is shed and regrown as part of the menstrual cycle.*
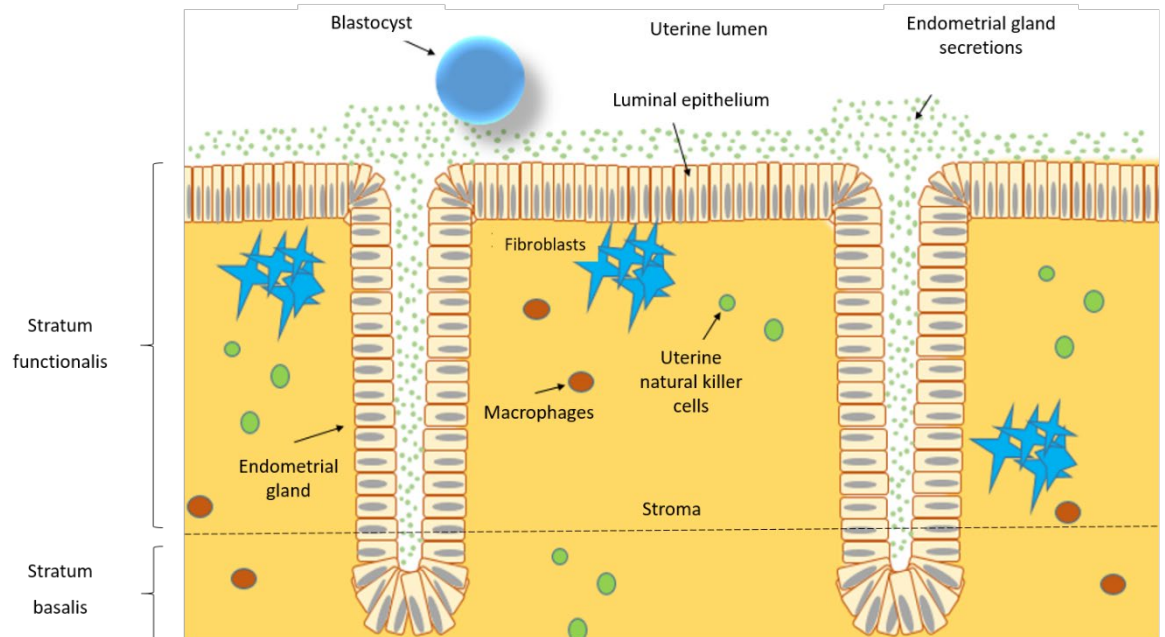
Figure 1.2 *Schematic of the endometrium, showing the stratum basalis and the stratum functionalis. The endometrial glands are invaginations of the luminal epithelial surface, while the stroma consists of different immune cell types.*

1.2.2   The menstrual cycle

The stratum functionalis is shed and re-grown to a thickness of approximately 5-7 mm as part of the monthly menstrual cycle (McLennan & Rydell, 1965). The majority of women have a 28-30 day menstrual cycle driven by cyclic hormones (Snijders et al., 1992). The menstrual cycle consists of two main uterine stages the proliferative phase and the progesterone-dominant secretory phase characterised by morphological and functional changes (Figure 1.3, Noyes et al., 1975). The secretory phase is also called the luteal phase.

The morphological changes observed in the luteal phase endometrium occur in a predictable pattern (Li et al., 1988; Noyes et al., 1975). The Noyes Criteria were established to assign the endometrium to a stage of the menstrual cycle by histological examination (Figure 1.3). These criteria were based upon the histological examination of approximately 8000 endometrial biopsies across the menstrual cycle, assuming ovulation, the release of an egg from the ovary, occurs on day 14 and menstruation, and the shedding of the endometrium, occurs on day 28 (Noyes et al., 1975).
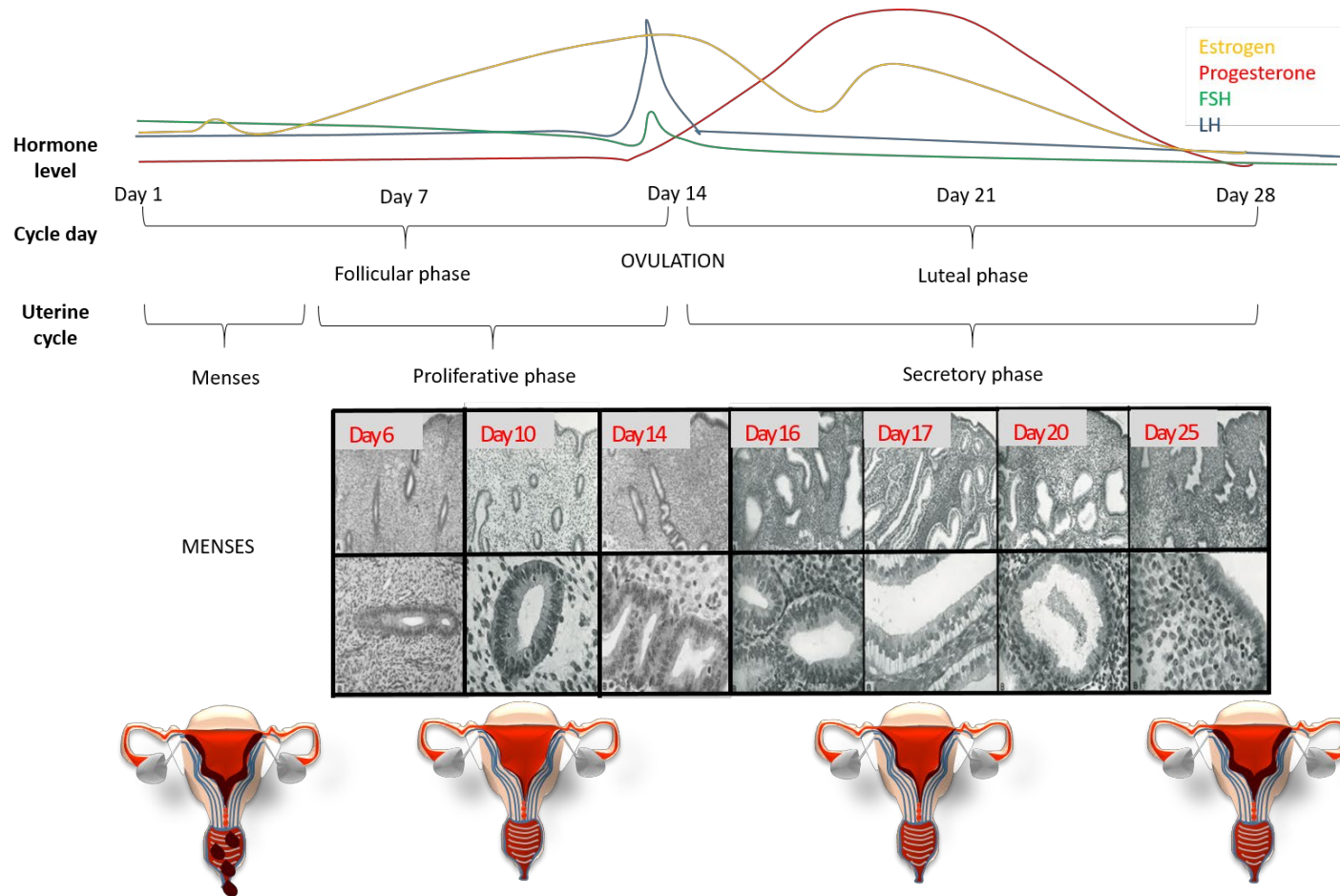
Figure 1.3 *The female menstrual cycle is regulated by cyclic changes in hormone levels. Including progesterone, estrogen, follicle stimulating hormone (FSH) and luteinising hormone (LH). In a regular menstrual cycle, ovulation occurs on day 14 and menstrual bleeding begins between days 28-30. Endometrial histology by the Noyes criteria of endometrial dating, images adapted from 'Dating the Endometrial Biopsy' (Noyes et al., 1950).*

The Noyes criteria uses endometrial gland morphology during the proliferative phase, while stromal cell and decidualization characteristics are used during the secretory phase (Noyes et al., 1975). At the beginning of the proliferative phase, after menses (day 6), the surface epithelium is relatively thin, stroma is compact and endometrial glands are straight, narrow and short. Mid proliferative phase (day 10), epithelial cells begin to have a columnar cell shape, and curved endometrial glands extend in length. By the late proliferative stage (day 14), endometrial glands show a tortuous shape, active growth and pseudostratification of the epithelium.

Following a luteinising hormone (LH) surge from the anterior pituitary gland in the brain, ovulation occurs on day 14 of the menstrual cycle, marking the start of the secretory phase. The secretory phase of the menstrual cycle is characterised by nuclei alignment, sub-nuclear vacuolation of the gland epithelium, and an increase in gland diameter and tortuosity. During mid-secretory phase (day 21), the window of implantation, endometrial gland vacuoles secrete their content into the endometrial gland lumen. Tissue oedema becomes evident on day 21 of the menstrual cycle, where the stromal cells appear small and dense. By menstrual cycle day 23 the spiral arterioles become prominent.

After the implantation period of the menstrual cycle (days 21 – 24), the stromal cells become decidualised accompanied by the influx of lymphocytes. In the absence of pregnancy, menstrual shedding is initiated (Noyes et al., 1975). Late secretory phase endometrium glandular epithelia consist of tall columnar cells, with substantial microvilli, interspersed with numerous ciliated cells. In contrast, glands at the proliferative stage are made up of smaller cuboidal cells with a flatter surface and fewer microvilli (Garry et al., 2010).

In summary, the endometrium goes through hormonally driven morphological changes over the course of the menstrual cycle. Morphological changes have been categorised by the Noyes criteria, based on a 'normal' 28-day cycle. Clinical investigations use the Noyes criteria to make a histological evaluation of the luteal phase endometrium in cases of infertility and miscarriage, known as endometrial dating.

1.2.3   Endometrial dating

Endometrial dating by the Noyes criteria is currently considered the gold standard for clinically evaluating endometrial histology. Endometrial dating has been used to diagnose a luteal phase defect, defined as the retardation of endometrium development, by more than 2 days from the expected morphology based on the chronological date from the LH surge (Li & Cooke, 1991). A national survey demonstrated that 62.5% of board-certified reproductive endocrinologists used the endometrial biopsy to confirm ovulation and the quality of luteal function when assessing patients who are unable to conceive (Glatstein et al., 1997).

It has been suggested that histological investigation of the endometrium alone is not accurate in dating fertile women, nor the clinical investigation of the endometrium from women with infertility or miscarriage (Coutifaris et al., 2004; Murray et al., 2004). Additional cell types such as uterine natural killer (uNK) cells have been counted alongside endometrial histological dating. uNK cell count on its own, however did not have a significant correlation to pregnancy outcome. Combining endometrial dating results with uNK cell count lead to an improved prognostic value (Liu et al., 2014). These results suggest that additional histological parameters may improve endometrial dating.

There have been several attempts to identify a receptive endometrium during the window of implantation. Endometrial histological dating has been compared to a new endometrial diagnostic tool, the endometrial receptivity array (ERA) (Díaz-Gimeno et al., 2013). The ERA consists of 238 pre-selected genes found to be differentially expressed in a receptive endometrium compared to a pre-receptive endometrium (Horcajadas et al., 2007). The ERA uses the pre-selected genes and machine learning to test if an endometrial sample has a receptive profile, independently of histological dating. Initial studies suggested that the ERA was more accurate than histological dating, however these methods did not account for different endometrial cell types with different functions (Díaz-Gimeno et al., 2013). Ultrasound examination of endometrial thickness and blood flow have also been used clinically to identify an unreceptive endometrium, however, it has a poor predictive value for a receptive endometrium (Alcázar, 2006).

In summary, while dating by Noyes criteria is currently the gold standard for clinical investigation of an endometrial biopsy, this evaluation takes a snapshot of the endometrium only. There is evidence to suggest that the endometrium might experience cycle-to-cycle variation (Mariee et al., 2012). Inter-cycle variation alongside histological endometrial dating inaccuracies suggest further work is required to create an endometrial dating tool.

1.2.4 Endometrium regeneration

Endometrial regeneration of the stratum functionalis is vital for embryo implantation, generating an endometrial lining upon which an embryo can implant. Endometrial gland re-growth is thought to stem from an epithelial stem cell population in the stratum basalis, in an upwards direction towards the uterine cavity (Valentijn et al., 2013).

Evidence for a stem cell population in the stratum basalis

Rapidly proliferating cells in the stratum functionalis originate from stem cells in the stratum basalis, close to the endometrium-myometrium junction (Padykula, 1991). In a primate model, radioactive [^{3}H] thymidine labelled progenitor epithelial cells were reported to have increased by more than 30% in the stratum basalis and stratum functionalis regions of the endometrium in the progesterone dominant phase of the rhesus menstrual cycle (Padykula et al., 1989).

Characterisation of the basalis epithelial stem cell populations began by cell-cloning studies (Gargett, 2007). An individual stem cell will multiply to form a colony, where distinct cell boundaries can be identified. It was hypothesised that stem cells for both epithelial cells and stromal cells would be present in the endometrium (Gargett, 2004, 2006). The cloning potential of endometrial cells was demonstrated by colonising purified cell suspensions of hysterectomy samples. Both endometrial stromal cells and epithelial cells formed individual colonies of more than 50 cells per colony (Chan et al., 2004).

Clonogenic endometrial epithelial cells and stromal cells require growth factors for colony formation. Growth factors include epidermal growth factor, platelet-derived growth factor-BB and transforming growth factor -alpha. This suggests that both epithelial and

stromal progenitors express epidermal growth factor and platelet-derived growth factor cell surface receptors (Chan et al., 2004; Schwab et al., 2005). Large endometrial stromal colonies exhibit multi-lineage differentiation similar to bone marrow and adipose tissue, such as adipocytes, smooth muscle cells, chondrocytes and osteoblasts (Gargett et al., 2005). Finally, the percentage of clonogenic cells are not believed to vary across the menstrual cycle (Schwab et al., 2005).

In summary, cell-cloning studies have demonstrated progenitor cell populations for both endometrial stromal cells and epithelial cells, showing similar differentiation capabilities to bone marrow.

Endometrial stem cell markers

The regenerative endometrium has been compared to the regenerative intestine, sharing characteristics of the Wnt/ β-catenin signalling pathway (Valentijn et al., 2013). The endometrium is regenerated monthly, while the luminal surface of the intestine is regenerated constantly. The Wnt signalling pathway activates cell surface receptors, inducing the transcription of target genes. Inactivation of β-catenin in the intestine results in a loss of intestinal epithelial cells (Fevr et al., 2007; Wetering et al., 2002). β-catenin is important for normal endometrial epithelial function, demonstrated by fertility defects in β-catenin mutant mice (Jeong et al., 2009).

Regenerative and non-regenerative endometrium were compared between pre and postmenopausal women. Key Wnt molecules were differentially regulated in the regenerative endometrial epithelium compared to the non-regenerative endometrium, including Wnt transcription factor SRY-box 9 (SOX9). Immunostaining also demonstrated Wnt-regulated genes to be located in the glandular epithelium (Nguyen et al., 2012). SOX9 is understood to inhibit the Wnt/β-catenin signalling pathway in the intestine (Bastide et al., 2007). To investigate SOX9 expression in the basalis endometrium, the cell surface marker stage-specific embryonic antigen-1 (SSEA-1) was specifically localised to basalis endometrial gland epithelium. *In vitro* gland-like structures were also generated by epithelial sub-populations that expressed SSEA-1 and SOX9 (Valentijn et al., 2013).

A transmembrane receptor, Leucine-rich repeat-containing G-protein coupled receptor 5 (LGR5) is another specific cell marker of proliferative epithelial stem cells in the

intestine (Barker et al., 2007). LGR5 is understood to exist in the endometrial epithelia (Krusche et al., 2007). The location of *LGR5* gene expression in the endometrium, correlated with epithelial proliferation and progenitor markers SOX9 and SSEA-1. *LGR5* expression followed the same endometrial cyclic pattern as SOX9 and SSEA-1, however, was most prominent in the luminal epithelial surface and not the stratum basalis (Tempest et al., 2018).

In summary, stratum functionalis regeneration builds the foundation for a receptive endometrium during the window of implantation. Stratum basalis progenitor cell population and progenitor cell markers have been identified, yet further work is required to characterise progenitor cell types and how they impact upon glandular and stromal formation.

1.2.5   Embryo implantation requires endometrial glands

Successful implantation is a three stage process that requires communication between the implanting blastocyst and a receptive endometrium (Wang et al., 2013). The human conceptus undergoes implantation, beginning around day seven post-fertilisation and complete by days 10 to 12 (Burton et al., 2011). The three phases of implantation are apposition, attachment and invasion. Apposition is identified by the close association of the trophoblast to the luminal epithelium (Tabibzadeh & Babaknia, 1995). When the trophectoderm adheres to the endometrial surface it undergoes transformation to the syncytiotrophoblast, where trophectoderm projections penetrate between the endometrial epithelial cells and into the underlying stroma. As the mantle of syncytiotrophoblast enlarges, it encircles and erodes into the necks of the glands. Connections between gland lumens and the developing inter-villous space of the placenta can be observed as early as day 17 post-fertilisation and throughout the first trimester (Burton et al., 2002). Endometrial epithelial to stromal cell interactions are important for embryo implantation (Zhang et al., 2013).

Investigating the implantation period in humans is difficult due to ethical concerns and technical issues, therefore, the majority of the literature focuses on animal models to identify cellular pathways and interactions. The mouse model is widely used; however, the physiological mechanisms of mouse embryo implantation differs from humans. The mouse

endometrium decidualises in the presence of an embryo, while the human endometrium decidualises monthly regardless of pregnancy.

Gene knockdown models in the mouse demonstrate that disrupted endometrial gland development results in unsuccessful implantation. Gene knockdowns include β-catenin (Jeong et al., 2009), E-cadherin (Reardon et al., 2012) and leukaemia inhibitory factor (*Lif*) (Stewart et al., 1992). Forkhead box A2 (FOXA2) is also expressed specifically in the uterine glandular epithelium (Besnard et al., 2004). Ablation of *Foxa2* in mice resulted in defective endometrial gland formation and dysfunctional endometrial stroma unable to decidualize (Bazer, 2010; Jeong et al., 2010).

In summary, embryo implantation is a complex process that requires endometrial glands. Animal models have helped identify important genes essential for endometrial gland development; however, more work is required to translate this to humans.

1.2.6   Uterine natural killer cells

Uterine natural killer (uNK) cells are a type of endometrial stromal cell and part of the innate lymphoid cell (ILC) family. Other endometrial stromal cell types include macrophages, stromal cells, dendritic cells and neutrophils (Olmos-Ortiz et al., 2019). uNK cells are phenotypically different to peripheral natural killer (pNK) cells that circulate in the blood stream, and are understood to play important roles in immune tolerance at the maternal-fetal interphase, spiral artery remodelling and trophoblast invasion.

Innate lymphoid cell family

The ILC represent a group of hematopoietic effectors, which classify into two main groups; the cytotoxic ILC's and the non-cytotoxic ILC's (Chang et al., 2020). The non-cytotoxic ILC's can be further subdivided into three sub-groups; ILC1, ILC2 and ILC3 (Spits & Di Santo, 2010). Other than uNK cells, ILC3's have been identified in human decidua (Doisne et al., 2015). ILC's act in tissue repair, remodelling and tissue homeostasis (Spits & Di Santo, 2010).

Phenotype of uNK cells

uNK cells are distinguished from pNK cells by the differential expression of cell-surface antigens CD56, CD16, CD94 and CD69 (Artis & Spits, 2015; Blumer & Lash, 2005). The uNK cell phenotype is CD56^{bright} CD16^{-}, while the pNK cell phenotype is CD56^{dim}, CD16^{+}. uNK cells are also recorded as CD56^{superbright} in some cases (Gaynor & Colucci, 2017). uNK cells demonstrate menstrual cycle variability, characterised by their increased size and granulation during the progesterone-dominated secretory phase of the menstrual cycle (King et al., 1989). Despite uNK cells having internal granule structures they are poorly cytotoxic (Koopman et al., 2003; Vujaklija et al., 2011). Single cell RNA sequencing has identified three distinct uNK transcriptomic signatures in the endometrium of a control cohort and in first trimester decidua (Lucas et al., 2020; Vento-Tormo et al., 2018).

uNK cell receptor expression provides uNK cells with the ability to identify trophoblast cells of an implanting blastocyst without generating a cytotoxic response, therefore mediating immune tolerance between the maternal decidua and the blastocyst during implantation and early pregnancy (Moffett-King, 2002). uNK receptors recognise antigens of the trophoblast major histocompatibility complex (MHC) class I. MHC class I are cell surface molecules, which present antigens from within its cell allowing self versus non-self antigen identification by uNK cell receptors. uNK cells express natural killer group 2 receptors (NKG2) and killer-cell immunoglobulin-like receptors (KIR) which recognise HLA – E and C. Sixteen KIR genes have been identified which have specific binding affinities to the MHC class I (Braud et al., 1998; Hilton et al., 2015).

Together, these studies highlight the complexity of the uNK phenotype, in respect of their cell surface antigen and receptor profile.

Origin of uNK cells

The origin of uNK cells is disputed, with two opposing theories. The first theory suggests that uNK cells stem from *in situ* progenitors (Manaster & Mandelboim, 2010). The second theory suggests that pNK cells traffic into the uterus and differentiate into uNK cells (Kitaya et al., 2007).

A theory was proposed that CD34$^+$ hematopoietic progenitor cells in the human decidua mature locally into active uNK cells on interaction with endometrial stroma cells (Vacca et al., 2011), in the presence of cytokine interleukin (IL) -15 (Verma et al., 2000). The presence of *in situ* hematopoietic progenitor cells would also account for the CD56$^+$ uNK cells detected in human endometrial tissue which had been xenografted into hormone-treated immuno-deficient mice (Matsuura-Sawada et al., 2005).

uNK cells could also be derived by pNK cells (Peel & Stewart, 1984). Mice were subjected to irradiation while one uterine horn remained protected by a lead shield. Meanwhile, rat bone marrow cells were transferred. Within the irradiated uterine tissue, only uNK cells of rat origin could be identified indicating that pNK cells contribute towards uNK cells (Peel & Stewart, 1984). Paracrine factors such as IL -15 and steroid hormones have been reported to mediate the migration of pNK cells to the decidua (Gibson et al., 2015). Fractalkine, the main NK cell chemoattractant, is also expressed by the endometrium which could mediate uNK cell migration into the uterus (Hannan et al., 2004). Transforming growth factor beta (TGF-β) has been reported to regulate the differentiation of pNK cells (particularly CD16$^+$) to uNK cells (CD16-) (Keskin et al., 2007).

Combining evidence of locally derived and peripherally infiltrated uNK cells suggests that neither contribution should be discounted.

Clearance of senescent decidualised cells by uNK cells

During the secretory phase of the menstrual cycle the endometrial stroma is remodelled to form decidualised stroma by a multi-step process. Elevated progesterone levels and intracellular cAMP production during the mid-luteal phase of the menstrual cycle is accompanied by an increase in uNK cells in the endometrium (Gellersen & Brosens, 2014). The first phase of decidualization is characterised by an inflammatory response that

occurs for only two to four days, remodelling the endometrium into a receptive state for an implanting embryo (Salker et al., 2012). Following this initial inflammatory response, the embryo can be imbedded into the decidualised stroma. A subpopulation of endometrial stromal cells have been reported to demonstrate a senescent phenotype, characterised by cells in a permanent state of cell cycle arrest and the secretion of inflammatory mediators (Brighton et al., 2017). uNK cells have been reported to clear senescent decidual cells by perforin and granzyme exocytosis (Brighton et al., 2017). Decreased embryo implantation rate in the mouse has been associated with the knockdown of inflammatory regulators, suggesting inflammatory mediators are key in the implantation process (Salker et al., 2012). Successful embryo implantation requires a balance between the induction and clearance of senescent cells, allowing for an inflammatory response (Lucas et al., 2020). The number of uNK cells and uNK function may impact upon the initial inflammatory response and therefore receptivity state of the endometrium during embryo implantation.

Early pregnancy spiral artery remodelling by uNK cells

Remodelling of the maternal spiral arteries is an essential adaptation to pregnancy, which transforms the arteries supplying the fetus to less resistant non-turbulent vessels (Burton et al., 2009). In humans, the initial stages of vascular transformation occur during the secretory phase of the menstrual cycle and become more pronounced in early pregnancy (Kam et al., 1999). The maternal vessels during these stages are closely associated with leukocytes, particularly macrophages and uNK cells.

Mouse models highlight the key role that uNK cells play in vascular remodelling. uNK deficient mice demonstrated defected decidual vascular remodelling, characterised by narrow vascular lumens and thick vascular walls, causing turbulent blood flow (Boulenouar et al., 2016). uNK cells are understood to mediate decidual vascular remodelling via the release of cytokines, such as interferon-gamma (Ashkar et al., 2000). Since interferon-gamma is a cytokine involved in macrophage activation, it is possible that uNK cells mediate vascular remodelling through macrophage stimulation (Kieckbusch et al., 2014). uNK cells also produce proteolytic matrix metalloproteinases (MMP), in particular MMP-7, MMP-9, MMP-19 and MMP-23 which mediate vascular remodelling (Hazan et al., 2010). Increased levels of MMPs are also thought to stimulate trophoblast invasion (Jovanovic et al., 2010).

The degree at which spiral artery transformation is dependent upon uNK cells in a mouse pregnancy compared to a human pregnancy may be variable (Georgiades et al., 2002).

Trophoblast invasion by uNK cells

Trophoblast invasion is a complex process, consisting of cellular interactions between uNK cells and the fetal trophoblast (Moffett & Colucci, 2014). These interactions are mediated through cytokine release and uNK receptor to trophoblast MHC class I interactions (Sharkey et al., 2008).

The invasive extra villous trophoblast expresses a unique combination of HLA ligands, including HLA-C, E and G, but not HLA-A and B or MCH class II. Distinct uNK receptor- HLA interactions allow recognition of the blastocyst during the apposition stage of implantation. Fetal endothelial cells and the extra villous trophoblast also express receptor XCR1 for uNK cell cytokine XCL1, reinforcing communication between the trophoblast and uNK cells (Kennedy et al., 2016). uNK cell cytokines have been shown to mediate the onset and inhibition of extra villous trophoblast invasion. IL-8 enhances the motility of the trophoblast in cell migration and invasion assays (Jovanovic et al., 2010). TGF-β however, has been reported to impair the invasive properties of primary trophoblast *in vitro* (Lash et al., 2005).

In summary, the uNK cell phenotype consists of at least three different transcriptional cell states and vary in HLA activation. uNK cells are important in mediating immune tolerance at the maternal-fetal interphase, modifying the decidua for pregnancy and trophoblast invasion.

1.2.7 Endometrial transcriptome during the window of implantation

Studies have attempted to identify a gene profile associated with a receptive endometrium during the window of implantation, yet a consistent pattern of receptivity associated gene expression has not been established. One reason for this may be that the endometrium is a heterogeneous tissue and cell specific expression patterns associated with receptivity may be obscured by other cell types.

Several studies have used a pre-selected panel of genes to identify a receptive endometrium from a non-receptive endometrium. This includes the endometrial dating tool the ERA, discussed previously in section 1.2.3 (Díaz-Gimeno et al., 2011; Enciso et al.,

2018). Potential gene targets associated with a receptive endometrium have been interpreted against the use of the drug mifepristone used for pregnancy termination. The secreted phosphoprotein (*SPP1*) gene was upregulated in the receptive endometrium, but down regulated under the influence of mifepristone (Cuevas et al., 2016). *SPP1* was also reported in the ERA (Díaz-Gimeno et al., 2011). Increased secretion of endometrial gland SPP1 during implantation in a ovine model reinforces SPP1 could be associated with a receptive endometrium (Dunlap et al., 2008).

Single cell RNA sequencing studies have been carried out on non-pregnant endometrial biopsies across the menstrual cycle, identifying six major endometrial transcriptional cell states by T-distributed stochastic neighbour embedding analysis. These include the ciliated epithelium, the un-ciliated epithelium, stromal cells, endothelium, macrophages and lymphocytes (Wang et al., 2018). Endometrial cell types have been further divided into endometrial cell subtypes, including three distinct uNK cell sub-populations in the non-pregnant endometrium and three NK cell sub-populations in first trimester decidua (Lucas et al., 2020; Vento-Tormo et al., 2018), previously described in section 1.2.6.

Total endometrial epithelial and stromal cell components have been isolated prior to single cell RNA sequencing to identify transcriptomic signatures associated to these cell types. Endometrial stromal cells were identified by the marker CD13 and epithelial cells by the marker CD9 (Krjutškov et al., 2016). These approaches and a meta-analysis of gene expression studies between a receptive and a non-receptive endometrium begin to separate the endometrium by its cell types (Altmäe et al., 2017). However, previous studies have used total epithelium which does not distinguish between the luminal epithelium and the glandular epithelium.

In summary, previous studies have identified genes associated with a receptive endometrium during the window of implantation and early pregnancy decidua. Studies have identified gene expression profiles associated with endometrial stromal cells and combined luminal and glandular epithelium. The transcriptomic profile of endometrial glands is not understood. Isolating endometrial glands form endometrial tissue will allow the transcriptome of endometrial glands to be studied.

1.2.8   Endometrial glands

Endometrial glands are important for successful pregnancy, where glandular products create an environment for the implanting embryo (Filant & Spencer, 2014). The glandular epithelium is abundant in apical cellular projections including microvilli and pinopodes (Bartosch et al., 2011). The glandular epithelium also contains secretory cells and ciliated cells (Wang et al., 2018). During early pregnancy, endometrial glands provide histotrophic nutrition before the maternal blood flow is initiated in the placenta at approximately 10 weeks of gestation (Hempstock et al., 2004). Endometrial glands are typically regarded as secretory, however, one alternative view proposed that endometrial glands play a role in absorbing mucus under progesterone dominance in the rat (Naftalin et al., 2002). The importance of endometrial gland function and secretions have been reported by gene knockout models, meanwhile, human endometrial organoid cultures have provided an *in vitro* model to study specific aspects of endometrial gland function.

Endometrial glands create an environment for the early embryo

Steroid hormone mediated endometrial gland secretion may alter the uterine environment and affect blastocyst hatching (O'Sullivan et al., 2002). Estrogen receptors and progesterone receptors are found on human endometrial glandular cells (Snijders et al., 1992). Estrogen-dependent endometrial gland factors such as osteopontin have been reported to activate blastocyst adhesion in embryo culture experiments (Chaen et al., 2012). Two proteins associated with blastocyst hatching and endometrial invasion, implantation serine proteinase -1 and 2 tryptases, are secreted by endometrial glands during the implantation period. Implantation serine proteinase -1 and 2 are regulated positively at the transcriptional level by progesterone, while negatively at post-transcriptional level by estrogen (O'Sullivan et al., 2004). Meanwhile glandular specific FOXA2 was ablated in a mouse endometrium following progesterone treatment leading to insufficient gland development (Kelleher et al., 2016).

Knockout models in mice and sheep show that insufficient glandular function leads to the endometrium's inability to support implantation and pregnancy (Filant & Spencer, 2013). Animal models have been used to investigate endometrial glands, due to ethical concerns and technical issues regarding human studies. An ovine uterine gland knockout

(UGKO) model was used to investigate ovine blastocyst survival. In the UGKO model, blastocysts hatched but failed to survive or elongate. It was concluded that blastocyst defects in UGKO ewes were due to the absence of endometrial glands and their secretions, rather than alterations in expression or adhesive molecules of the luminal epithelial surface of the endometrium (Gray et al., 2002).

Different factors of endometrial glands have been investigated via mouse knockout models, demonstrating their importance in gland function and early pregnancy (previously described in section 1.2.5). LIF is secreted by endometrial glands, acting in the communication between the trophoblast and the endometrium (Zhang et al., 2013). A knockout model of *Lif*-null mice were infertile due to failure of blastocyst implantation (Stewart et al., 1992). Other genes investigated in endometrial gland function include Lymphoid enhancer factor 1 (Shelton et al., 2012) and catenin cadherin associated protein beta 1 (Jeong et al., 2009). These studies highlight that endometrial glands produce secretions, which contribute towards an environment that supports embryo implantation and successful pregnancy.

Organoid culture

Organoid culture models have been developed to model human endometrial glands in non-pregnant endometrium and decidua (Boretto et al., 2017; Fitzgerald et al., 2019; Luddi et al., 2020; Turco et al., 2017). 'Organoids are self-organising, genetically stable, 3D culture systems containing both progenitor/ stem and differentiated cells that resemble the tissue of origin' (Turco et al., 2017). To assess the similarity between organoid cultures and endometrial glands from the same patient sample, the global gene expression profiles were analysed. 287 genes were commonly upregulated in organoids and glands compared with the stroma. Known glandular markers were identified in the organoid cultures, including markers of epithelial cells (*CDH1*, *CLDN10* and *EPCAM*), mucosal secretory cells (*PAX8* and *MUC1*) and endometrial glandular products (*PAEP* and *MUC20*) (Turco et al., 2017). Organoids could become a useful tool in the study of endometrial development, allowing functional studies to be performed.

Endometrial gland secretions

Proteomic studies have enabled the identification of multiple proteins present in human endometrial secretions. Endometrial cavity flushing's however, must be taken with caution due to the cavity being an admixture of oviduct fluid, endometrial and endometrial gland secretions (Cheong et al., 2013). Glandular secretions alone cannot be collected from uterine fluid in humans, therefore immunohistochemistry studies can locate endometrial gland secretions to the glandular epithelium.

Endometrial gland secretions change across the menstrual cycle. For example, human defensin-5 and IL-6 are highly expressed in the glandular epithelium at the secretory phase of the menstrual cycle and more specifically IL-6 at the implantation window (Quayle et al., 1998; Von Wolff et al., 2002). Primary cell culture has been used as a means of endometrial epithelial investigation in humans, however only the stage of the menstrual cycle such as the proliferative, secretory or late secretory phase was disclosed (Table 1.1).

Endometrial production of microvesicles

Animal models have provided evidence of endometrial extracellular vesicles and their role in transporting microRNA (miRNA) cargo in endometrial-conceptus communication (Bidarimath et al., 2017). Extracellular vesicles are a heterogeneous mix of membrane bound structures released by exocytosis, including exosomes and microvesicles. Microvesicles have been found in the uterus of fertile women and may be influenced by steroid hormones (Simon et al., 2018). These microvesicles are thought to play a role in endometrial–trophoblast communication (Evans et al., 2019; O'Neil et al., 2020). O' Neil et al., (2020) reviewed *in vitro* experiments highlighting over 200 miRNAs derived from an endometrial epithelial cell line, predicted to regulate genes involved in embryo implantation (O'Neil et al., 2020).

Table 1.1 *Human studies investigating endometrial gland secretion.*

Gland secretion	Stage of menstrual cycle	Patient groups	Reference
Interleukin (IL-6)	Across the menstrual cycle	Benign hysterectomy cases (n = 33)	(Von Wolff et al., 2002)
Vascular endothelial growth factor (VEGF)	Not specified	Laparoscopy with fibroids (n = 6)	(Hornung et al., 1998)
Metalloproteinase production	n/a	Human uterine stromal cells and human uterine epithelial cell line (n = 3)	(Braundmeier et al., 2012)
Migration inhibitory factor (MIF)	Proliferative phase or secretory phase	Benign hysterectomies (n = 16)	(Schaefer et al., 2005)
CA125 synthesis	Proliferative phase or secretory phase	Benign hysterectomies (n = 27)	(Weintraub et al., 1990)
Placental growth factor	Proliferative phase or secretory phase	Benign hysteroscopies (n = 7)	(Binder et al., 2016)
Lleukaemia inhibitory factor (LIF)	Not specified	Not specified	(Xu et al., 2008)
Inhibin	Proliferative phase or secretory phase	Benign hysterectomies (n = 34)	(Mylonas et al., 2003)
Ectonucelotide pyrophosphatase/phosphodiesterase family (ENPP3)	LH + 7 days	Fertile women (n = 9)	(Boggavarapu et al., 2016)
Human defensin-5 (HD-5)	Proliferative phase or secretory phase	Hysterectomies for fibroids or endometriosis (n = 28)	(Quayle et al., 1998)
Mucin 1 (MUC1)	LH surge + 2 to 9 days	Comparing recurrent miscarriage and controls	(Hey et al., 1995)
Glycodelin A	Proliferative phase or secretory phase	Benign hysterectomies (n = 17)	(Mylonas et al., 2000)

n/a = not applicable, LH = luteinising hormone

Proteins have been identified within endometrial extracellular vesicles which are associated with endometrial receptivity. Microvesicles from total glandular and luminal epithelial cells of the implantation window conditioned medium, expressed intact EMMPRIN protein. Treatment with estradiol increased the release of the extracellular matrix metalloproteinase inducer (EMMPRIN) containing vesicles (Braundmeier et al., 2012). Ectonucleotide Pyrophosphatase/Phosphodiesterase (ENPP) has also been reported in exosomes and on the apical epithelium of endometrial glands, suggesting ENPP3 is released into the endometrial gland lumen (Boggavarapu et al., 2016). ENPP3 can either increase or decrease the activity of glycans, which are present in both the endometrium

and endometrial secretions, reinforcing the important role of ENPP3 in the receptive endometrium (Korekane et al., 2013).

In summary, animal models and human studies have established key endometrial secretions, controlled in a cyclic manner by steroid hormones. Endometrial gland secretory mechanisms are less understood.

1.2.9   Cilia in the endometrium

Endometrial glands consist of secretory cells and ciliated epithelial cells (Bartosch et al., 2011; Wang et al., 2018). Cilia are fine 'hair-like' structures that project from specialised cells, providing biologically important functions in the human body (Boutin & Kodjabachian, 2019). These include movement of the embryo down the fallopian tube, unidirectional movement of mucus in respiratory tracts and cerebrospinal fluid within brain ventricles (Guirao et al., 2010; Horani et al., 2016; Leigh et al., 2009).

The last two decades saw a growing interest in the investigation of cilia and ciliopathies, however, the role of cilia on the endometrial epithelial surface and inside endometrial glands remains undetermined. Fallopian tubal cilia morphology is understood to change over the course of the menstrual cycle, under the influence of estrogen and progesterone (Critoph & Dennis, 1977). Endometrial cilia are also understood to act in a cyclic manner, increasing during the proliferative phase, remain until ovulation and then declining to approximately 20% (Bartosch et al., 2011; Masterton et al., 1975). A ciliated epithelial cell transcriptomic signature has been reported in the healthy endometrium, co-expressed to a cell signature with no functional annotation (Wang et al., 2018). These findings highlight the need for functional studies to understand endometrial gland cilia in both health and disease phenotypes.

Cilia are classified into three categories based on their internal axoneme microtubule arrangement, primary cilia, motile cilia and nodal cilia (Figure 1.4). The microtubule arrangement is uniform from base to tip, encompassed by plasma membrane contiguous to the cellular plasma membrane. Motile cilia cross-sections consist of nine outer doublet microtubules and one central pair, a 9 + 2 axoneme arrangement. The outer microtubule lattice acts in a sliding manner across each other, allowing cilia to move.

Microtubule motor proteins called dynein arms bind to the outer microtubule lattice and are responsible for generating a force that initiates cilia movement. Nexin inter-doublet linkages, between the microtubule doublets, keep the nine outer microtubule doublets in a tight microtubule lattice. C-terminus regions of individual microtubules decorate the outer microtubule lattice, creating key interaction sites prone to post translational modifications.
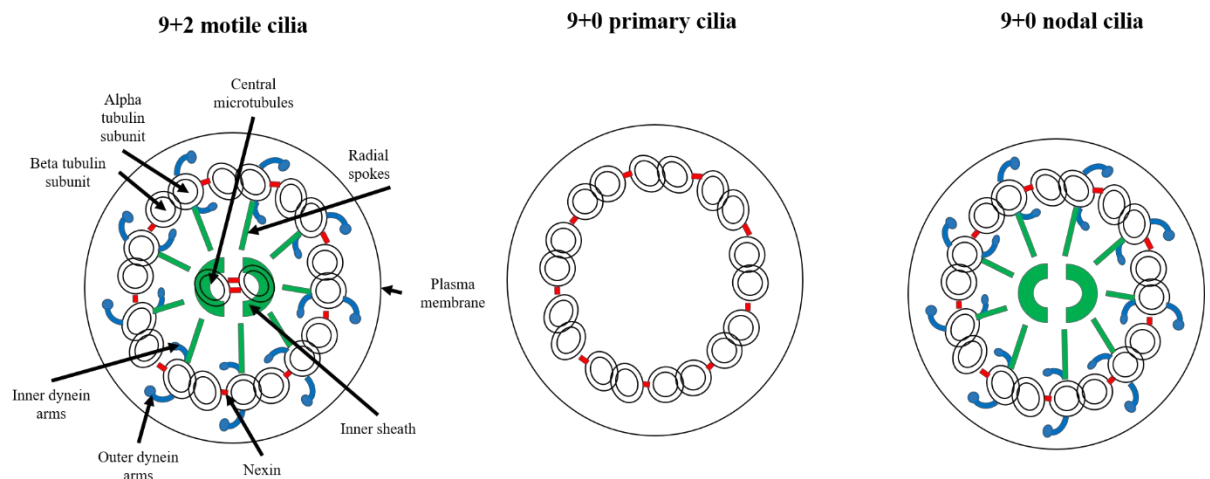
Figure 1.4 Cilia are classified into three categories by their internal axoneme microtubule arrangement, demonstrated by transverse cross-section in schematic.

A cilium is anchored to the cell at the proximal end by a ciliary basal body, consisting of two appendages, a rootlet and the basal foot, which dictates the cilia beating direction. By linking the basal bodies together provides coordinated cilia orientation in a multi-ciliated cell, also known as rotational polarity (Spassky & Meunier, 2017). The coordination of cilia on an epithelial cell surface is facilitated by cilia basal body polarisation (Boutin & Kodjabachian, 2019). Super resolution imaging techniques such as STORM microscopy have made it possible to investigate the spatial arrangement of basal feet in primary and motile cilia (Liu et al., 2020).

To generate cilia movement, motor proteins attached to the alpha tubulin subunits must be activated inside the cilium. Motor protein activation is thought to be mediated by central pair to radial spoke head interactions. Radial spoke head proteins are attached to the outer microtubule doublets and radiate into the centre of the cilium close to the central pair. The central pair is understood to have the ability to twist. As the central pair twists it interacts with the different radial spoke head proteins and activates their respective dynein

arms, mediated by kinesin enzymes (Omoto et al., 1999; Sawin et al., 1992). The precise role of the central pair is not established. Asymmetry in the central pair microtubules also implies selective control of the forward and backward bend in cilia. There are conflicting suggestions in the literature regarding the direction of the cilia beat, to be parallel or perpendicular to the central pair plane microtubule bridge between microtubule doublets 5 and 6 (Satir et al., 2014; Smith & Yang, 2004).

Primary cilia are individual cilia which protrude from the apical surface of many cell types, understood to play a sensory role through cellular signalling pathways such as Notch, Wnt and hedgehog signalling (Sreekumar & Norris, 2019; Wheway et al., 2018). Primary cilia have a 9 + 0 axoneme arrangement, lacking a central pair and motor proteins associated with the outer microtubule doublets, therefore lacking motility function. A third cilia type is the nodal cilium, present in the early embryo during the establishment of left-right asymmetry (Wagner & Yost, 2000). Cilia are under a constant status of microtubule turnover, maintaining a constant cilia length. The process of ciliogenesis is of particular interest in the endometrium, due to the monthly shedding and regeneration as part of the menstrual cycle.

Ciliogenesis

Ciliogenesis is an assembly process that builds and maintains cilia through motor-driven intraflagellar transport of tubulin subunits (Figure 1.5). To initiate ciliogenesis, basal bodies are generated from centriole replication, which then dock to the cellular plasma membrane. At the base of the cilium, the 'transition zone' has been proposed to act as a 'lipid gate' maintaining separation between cellular and cilia regions (Gonçalves & Pelletier, 2017). Ciliary pockets, located at the base of the cilium, also act as an interphase between cellular and cilia regions, however their full role is not fully understood. The cilia plasma membrane itself, is rich in phosphoinositols, where mutations to the ciliary membrane regulator poly-phosphate-5-phosphatase E result in primary cilia signalling defects (Jacoby et al., 2009). The basal body rootlet and the basal foot anchor on the apical plasma cell membrane ready for cilia construction and growth outside the cell (Ishikawa & Marshall, 2011).
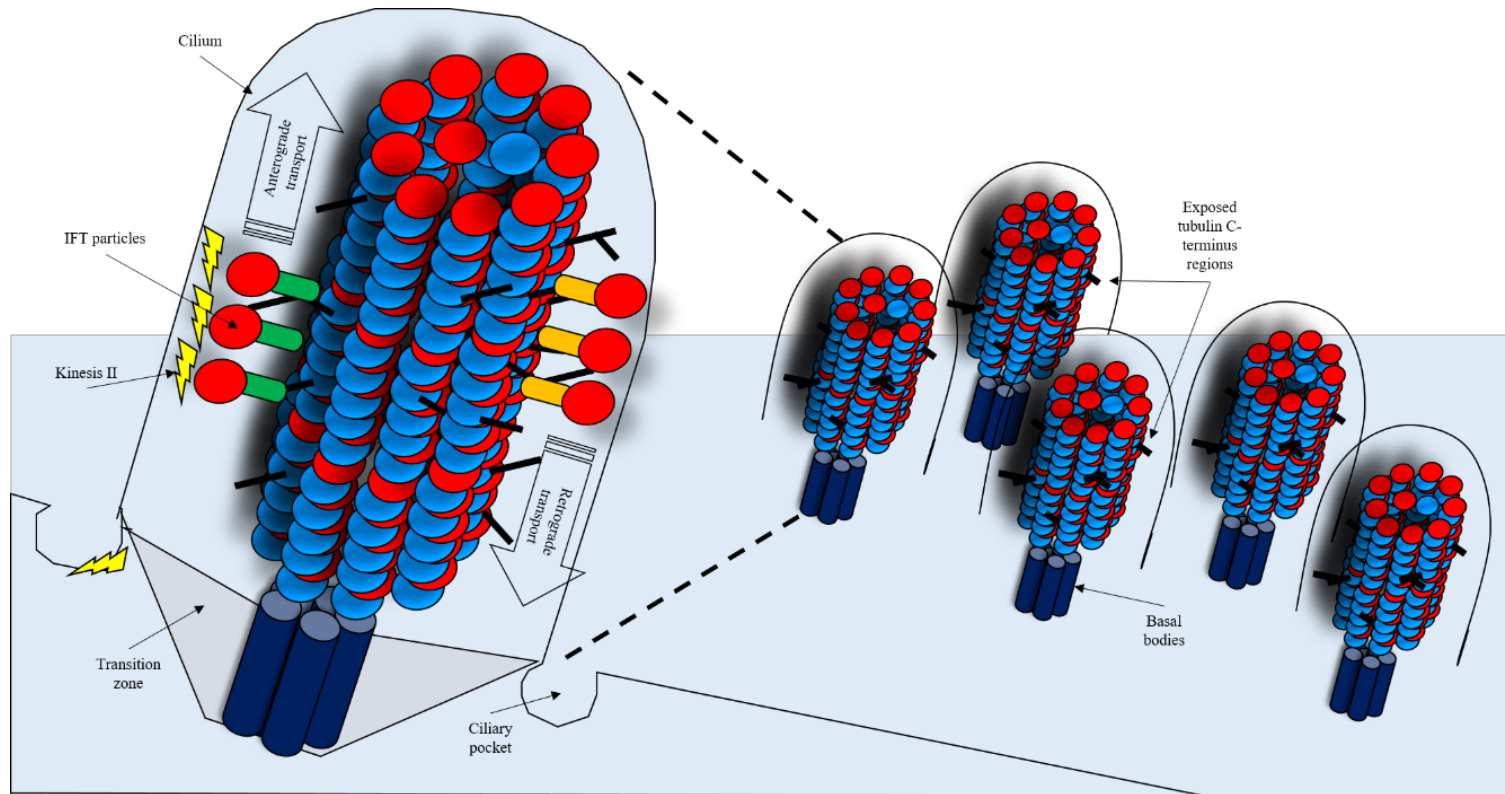
Figure 1.5 *Intraflagellar transport (IFT) of tubulin subunits is responsible for the turnover of the microtubule lattice, catalysed by kinesin II. Anterograde transport is the movement of tubulin subunits up the cilium to the ciliary tip, and retrograde transport is the movement of old tubulin subunits down to the cilium base. The microtubule lattice is decorated with exposed tubulin C- terminus regions, and anchored to the cell membrane by the basal bodies. Transition zone and the ciliary pockets act as an interphase between ciliary and cellular compartments.*

Motor protein Kinesin II is responsible for anterograde transport of microtubule cargo, towards the tip, and cytoplasmic dynein is responsible for retrograde transport. It is reported that a lack of Kinesin II can cause an imbalance in intraflagellar transport, leading to impaired cilia (Gerdes et al., 2009). In order for microtubule subunits to be used in intraflagellar transport, they are selectively passed from the cellular cytoplasm into the cilium cytoplasm via the transition zone where microtubules are converted from triplet microtubules into doublet alpha (α) and beta (β) microtubules (Gonçalves & Pelletier, 2017).

Ciliogenesis is regulated by transcription factors acting on different cilia structural components. Target genes have been identified by experimental work on model organisms, such as Drosophila and C. elegans (Burghoorn et al., 2012; Newton et al., 2012). The Regulatory factor X (*RFX*) gene family have been reported to act upon intraflagellar transport and the transition zone. Meanwhile, transcriptional factor Forkhead box protein J1 (FOXJ1) is understood to act upon cilia axoneme structures such as the central pair, radial spoke heads and dynein motor proteins. Two members of the *RFX* gene family, *RFX2* and *RFX3*, are vital for motile cilia function. Altered *RFX2* and *RFX3* gene expression lead to impaired cilia motility (Chung et al., 2012; El Zein et al., 2009). *FOXJ1* knockout mice have reported an altered 9 + 2 motile cilia axoneme arrangement, and impaired basal body docking to the apical cell membrane. Different signalling pathways may regulate the RFX/FOXJ1 ciliogenic network, including WNT FGF and NOTCH signalling. In the airways, higher notch activity is hypothesized to favour creation of secretory cells over ciliated cells (Rock et al., 2011; Whitsett & Kalinichenko, 2011). These transcriptional studies highlight the important role of transcription factors in ciliogenesis.

In summary, cilia consist of a complex axoneme structure surrounded by a plasma membrane which require coordination for motility function. Functional animal studies have demonstrated RFX/FOXJ1 cascades are responsible for ciliogenesis and constant turnover of the microtubule lattice to maintain cilia length. Endometrial cilia morphology has been described by traditional 2D microscopy techniques and a transcriptomic profile has been established for the endometrial ciliated epithelial cell type. Functional studies however, are required to understand the role of cilia inside endometrial glands.

1.2.10 Tubulin

Two tubulin superfamilies' α-tubulin and β-tubulin polymerise to form microtubules in eukaryotic cells, which perform essential cellular functions such as the movement of fluid across specialised tissues and mitotic spindle during cell division. β-tubulin proteins are encoded by nine genes (*TUBB1-9*) and different isoforms are more or less prone to post translational modifications at the C-terminus tail regions that decorate the outside of the microtubule lattice (Figure 1.5). The expression and incorporation of these tubulin isoforms into the microtubule lattice can affect the structure and function of a cilium.

Tissue specific tubulin enrichment

Multiple tubulin protein isoforms can intermingle in the microtubule lattice (Lewis et al., 1987), therefore a cilium does not consist of just one tubulin gene (*TUBB*) isotype only. Specific ciliated cell types are enriched in tubulin isotypes, for example, neuronal microtubules are enriched in *TUBB3*, where point mutations of this gene lead to neuronal diseases (Joshi & Cleveland, 1989; Tischfield et al., 2010). Meanwhile, platelet marginal bands are enriched in *TUBB1*, where point mutations in this gene lead to bleeding disorders (Fiore et al., 2017; Wang et al., 1986). The mechanism of tubulin enrichment selectivity has been reported to involve the selective interaction between the motor protein kinesin II and α-tubulin. Affinity chromatography has been performed to identify different tubulin isoforms co-purified with kinesis-2 tail fragments, reporting a preferential association with α-tubulin-1 isotype. No β-tubulin isoforms however, were identified from the tubulin pool (Girotra et al., 2017). These mechanisms, among others, could be responsible for tubulin enrichment in different tissue types.

Tubulin post-translational modifications

Post-translational modification is the process where proteins are modified after they have been synthesised, such as the addition or modification of functional groups. α-tubulin and β-tubulin are modified on their C-terminus end, most commonly by tyrosination, glutamylation and glycylation. Tyrosination is specific to α-tubulin, and is the reversible addition of a tyrosine group to tubulin (Arce et al., 1975). Tyrosination is

catalysed by the enzyme tubulin tyrosine ligase (TTL), however the enzyme catalysing the reverse step tyrosination is not fully established (Prota et al., 2013).

Glutamylation and glycylation modify the C-terminus region of α-tubulin and β-tubulin by the enzymatic addition of a glutamate or glycine residue (Eddé et al., 1990; Redeker et al., 1994). Subsequent additions of glutamate of glycine residues is called polyglutamylation and polyglycylation. Glutamylases and glycylases catalyse these reactions, where enzymes have a preference for α-tubulin or β-tubulin. Primary cilia polyglutamylation regulation was investigated in a human retinal pigment epithelium cell line Htert-rpe-1. Glutamylases TTLL5 and TTLL6 were reported to regulate the level of polyglutamylation. A co-depletion of TTLL5 and TTLL6, however, did not bring the glutamylation signal in the cytoplasm-cilia entry zone, the transition zone, to a stop. This suggests that other glutamylases regulate polyglutamylation in primary cilia (He et al., 2018). Targeting pathways at the point of cilia entry could lead to potential therapeutics. Polyglutamylation has been reported to regulate flagellar dynein motors, in turn affecting cilia beat function (Kubo et al., 2010). In contrast to polyglutamylation, polyglycylation is understood to regulate axoneme stability in a zebrafish model (Pathak et al., 2011).

Other types of post-translational modification include acetylation, which is the addition of an acetyl group into the lumen of the microtubule lattice. Access to the microtubule lumen is therefore essential (Coombes et al., 2016). A β-tubulin acetylation event was confirmed on lysine 252 expected to be associated with microtubule polymerisation (Chu et al., 2011).

In summary, tubulin enrichment and post-translational modification susceptibility are important contributors to axoneme structure and function, and in turn cilia motility.

1.3   Altered endometrial phenotype in unsuccessful pregnancy

1.3.1   uNK cells in recurrent pregnancy loss

Endometrial stromal cells play important roles during embryo implantation, including recruitment of immune cell populations, hormone signalling to the luminal surface

epithelium and stromal-epithelial cross talk (Hantak et al., 2014; Chen et al., 2013; Gellersen & Brosens, 2014). uNK cells have been studied as immunological markers for recurrent pregnancy loss and are thought to play a role in reproductive performance (Moffett & Shreeve, 2015; Quenby et al., 1999). A lack of HLA-C groups and KIR activation has been reported in women with a history of recurrent pregnancy loss (Hiby et al., 2009). Recurrent pregnancy loss has also been associated with a pro-senescent decidual response, including altered gene expression of Scavenger Receptor Class A Member 5 (*SCARA5*) and Iodothyronine Deiodinase 2 (*DIO2*) (Lucas et al., 2020) and a lack of mesenchymal stem cell differentiation (Lucas et al., 2016). uNK cells have been reported to clear senescent decidual cells, so a pro-senescent response could suggest a change in uNK regulation (Brighton et al., 2017).

To investigate uNK cells in endometrial tissue of recurrent pregnancy loss patients, uNK cell numbers have been histologically compared between recurrent pregnancy loss patients and control groups. These methods have included a measure of cell count and cell percentage of the relative endometrial tissue sections. A review by Seshadri and Sunkara (2014) highlight the discrepancies between study outcomes when uNK cell populations are quantified by different 2D immunohistochemistry quantification methods. Results varied dependent on the method of uNK quantification. No significant difference was found in recurrent pregnancy loss versus controls when evaluating uNK cells as a percentage of stromal cells (Lachapelle et al., 1996; Michimata et al., 2002; Quenby et al., 1999; Shimada et al., 2004; Tuckerman et al., 2007). uNK cell numbers in women with recurrent pregnancy loss were significantly higher compared with controls, when uNK cells were presented as numbers reported (Clifford et al., 1999). An increased infiltration of uNK cells and Treg cells has also been associated with an increased risk of recurrent pregnancy loss, uNK cells counted as number of cells/ mm^2 (Lyzikova et al., 2020).

There is a need to standardise uNK measurements, in order to reduce variation of results between clinical centres and allow translation of NK research into clinical practise (Chiokadze and Kristesashvili 2019). Less uNK cell variation was reported when a standardised method of 2D immunohistochemistry uNK cell measurements was applied by multiple clinical centres (Lash et al., 2016). These standardised uNK methods have

been applied to recent 2D immunohistochemistry studies, where results demonstrate a decrease in uNK cells in endometrium from women with recurrent pregnancy loss compared to controls (Lucas et al., 2020).

Stromal-epithelial cross talk has been shown via two distinct cell pathways; the canonical WNT/β-catenin-dependent pathway and the non-canonical β-catenin-independent pathway. Mouse studies have proposed that WNT5a signalling through a non-canonical pathway alters the E-cadherin-β-catenin complex in the uterine epithelium resulting in a lack of epithelial cell breakdown and subsequent embryo implantation (Hantak et al., 2014). The non-canonical WNT receptor Ror-2 has been investigated in the mouse model, and shown to be expressed in uNK cells during early pregnancy (K et al., 2010).

In summary, there are discrepancies between the number of uNK cells reported when endometrial biopsies are investigated by 2D immunohistochemistry techniques. Further work is required to establish the 3D arrangement of uNK cells in the endometrium of women with recurrent pregnancy loss, which will contribute towards standardising uNK measurements between different clinical settings.

1.3.2 Endometrial gland morphology in recurrent pregnancy loss

Reduced concentrations of glandular products MUC-1, LIF and Glycodelin have been reported in the uterine flushing's of women with recurrent pregnancy loss (Dalton et al., 1998; Mikołajczyk, et al., 2003). Altered glandular secretions suggest abnormal glandular function, yet the structure and function of endometrial glands in recurrent pregnancy loss is yet to be determined. Endometrial gland morphology has been investigated by a variety of histology techniques including light microscopy, transmission electron microscopy (TEM) and scanning electron microscopy (SEM) in clinical groups including pre-pregnancy endometrium, early pregnancy, recurrent implantation failure, endometriosis and miscarriage (Bahar et al., 2015; Bidarimath et al., 2017; Kara et al., 2007; Roshangar et al., 2013).

Glandular ultrastructural changes have been reported in the endometrium of women with recurrent implantation failure. The number of pinopodes at the apical surface of the endometrium were lower in women with recurrent implantation failure (Bahar et al., 2015). Luminal epithelial pinopode number has been proposed as an endometrial receptivity marker associated with the clinical pregnancy rate and the implantation rate following IVF procedures (Jin et al., 2017; Qiong et al., 2017). Artificial hormone replacement therapy however, was applied prior to endometrial biopsy collection, which would not represent the natural cycling endometrium (Jin et al., 2017). Endometrial pinopodes can be used alongside the quantification of endometrial secretory cells and ciliated cells to determine if there is a morphological phase delay in the endometrium (Aunapuu et al., 2018). No change in pinopode coverage was reported however, in the endometrium of women with recurrent pregnancy loss (Xu et al., 2012). The role of increased extracellular protrusions during endometrial receptivity, is yet to be determined.

Miscarriage decidua ultrastructure was compared to normal pregnancy decidua by SEM and TEM. Decidual cells were demonstrated to possess several polyploidic protrusions on cell membranes. Decidual cells from non-miscarriage cohort were found to develop jap-junctions in interfaces between each other. In contrast, decidual cells obtained from miscarriages showed infiltration to be significantly lower, thus in miscarriage it is hypothesised that intercellular communications are lacking, associated with an increase in the number of uNK cells (Kara et al., 2007).

In summary, glandular structural differences in the endometrium of recurrent pregnancy loss is not well understood. 3D imaging techniques could enhance our understanding of glandular structures and their spatial relationships.

1.3.3 Endometrial gland transcriptome in recurrent pregnancy loss

Candidate gene and microarray studies have attempted to identify a gene expression profile that predicts the endometrial status in terms of receptivity or implantation success (Díaz-Gimeno et al., 2011). The gene panel used by the ERA did not associate a non-receptive endometrium with implantation failure (Ruiz-Alonso et al., 2013). Microarray and RNA sequencing studies however, have indicated an association between an altered

endometrial gene expression profile and implantation failure during the window of implantation (Chen et al., 2018; Koot et al., 2016; Macklon, 2017). There has not been a consistent pattern of gene expression across all studies that relates to these conditions, potentially due to the differences in methodology and endometrial heterogeneity not being taken into account (Table 1.2).

The gene expression profile of endometrium from women with recurrent pregnancy loss is less established. The endometrium from women with recurrent pregnancy loss has been compared to the endometrium from other unsuccessful pregnancy patient groups such as recurrent implantation failure (Huang et al., 2017). Recent single cell RNA sequencing approaches have also identified cell signatures in control endometrium and a differential gene expression profile in stromal cell types of endometrium from women with recurrent pregnancy loss (Lucas et al., 2020). A comparative gene expression analysis, however has not been performed between endometrial glands from women with recurrent pregnancy loss and fertile controls. This approach would allow the transcriptome from endometrial glands to be analysed without being obscured by other endometrial cell types.

Table 1.2 Endometrial transcriptome study comparison

Method	Animal model	Study groups/tissue	Finding	Reference
Microdissection of isolated cell types RNA-sequencing	Sheep	Endometrial luminal epithelium, glandular epithelium, the conceptus and endometrial luminal fluid during the peri-implantation period of pregnancy	Genes expressed in luminal epithelium and glandular epithelium involved in cell survival and growth	(Brooks, Burns, Moraes, & Spencer, 2016)
RNA-sequencing	Human	Comparing long noncoding RNA and messenger RNA in endometrium of women with RIF following IVF embryo transfer and control (LH + 3 - 7)	Identified 742 long noncoding RNA differentially expressed genes and 460 m RNA. Cis-regulated target genes of long noncoding RNA were clustered into TNF signalling pathways and toll-like receptor signalling pathway	(Chen et al., 2018)
FACS cell sorting RNA-sequencing	Human	2 samples (1) (LH + 8) and (2)- Day 25 late secretory with known endometriosis. CD39 stroma and CD9 epithelium	Genes more active in cultured stromal cells compared to biopsy. Low RNA yield from cultured epithelium caution	(Krjutškov et al., 2016)
RNA-sequencing	Human	Pre-receptive (LH + 2) versus receptive endometrium (LH + 7).	1099 genes were up-regulated at LH + 7 compared to LH + 2, and 1273 down-regulated. Mineral absorption pathway was most active for upregulated genes while cell cycle for down regulated	(Hu et al., 2014)
Microarray	Human	RIF vs controls (LH + 6 - 7)	303 genes predictive of RIF, suggestive that RIF is primarily associated with reduced cellular proliferation	(Koot et al., 2016)
RNA-sequencing	Human	RIF/RM vs controls (LH + 7)	Complementary and coagulation cascades pathway was up-regulated in RIF, while down regulated in RM.	(Huang et al., 2017)

1.3.4   Ciliopathies in reproduction

Ciliopathies can result from gene mutations, affecting cilia structure and function. Motile cilia in the fallopian tubes are important in gamete and embryo transport. Infections such as chlamydia, are understood to reduce the cilia beat frequency of tubal mucosa (Lyons et al., 2006), clinically recognised as 'immotile cilia syndrome' or tubal infertility. Endometrial cilia, investigated by TEM, are identified on the luminal epithelial surface and endometrial glands (Bartosch et al., 2011). Cilia axoneme defects have been reported in a recurrent implantation phenotype, including impaired microtubule arrangement in the ciliary shafts and the deletion of central tubules (Denholm & More, 1980; Fedele et al., 1996), associated with a disrupted hormonal milieu (More & Masterton, 1976). These ciliary structural impairments may influence cilia beating and coordination.

The 3D structure of endometrial gland cilia and their role in moving glandular products is not understood. The ciliopathy primary cilia dyskinesia (PCD) is a well-studied condition which impacts the motile ciliary beat function of the mucosal-ciliary elevator in the respiratory system.

Primary ciliary dyskinesia

PCD is a genetic defect which causes reduced or non-functional cilia, with the main consequence being frequent respiratory infections (Van's Gravesande & Omran, 2005). Of those women that have PCD, approximately 30% will be infertile. PCD provides a well-studied reference point for associated genetic and structural ciliary axonemal impairments. Multiple methods can be used to clinically assess PCD, including genetic profiling, electron microscopy and cilia beat frequency. The results of these investigations are not always consistent, such that cilia may only be shown to be impaired in one or more but not all techniques. Approximately 30 known gene mutations have been found to underlie PCD (Lucas et al., 2017). Studies applying TEM or genetic profiling as the standard method of PCD assessment could exclude PCD patients where the cilia axoneme ultrastructure is normal or the genetic mutation is unknown (Lucas et al., 2017). This reinforces that ciliopathy identification, in the respiratory system or the endometrium, requires a more established understanding of gene mutations and their respective structural impairments.

Ciliary function in the airways is understood to be regulated by genetic and environmental factors. There is emerging evidence of an association between lung disease and environmental stimuli such as air pollutants and smoking (Cao, et al., 2020), via the chemosensory ability of motile cilia (Shah et al., 2009). Women who smoke have an increased risk of ectopic pregnancy and increased incidence of tubal infertility (Bouyer et al., 2003). Together, these studies provide evidence that glandular cilia could be influenced on a genetic and an environmental level, influencing the regrowth and differentiation of cilia at every menstrual cycle.

1.4   3D imaging of the endometrium

3D imaging provides a more representative approach to studying biological samples, overcoming some restrictions imposed by traditional 2D imaging techniques, as reviewed in the placenta (Lewis & Pearson-Farr, 2020). 3D modelling has been applied to endometrial animal models, providing insights into the site of embryo implantation, the long axis of the endometrial horn and endometrial gland organisation (Hondo et al., 2007). Changes made to the luminal surface of the endometrium during implantation preparation have also been reported (Arora et al., 2016).

Three-dimensional imaging

A 3D reconstruction of the mouse uterus was prepared using paraffin cross sections from pregnant and non-pregnant uteri (Hondo et al., 2007). Both the 'lateral edge' being the luminal epithelium and gland outline were traced on a digital image and then aligned together using image software. Their evidence suggests that the implantation site in mice is programmed to form relative to the long axis of the endometrial horn, and an embryo is implanted in the region where endometrial glands are localised from the lateral to the anti-mesometrial region of the endometrial horn (Hondo et al., 2007). Changes to mouse endometrial gland orientation have been identified during early pregnancy. Reorientation was demonstrated to be concurrent with implantation at gestational day 4.5, in comparison to non-pregnant endometrial glands. Endometrial glands of a pregnant mouse also demonstrated further coiling (Arora et al., 2016).

In summary, 3D imaging approaches have shed light on the macroscale of endometrial glands, alterations made during early pregnancy and the location of endometrial glands. Advances in automated image segmentation and machine learning has the ability to distinguish between different endometrial cell types (Downing et al., 2019). By investigating endometrial 3D ultrastructure with automated/semi-automated image analysis methods, will provide novel insights into endometrial structure and function.

1.5 Aims

This thesis aims to apply multi-scale 3D imaging techniques to investigate if there is an association between recurrent pregnancy loss and the spatial relationships of endometrial glands. The project aims to start with whole endometrial tissue, and then work progressively to the glandular cilia subunits important for the glandular milieu (Figure 1.6).

1)   To investigate the association between recurrent pregnancy loss and the 3D spatial relationships of endometrial stromal cells to endometrial glands using a novel 3D approach

2)   To investigate endometrial gland architecture by multiscale and multimodal 3D imaging

3)   To investigate the association between recurrent pregnancy loss and the gene expression profile of isolated endometrial glands

4)   To investigate the association between recurrent pregnancy loss and β-tubulin expression in endometrial gland cilia

Whole endometrial tissue

Endometrial glands

Endometrial gland beta tubulin

1) Spatial relationships of endometrial stromal cells to endometrial glands

2) Endometrial gland architecture

3) Endometrial gland gene expression profile

4) Beta tubulin subunit of endometrial gland cilia
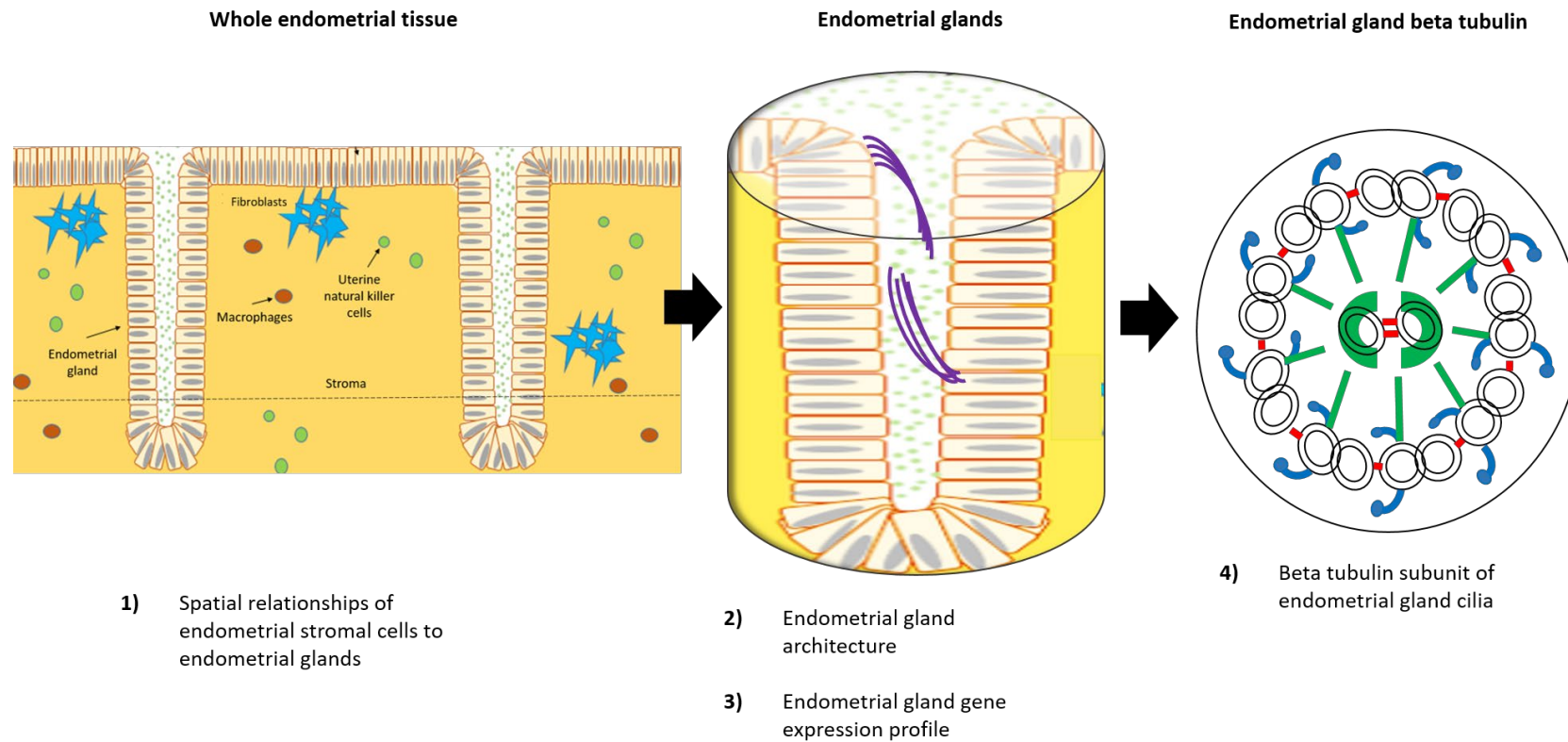
Figure 1.6 *A multi-scale and multi-modal approach to investigating the architecture and gene expression profile of endometrial glands during the window of implantation. 1) From endometrial cellular spatial relationships, 2) and 3) endometrial glands (purple lines represent glandular ciliated epithelial cells) to 4) subunits of endometrial gland cilia.*

Chapter 2   General methods

2.1 Contributions

Work was carried out by myself, other than the techniques stated below:

- Dr Sybil Jongen carried out RNA extraction, bioanalyser quality check, library preparation, RNA sequencing and differential gene expression analysis of isolated endometrial glands that I had prepared.

- Patricia Goggin drove the 3-view serial block face SEM on 3-view pins I had prepared.

- Regan Doherty drove the tilt Hitachi TEM to image glandular cilia ultrastructure of thin sections (90 nm) that I had prepared.

2.2 Participant recruitment and endometrial tissue collection

2.2.1 Participant recruitment

Participants that met the study criteria (Table 2.1), were recruited for collection of an endometrial tissue biopsy at a tertiary fertility and gynaecology referral centre in Southampton. These included recurrent pregnancy loss, subfertility and control participants. Control participants were recruited from healthy fertile women who elected to donate eggs at the local fertility centre in Southampton having met the criteria for egg donation. Informed written consent was given by all participants, and ethical approval for this study was given by the Isle of Wight, Portsmouth & South East Hampshire Research Ethics Committee (08/H0502/162).

An anonymous study ID number was given to the participant, which was linked to participant clinical characteristics. Demographics included age and body mass index (BMI). Menstrual cycle characteristics included day of the menstrual cycle, length of menstrual cycle, number of days bled, and whether the menstrual cycle was regular or irregular. Fertility history included contraceptive use, number of pregnancies, live births, and subsequent miscarriages. Smoking status and sexually transmitted infection history were also recorded.

Table 2.1 *Participant inclusion and exclusion criteria.*

Participant Criteria
Aged between 18-45 years old
Not suffering from premature ovarian failure or any infective processes
Not receiving treatment for any systemic infection
Not on hormonal treatment

2.2.2 Endometrial tissue collection

Endometrial biopsies were collected within a seven-day window of the menstrual cycle, 4-10 days post the luteinising hormone surge (LH + 4 - 10), encompassing the window of implantation (LH + 7 - 10). A consistent sampling collection period was important to ensure all samples were in a similar biological state, as the endometrium changes to a receptive state during the window of implantation only. A seven-day sampling window was used in this study, due to sample availability at the time of tissue processing. Menstrual cycle day was self-reported, based on a participant's last menstrual bleed.

Endometrial biopsies (approximately 1.5 cm x 0.5 cm) were collected by a Pipelle sampler (Laboratorie C.C.D) (Stocker et al., 2017) by the clinician prior to any surgical intervention, if any. One endometrial sample was obtained per participant and divided into five. One endometrial piece was immersed into the main electron microscopy fixative (3% glutaraldehyde in 0.1 M cacodylate buffer at pH 7.4), two endometrial pieces were immersed into RNAlater® (Thermo Fisher Scientific, UK) to stabilise RNA, and the remainder of the tissue biopsy divided in half. The first half was placed in a serum free 50:50 mix of Dulbecco's modified Eagle's medium (DMEM, Lonza, Cambridge, UK) and Ham's F12 nutrient mixture (Lonza, Cambridge, UK) supplemented with 5% penicillin streptomycin (Lonza, Cambridge, UK) for endometrial gland isolation. The remaining half was fixed for 2 h at 4°C in 4% paraformaldehyde (PFA, Sigma Aldrich, UK) in phosphate buffered saline (PBS, 0.01 M phosphate buffer 0.0027 M potassium chloride and 0.137 M sodium chloride at pH 7.4, Sigma, Dorset, UK) for imaging (Figure 2.1). After fixation the tissue was stored in 0.1% sodium azide (Fisher Scientific, UK) in PBS at 4°C. The endometrial piece immersed in the main electron microscopy fixative (3% glutaraldehyde in 0.1 M cacodylate buffer at

pH 7.4) was stored at 4°C until processing for electron microscopy. Endometrial pieces in RNAlater® were stored at 4⁰C overnight and then long-term at -80⁰C. All samples were labelled appropriately with their participant anonymous study ID, referencing the study number and date of collection.
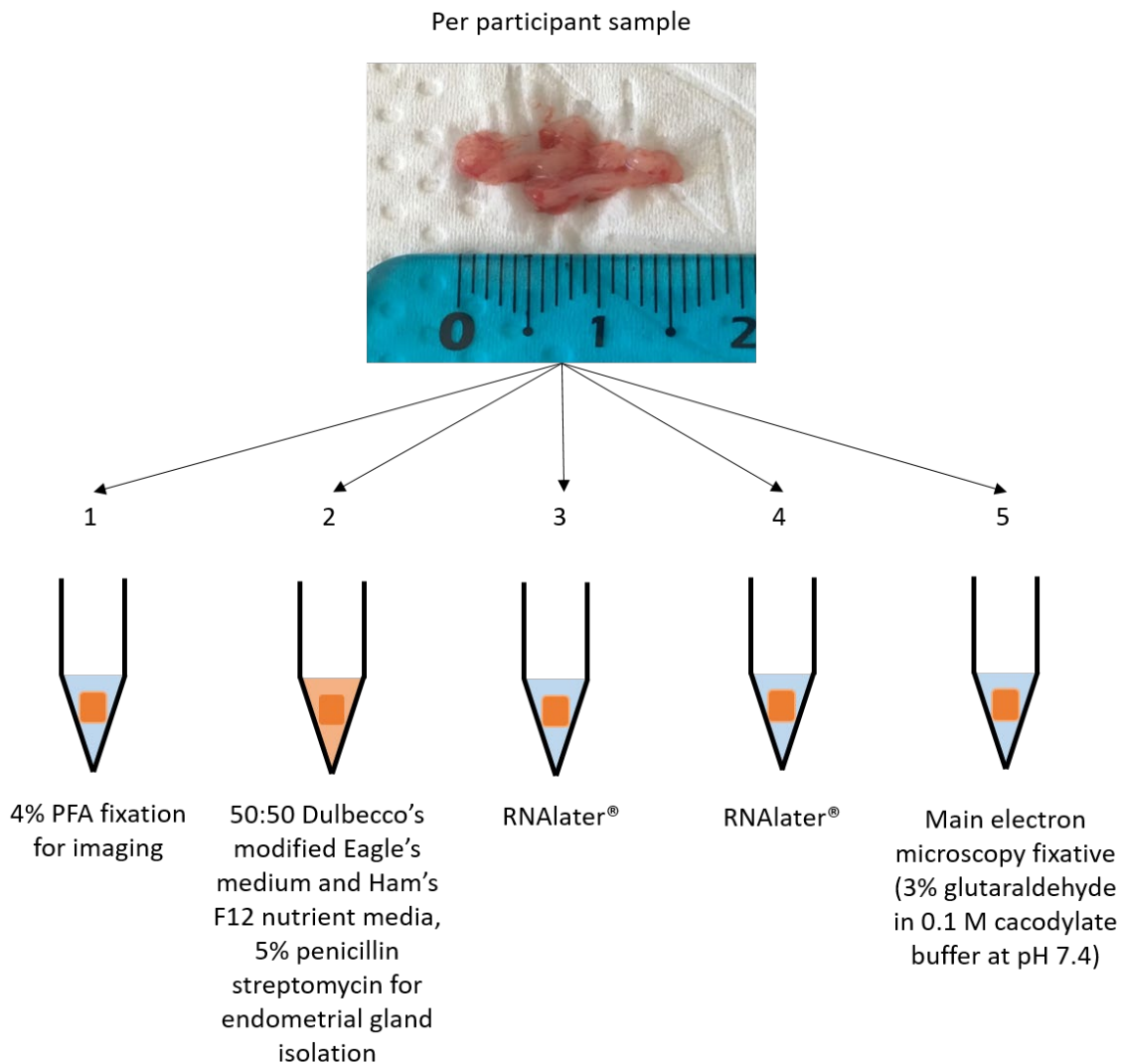
Figure 2.1 *The separation of an endometrial biopsy for different applications.* ***1)*** *Tissue fixation for imaging,* ***2)*** *media for endometrial gland isolation,* ***3 and 4)*** *RNAlater® for RNA extraction and* ***5)*** *main electron microscopy fixative for high resolution microscopy.*

2.3   Immunohistochemistry on tissue sections

Fluorescence immunohistochemistry was carried out on 10 µm endometrial tissue sections to establish optimal antibody dilutions for wholemount immunohistochemistry. Immunohistochemistry was also carried out on nasal brushing culture preparations. These were used as wholemount immunohistochemistry positive controls (donated by Southampton PCD team Professor Lucas, Southampton and South West Hampshire Research Ethics Committee A CHI395, 07/Q1702/109).

2.3.1   Principles of immunohistochemistry

Immunohistochemistry is a common application that uses positive immune-reactivity of antibodies raised to specific cell markers, first established by Albert Coons in 1941 (Coons et al., 1941). Visualising an antigen-antibody interaction is achieved in multiple ways by the addition of secondary antibody-mediated detection. The two most popular methods of secondary antibody detection are enzyme mediated chromogenic detection, through the production of coloured pigments, and fluorophore mediated detection by fluorescent detection. In chromogenic detection, an enzyme label reacts with a substrate to yield a coloured product that precipitates at the site of the antigen, which is detected by light microscopy. Alternatively, a fluorescent secondary antibody can be added with specific binding for the host species of the primary antibody, detected on a fluorescent microscope. Fluorescent imaging was the chosen application for this study.

2.3.2   Principles of fluorescence

Fluorescence is a process where an electron absorbs light at a given energy level and wavelength (Willem Borst & Visser, 2010). An electron begins at ground energy state (S_0). The electron is then raised to higher energy levels 1 (S_1) and 2 (S_2) when absorbing excitation light (Figure 2.2) (Jablonski, 1933). A concept known as the Stokes shift then occurs where a lower energy and longer wavelength is then emitted (Stokes, 1852). The fluorescence lifetime *(Tnsec)* is the time that a molecule will remain at the excited state

before returning to the grounded energy state (Lleres et al., 2007). Fluorescently conjugated secondary antibodies allow positive primary immuno-reactivity to be identified.
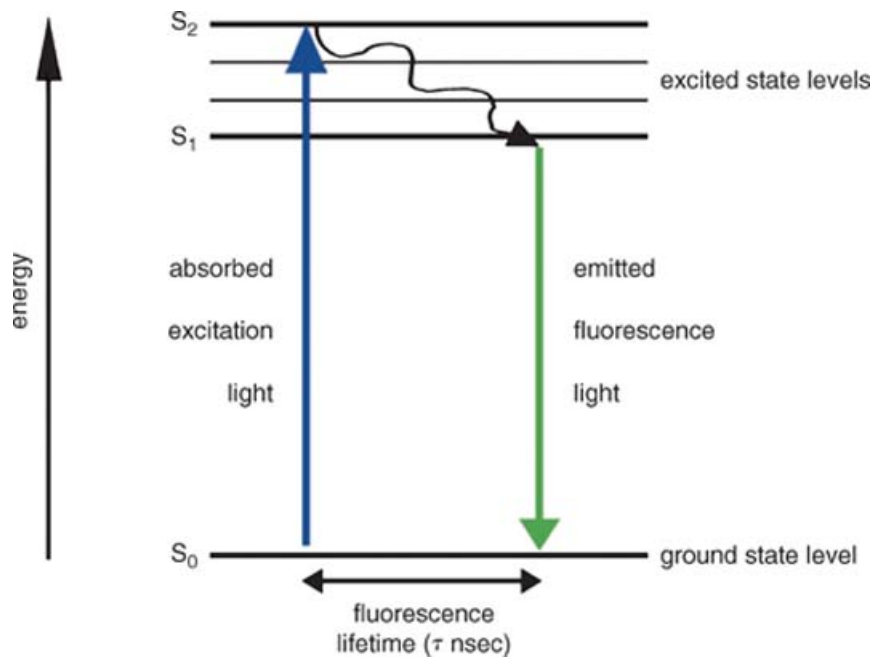
Figure 2.2 *Jablonski energy diagram demonstrating the change in energy state of an electron during fluorescence, adapted from lleres et al., 2007.*

One problem associated with fluorescence imaging is autofluorescence, which can emit a stronger signal than that given by the immunofluorescence of cells/proteins of interest. Autofluorescence occurs when components of fixed human tissue emit bright fluorescence when exposed to fluorescent light, with no need for antibody staining. Components such as the extracellular matrix emit a large amount of autofluorescence, due to their relatively high quantum yield, which hold a high fluorescence intensity (Monici, 2005).

2.3.3 Immunohistochemistry of tissue sections for fluorescence microscopy

Immunohistochemistry was performed on endometrial cryo-sections and nasal brushing culture preparations (Figure 2.3), immunohistochemistry reagents (Table 2.2). Endometrial samples were snap frozen in liquid nitrogen and cut into 10 µm sections on the cryostat at -20°C by Jon Ward from the Histology Research Unit. Nasal brushing culture preparations were donated by Southampton PCD team Professor Lucas. Nasal brushings
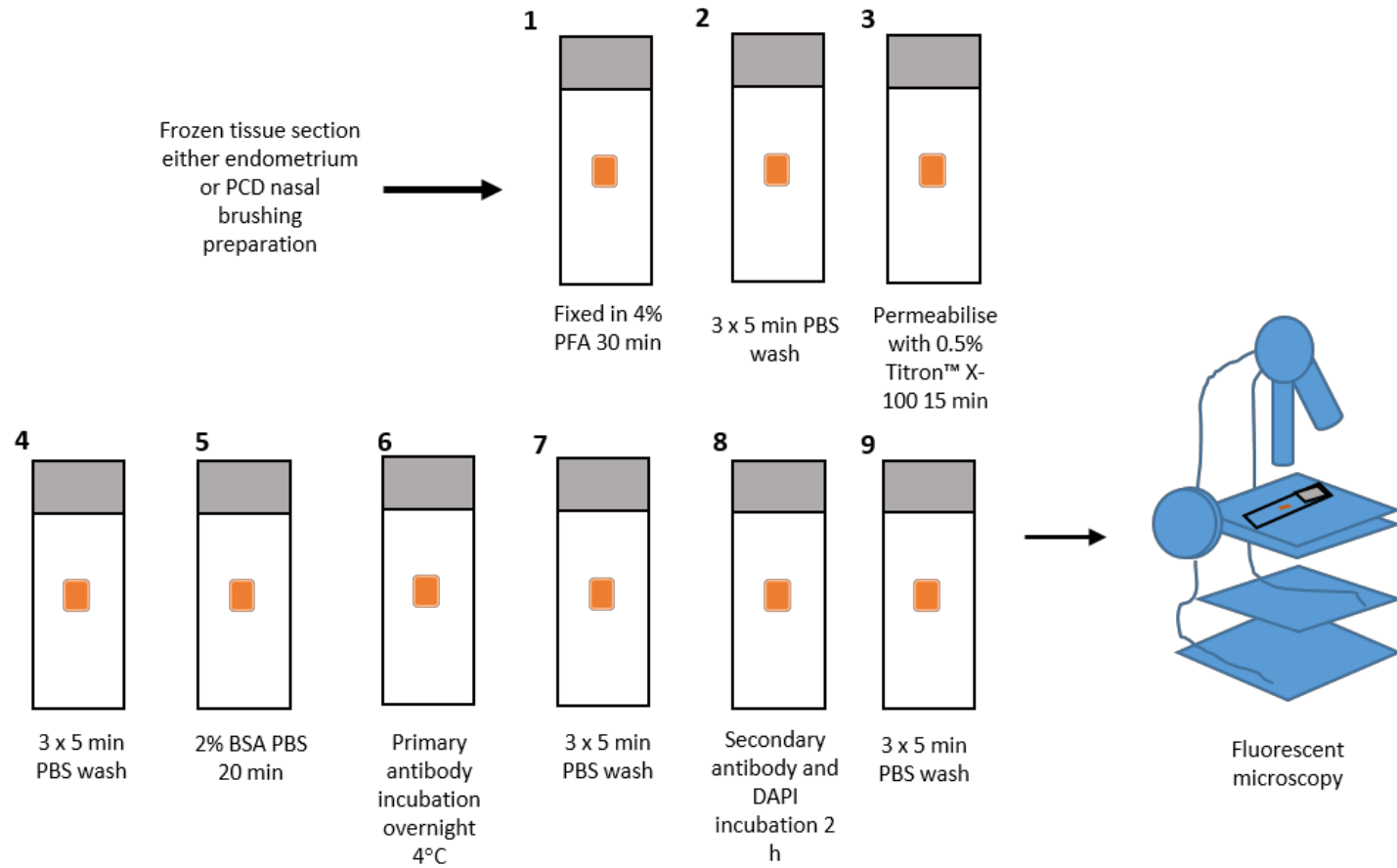
Figure 2.3 *Immunohistochemistry on endometrial tissue sections and nasal brushing epithelial cells for fluorescent microscopy. PFA = paraformaldehyde, PBS = phosphate buffered saline, BSA = bovine serum albumin, DAPI = 4',6-diamidino-2-phenylindole.*

were retrieved from healthy volunteers, were cultured to re-establish functional motile ciliated cells on a glass slide and frozen at -20°C. Immunohistochemistry experiments were accompanied by a negative control where the primary antibody was omitted, which checks for non-specific binding of the secondary antibody. To demonstrate a positive immunohistochemistry reaction, western blot validation is required.

Pre-immunohistochemistry, antigen retrieval experiments were carried out as part of antibody optimisation. Heat treatment in 2 ml citrate buffer (0.01 M citrate buffer pH 6.0) and pronase enzyme treatment (1% pronase in PBS) were applied.

Immunohistochemistry was carried out at room temperature unless stated otherwise. Tissue sections were fixed in 4% PFA for 30 min, followed by 3 x 5 min PBS washes. Tissue sections were then permeabilised with 0.5% Titron™ X-100 for 15 min, followed by 3 x 5 min PBS washes. To block non-specific antibody binding sites, tissue sections were incubated in 2% bovine serum albumin (BSA) in PBS for 20 min. Incubation with the respective primary antibodies was undertaken at 4°C overnight, followed by 3 x 5 min PBS washes. Tissue sections were incubated with respective secondary antibodies and a nuclear stain 4',6-diamidino-2-phenylindole (DAPI) at 2 µg/ml for 1 h, followed by final 3 x 5 min PBS washes.

Table 2.2 *Reagents for immunohistochemistry.*

- 4',6-diamidino-2-phenylindole (Sigma Aldrich, UK)
- Bovine serum albumin (Sigma, Dorset, UK)
- Citrate acid crystals (Fisher Scientific, UK)
- Paraformaldehyde (Sigma Aldrich, UK)
- Phosphate buffered saline (Sigma, Dorset, UK)
- Pronase (Dako, UK)
- Sodium hydroxide (Fisher Scientific, UK)
- Titron™ X-100 (Sigma Aldrich, UK)

2.3.4   Fluorescent microscopy of tissue sections

Endometrial tissue sections were imaged on the Fluorescent microscope Zeiss KS400 (Ziess, UK), at 10 x and 40 x magnification, images saved to the Biomedical Imaging Unit file store. A fluorescence microscope works by illuminating the tissue section with a high-energy source, which is absorbed by fluorophores attached to the tissue indirectly by secondary antibody application. Fluorophores emit a longer lower energy wavelength light, which can be separated from the surrounding light by filters designed for specific wavelengths. The detection of different wavelengths is made possible by using different emission filters.

2.4   Wholemount immunohistochemistry

2.4.1   Principles of wholemount immunohistochemistry

The principles of immunohistochemistry and fluorescent imaging hold true for wholemount immunohistochemistry, described in section 2.3. Wholemount immunohistochemistry overcomes the requirement to cut the tissue into individual sections, allowing the investigation of whole tissue pieces, therefore, less disruptive compared to immunohistochemistry on tissue sections. Samples processed by wholemount immunohistochemistry were imaged via the fluorescent confocal laser-scanning microscope. After secondary antibody incubation, endometrial samples underwent optical clearing with organic solvent 2,2' Thiodiethanol (TDE) to overcome the limitation of light scatter, allowing a whole piece of tissue to be imaged, whilst resolving the 'micro' details (Richardson & Lichtman, 2017).

2.4.2   Wholemount immunohistochemistry of endometrial tissue pieces for confocal laser scanning microscopy

A wholemount immunohistochemistry protocol was carried out on endometrial tissue pieces (approximately 1.5 mm^3, Figure 2.4) to prepare them for confocal-laser scanning microscopy (Figure 2.6). All steps were carried out on a specimen roller at room

temperature to ensure that the tissue was constantly moving in solution, unless stated otherwise. A negative control sample was also processed by omission of the primary antibody, to check for non-specific staining of the secondary antibody. Reagents for wholemount immunohistochemistry (Table 2.3).

Endometrial tissue pieces were washed in 5 ml PBS and then permeabilised with 0.5% Titron™ X-100 for 1.5 h, followed by 3 x 5 min PBS washes. The tissue was then blocked with 2% BSA in PBS for 1 h at room temperature. Following tissue blocking, primary antibody incubation was carried out immediately. Primary antibody incubation was undertaken in 75 µl PBS via a droplet technique at 4°C overnight (Figure 2.5). The rationale behind the droplet technique was to ensure a concentrated liquid around the samples during their primary incubation. Droplets were made on a parafilm surface in a closed container, above damp cloths to ensure the droplets did not dry out.

Following another 3 x 5 min PBS washes, the secondary antibody incubation was carried out with DAPI at 2 µg/ml for 2 h on a moving plate, followed by 3 x 5 min PBS washes. Endometrial tissue pieces were optically cleared by gradually displacing PBS with TDE, via stages 10% 25% 50% and 97%. Each tissue clearing step was left for a minimum of 30 min. Once complete, the tissue pieces were stored in 97% TDE in PBS at 4°C until imaging on the confocal laser scanning microscope.
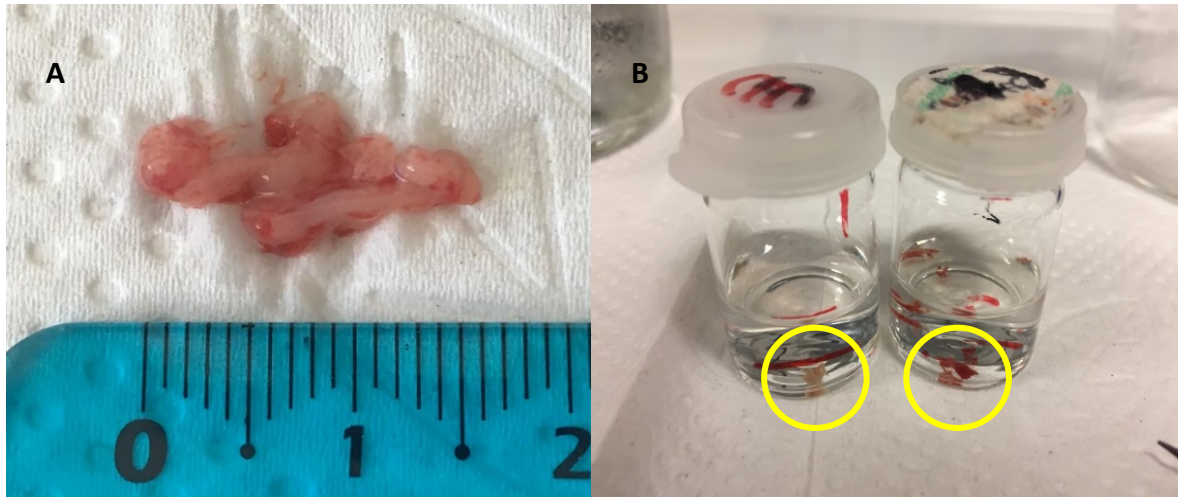
Figure 2.4 *Endometrial pipelle biopsies prepared for wholemount immunohistochemistry.* ***A)*** *Fixed endometrial biopsies were cut into* ***B)*** *small pieces of approximately 1.5 mm³.*
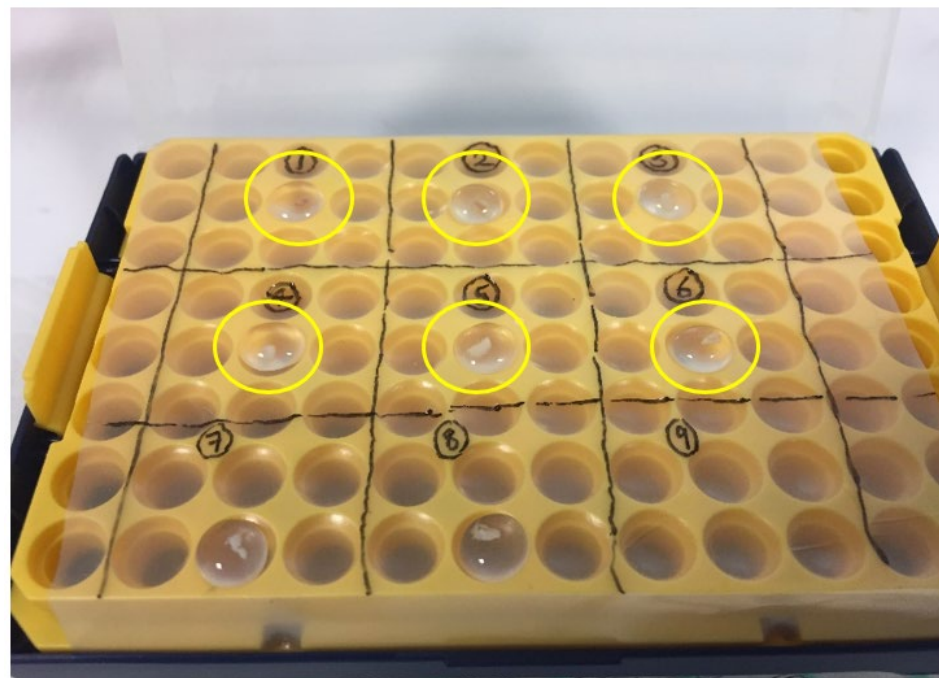
Figure 2.5 *The droplet technique developed for primary antibody incubation overnight. Droplets on parafilm in a humidified container. Incubation in this way reduces the amount of antibody required.*
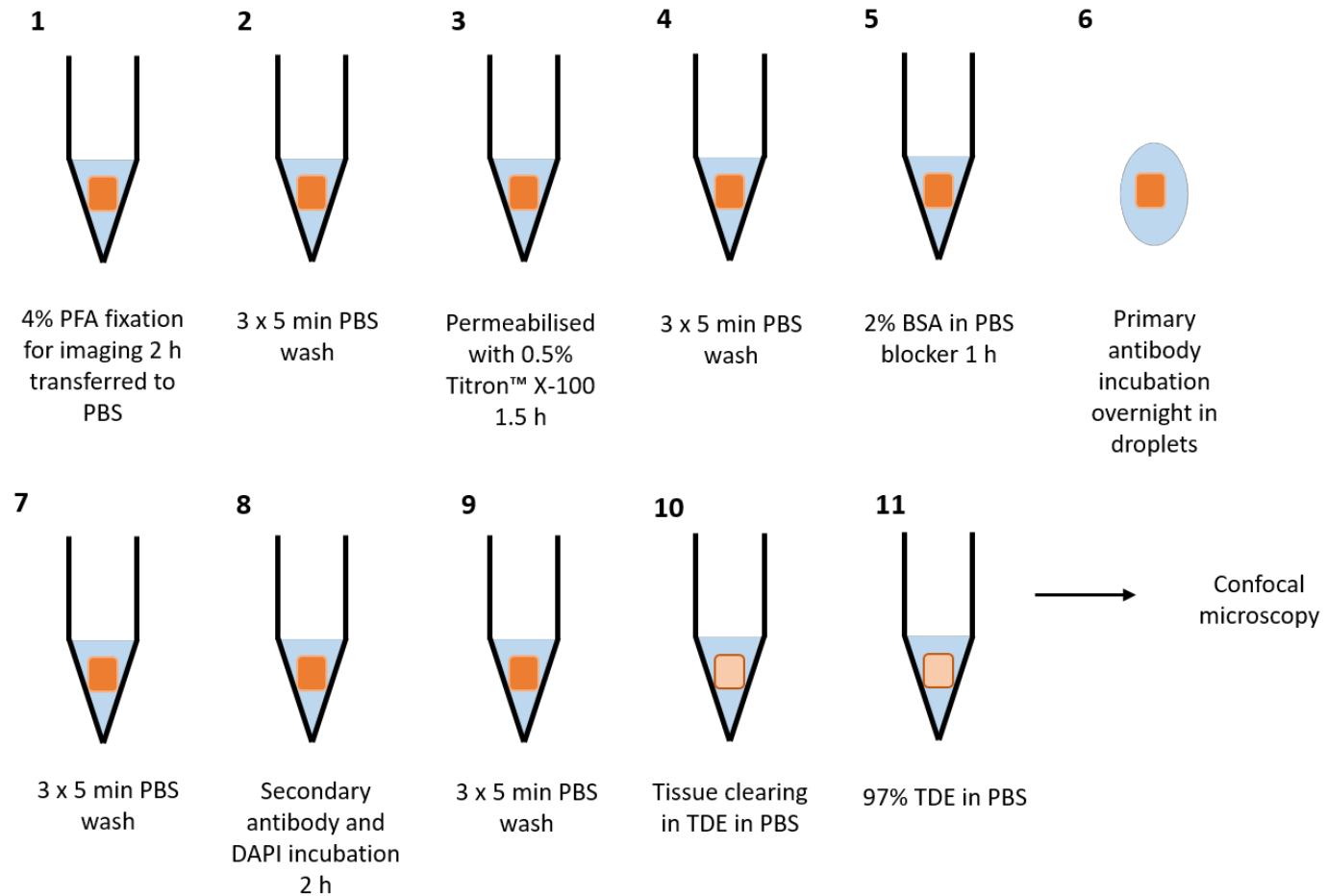
Figure 2.6 Processing of endometrial tissue pieces (orange) by wholemount immunohistochemistry for confocal laser scanning microscopy.
PFA = paraformaldehyde, PBS = phosphate buffered saline, BSA = bovine serum albumin, DAPI = 4',6-diamidino-2-phenylindole, TDE = 2,2'
Thiodiethanol.

***Table 2.3** Reagents for wholemount immunohistochemistry.*

- $1.5 - 3$ mm^3 human tissue fragments
- 2,2' Thiodiethanol (Fluka Analytical)
- 4',6-diamidino-2-phenylindole (Sigma Aldrich, UK)
- Bovine serum albumin (Sigma, Dorset, UK)
- Paraformaldehyde (Sigma Aldrich, UK)
- Phosphate buffered saline (Sigma, Dorset, UK)
- Titron^{TM} X-100 (Sigma Aldrich, UK)

2.5   Confocal laser scanning microscopy

2.5.1   Principles of confocal laser scanning microscopy applied to tissue samples

The confocal microscope is a multi-laser fluorescent microscope, which allows samples to be imaged in 3D by optical sectioning. Endometrial tissue that has been optically cleared into 97% TDE in PBS (described in principles of wholemount immunohistochemistry) is placed into a chamber and covered with 97% TDE, so to prevent the tissue drying out during imaging. The chamber containing the endometrial tissue sample is placed onto the confocal microscope stage for imaging.

Multiple lasers of different wavelengths scan the tissue sample (Figure 2.7), each exciting fluorophores within its wavelength. Fluorophores attached to a specific cell marker, are detected and imaged in the z-direction by optical sectioning. Optical sectioning scans the sample from top to bottom, or vice versa, creating a stack of consecutive images per cell marker, depicted as one channel. Multiple channels are imaged at once by avoiding the crossover of emission and excitation wavelengths between different fluorophores. This is important in experimental planning and scanning settings. Sequential imaging arranges a set sequence of lasers, so that lasers of a similar wavelength do not excite the tissue at the same time. Confocal laser components such as the pinhole and the dichromic mirrors, allow laser wavelength spectrum to be adjusted, for example narrowed, before the laser excites the tissue with a high energy source.
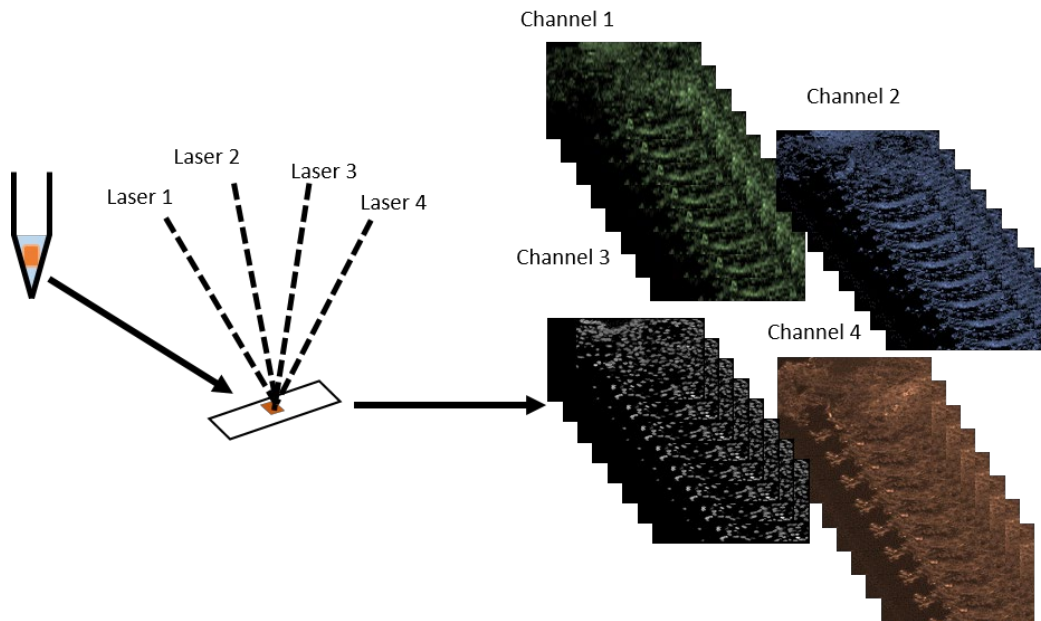
Figure 2.7 *Principles of confocal laser scanning microscopy. Fluorophores on a sample (orange) are excited by lasers with specific wavelengths and the resulting emissions detected by the microscope. Focusing the microscope at different depths allows a stack of consecutive images can be generated providing 3D information. By exciting different fluorophores with different wavelengths lasers multiple cell markers can be identified.*

2.5.2 Wholemount confocal laser scanning microscopy of endometrium

Endometrial tissue pieces were imaged on the SP8 confocal laser-scanning microscope (Leica Microsystems, Germany), by laser scanner settings (Table 2.4). For each experiment, negative control samples, by omission of the primary antibody, were used to check for no non-specific binding of the secondary antibody and set the microscope laser settings for the respective study samples. Different lasers were used to detect individual cell markers, fluorophore information (Table 2.5). The objective and voxel size were specific by experiment. All data files saved onto the Biomedical Imaging Unit file store.

Table 2.4 *Settings applied for the SP8 confocal laser-scanning microscope.*

Setting	Applied
Smart offset (%)	-1.0
Scan field rotation (°)	90.00
Pinhole (AU)	1.00
Zoom	0.75
Format (pixels)	1024 x 1024
Scan speed (Hz)	600
Line average	4

AU = airy unit, Hz = hertz

Table 2.5 *Excitation and emission wavelengths for fluorophores used.*

Secondary antibody/ fixed conjugate	Excitation wavelength (nm)	Emission wavelength (nm)	Confocal laser (nm)
DAPI	359	461	405
FITC	495	519	488
Dylight 550	558	576	561
Streptavidin 680	677	705	633
Dylight 594	593	617	594
CF^{TM}633	629	657	633

2.6 Transmission electron microscopy

2.6.1 Principles of transmission electron microscopy

Transmission electron microscopy (TEM) is a high-resolution imaging technique used to investigate tissue ultrastructure. Glutaraldehyde fixed tissue samples are stained with heavy metals and polymerised in a resin block. Ultrathin tissue sections (approximately 90 nm), cut from the resin block are mounted into the electron microscope for imaging. An electron gun produces a beam of electrons, which transmit onto the specimen via the contribution of different lenses. Electrons that pass through and interact with the specimen generate an image, whereas electrons that are reflected off the sample do not generate an image (Figure 2.8). Heavy metals create contrast in the tissue sample features.
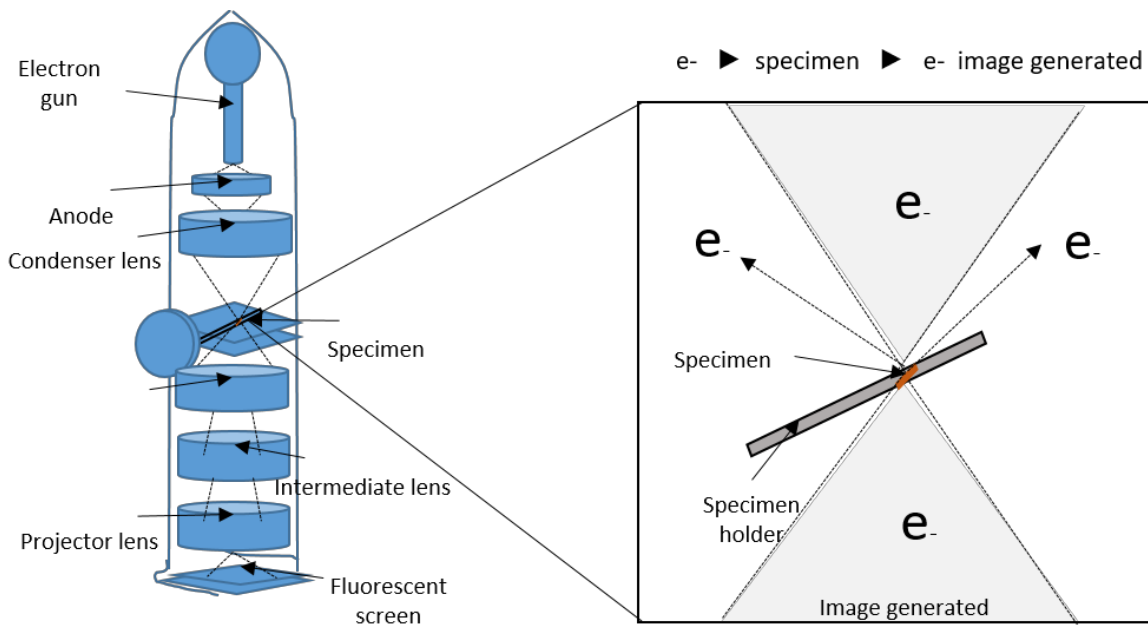
Figure 2.8 *Principles of transmission electron microscopy. An electron gun produces a beam of electrons (e-) which are focused onto the specimen. Electrons that pass through the tissue specimen produce an image.*

2.6.2   Tissue processing for imaging by TEM

The protocol and solutions used for TEM processing were taken from general protocols used at the biomedical imaging unit (Figure 2.9). All steps were carried out with reagents (Table 2.6) at room temperature and in a rotator unless stated otherwise.

Endometrial tissue pieces of 2-3 mm^3 were collected into the main electron microscopy fixative and stored at 4°C until tissue processing, as described in 1.2. At the time of tissue processing, the endometrial pieces underwent 2 x 10 min cacodylate buffer washes (0.1 M sodium cacodylate buffer at pH 7.4 plus sucrose and 2 mM CaCl$_2$). Then the endometrial pieces were incubated with the post electron microscopy fixative (2% osmium tetroxide in 0.1 M sodium cacodylate buffer at pH 7.4) for 2 h. Following a brief rinse in distilled water for 30 sec, the endometrial pieces were incubated in 2% uranyl acetate in ddH$_2$0 for 30 min, followed by another distilled water rinse for 30 sec.

A dehydration process was then undertaken. The endometrial pieces were incubated in 70% ethanol and 95% ethanol for 10 min, followed by absolute ethanol 2 x 20
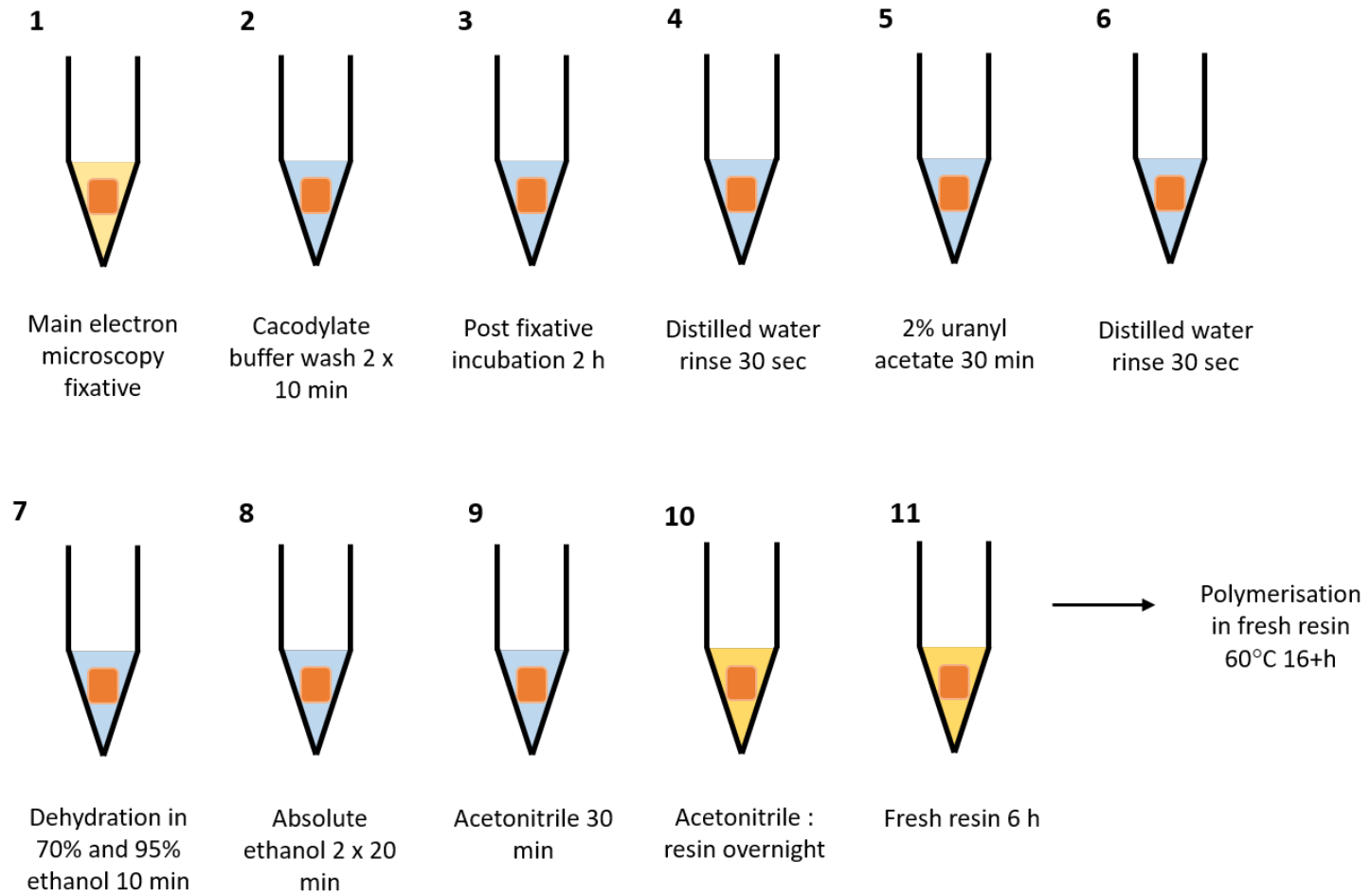
Figure 2.9 *Tissue processing for transmission electron microscopy. Tissue (orange) is fixed, stained with heavy metals and then dehydrated before embedding in a resin block.*

min and acetonitrile for 30 min. Finally, 50:50 acetonitrile: resin incubation overnight. The samples were incubated in fresh resin for 6 h the following morning, before being polymerised and encapsulated in fresh resin at 60°C for 16+ h. The resin blocks were taken forward for cutting and imaging by TEM.

2.6.3 Resin tissue quality check and thin sectioning for TEM

Tissue quality check

Thick endometrial tissue sections (0.5 µm) were stained with 1% toluidine blue in ddH$_2$0 and examined for tissue quality on the standard light microscope (Figure 2.10). In order to prepare the slides for examination, glass knives were cut by the knife maker type 7801-A (LKB-Produkter AB, Bromma, Sweden) and thick sections were cut on the Ultracut E microtome (Ultracut Reichert-Jung, UK), before being transferred onto a droplet of double filtered water on a microscope slide. The microscope slide was then dried on a hot plate for 20 min. The section was stained with 1% toluidine blue tissue stain, dried for a second time before mounted with a cover slip. The slides were investigated at both low magnifications 5 x for overall tissue structure and 40 x to check for cellular integrity.
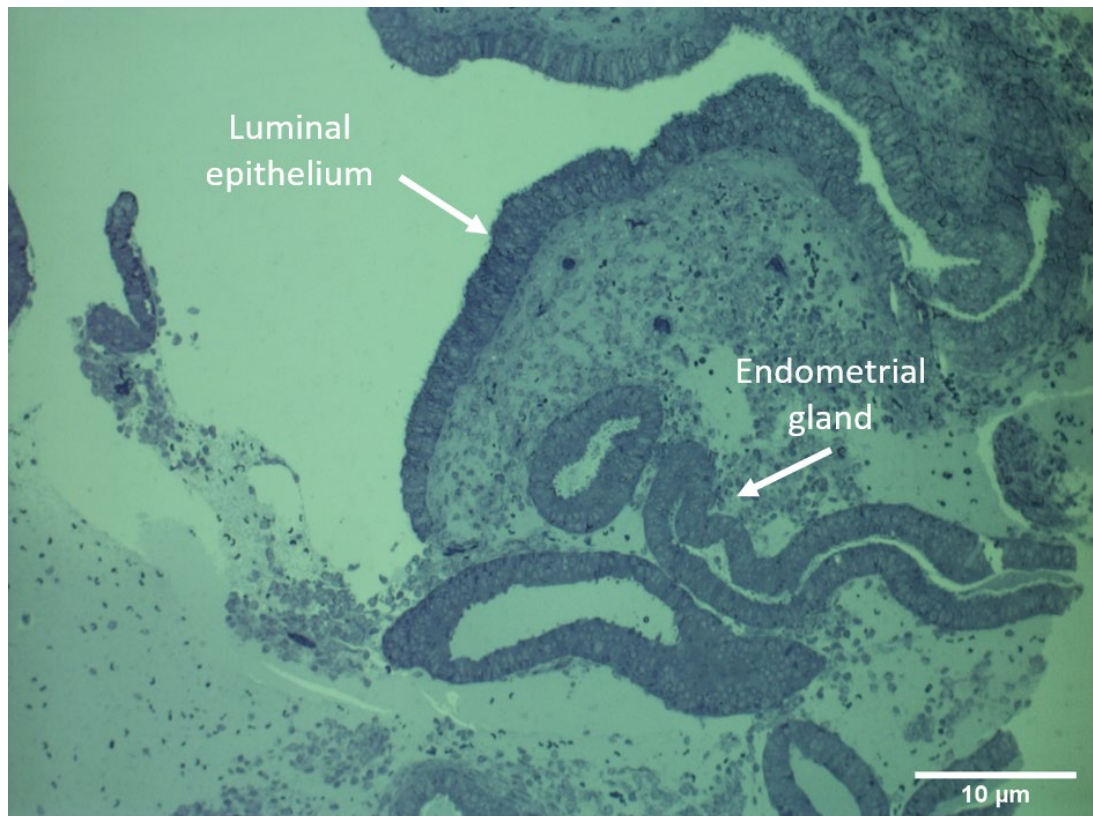
Figure 2.10 *Representative image of a 0.5 µm thick endometrial tissue section. Tissue stained with 1% toluidine in ddH$_2$0 blue tissue stain.*

Ultra-thin section preparation

Thin endometrial tissue sections of 90 nm were cut on the Ultracut E microtome and placed onto copper grids, ensuring a silver section with no wrinkles. The copper grids were stained with lead citrate to enable contrast during imaging. Inside a petri dish, a lead citrate droplet was placed onto the wax strip alongside 1 M sodium hydroxide NaOH pellets. A TEM grid was placed face down onto the lead citrate for a 5 min incubation. Grids were washed in distilled water and then dried on filter paper.

Table 2.6 *Reagents for TEM.*

- Toluidine blue (Agar Scientific, UK)
- Acetonitrile (Fisher Scientific, UK)
- Cacodylate buffer: made by the Biomedical Imaging Unit
- Chloroform (Fisher Scientific, UK)
- Ethanol (Fisher Scientific, UK)
- Lead citrate (Agar Scientific, UK)
- Lead nitrate (Agar Scientific, UK)
- Main electron microscopy fixative, made by the Biomedical Imaging Unit
- Sodium hydroxide pellets (Fisher Scientific, UK)
- Post electron microscopy fixative, made by the Biomedical Imaging Unit
- Spurr resin, made by the Biomedical Imaging Unit
- Uranyl acetate (Agar Scientific, UK)

2.6.4   TEM

Ultra-thin sections cut at 90 nm were imaged on the TEM FEI Tecnai T12 or the TEM Hitachi HT7700. All images stored on the Biomedical Imaging Unit file store.

2.7   Serial block face scanning electron microscopy

2.7.1   Principles of serial block face scanning electron microscopy

Serial block face scanning electron microscopy (SBFSEM) is a technique that generates a consecutive stack of electron microscopy images. A piece of endometrial tissue is processed with heavy metals and embedded in a resin block. The tissue region of interest is identified on the uppermost facing surface of the block, and the block is cut down to 1 mm x 1 mm x 3 mm deep. The tissue block is then inserted into the microscope, with the region of interest facing upwards. A beam of electrons scans the sample, where backscatter electrons are picked up by a detector and an image generated. An inbuilt ultramicrotome then cuts sections of tissue from the face of the block at a programmed depth, for example 50 nm. The process is then repeated to create a serial stack of images (Figure 2.11).
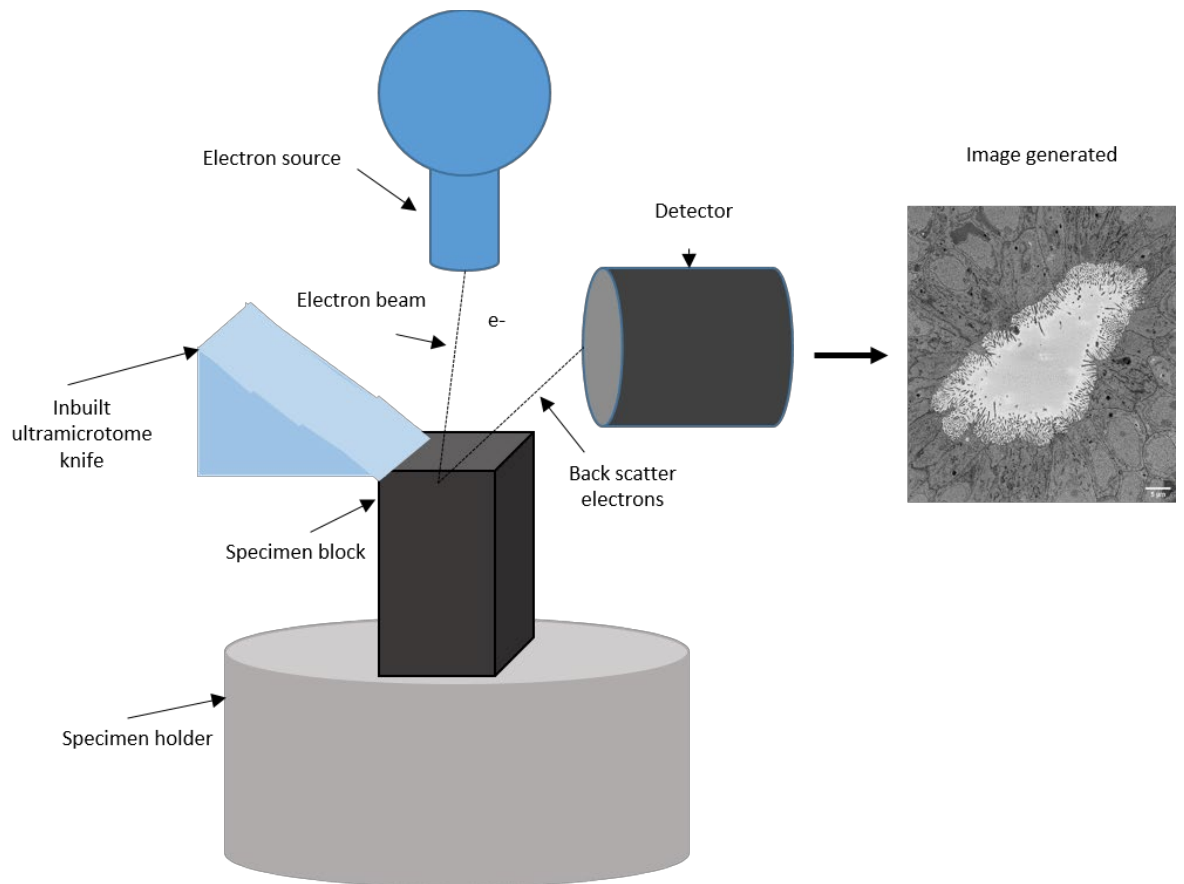
Figure 2.11 *Principles of serial block face scanning electron microscopy. A beam of electrons (e-) scan the surface of the resin block, backscatter electrons picked up by a detector and an image is generated.*

2.7.2   Tissue processing for SBFSEM

Endometrial tissue pieces were processed for SBFSEM (Palaiologou et al., 2017, Figure 2.12). All incubation steps were carried out at room temperature and in a rotator, unless stated otherwise. Reagents are listed in Table 2.7.
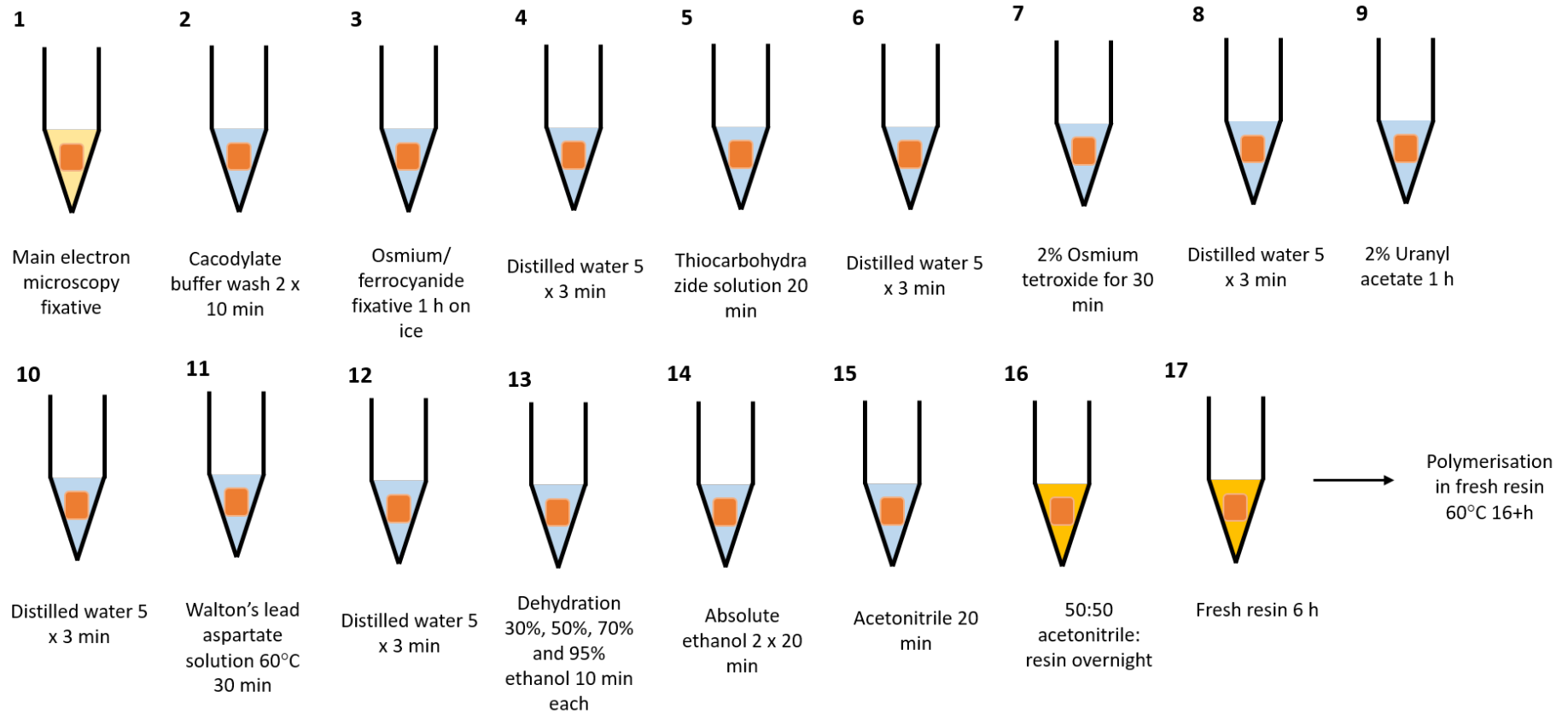
Figure 2.12 *Endometrial tissue processing for serial block face scanning electron microscopy. Endometrial samples (orange) were glutaraldehyde fixed, stained with heavy metals and polymerised in a resin block.*

Endometrial tissue pieces of 2-3 mm^3 were collected into the main electron microscopy fixative and stored at 4°C until tissue processing, as described in section 2.2.2. At the time of tissue processing the endometrial pieces were treated with 2 x 10 min cacodylate buffer rinses. The endometrial tissue pieces were then incubated with solutions in order: Osmium/ ferrocyanide fixative (1.5% potassium ferrocyanide plus 2% osmium tetroxide in 0.15 M cacodylate buffer plus 2 mM calcium chloride pH 7.4) for 1 h on ice, Thiocarbohydrazide solution for 20 min, 2% Osmium tetroxide for 30 min, 2% Uranyl acetate for 1 h and Walton's lead aspartate solution at 60°C for 30 min. Between each incubation and after the Walton's lead aspartate solution all endometrial pieces were treated with 5 x 3 min washes in distilled water.

A dehydration process was then undertaken. The endometrial pieces were incubated in 30%, 50%, 70% and 95% ethanol for 10 min, followed by absolute ethanol x2 for 20 min and acetonitrile for 20 min. Finally, 50:50 acetonitrile: resin incubation overnight. The samples were incubated in fresh resin for 6 h the following morning, before being polymerised in a final resin change at 60°C for 16+ h.

2.7.3   Tissue quality check for SBFSEM

3-view blocks were investigated for tissue quality. In short, thick endometrial tissue sections (0.5 µm) were checked with a 1% toluidine blue in ddH$_2$0 tissue staining on a light microscope and ultra-thin endometrial tissue sections were prepared on copper grids for the TEM, as described in section 2.6.3. From this investigation, the tissue regions of interest were identified.

2.7.4   SBFSEM pin preparation

A 1 mm^3 tissue block was cut from the resin block to incorporate the tissue region of interest and mounted onto a 3-view pin with adhesive conductive epoxy to create a conductive surface. The block mounted to the 3-view pin was spluttered with a goal/palladium coating, preventing a negative charge build up and encouraging the backscatter electrons to dissipate away from the block face.

Table 2.7 *Reagents for SBFSEM.*

- 0.22 µm millipore filter (Fisher Scientific, UK)

- 3-view pin (EM Resolutions)

- Adhesive conductive epoxy (Farnell, UK)

- Aspartic acid (Agar Scientific, UK)

- Ethanol (Fisher Scientific, UK)

- Osmium tetroxide (Oxkem, UK)

- Potassium hydroxide (Fisher Scientific, UK)

- Spurr resin, made by Biomedical Imaging Unit

- Thiocarbohydrazide (Fisher Scientific, UK)

- Uranyl acetate (Agar Scientific, UK)

2.7.5 SBFSEM microscopy

Pins were imaged by Gatan 3View inside a FEI Quanta 250 FEGSEM microscope at 3.0kV accelerating voltage and a vacuum of 40 Pa. A stack of consecutive images were generated at a constant voxel size of 0.01 x 0.01 0.05 µm. Raw data sets consisted of consecutive ".dm3" images.

2.7.6 3D image analysis and reconstruction

Raw data ".dm3" images were converted to .tiff files in Fiji Image J. Image analysis workflows were developed in Avizo (version 9.5.0), all work carried out on IRIDIS 5 High Performance Computing Facility.

2.8 Endometrial gland isolation

2.8.1 Principles of endometrial gland isolation

Endometrial gland isolation technique uses enzyme digestion to break apart endometrial tissue to release endometrial glands. Once endometrial tissue has been digested to separate endometrial glands, a 50 µm cell sieve is used to separate the

endometrial glands from other endometrial cell types. Endometrial glands were then taken forward for other applications including high speed video, RNA extraction and digestion into a glandular single cell suspension (Figure 2.13).

2.8.2   Endometrial gland isolation protocol

Fresh endometrial tissue pieces of 0.5 - 1.0 cm^3 were collected into 50:50 DMEM and Ham's F12 nutrient media, 5% streptomycin without serum as described in section 2.2.2. The gland isolation protocol began within 30 min of tissue collection, reagents are listed in Table 2.8. Endometrial tissue was cut into pieces (1 – 2 mm^3) for digestion in 0.7 mg/ml type 1A collagenase in complete media without serum at 37°C for 15 min. The tissue was then agitated by shaking for 20 s. The 15 min incubation was then repeated, followed by a second agitation. The digested solution was then pipetted through 8 ml of 10% fetal bovine serum DMEM and Ham's F12 nutrient media, 5% streptomycin to separate the red blood cells in the top 2 ml and the remaining tissue debris in the bottom 2 ml. The remaining solution was put through a 50 μm cell sieve. The endometrial glands should remain on the sieve, where they were backwashed off the sieve with sterile PBS. Both the solution that passed through the sieve, referred to as 'remaining endometrial cells' and the backwashed glands were centrifuged at 300 rpm for 5 min to pellet the cells. The pellets were re-suspended in 2 ml complete culture media with serum.

***Table 2.8** Reagents for endometrial gland isolation.*

- 12 well plates (Corning, USA)
- 50 µm cell sieve
- Dulbecco's modified Eagle's medium (Lonza, Cambridge, UK)
- Fetal bovine serum, Lonza, Cambridge, UK)
- Ham's F12 nutrient mixture (Lonza, Cambridge, UK)
- QIAol Lysis Reagent (Qiagen, UK)
- Sterile PBS (Lonza, Cambridge, UK)
- Penicillin streptomycin (Lonza, Cambridge, UK)
- Type 1A collagenase (Sigma, Dorset, UK)
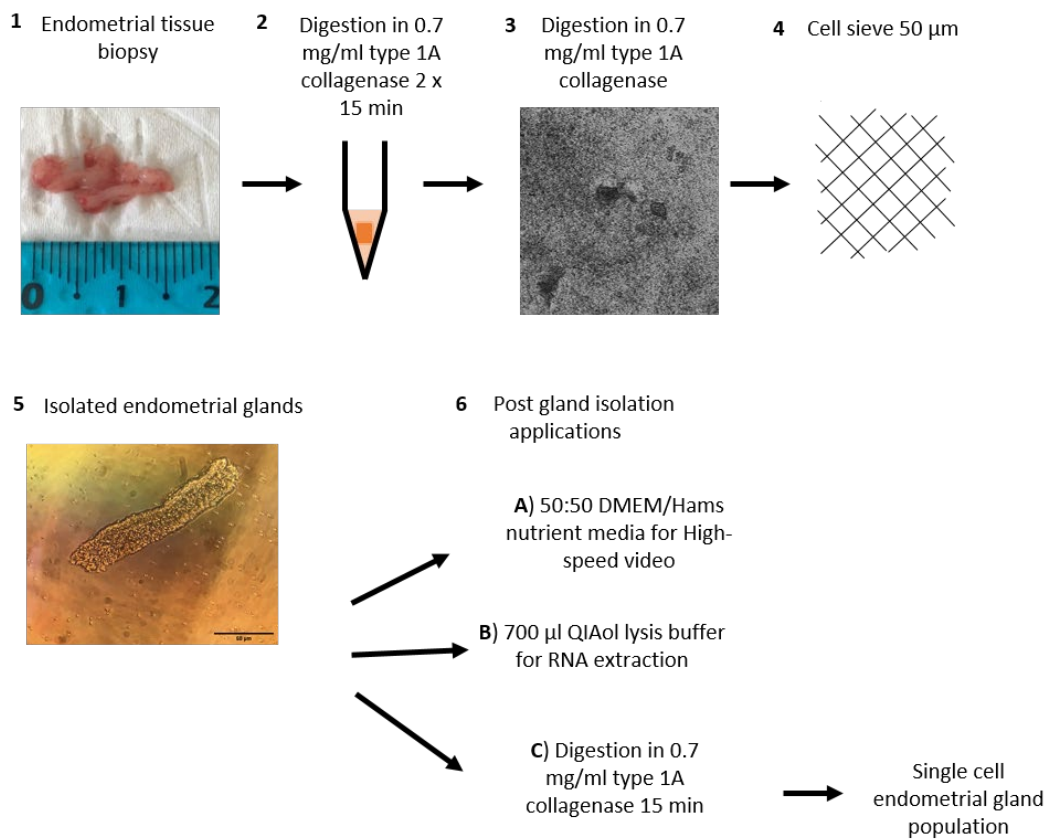
***Figure 2.13** Isolation of endometrial glands from a fresh endometrial tissue biopsy. **1)** A fresh endometrial biopsy was **2)** enzymatically digested with gentle agitation and **4)** passed through a 50 µm cell sieve. **5)** Isolated endometrial glands where used for different applications including **A)** high-speed video, **B)** RNA extraction and **C)** digestion to glandular single cell population.*

2.8.3   Experiments performed on isolated endometrial glands

Preparing isolated endometrial glands for high-speed video

1.5 ml of isolated endometrial gland suspension in 50:50 DMEM and Ham's F12 nutrient media, 5% streptomycin with serum were plated into a corning 12-well plate (22.1 mm well diameter) and incubated at 37°C until imaging with high-speed video. High-speed video took place within 1 h of completed endometrial gland isolation.

Preparing isolated endometrial glands for RNA extraction

Isolated endometrial glands were re-suspended in 700 μl QIAol lysis reagent. Samples stood at room temperature for 5 min before being frozen on dry ice. Samples stored at -80°C until RNA extraction.

Preparing isolated endometrial glands for flow cytometry

Isolated endometrial glands underwent another digestion step to break the isolated glands up into a single cell suspension, followed by paraformaldehyde fixation. Isolated endometrial glands were re-suspended in 0.7 mg/ml type 1A collagenase in 50:50 DMEM and Ham's F12 nutrient media, 5% streptomycin without serum, and incubated at 37°C for 15 min. Samples were agitated by shaking for 20 sec. Following this, the cell suspension was centrifuged at 300 rpm for 5 min and re-suspended in 2 ml 4% PFA for fixation overnight at 4°C. The following morning, the cells were centrifuged at 300 rpm for 5 min and re-suspended into 2 ml sterile PBS, and stored at 4°C until flow cytometry.

2.8.4   High-speed video of isolated endometrial glands

Isolated endometrial glands in 50:50 DMEM and Ham's F12 nutrient media, 5% streptomycin with serum were imaged by high-speed video microscopy, no longer than 3.5 h after tissue collection. 100 μl of gland suspension was mounted into a cover well chamber gasket (diameter 20 mm, depth 0.5 mm), that was then attached to a glass slide. The chamber gasket allows endometrial glands to be suspended in complete media, by the separation of the coverslip and the glass slide. The glass slide was inserted onto the

microscope (Olympus 1 X 71) on an anti-vibration table, encased in a custom-built environmental chamber at 37°C. Cilia acclimatized for 30 min before imaging commenced.

Steps followed those used to clinically assess cilia in the airway disorder (PCD, by the training and guidance of PCD microscopists (Southampton PCD team Professor Lucas). Approximately three isolated endometrial glands were present in the 100 µl aliquot per participant. The chamber gasket was systematically investigated from left to right and cilia beat frequency (CBF) determined, via Photron fastcam MC2 high speed video (Photron FASTCAM analysis), for all cilia visualised. CBF was calculated by counting how many frames it took for the cilia to make 10 complete forward and backward strokes, to get a parameter of beats per second (Hz).

2.9 Flow cytometry

2.9.1 Principles of flow cytometry

Flow cytometry is used to characterise cell populations by fluorescence detection. A fixed single cell suspension is prepared by labelling cell components with fluorophores. The single cell suspension is then run on the BD FACSCalibar (Becton Dickinson), which enables fluorescence-activated cell detection. This system uses a 488 nm laser to excite cells tagged with fluorophores, and detects three different emission wavelengths, spectrally split by in-built dichroic mirrors and filters. The three emission spectra include 530/30 nm, known as the Fluorescein Isothiocyanate (FITC) channel, 585/42 nm, known as the Phycoerythrin (PE) channel, and 650 nm, known as the Peridinin Chlorophyll Proetin Complex (PerCP) channel.

Single cells are run through a chamber called a flow cell, where the excitation light is focused. When a cell intercepts the laser light, scattered light is emitted which provides information on cell characteristics. A gating system of forward scatter and side scatter are used in tandem to identify cells by their size and granularity (complexity). During the use of multiple cell labels, the laser settings are prepared, so as to prevent spectral overlap between different channels. These gating parameters are acquired by the use of

compensation beads. Compensation beads are microspheres that capture species specific antibodies, and can be run on the BD FACSCalibar prior to the single cell suspension.

2.9.2   Flow cytometry cell preparation

The cell suspensions were adjusted to 1,000,000 cells per ml of PBS, and then prepared for flow cytometry. Cell concentration was calculated on the Beckman Coulter Z1 Particle Counter (Beckman Coulter) by adding 20 µl of cell suspension to 10 ml of isoton II Dilutent (Beckman Coulter). The number of cells in 500 µl of isoton solution was counted twice and added together giving the number of cells in 1 ml of isoton solution. This result was then multiplied by 500 to account for the dilution, giving the number of cells per ml of cell suspension.

200 µl single cell suspension and compensation beads (Becton Dickinson) at 1,000,000 cells / ml were incubated with antibodies conjugated with FITC, PE and PerCP for 15 min. 1 ml of washing solution (1% BSA 0.1% sodium azide in PBS) was added to the glass tube and centrifuged at 1000 rpm for 5 min. Cells were re-suspended in 500 µl PBS. Three channels of fluorescence detection: channel 1: FITC, channel 2: PE and channel 3: PerCP were acquired on the flow cytometer BD FACSCalibur (Becton Dickinson) and the software CellQuest. A blank sample was prepared and run for each experiment, without antibody labels. This allowed positive staining to be distinguished from background fluorescence.

2.9.3   Flow cytometry analysis

Events, defined as single particles detected by the BD FACSCalibar were analysed by FlowJo software (USA). FlowJo analysis consisted of setting gated thresholds, which refers to the process of selecting a subset of events to take forward for analysis. A threshold gating was set up using the blank sample to distinguish cells from background fluorescence. This gating was then applied to samples with fluorophores FITC, PE and PerCP. The output of these analyses, were the number of cells positive for the cell label.

2.10 RNA extraction and quantification

2.10.1 RNA extraction protocol

Isolated endometrial glands were previously stored in 700 μl QIAol lysis reagent, which facilitates the lysis of endometrial glands and inhibit RNases, as described in section 2.8.3. RNA extraction is the purification of total RNA from biological tissue. Dr Sybil Jongen purified RNA from isolated endometrial glands, all materials and reagents used were part of the Qiagen miRNeasy extraction kit as per manufacturer's instructions (Figure 2.14). Other reagents are listed in Table 2.9.
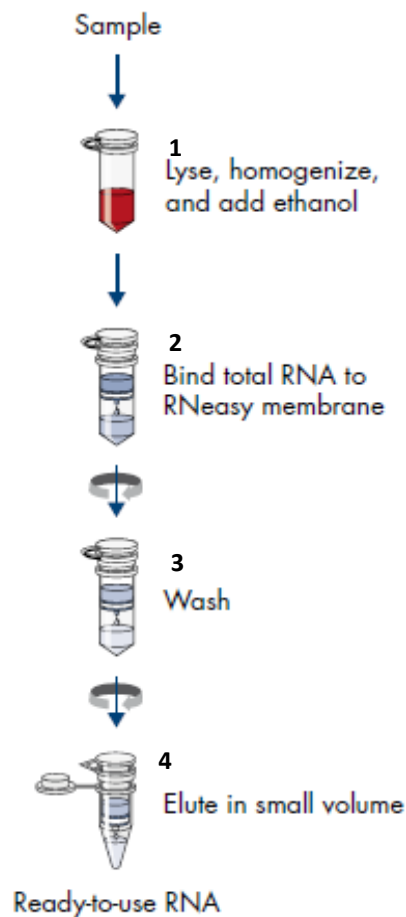
Figure 2.14 *Flow diagram summarising extraction of RNA from biological tissue, adapted from Qiagen.*

Endometrial gland samples in QIAol lysis reagent were defrosted on ice and then left to incubate at room temperature for 5 min. The lysate was then vortexed for 5 sec. 140

µl of chloroform was added to the lysate, and shaken vigorously for 15 sec. The lysate was left for another 3 min at room temperature. The addition of chloroform separates the homogenates into aqueous and organic phases. Centrifugation was initiated at 12,000 x g for 15 min at 4°C. Other centrifugations were carried out at room temperature.

350 µl of the upper aqueous phase of the centrifuged homogenate was transferred to a new collection tube, and 525 µl of 100% ethanol was added and mixed thoroughly. 700 µl of the sample was pipetted onto a RNeasy Mini spin column, and centrifuged at 8000 x g for 15 sec. The remainder of the sample was pipetted onto the RNeasy spin column, and centrifuged. The flow-through was discarded here, and after each wash step. 350 µl of buffer RWT was pipetted onto the RNeasy spin column and centrifuged at 8000 x g for 15 sec. The sample was incubated with 80 µl DNase (in RDD buffer), applied directly to the RNeasy spin column and incubated for 15 min. Following this step, a buffer RWT wash of 350 µl was applied, and centrifuged at 8000 x g for 15 sec. 500 µl buffer RPE was added to the RNeasy spin column and centrifuged at 8000 x g for 15 sec. 500 µl buffer RPE was added to the RNeasy spin column and centrifuged at 8000 x g for 2 min. Before the RNA elution step, the RNeasy spin column was centrifuged 8000 x g for 1 min to dry the membrane.

Finally to elute the RNA, the RNeasy spin column was transferred to a new 1.5 ml collection tube. 20 µl RNase-free water was added to the RNeasy spin column and centrifuged at 8000 x g for 15 sec. Eluted RNA was stored at -80°C.

2.10.2 Determination of RNA yield and quality

Dr Sybil Jongen used the nanodrop spectrophotometer and the bioanalyser to assess RNA yield and quality from isolated endometrial glands. Due to the limited isolated endometrial gland RNA available, gel electrophoresis was not carried out as an additional RNA assessment.

Determination of RNA yield and quality using a Nanodrop 1000 Spectrophotometer

A Thermos Scientific Nanodrop 1000 Spectrophotometer (Thermo Scientific, UK) was used to determine the concentration and quality of RNA samples in solution. First, the

spectrophotometer was blanked, thus ensuring background absorbance was not included in RNA concentration calculations. Blanking was carried out by loading 1 µl of ddH$_2$0 onto the pedestal and measuring the absorbance across the full range of wavelengths. For RNA concentration calculations thereafter, the blank measurements were removed by the software. 1 µl RNA samples were loaded onto the pedestal and an absorbance spectrum measured. Concentration was calculated by the software using the Beer-Lambert equation detailed below:

A= E * b * c

(A is absorbance represented in absorbance units, E is the wavelength dependent molar coefficient, b is the path length in cm and c is concentration in moles/litre)

The molar absorptivity coefficient for RNA A$_{260}$ of 1.0 = 40 µg/ml of pure RNA. The Nanodrop assesses the purity of RNA by the ratio of 260/280 nm absorbance and 260/230 nm absorbance. For 260/280 nm absorbance, a value of approximately 1.8 indicates pure RNA, while values lower than this suggests protein contamination or the contamination of other substances absorbing around 280 nm. Moreover, for 260/230 nm absorbance, a value of between 1.8 and 2.2 indicate pure RNA, while a value lower again suggests contamination.

Determination of RNA quality using a Bio-analyser

RNA samples were run on the Agilent 2100 Bioanalyser (Lapchip Caliper G2939A). The bioanalyser uses a microfluidics chip to perform a RNA quality check. The RNA sample moves through microchannels and RNA components are electrophoretically separated, where smaller components migrate faster than larger components. Fluorescent dye molecules intercalate into RNA strands, where they are detected and translated into gel-like images and electropherograms. The output of the 2100 bioanalyser is a measurement of RNA quality in the form of a RNA Integrity Number (RIN). The RIN assigns an electropherogram a value of 1 to 10, with 10 being the least degraded (Figure 2.15).
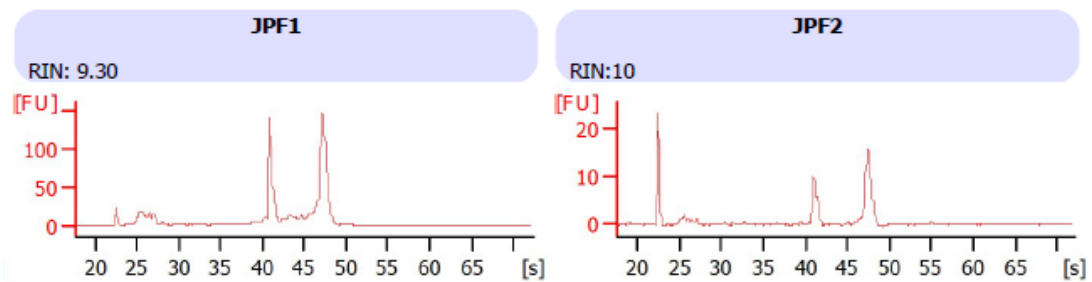
Figure 2.15 *Representative non-degraded RNA sample. RIN = RNA integrity number.*

Table 2.9 *Reagents for RNA extraction.*

- Agarose (Sigma, Dorset, UK)

- Buffer RDD (Qiagen, UK)

- Chloroform (Acros Organics)

- Deionised formamide (Sigma Aldrich, UK)

- DNase (Qiagen, UK)

- GelRed™ (Biotium, USA)

- Loading dye (Ambion, Thermo Fisher Scientific, UK).

- miRNeasy extraction kit (Qiagen, UK)

- RNA ladder (Promega, USA).

2.11 RNA sequencing

Library preparation

RNA sequencing was carried out by Dr Sybil Jongen, to compare the gene map of isolated endometrial glands from healthy women to those with recurrent pregnancy loss. In brief, library preparation was carried out (TruSeq, Illumina) to convert RNA to cDNA, add index adapters and flow cell adapters, to allow sample quantification and sequencing on the flow cell. The cDNA library was quantified by a Roche KAPA library quantification kit (Illumina). This kit uses qPCR to quantify Illumina sequence adapters only. A six point standard curve is used to convert crossing point (Cp) values of cDNA libraries to concentration. Once the concentration of the cDNA library was established, all samples were combined for the flow cell at 10 nM per sample. A final RNA quality check using a

bioanalyser (section 2.10.2) was performed, before RNA sequencing was run on an Illumina NextSeq 550 and data management was carried out using Iluminas platform Basespace.

Processing raw data to count data

The Illumina platform Basespace creates FASTq files. These FASTq files were then translated to count data per gene ensemble ID on Iridis 4, in which the data underwent quality checks by FastQC, and were aligned to the human genome via STAR 2.7.3a alignment using human genome 38.

Differential expression analysis

Gene count data were normalised, and differential expression analysis was carried out in RStudio R-3.6.2 package DESeq2 to compare participant groups. Genes were mapped to pathways using the publicly available software Toppgene (Division of Bioinformatics, Cincinnati Children's Hospital Medical Centre).

2.12 Reverse transcription

Reverse transcription is the generation of complementary DNA (cDNA) from RNA, a more stable transcript which can be amplified in quantitative polymerase chain reaction (qPCR) to measure gene expression. Reverse transcription was carried out on endometrial gland RNA samples to validate the findings of RNA sequencing. All reagents for reverse transcription were obtained from Promega (UK).

A set of seven standards (S1 – S7) were run at known RNA concentrations, alongside the RNA samples. The standards will be used during qPCR to convert the Cp value, the point at which a samples amplification curve has reached its maximum fluorescence signal detection, to cDNA concentration. The standards were pooled from whole endometrium RNA due to the limited gland RNA available, where the highest standard, S1, was prepared at a concentration of 0.2 µg/µL (1000 ng/5 µl). S2 - S7 were prepared by a double dilution.

Gland RNA samples were prepared to a final concentration of 0.25 µg in 13 µl final volume using ddH$_2$O. In addition to RNA samples, six coefficients of variation (CV) controls (C1 – C6) were prepared to a final concentration of 0.05 µg/µl and no enzyme controls

(NECs) were prepared with ddH$_2$O in the place of the reverse transcriptase enzyme. CV controls test for experimental variation, while NEC tests for the presence of DNA contamination in the RNA preparation. 13 µl (0.25 µg) RNA and 0.25 µg of C1 – C6 were added to each reaction tube. 2 µl of master mix one including random primers (C1181, Promega UK, 250 ng per reaction) was added to each reaction, preparing a final volume of 15 µl. Samples were vortexed and centrifuged for 10 sec to force the sample to the bottom of the tube, and incubated in the PCR cycler (Verti 96 well thermal cycler, Applied Biosystems) at 70°C for 5 min to allow primers to anneal and melt secondary structures which may be present in the RNA. Samples were vortexed and centrifuged once complete.

A second master mix was prepared in ddH$_2$O to include 5X Reverse Transcriptase Buffer, 0.5 mmol/L Deoxynucleotide Triphosphates (dNTPs, U1511, Promega, UK), 12.5 units Recombinant RNasin® Ribonuclease Inhibitor (N2511, Promega, UK), 100 units Moloney Murine Leukaemia Virus Reverse Transciptase (MmLV RT, M1701, Promega, UK) per sample. 10 µl of the second master mix was added to each reaction, giving a final volume of 25 µl. Samples were vortexed and centrifuged again for 10 sec to force the sample to the bottom of the tube. Samples were run on the PCR cycler, to perform reverse transcription by heating at 37°C for 60 min to allow reverse transcriptase to elongate the annealed primers and 95°C for 10 min to inactive the reverse transcriptase enzyme. Samples were then kept at 4°C continuously until samples were collected. cDNA samples were centrifuged and stored at -20°C.

2.13 Quantitative polymerase chain reaction (qPCR)

qPCR was carried out on endometrial gland cDNA, to compare the levels of messenger RNA (mRNA) between participant groups. Primer assays were designed for genes of interest in coordination with the Roche Universal Probe Library (West Sussex UK), and produced by Eurogentec (UK). Primers were designed using the Roche Universal Probe Library Assay Design Centre (http://lifescience.roche.com/en_gb/brands/universal-probe-library.html#assay-design-center). Designed assays were run on the Roche Lightcycler 480 with 2X MasterMix (Roche Lightcycler 480 Probes 2X concentration MasterMix).

Housekeeping genes, understood to remain stable in the endometrium, were run via Primer Design custom designed double-dye assays (Primer Design, UK). These assays were run on the Roche Lightcycler 480 with PrecisionPLUS qPCR Master Mix (Primer Design, UK).

For all assays, gland cDNA samples were run alongside seven standards, 6 CV controls, NECs and a no template control (NTC). No template controls tested for reagent contamination. Samples were run in triplicate to account for pipetting error.

2.13.1 qPCR Roche assay genes of interest

The cDNA samples for standards were diluted 1:10, while controls and samples were diluted 1:20. The master mix was prepared with Roche qPCR Master Mix (half final reaction volume), forward primers (200 nM), reverse primers (200 nM), probe (100 nM) and ddH$_2$O. 7 µl of master mix was added to each well according to the plate layout. Then 3 µl of each cDNA sample was added into its appropriate well, including standards S1 – S7, CV controls C1 – C6, and NECs. 3 µl ddH$_2$O was also added for NTC wells, final volume for all wells was 10 µl. Plate was sealed, vortexed and spun and then run on the Roche light cycler 480 machine, for Roche mono probe FAM dye. The run settings were as follows 95°C 10 min to activate the 'hot start' polymerase, followed by 40X cycles of 95°C 15 sec to denature cDNA and 60°C 60 sec for annealing and elongation.

2.13.2 qPCR double dye assay housekeeper genes

The cDNA samples for standards were diluted 1:10, while controls and samples were diluted 1:20. The master mix was prepared with 2x PrecisionPLUS® qPCR Master Mix, double dye primer and probe mix and ddH$_2$O (0.5 µl of primer probe mix and 5 µl 2x PrecisionPLUS® qPCR Master Mix per 10 µl reaction volume). 7 µl of master mix was added to each well according to the plate layout. Then 3 µl of each cDNA sample was added into its appropriate well, including standards S1 – S7, CV controls C1 – C6, and NECs. 3 µl ddH$_2$O was also added into the NTC wells, final volume for all wells was 10 µl. All samples prepared in triplicate. Plate was sealed, vortexed and spun and then run on the Roche light cycler 480 machine. The run settings were as follows 95°C 2 min to activate the 'hot start'

polymerase, followed by 40X cycles of 95°C 15 sec to denature cDNA and 60°C 60 sec for annealing and elongation.

2.13.3 qPCR data analysis

During the PCR reaction fluorescently labelled probes bind downstream of the primers, producing a fluorescent signal when amplified. At the 3' end of the probe, a quencher hinders the fluorescent signal. When the assays were run, an amplification curve was created per cDNA sample. Cp values were determined by the Roche Lightcycler software second derivative method, recording the number of cycles at which a samples fluorescence signal has reached its maximum acceleration on the amplification curve.

Cp values were then plotted against log cDNA of the seven point standard curve of known cDNA concentrations. cDNA concentration for all samples were calculated using the equation $x = 10^{((y-c)/m)}$, where y refers to the sample Cp value, m to the gradient of the line and c to the y intercept. CV controls were assed to check for experimental variation by the equation 'CV = (Standard deviation / mean) x 100'. cDNA concentration of all samples were then normalised to housekeeping genes, by the division of the geometric mean.

2.14 Protein analysis by Western blotting

The protein fraction of paired whole endometrium and isolated endometrial glands were extracted and analysed by Western blotting. Western blotting is a technique used to separate and detect specific proteins in a given sample by antibody application, composed of three main steps. The first step is protein separation by sodium dodecyl sulphate - polyacrylamide gel electrophoresis (SDS-PAGE) under reducing conditions, where by proteins are denatured by incubation with β-mercaptaethanol. Negatively charged proteins move towards the positive anode, separated by their mobility through the polyacrylamide gel, which is determined by molecular weight. Secondly the separated protein is blotted and dried onto a membrane, and finally proteins of interest are labelled by antibody binding and detected by chemiluminescence.

2.14.1 Protein extraction and quantification

The protein fraction was extracted from paired whole endometrial tissue pieces and isolated endometrial glands. Previously, whole endometrial tissue pieces were collected from a fresh endometrial biopsy and stored in RNA later®, described in section 2.2.2. Meanwhile, endometrial glands were previously isolated from a fresh tissue biopsy and stored in QIAol lysis buffer for RNA extraction, described in section 2.8. Reagents for protein extraction and quantification are listed in Table 2.10.

Protein extraction from whole endometrium samples in RNA later®

All steps were conducted at 4°C, to help prevent the action of proteases released during cell lysis. Whole endometrium tissue samples in RNA later® where defrosted on ice and placed into 300 µl 1x Radioimmunoprecipitation assay buffer (RIPA) buffer (0.15 M sodium chloride, 1% NP40, 0.5% sodium deoxycholate, 0.1% SDS, 0.005 M Tris base pH 8.0) with proteinase inhibitors (1:100). Samples were incubated on ice for 2 h with gentle agitation. Cells were then centrifuged at 12000 rpm for 20 min 4°C to remove insoluble material, and the lysate was stored at -20°C.

Protein extraction from isolated endometrial glands in QIAol lysis buffer

Isolated gland samples in QIAol lysis buffer were defrosted on ice and incubated at room temperature for 5 min to lyse the cells. Samples were then vortexed to encourage cell lysis. To separate the lysate into aqueous phases, 140 µl of chloroform was added, samples shaken vigorously for 15 sec, incubated at room temperature for 3 min and then centrifuged for 15 min at 12000 g at 4°C. The upper aqueous phase containing RNA was removed and frozen.

To precipitate the protein, 210 µl of 100% ethanol was added, mixed by inverting several times and incubated at room temperature for 3 min. Sample were centrifuged at 2000 g for 5 min 4°C to pellet the DNA. The phenol-ethanol supernatant was transferred to a new tube, 1050 µl of isopropanol were added and incubated at room temperature for 10 min. To pellet the proteins samples were centrifuged for 10 min at 12000 g 4°C, and the supernatant discarded.

The proteins were then washed in 50 μl protein wash solution (0.3 M guanidine HCL in 95% ethanol) and stored at -20 °C overnight. Samples were defrosted and centrifuged for 5 min at 7500 g 4°C to pellet the proteins and supernatant discarded. The protein pellet was air dried and then re-suspended in 50 μl 1x SDS to dissolve the protein pellet. Finally samples were centrifuged for 10 min 10000 g 4°C to remove insoluble material and the supernatant stored at -20°C.

Protein quantification

Protein quantification was carried out via the DC Protein Assay (Bio Rad). Lysate samples were run alongside a seven point BSA standard curve (S1 – S7) and blank samples (1x RIPA for whole endometrium lysate and 1x SDS for isolated endometrial gland lysate) to account for the detergent absorbance. The highest BSA standard (S1) was at a concentration of 1.5 mg/ml, with all samples run in triplicate.

Protein detection was determined by a characteristic blue colour change, with an absorbance of 405 – 750 nm. This blue colour is the product of proteins in the lysate reacting with copper in the alkaline copper tartate solution, which subsequently reduces the Folin reagent by the loss of oxygen atoms. The relative absorbance was recorded by a 750 Absorbance plate reader. These absorbance values were corrected by the blank sample, to account for detergent absorbance. The seven point BSA standard curve (S1 – S7) absorbance were plotted against the known BSA concentrations to construct a calibration curve, and the equation of the line was determined. Sample protein concentrations (mg/ml) were then calculated by the equation:

'Lysate concentration = average corrected absorbance/ slope of the line'

2.14.2 Sodium dodecyl sulphate – polyacrylamide gel electrophoresis (SDS-PAGE)

SDS-PAGE was carried out on all samples. 10% separating gels in ddH$_2$0 (0.375 M Tris-HCL, pH 8.8, 0.1% SDS, 10% Acrylamide/Bis, 0.05% APS, 0.05% TEMED) and 4% stacking gels in ddH$_2$0 (0.125 M Tris-HCL, pH 6.8, 0.1% SDS, 4% Acrylamide/Bis, 0.05% APS, 0.05% TEMED) were casted via Bio Rad casting apparatus, by the combination of monomers listed

in Table 2.10. The stacking gel concentrates the protein into a unified line before it enters the separating gel of a smaller pore size. Gels were left to polymerise for 45 min by the action of tetramethylethylenediamine and ammonium persulphate polymerisation agents. Gels were then attached to electrophoretic chamber (Bio Rad), and the chamber was filled with 1x running buffer (0.025 M tris-base, 0.192 M glycine, 0.1% SDS).

Protein samples and molecular weight ladder (Precision Plus Protein Duel Colour Standard) were diluted in 1x sample reducing buffer (0.063 M tris-HCL, pH 6.8, 2% SDS, 10 % glycerol, 0.25 % bromophenol blue, 5% [10]β-mercaptoethanol). Only the samples were heated for 4 – 10 min at 95°C. Samples were allowed to cool to room temperature and centrifuged briefly to collect the sample at the bottom of the tube. 15 – 30 μg of protein were loaded onto the gel per sample. Empty wells were loaded with 1x sample reducing buffer. SDS-PAGE was run at 200 V for just under 1 h, until the dye front had run off the gel.

2.14.3 Protein blotting

Protein blotting was carried out onto methanol activated PVDF membranes by semi-dry transfer (Bio Rad). An electric current is passed through a 'transfer sandwich' causing negatively charged proteins to pass from the gel onto an activated membrane.

PVDF membranes were activated by emersion in 100% methanol for 30 - 60 sec, ddH$_2$0 for 2 min and 1x transfer buffer (48 mM tris-base, 39 mM glycine, 0.037% SDS, 20% methanol) for 5 min. The gel was taken out of the SDS-PAGE chamber and immersed in 1x transfer buffer. A 'transfer sandwich' was assembled on the anode. This included six pieces of filter paper briefly immersed in 1x transfer buffer, methanol activated membrane, gel, and six additional pieces of filter paper briefly immersed in 1x transfer buffer. The cathode was placed on top of the 'transfer sandwich', and run for 1.5 h at 25 V limit and constant 75 mA. Once complete, the membrane was taken away and allowed to dry at room temperature for 15 – 20 min to fix the proteins onto the membrane.

2.14.4 Antibody staining

Membranes were blocked in 2% BSA to prevent non-specific binding, and then Western blotting primary antibody incubation was carried out overnight at 4°C with gentle agitation. All following Western blotting steps were carried out at room temperature with gentle agitation. Three 1x tris buffered saline plus tween20 (TBST, 0.001% tween20, 0.0027 M potassium chloride and 0.137 M sodium chloride, 0.05 M tris base pH 7.4) washes in-between steps. Membranes were incubated with HRP – bound anti-mouse secondary (cell signalling #7076) for 1 h, a Precision Protein™ Strep-Tactin-HRP conjugate (Bio Rad #161-0380) for 1 h and a HRP- conjugated β-actin loading control (Sigma, 1:10000, 45 kDa) for 1 h.

2.14.5 Chemiluminescence acquisition

Chemiluminescence detection was carried out using the Amersham ECL Western Blotting Detection Kit (Cytiva, #RNP2108) on the Ingenius Gel Doc visualisation system. Exposure times were recorded.

Table 2.10 Reagents for protein extraction and Western blotting

- Acrylimide-Bis (Sigma, UK)
- Ammonium persulphate (#A3426 Sigma, UK)
- Bovine serum albumin (Sigma, UK)
- Chloroform (Acros Organics)
- DC Protein Assay (Bio Rad)
- Ethanol (Fisher Scientific, UK)
- Isopropanol (Fisher Scientific, UK)
- Methanol (Fisher Scientific, UK)
- Precision Plus Protein Duel Colour Standard (Bio-Rad)
- Proteinase inhibitors (Sigma, UK)
- PVDF immobilon transfer membrane (# IPVH00010, Merck, UK)
- Sodium dodecyl sulphate (SDS, Bio Rad)
- Tetramethylethylenediamine (#161-0800 Bio Rad)
- Tris (Merck, UK)

2.15 Data storage for all study data

Participant data is stored securely, where file names are kept by study ID. All imaging files are saved on the Biomedical Imaging Unit file store, which is backed up daily. Work files carried out on IRIDIS 5 High Performance Computing Facility are also backed up daily

.

Chapter 3 Investigating the 3D spatial relationships between stromal cells and endometrial glands in recurrent pregnancy loss

3.1 Introduction

Recurrent pregnancy loss occurs in 2% of women, placing an unseen burden on families (Ford & Schust, 2009). The underlying cause of recurrent pregnancy loss is thought to be multifactorial. Chromosomal abnormalities are a known contributor of recurrent pregnancy loss, however most cases are deemed as unexplained. Consistent biomarkers and therapeutic treatments for women with recurrent pregnancy loss are not established (Odendaal et al., 2019). During the luteal phase of the menstrual cycle, endometrial stromal cells undergo a multi-step process to become decidualised (Gellersen & Brosens, 2014). The endometrial stroma consists of different cell populations including lymphocytes, and dendritic cells. Stromal cells play important roles in the endometrium, such as stromal-epithelial communication (Hantak et al., 2014; Li et al., 2011). uNK cell abundance in the endometrium of women with recurrent pregnancy loss during the window of implantation has been investigated by 2D immunohistochemistry, however, there are discrepancies between results (Seshadri & Sunkara, 2014). In this chapter, I apply quantitative 3D imaging to endometrial tissue, to study the spatial relationship between endometrial stromal cells and endometrial glands from women with recurrent pregnancy loss.

During the mid-luteal phase of the menstrual cycle and just before menstrual shedding, senescent decidualised cells, defined as cells in a permanent state of cell cycle arrest, become more abundant and secrete inflammatory mediators (Brighton et al., 2017). Successful embryo implantation and pregnancy requires a balance between the induction and clearance of senescent cells (Lucas et al., 2020). Decreased embryo implantation rate in the mouse has been associated with the knockdown of inflammatory regulators, suggesting inflammatory mediators are key in the implantation process (Salker et al., 2012). Recurrent pregnancy loss has been associated with increased cellular senescence and a lack of mesenchymal stem cell differentiation in the endometrium, characterised by low gene expression of SCARA5, high expression of DIO2 and low abundance of uNK cells (Lucas et al., 2016, 2020).

uNK cells play an important role in the balance of senescent cells in the endometrium, in clearing senescent decidualised cells by granule exocytosis (Brighton et al., 2017). Three

uNK cell subtypes have been reported in the endometrium of healthy women (Lucas et al., 2020). Recurrent pregnancy loss has also been associated with altered uNK cell activation, which could be due to different uNK subtypes characterised by different maternal uNK KIR cell receptor regions (Faridi et al., 2011; Vento-Tormo et al., 2018). uNK cell abundance has been investigated in the endometrium from women with recurrent pregnancy loss by immunohistochemistry. The results between studies however, have been inconsistent showing both an increase and a decrease in the number of uNK cells in the endometrium from women with recurrent pregnancy loss (Seshadri & Sunkara, 2014) (Table 3.1). These findings suggest uNK cells are functioning differently in the endometrium from women with recurrent pregnancy loss, yet their spatial arrangement and spatial relationship to endometrial glands remains undetermined.

uNK cell count has been considered as an additional parameter for endometrial dating (Liu et al., 2014). To incorporate uNK cell measurements into clinical practise they must be standardised to reduce variation between clinical centres (Chiokadze & Kristesashvili 2019). A standardised protocol was formulated to quantify uNK cells from tissue sections, where uNK cells were reported as the percentage of endometrial stromal cells (Lash et al., 2016). 2D methods have also been established to determine the spatial arrangement of uNK cells and macrophages however, these methods do not take into account the endometrial tissue volume (Helige et al., 2014; Russell et al., 2011).

In this chapter, I apply confocal laser scanning microscopy and 3D image analysis to stromal cells in whole pieces of undisrupted endometrium, to provide an insight into the spatial relationship of stromal cells to endometrial glands from women with recurrent pregnancy loss. These 3D methods provide a more representative analysis of uNK cells in a piece of endometrial tissue compared to 2D tissue sectioning, and have the potential to contribute towards clinical uNK cell biopsy standardisation.

3.2 Aims

To develop a wholemount confocal imaging approach to study:

1) The 3D spatial arrangement of endometrial stromal cells during the window of implantation in women with recurrent pregnancy loss versus controls.

2) The 3D spatial relationship between endometrial stromal cells and endometrial glands during the window of implantation in women with recurrent pregnancy loss versus controls.

Table 3.1 *Comparison of studies investigating uNK cells in the endometrium between controls and women with recurrent pregnancy loss during the implantation stage of the menstrual cycle.*

Reference	Recurrent pregnancy loss population	Control population	Endometrial biopsy stage	uNK quantification method	Pregnancy outcome	CD56	CD16
Clifford et al., 1999	Early pregnancy loss	Laparoscopic sterilization	LH + 7 to 9 days	Cell count	X	↑	X
Quenby et al., 1999	Idiopathic recurrent pregnancy loss	Obstetric histories	Day 19 to 22 of cycle	Cell count	Y	↑	↑
Michimata et al., 2002	Two successive spontaneous abortions	Male factor infertility	Pre-implantation period	Cell count	Y	N	N
Tuckerman et al., 2007	Unexplained recurrent pregnancy loss	Control information not disclosed	LH + 7 to 9 days	Cell count	Y	↑	X
Giuliani et al., 2014	Unexplained recurrent pregnancy loss	Controls – no history of infertility or endometriosis	LH + 7 to 9 days	Cell %	X	N	↑
Chen et al., 2017	Unexplained recurrent pregnancy loss	Ovulatory fertile controls	LH + 7 days	% positive uNK cell per total stroma	X	↑+↓	X
Kuon et al., 2017	Idiopathic recurrent pregnancy loss	Egg donors fertility patients	LH + 7 to 9 days	Cell concentration	X	↑	X
Lucas et al., 2020	Recurrent pregnancy loss 3 or more miscarriages	Women awaiting IVF	LH + 7 to 10 days	Cells per 100 stromal cells in luminal epithelial proximity	X	↓	X
Lyzikova et al., 2020	Recurrent miscarriage	Without recurrent miscarriage	LH + 7 to 9 days	Cells per mm^2	X	↑	X

LH= luteinising hormone, uNK = uterine natural killer, IVF = in-vitro fertilisation, Y = included, ↑ = increase, ↓ = decrease, N = no change, X = not included in the study

3.3 Methods

To investigate the association between the 3D spatial relationships of endometrial stromal cells to endometrial glands and recurrent pregnancy loss, endometrial pieces were processed by wholemount immunohistochemistry, imaged by confocal laser scanning microscopy and the 3D spatial parameters quantified.

3.3.1 Endometrial biopsy collection

Endometrial pipelle biopsies were collected from two participant populations across a seven-day window of the menstrual cycle (LH + 4 - 10), as described in *General methods* section 2.2 (Stocker et al., 2017). This collection window, inclusive of the window of implantation (LH + 7 - 10), was chosen for practical and logistical purposes, to facilitate the collection of samples over a wide enough time frame for the participants enrolled in the study. Two participant populations included egg donor controls (n =10) and those with recurrent pregnancy loss (n = 11). Control participants were healthy fertile women who elected to donate eggs at the local fertility centre in Southampton having met the criteria for egg donation. Recurrent pregnancy loss participants had a history of three or more miscarriages and were recruited at the local gynaecology referral centre in Southampton.

Briefly, endometrial pipelle biopsies were collected from participants during their routine procedures and immediately fixed into 4% paraformaldehyde. Following 2 h fixation, endometrial samples were stored in 1% sodium azide PBS at 4°C until tissue processing for wholemount immunohistochemistry.

3.3.2 Wholemount immunohistochemistry

Wholemount immunohistochemistry protocol optimisation

Wholemount immunohistochemistry experimental parameters were optimised for endometrial stromal cell markers (Table 3.2), including uNK cell marker mouse anti-human CD56 [123c3] (Bio Rad #MCA2693GA), uNK progenitor cells marker mouse anti-human CD34 [QBEND/10] (Bio Rad #MCA547GT), macrophage marker mouse anti-human CD163+

[EDHu-1] FITC conjugate (Bio Rad #MCA1853T) and stromal cell markers rabbit anti-human anti-vimentin [EPR3776] (Abcam #Ab92547) and rabbit anti-human anti-vimentin [SP20] (Abcam #Ab16700). A strong antibody signal in whole pieces of endometrial tissue allowed for endometrial stromal cell markers to be used in post-imaging 3D analysis.

All optimisation experiments were carried out using a wholemount approach, apart from establishing the working dilutions of uNK antibodies CD56 [123c3] and CD34 [QBEND/10] which were performed on 10 µm cryo-sections as described in *General methods* section 2.3. With respect to antigen retrieval pre-treatments, for antibodies CD56 [123c3] and CD34 [QBEND/10] the manufacturer recommended heat treatment with citrate buffer and pronase enzyme treatment. Three heating temperatures were compared (i) room temperature (overnight), (ii) 95°C (25 min) and (iii) 50°C (25 min). Treatment (iv) was the pronase treatment. Tissue permeabilisation 0.5% and 1.0% Titron™ X-100 were also compared.

Table 3.2 *Summary table of endometrial stromal cell markers optimised for wholemount immunohistochemistry.*

Primary Antibody	Primary working dilution	Secondary antibody	Secondary dilution	Endometrial tissue target	Tissue permeabilisation	Antigen retrieval
CD56 [123c3] (Bio Rad #MCA2693GA)	1:50	Donkey anti-mouse IgG 550 (Thermo fisher)	1:200	uNK cells	0.5 % Titron™ X-100 1.5 h	Positive result for pronase treatment
CD34 [QBEND/10] (Bio Rad #MCA547GT)	1:50	Donkey anti-mouse IgG (Thermo fisher)	1:200	uNK progenitor cells	N/A	Negative result
CD163+ *[EDHu-1]* FITC conjugate (Bio Rad #MCA1853T)	1:300	N/A	N/A	Macrophages	0.5 % Titron™ X-100 1.5 h	N/A
Anti-vimentin [EPR3776] (Abcam #Ab92547)	1:200	Donkey anti-rabbit 594 IgG (Thermo scientific	1:200	Stromal cells	N/A	N/A
Anti-vimentin [SP20] (Abcam #Ab16700)	1:500	Goat anti-rabbit CF™633 conjugate (Sigma-Aldrich)	1:200	Stromal cells	0.5 % Titron™ X-100 1.5 h	N/A

N/A = not necessary, uNK cells = uterine natural killer cells

Wholemount immunohistochemistry protocol

The person processing was blinded to the endometrial sample groups prior to tissue processing to avoid sample bias. Subsequent endometrial sample un-blinding was carried out once 3D analysis had been completed.

At the time of tissue processing a wholemount immunohistochemistry protocol was carried out on endometrial samples from egg donor controls (n = 10) and women with recurrent pregnancy loss (n = 11), as described in *General methods* section 2.4. In short, endometrial samples were permeabilised in 0.5% Titron X-100 in PBS for 1.5 h, washed in 1 x PBS and then blocked with 2% BSA for 1 h.

Primary antibody incubations were carried out in 75 µl droplets overnight at 4°C, in two sessions to keep the two antibodies raised in a mouse separate. Master-mix solutions were made up for all primary and secondary antibody incubations. The first primary antibody incubation included the uNK cell marker mouse anti-human CD56 [123c3] (1: 50) and the stromal cell marker rabbit anti-human vimentin [SP20] (1:500), followed by 3 x PBS washes. The second primary antibody incubation included only the macrophage marker mouse anti-human CD163+ FITC conjugate (1:300). Following 3 x PBS washes, the secondary antibody incubation was carried out at room temperature for 2 h in 50 µl per endometrial sample. Secondary antibodies were donkey anti-mouse IgG 550 (1:200; Thermo fisher #SA5-10167), goat anti-rabbit CF^{TM}633 conjugate (1:200; Sigma-Aldrich #SAB4600140) and DAPI nuclear stain (1:250; Sigma-Aldrich #D9542). The macrophage primary antibody was FITC conjugated. Finally, samples were cleared using TDE and stored at 4°C until imaging.

3.3.3 Confocal imaging of endometrial gland portions

Endometrial tissue volumes were imaged sequentially by the SP8 confocal laser-scanning microscope as described in *General methods* section 2.5. Three replicate standard tissue volumes were imaged per participant (245.52 µm x 245.52 µm x 83.12 µm). Within the endometrial tissue volume, imaging sites were selected based on the presence of endometrial glands so that stromal-gland spatial relationships could be analysed.

The first gland portion was selected by exciting only the DAPI channel. Endometrial gland portions were identified by their tube-like and columnar cell structure. An endometrial tissue volume was then sequentially imaged in the z axis to encompass the gland portion identified (0.24 µm x 0.24 µm x 1.81 µm voxel resolution, x 63 objective, Figure 3.1). Subsequent gland portions two and three were chosen using a random method involving tossing a coin, where a head or a tail dictated if the field of view was moved in the X or Y direction to the next endometrial gland respectively. If the coin flip dictated I went back to a previously imaged gland this was ignored to prevent resampling. A stack of greyscale images were collected per tissue volume for each endometrial stromal cell marker, including DAPI nuclei stain, uNK cells, macrophages and stromal cells.
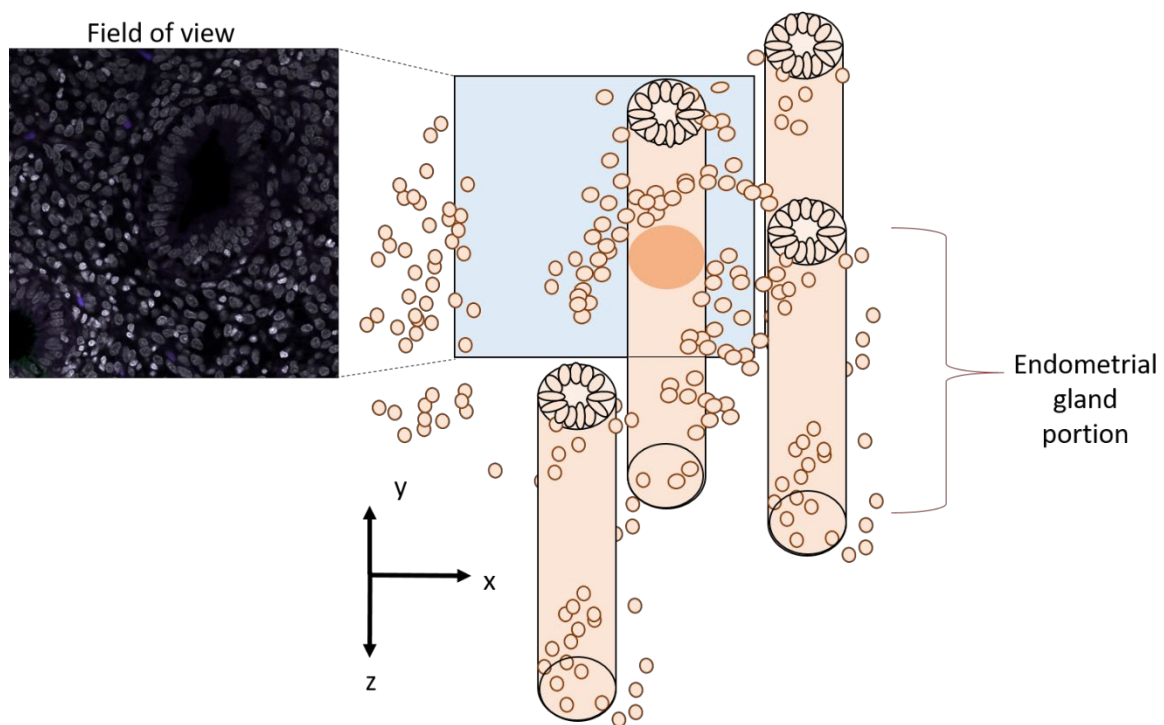
Figure 3.1 *Diagrammatic illustration of how endometrial gland portions were imaged on the confocal laser scanning microscope. An endometrial gland was identified by their tube-like columnar cell structure.*

3.3.4   3D spatial quantitative analysis

To investigate the association between the 3D spatial relationship of endometrial stromal cells to glands and recurrent pregnancy loss, 3D parameters were applied to image

stacks using the software Avizo (version 9.5.0) and Fiji Image J. All tissue volumes were imaged using the same conditions, however if the laser was not able to penetrate the tissue effectively and tissue staining became unclear, the deeper tissue volumes were cropped. To ensure image data were processed in the same way, Fiji macros were written to batch process binary stacks of images for 3D spatial parameters. These included the cell density per tissue volume, the distances between cells in a tissue volume, cell clustering and formatting binary image stacks for 3D distance mapping. Final 3D distance map analysis was carried out in Avizo (version 9.5.0). All image processing was carried out on the IRIDIS 5 High Performance Computing Facility.

3D analysis workflows required imaging datasets to be in a binary image format, where the voxels representing a stromal cell nuclei had a value of 1 while the remaining voxels had a value of 0. It was not possible to automatically threshold the greyscale data for the stromal cell markers due to tissue autofluorescence, therefore greyscale image data were converted into binary images by manually labelling cell nuclei positive for the stromal cell marker in Avizo (version 9.5, Figure 3.2). Nuclei staining was thresholded and converted into a binary image, and overlaid with the greyscale image of separate stromal marker staining. Stromal cell nuclei associated with positive staining for the stromal cell marker were labelled for all z slices that the cell nuclei was observed.

The staining produced for the stromal cell macrophage marker CD163 was unclear therefore, only uNK and stromal cell markers were taken forward for 3D spatial analysis.
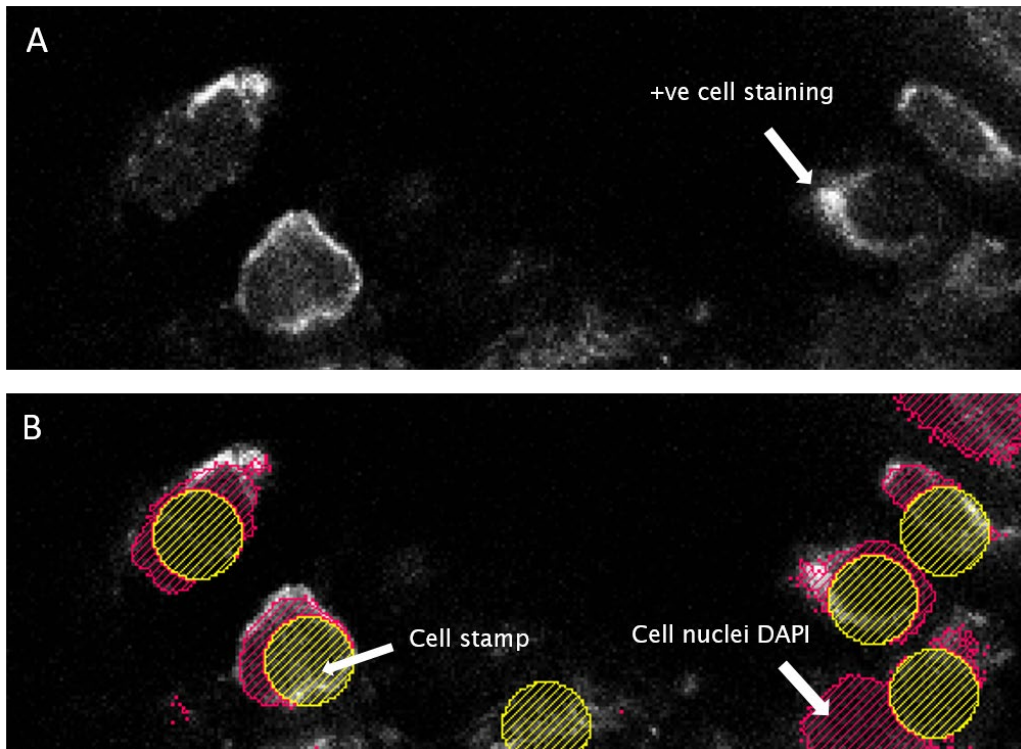
Figure 3.2 Representative images of manual cell nuclei labelling. A) Positive cell staining (white) for stromal cell marker, B) positive cell staining (white) was overlaid with DAPI nuclei staining (pink). Where a cell nuclei was associated with positive cell staining the nuclei was labelled (yellow) through all z slices the nuclei was observed.

Cell density and average distance between stromal cells

Cell density, calculated as the number of cells per tissue volume mm^3, and the distances between cells were calculated for uNK cells and stromal cells, using Fiji Image J 3D region of interest manager. The Fiji 3D region of interest manager takes nuclei stamps across multiple z-slices as one nuclei, allowing 3D nuclei to be identified and analysed. All endometrial samples were batch processed via the macro detailed in Appendix A 'Macro batch processing cell count and cell-cell distances'.

Clustering of stromal cells

Cell clustering was analysed for uNK cells and stromal cells using the Fiji Image J plugin 'Spatial distribution index' (SDI) (Andrey et al., 2010). Cell clustering data were generated via the SDI 'G function', by comparing the observed endometrial population to

a randomly generated population. All endometrial samples were batch processed in Fiji Image J via the macro 'macro batch processing cell clustering' detailed in Appendix A.

A manually created test population demonstrates the Spatial Distribution Index (Figure 3.3). During SDI analysis, each nuclei population distribution, called the observed distribution, generates their own randomly distributed population for comparison. The test population is an example of a clustered observed population (Figure 3.3A) accompanied by a cumulative frequency curve (red line) that sits to the left of a randomly generated population curve (black line, Figure 3.3B). For the randomly generated population (Figure 3.3C), generated from the observed population, the randomly distributed population curve (black line) and the observed populations curve (red line) are similar (Figure 3.3D). In comparison, a regularly spaced population would sit to the right-hand side of the randomly distributed population curve. A SDI value between 0 and 1 are also assigned to the observed distribution. A regularly spaced population has a SDI value of 1, and a clustered population had an SDI value of 0. A randomly spaced distribution has a SDI value close to 0.5.

3D distance maps of endometrial stromal cells to endometrial glands

To generate 3D distance maps, centroid points were generated in Fiji Image J and distance maps were generated in Avizo (version 9.5.0). Reducing cell nuclei stamps down to one voxel, centroid points, was necessary to create one 3D distance measurement per endometrial stromal cell nuclei. Cell nuclei stamps were batch converted in Fiji Image J into centroid image stacks by the macro 'macro batch processing 3D distance mapping' detailed in Appendix A.

The second phase of the analysis was carried out in Avizo (version 9.5.0), where 3D distance maps of uNK cells and stromal cell nuclei centroid points were generated against manually segmented endometrial gland portions. A 3D distance map was generated away from the endometrial gland, taking the endometrial gland as 0 μm. The 3D distance map than assigned the uNK cells and stromal cells a distance between them and the endometrial gland portions present in the imaged endometrial volume (Figure 3.4). The raw data output was cell count at a given distance from the endometrial gland portions. Data were presented as the distance between the endometrial gland portions and the closest uNK cell

or stromal cell. The distance between the endometrial gland portions and where 50% of uNK cells or stromal cells were located and the distance between the endometrial gland portions and the furthest uNK cell or stromal cell.
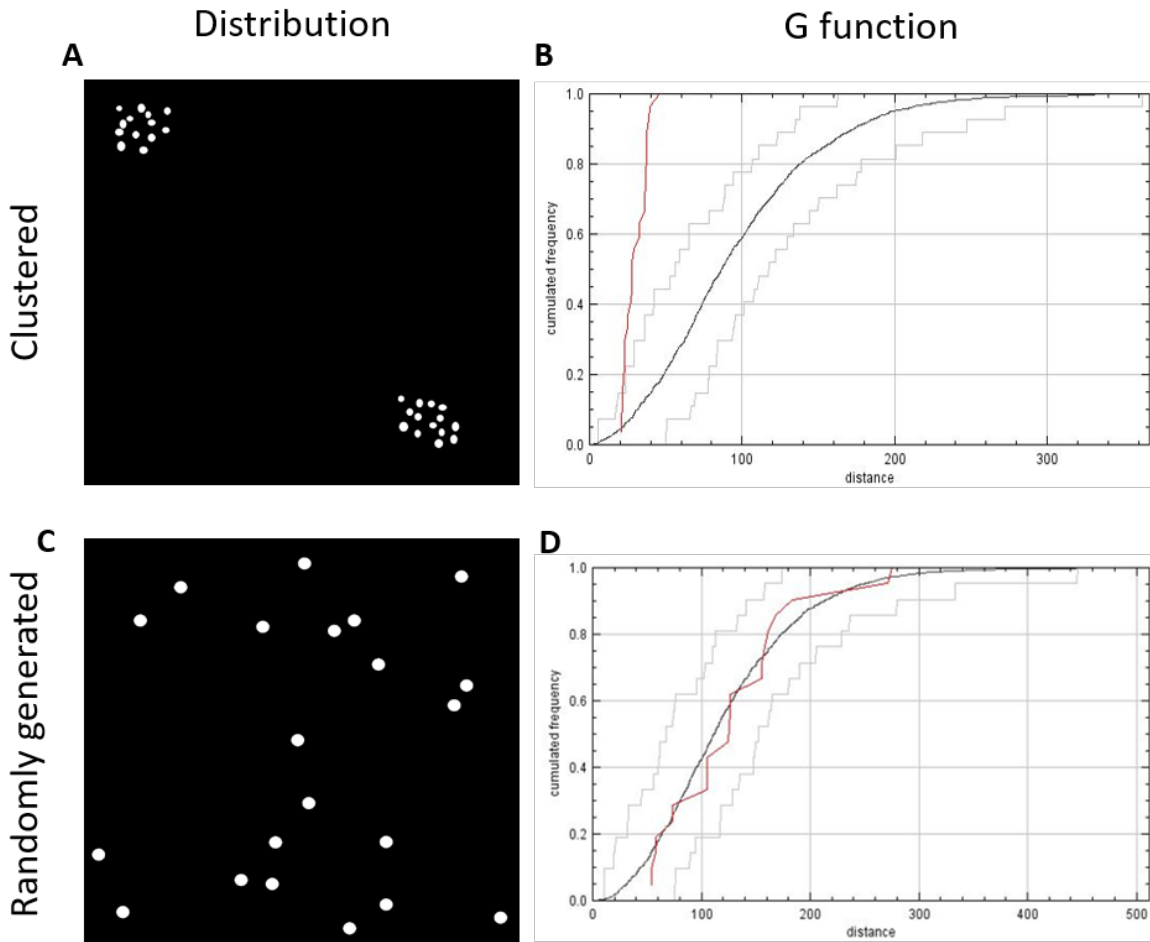
Figure 3.3 *A test clustered population analysed by the Spatial Distribution Index. **A)** a test observed clustered population created manually, **B)** cumulative frequency curves of the distance between cells comparing the observed population (red line) to the randomly generated population (black line) surrounded by 95% confidence limits (grey lines), the observed population curve (red) sits to the left of the randomly distributed curve **C)** a randomly generated population, and **D)** a cumulative frequency curve of the randomly generated population, A randomly distributed population curve sits within the 95% confidence limits.*
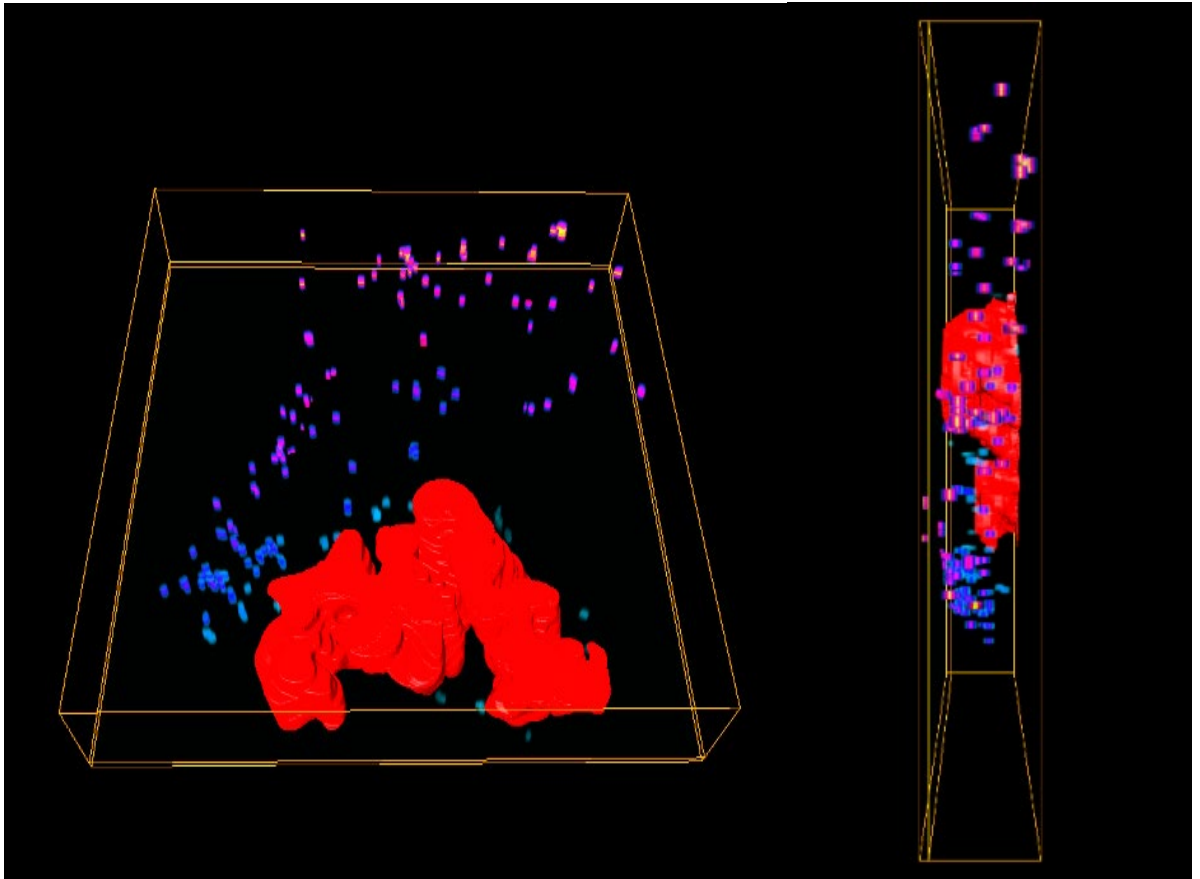
Figure 3.4 *Representative 3D distance map of endometrial stromal cells from endometrial gland (red). Blue is closest to the endometrial gland and yellow furthest away. Endometrial stromal cell centroid voxels have been dilated in order to visualise the cells.*

3.3.5   Data analysis

Data analysis and management was carried out in Prism 8 (GraphPad Software Inc., California, USA) and Microsoft excel 2016. Prior to carrying out this investigation, sample power calculations were calculated using data from previous 2D imaging experiments. Sample power calculations indicated that n = 10 per participant group would provide 80% power to detect a change in uNK cell number in the endometrium from women with recurrent pregnancy loss versus controls.

All data were tested for a normal distribution by the Shapiro-Wilk normality test before further statistical analysis was carried out. Data that were not normally distributed were presented as median and statistically compared using a Mann Whitney U test. Data

that were normally distributed were presented as the mean and statistically compared using a Welch's corrected t –test, which does not assume that two populations have the same standard deviation. An unequal variance test was chosen based on control and recurrent pregnancy loss populations demonstrating different standard deviations.

To investigate the association between stromal cell 3D spatial relationships and recurrent pregnancy loss, parameters cell density, average distance between cells and cell clustering were statistically compared between participant groups. To investigate the association between endometrial stromal to endometrial glands spatial relationships and recurrent pregnancy loss, 3D distance map data was statistically compared between groups. A p value of ≤ 0.05 was considered statistically significant.

3.4 Results

Participant demographics and self-reported menstrual cycle characteristics show no significant differences between these variables were observed when statistically analysed by a t-test (Table 3.3). The number of pregnancies and the number of miscarriages however, were significantly increased in recurrent pregnancy loss participants compared to egg donor controls (p < 0.01).

Table 3.3 *Demographics, menstrual cycle characteristics and fertility history of participants.*

Characteristic	Control (n = 10) mean (SD)	Recurrent pregnancy loss (n = 11) mean (SD)
Demographic characteristics		
Age	30.1 (3.5)	33.0 (4.0)
BMI	23.6 (4.4)	25.6 (3.7)
Menstrual cycle characteristics		
Day of menstrual cycle	20.6 (1.8)	20.8 (1.8)
Length of menstrual cycle	28.6 (0.9)	27.6 (1.3)
Fertility history		
Contraceptive use in last year	none	none
Number of pregnancies	0.7 (0.5)	5.4 (1.0) *
Number of miscarriages	0.0 (0.0)	4.0 (0.7) *
Met criteria for egg donation	Yes	n/a

* p < 0.01 indicates significantly different from control group, AMH = anti-mullerian hormone, n/a = not applicable.

3.4.1 Wholemount immunohistochemistry protocol optimisation summary

Endometrial stromal cell markers were optimised for wholemount immunohistochemistry, to provide strong antibody signals in whole pieces of endometrial tissue which could be quantified in 3D image analysis (Figure 3.5).

3.4.2 Association between the stromal cell 3D spatial arrangement and recurrent pregnancy loss

Endometrial tissue biopsies were processed by wholemount immunohistochemistry, imaged by confocal fluorescence microscopy and analysed by 3D workflows, so as to investigate the association between uNK cell and stromal cell 3D spatial

arrangements and recurrent pregnancy loss. 3D spatial arrangements were quantified from stromal cell nuclei, including cell density (number of endometrial stromal cells per mm^3), the average distance between stromal cells in a given tissue volume and cell clustering defined by the spatial distribution index (Figure 3.6).

uNK cell density was significantly increased in the endometrium from women with recurrent pregnancy loss (n = 11) compared to controls (n = 10, p = 0.03, Figure 3.7A). While stromal cell density in the endometrium from women with recurrent pregnancy loss (n = 9) was higher than controls (n = 10) in absolute terms, there was no significant difference (p = 0.50, Figure 3.7B). Total uNK cell and stromal cell density was significantly increased in the endometrium from women with recurrent pregnancy loss (n = 20 measurements) compared to controls (n =20 measurements, p = 0.04, Figure 3.7C).

uNK cells in the endometrium from women with recurrent pregnancy loss (n = 10) showed a higher degree of clustering compared to controls (n = 8), however, uNK cell clustering was not significantly different between groups (p = 0.19, Figure 3.7F). Stromal cells in the endometrium from women with recurrent pregnancy loss (n = 8) were significantly more clustered than controls (n = 8, p = < 0.05, Figure 3.7G). No association was observed between 3D spatial parameters and day of the menstrual cycle (Figure 3.8).
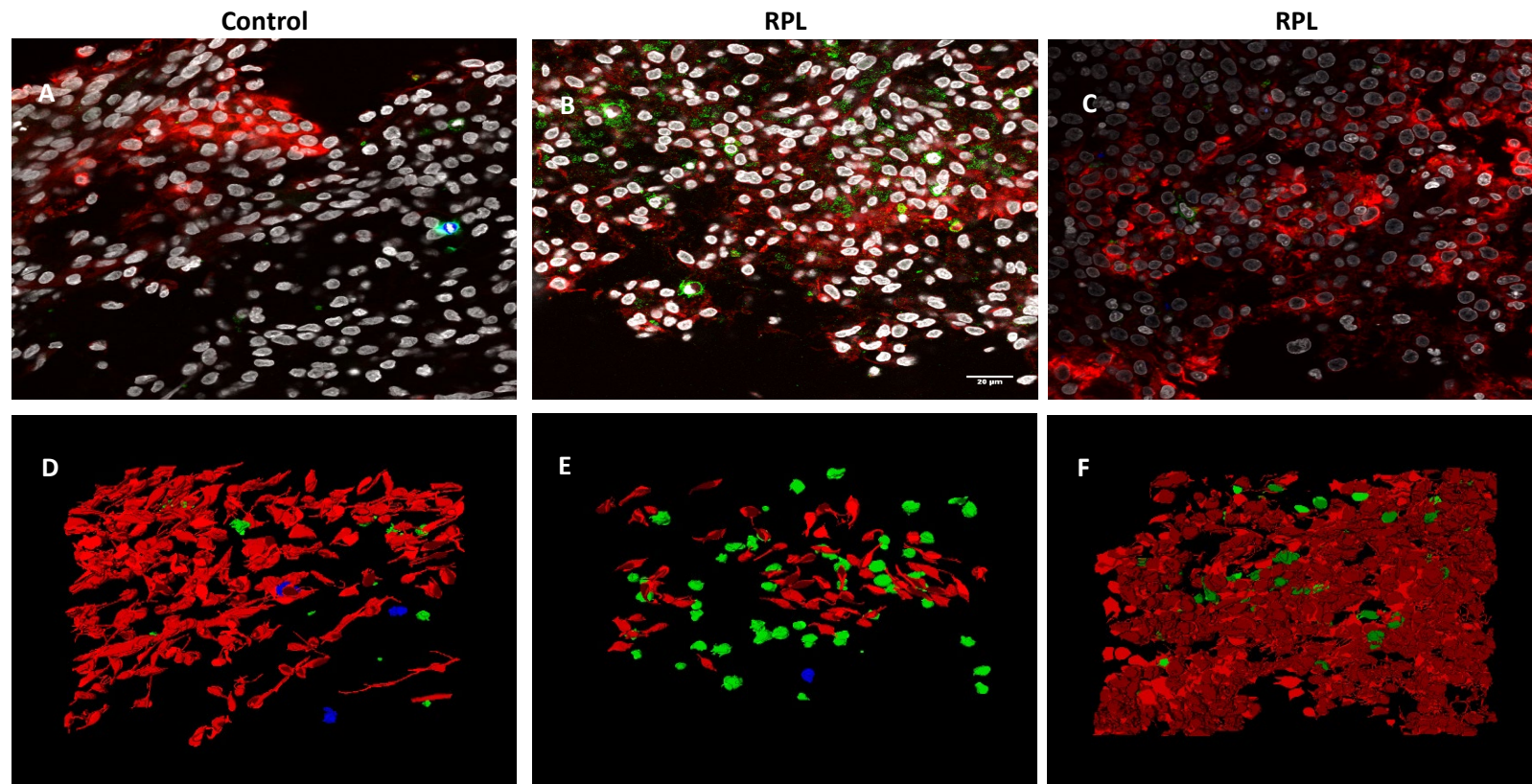
Figure 3.5 *Representative images and 3D reconstructions of endometrial stromal cell markers optimised in wholemount immunochemistry comparing endometrium from women with recurrent pregnancy loss (RPL) versus controls. Uterine natural killer cells (green, CD56 [123c3]), macrophages (blue, CD163+ [EDHu-1] FITC) and stromal cells (red, anti-vimentin [SP20]).*
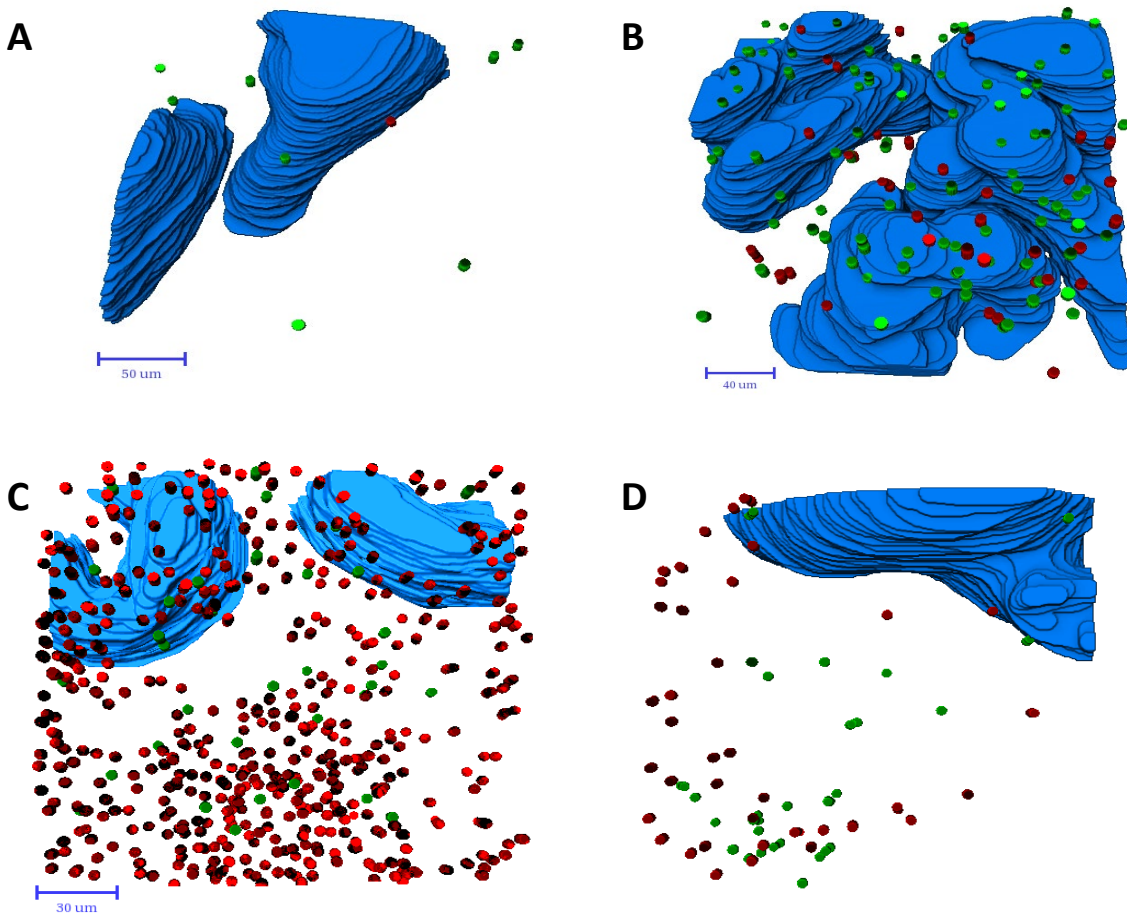
Figure 3.6 Representative 3D reconstructions showing stromal cell 3D spatial arrangements. A) Endometrial volume from control participants with a low uterine natural killer cell (green) and stromal cell (red) density versus B) an endometrial volume from women with recurrent pregnancy loss demonstrating an increased uterine natural killer cell and stromal cell density surrounding endometrial glands (blue). C) Representative 3D reconstructions of regularly spaced stromal cells and D) clustered stromal cells. Each cell is represented by its cell nuclei
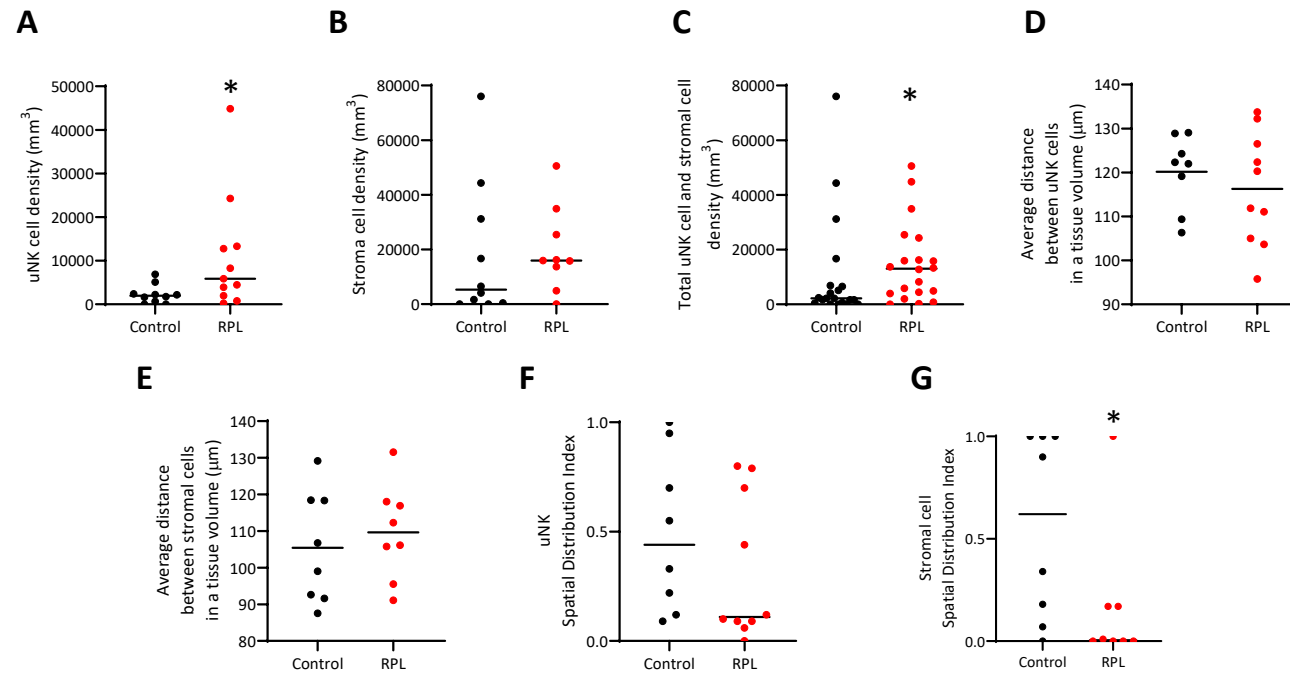
*Figure 3.7 Altered endometrial stromal cell 3D spatial arrangements in the endometrium from women with recurrent pregnancy loss versus controls. A) Endometrial stromal cell density (cells per tissue volume mm³) in uterine natural killer (uNK) cells, B) stromal cells and C) total uNK cells and stromal cells. A-C) Data presented as median and statistically analysed using a Mann Whitney U test. D) Average distance between stromal cells in a given tissue volume in uNK cells and E) stromal cells. D-E) Data presented as mean and statistically analysed by Welch's corrected t-test. F) Endometrial stromal cell clustering analysis for uNK cells and G) stromal cells. Spatial Distribution Index (SDI) range 0 (clustered) to 1 (regularly spaced). F-G) Data represented as median and statistically analysed using a Mann Whitney U test. * p ≤ 0.05 indicates RPL significantly different from control.*
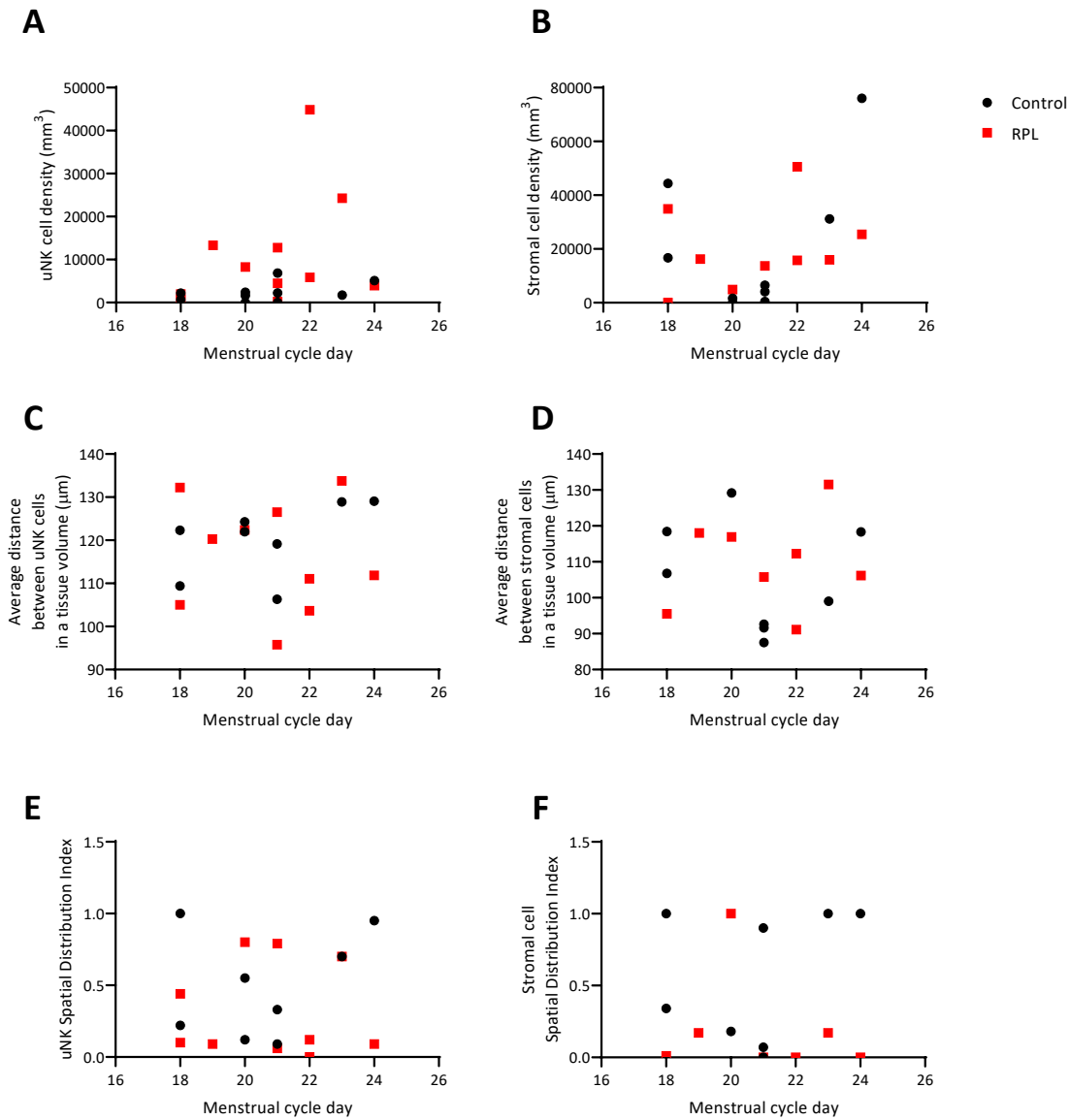
Figure 3.8 *No associations were observed between stromal 3D spatial arrangements and menstrual cycle day in endometrium from women with recurrent pregnancy loss (RPL) versus controls.* ***A)*** *Endometrial stromal cell density (cells per tissue volume mm³) in uterine natural killer (uNK) cells and* ***B)*** *stromal cells.* ***C)*** *Average distance between stromal cells in a given tissue volume in uNK cells and* ***D)*** *stromal cells.* ***E)*** *Cell clustering analysis for uNK cells and* ***F)*** *stromal cells.*

3.4.3 Association between stromal cells to glands 3D spatial relationships and recurrent pregnancy loss

To investigate the association between stromal cells to glands 3D spatial relationships and recurrent pregnancy loss, 3D distance maps were calculated between uNK cells, stromal cells and endometrial gland portions. The distance between endometrial gland portions and their closest uNK cell and stromal cell were calculated. The distance at which 50% of cells were located away from endometrial gland portions were calculated. Finally, the distance between endometrial gland portions and their furthest away uNK cell and stromal cell were calculated.

Spatial relationship of uNK cells to endometrial glands

The uNK cells furthest away from endometrial glands were significantly further away from endometrial glands in the endometrium from women with recurrent pregnancy loss (n = 10) compared to controls (n = 8, $p < 0.05$, Figure 3.9C). The distance at which 50% of uNK cells were located away from endometrial glands and the uNK cells closest to endometrial glands, however, were not significantly altered in the endometrium from women with recurrent pregnancy loss compared to controls (Figure 3.9A and B).

Spatial relationship of stromal cells to endometrial glands

The stromal cells closest to endometrial glands were significantly closer to endometrial glands in the endometrium from women with recurrent pregnancy loss (n = 8) compared to controls (n = 8, $p = 0.01$, Figure 3.9D). The distance at which 50% of stromal cells were located away from endometrial glands and the stromal cells furthest away from endometrial glands, however, were not significantly altered in the endometrium from women with recurrent pregnancy loss compared to controls (Figure 3.9E and F). No associations were observed between stromal – gland 3D spatial relationships and menstrual cycle day (Figure 3.10).

3D reconstruction of endometrial tissue volumes allows 3D spatial relationships to be represented and quantified, compared to 2D image sections (Figure 3.11).
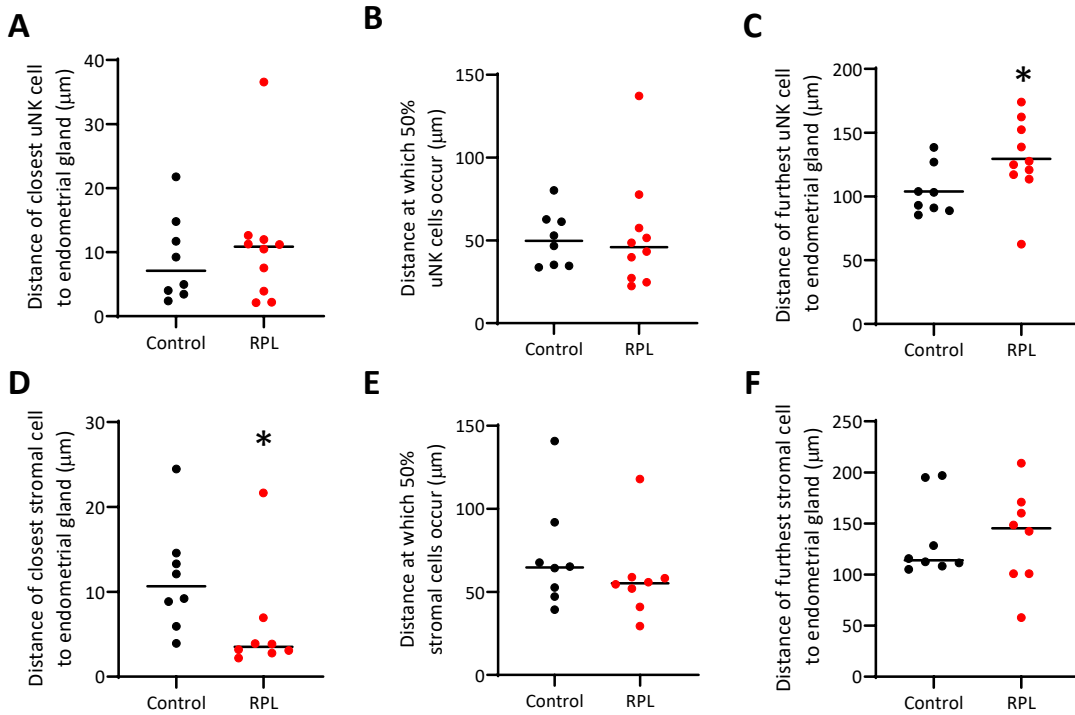
Figure 3.9 *Altered distance of uterine natural killer (uNK) cells and stromal cells to endometrial glands in the endometrium from women with recurrent pregnancy loss (RPL) versus controls. **A and D)** the closets cell to the endometrial gland portion, **B and E)** the distance at which 50% of cells are located away from the endometrial gland portion and **C and F)** the furthest cell from the endometrial gland portion. Data represented as median and statistically analysed using a Mann Whitney.* p ≤ 0.05 indicates RPL significantly different from control.*
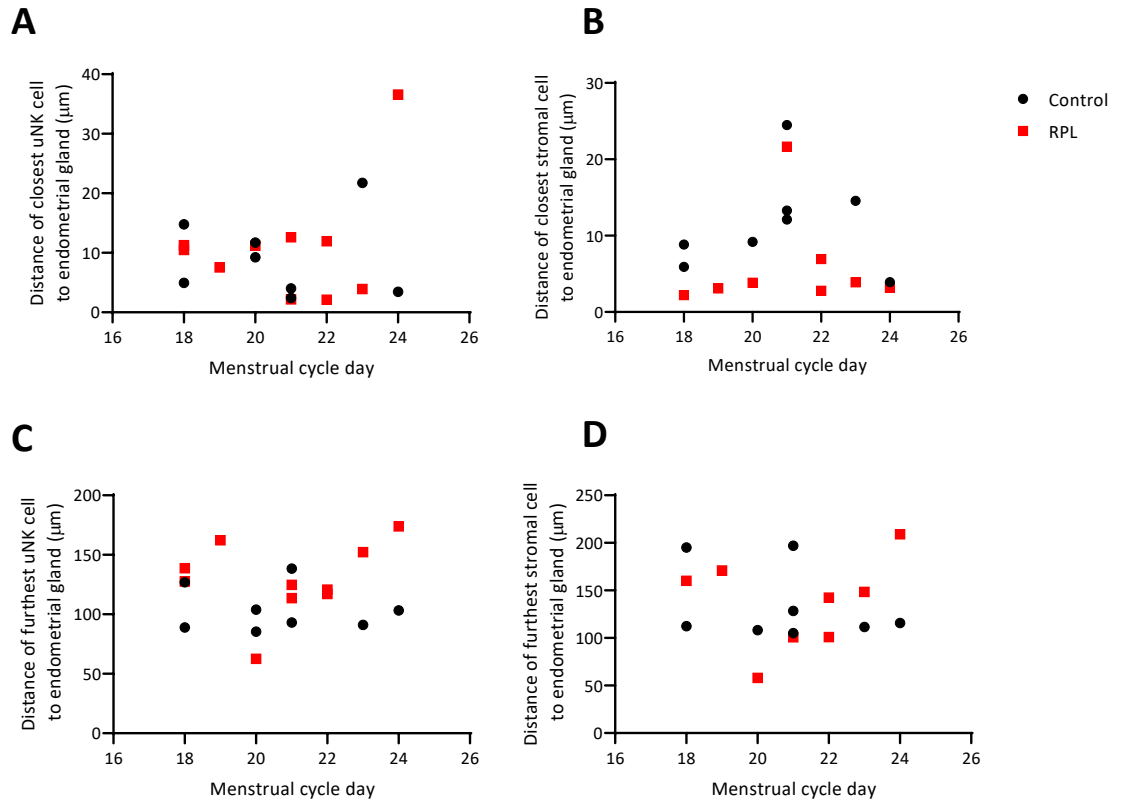
Figure 3.10 *No associations were observed between endometrial stromal – gland 3D distance maps and the day of the menstrual cycle in the endometrium from women with recurrent pregnancy loss (RPL) versus controls. **A and B)** uterine natural killer (uNK) cells and **C and D)** stromal cells.*
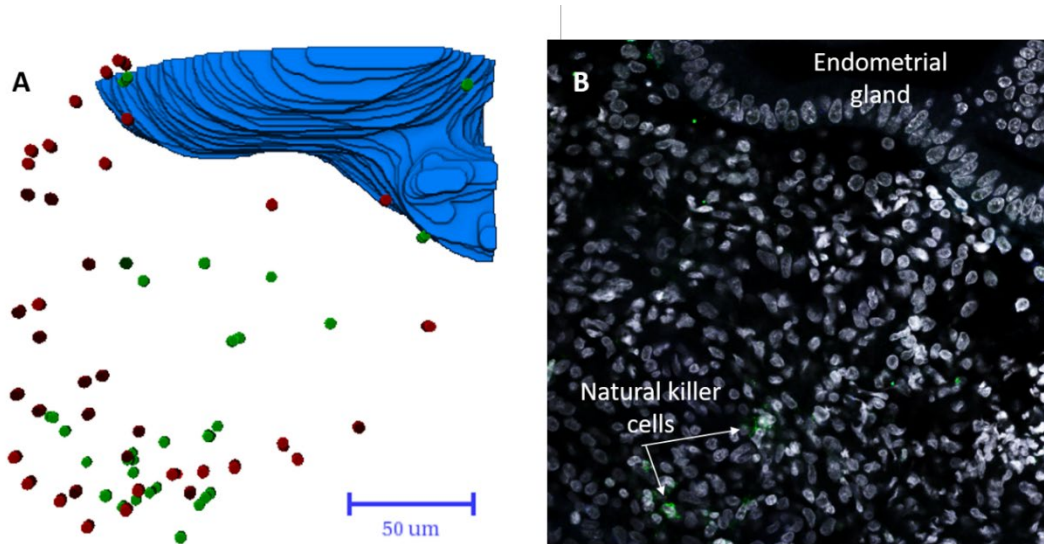
Figure 3.11 *3D endometrial reconstruction provides more volume information compared to a 2D image section.* ***A)*** *3D reconstruction demonstrates clustered uterine natural killer cells (green) and stromal cells (red).* ***B)*** *A 2D section from this stack used to generate image A shows the nuclei (white) and NK cells green. The gland epithelium can be seen at the top right.*

3.5 Discussion

This chapter described an innovative approach to investigating 3D structural changes in the endometrium of women with recurrent pregnancy loss, which may identify endometrial markers that can be used in clinical diagnostics. This study demonstrates for the first time that the 3D spatial relationships between endometrial stromal cells and glands can be quantified. Increased uNK cell density in the endometrium from women with recurrent pregnancy loss is consistent with those of previous 2D immunohistochemistry studies (Chen et al., 2017; Kuon et al., 2017; Quenby et al., 1999), however, this study has gone beyond cell density and has shown that the 3D spatial relationships of uNK cells and stromal cells are altered in recurrent pregnancy loss.

Endometrial biopsies are used in routine clinical workups for recurrent pregnancy loss patients. This 3D imaging study has demonstrated that uNK cells and stromal cells are clustered therefore endometrial cells could be missed or measured incorrectly when investigated using 2D imaging techniques. A larger number of 2D sections could account

for a 3D endometrial tissue volume, however, 3D imaging facilitates a more accurate and detailed approach to one region of the endometrium and provides spatial data.

The increase in uNK cells observed in this study could be an over compensation for increased senescent decidualised cells in the endometrium from women with recurrent pregnancy loss (Lucas et al., 2016). uNK cells could be activated to clear excess senescent decidualised cells by granule exocytosis and balance the number of senescent cells during the window of implantation (Brighton et al., 2017; Lucas et al., 2016). This may in turn affect the endometrial inflammatory response mediated by senescent cells. Changes to this inflammatory response in the endometrium from women with recurrent pregnancy loss may contribute towards an unsupportive uterine environment unable to sustain a pregnancy (Salker et al., 2012).

Excessive decidual senescence reported in the endometrium of women with recurrent pregnancy loss has been associated with a low percentage of uNK cells, which is different from the uNK cell profile determined in our study (Lucas et al., 2020). 3D uNK quantification versus 2D tissue sectioning methods may explain the difference in uNK cell outcome in the endometrium from women with recurrent pregnancy loss. 2D standardised methods also analysed uNK cells close to the luminal epithelium rather than the glandular epithelium (Lash et al., 2016). 3D quantitative imaging is more representative of an endometrial tissue volume compared to 2D tissue sectioning allowing spatial relationships to be determined. The relationship between uNK cells and senescent decidualised cells in the endometrium from women with recurrent pregnancy loss is yet to be established. To investigate this relationship, the 3D quantitative imaging methods described in this chapter could be performed on stromal cell markers associated with senescent decidualised cells such as SCARA5, DIO2 and senescence-associated β-galactosidase (SAβG) activity (Brighton et al., 2017; Lucas et al., 2020).

It has been reported that senescent decidualised cells form islets. Clustered uNK cells in the endometrium from women with recurrent pregnancy loss could be involved in clearing these grouped senescent decidualised cell regions (Brighton et al., 2017). Alternatively, clustered endometrial stromal cells may be forming due to their reduced

colony forming potential and therefore not as evenly distributed throughout the tissue (Lucas et al., 2016). Altered inflammatory signalling could also be responsible for changes to uNK spatial relationships in the endometrium of recurrent pregnancy loss, impacting upon the immune response (Salker et al., 2012) or the influence of progesterone indirectly through glucocorticoid receptors as uNK cells do not have progesterone receptors (Guo et al., 2012).

As well as demonstrating differences between clinical groups, this study found variation within clinical groups. Variation within participant groups could reflect different regions of the endometrium or differences in sampling site. A larger number of tissue volume replicates may be required per participant to make tissue sampling more representative. Alternatively, within participant group uNK cell spatial variation could be due to subtypes of uNK cell (Lucas et al., 2020). A lack of HLA-C groups and KIR activation in different uNK cell subtypes has been reported in women with recurrent pregnancy loss (Hiby et al., 2009). Sixteen KIR genes have been identified which have specific binding affinities to MHC -1 and could dictate uNK cell activation (Colucci & Gaynor, 2017).

The antibody used for this study was a general CD56 uNK cell marker and would not have identified subsets of uNK cells. To understand the uNK phenotype in the endometrium from women with recurrent pregnancy loss, single cell sequencing paired with targeted 3D image analysis could be performed to understand their gene expression profile and their location in relation to the glandular epithelium. Advanced wholemount *in situ* hybridisation technology such as the RNAscope® would allow differential gene expression to be identified and located in endometrial glands (Kann & Krauss, 2019). uNK cells exhibit fluctuation over the course of the implantation period, which could also be contributing to the variation within study groups (Russell et al., 2011). The overlap between control and recurrent pregnancy loss groups also reinforce that the underlying cause of recurrent pregnancy loss is multifactorial.

Different spatial relationships between uNK cells, stromal cells and endometrial glands may be due to a larger abundance of other cell types such as dendritic cells and lymphocyte T cells or Tregs. uNK cells further away from the endometrial gland portion may

be close to other endometrial glands outside the tissue volume, reinforcing that sampling site may have a direct influence on stromal cell analyses. Other stromal cell types such as dendritic cells and Tregs were not measured in this study due to the time constraints of 3D image processing. Other immune cells such as T cell populations have also been shown to be altered in the pre-pregnancy endometrium of women with recurrent pregnancy loss (Southcombe et al., 2017).

The clustering of endometrial glands, their size, shape and the gland to gland proximity may differ, and as such, these parameters must be taken into account for future 3D studies (Kara et al., 2007). Alternatively, uNK cell-epithelial signalling pathways could be altered if the uNK cells are further away from endometrial glands from women with recurrent pregnancy loss (Hantak et al., 2014; K et al., 2010), linked to an alteration in uNK cell cytokine secretion (Blois et al., 2017). This study has shown it is possible to quantify uNK 3D spatial relationships, future work should be carried out to determine uNK function in recurrent pregnancy loss such as uNK activation (Faridi & Agrawal, 2011).

It is not clear why endometrial stromal cells may be located closer to endometrial glands in the endometrium from women with recurrent pregnancy loss. Stromal cells secrete precursors for the extracellular matrix. Stromal cells may be closer to damaged or structurally abnormal endometrial glands in recurrent pregnancy loss to provide structural support (Kara et al., 2007). The type of collagens may be altered in the endometrium from women with recurrent pregnancy loss and therefore impacting on the spatial distribution of stromal cells. Alternatively, a change in stromal cell 3D spatial arrangements may stem from alterations in stromal cell – epithelium interactions, altering cytokine secretion, and other growth factors that influence epithelial proliferation (Chen et al., 2013; Li et al., 2011). Future work is required to answer these questions.

3D imaging is more representative compared to 2D tissue sectioning, allowing tissue volumes to be imaged and analysed. Although 2D imaging may use a bigger field of view, 3D imaging allows volume data to be acquired which 2D imaging does not. Decidualised stromal cell 3D spatial distributions may be a result of an underlying faulty mechanism,

causing an out of sync implantation window, predisposing recurrent pregnancy loss (Salker et al., 2012).

The endometrial stromal to epithelial 3D spatial relationships described in this study could be taken into account when standardising uNK clinical measurements (Lash et al., 2016). Endometrial biopsy dating is traditionally measured by glandular cellular proliferation and structure. The 3D spatial relationships of endometrial stromal cells could provide further insight into endometrial dating, especially as faster imaging techniques are developed such as artificial intelligence assisted segmentation (Lewis & Pearson-Farr, 2020).

3.6 Limitations

Access to clinical samples as well as practical and technical constraints mean that there are some limitations to what could be achieved in this study. The timing of the menstrual cycle was made on a participant's last menstrual bleed, reliant on self-reporting, and did not use ovulation sticks to time the LH surge. The window of implantation is typically considered to be LH + 7 - 10 but because of sample availability this study uses samples from LH + 4 - 10, due to the endometrial biopsies available at the time of tissue processing (June, 2019). The results are not changed if samples from only the standard implantation window are considered (LH + 7 – 10 days).

uNK results were not normalised to cycle day as in recent literature (Lucas et al., 2020) as no association was observed between 3D spatial parameters and menstrual cycle day, however future work could use a narrower window of implantation (LH + 7 - 10). No correlation between uNK cell and stromal cell spatial arrangements and the day of the menstrual cycle suggests that there may be variability in endometrial structure during the window of implantation.

Labelling stromal cell nuclei through a tissue volume was a time-consuming process. For this to be adopted clinically, accurate automated or semi-automated labelling would be required to streamline these workflows. This study used three replicates per patient sample due to imaging time and resource availability. A larger number of replicates may

have provided a better representation of the endometrial tissue volume and future experiments could be performed to determine the optimum number required. In this study there was a compromise between the area of the field of view and image detail. I choose to use the greatest detail with x63 objective, at a z depth of 83 μm. However, it may be that this is not required and future studies need to compare the results with higher resolution and greater precision or wider field of view and a more representative sample.

This 3D map analysis considers endometrial stromal cells to endometrial glands. During this analysis, however, there was no comparison of the endometrial gland sections between the endometrium from women with recurrent pregnancy loss and controls. Further investigation is needed to compare endometrial glands of control and recurrent pregnancy loss endometrium; such as endometrial gland volume or endometrial gland branching.

3.7 Future directions

Future work could study novel 3D spatial parameters of other endometrial stromal cell types including macrophages, dendritic cells, Tregs and T-cells. This will build a picture on the association between recurrent pregnancy loss and endometrial stromal 3D architecture. Using antibodies raised specifically to subpopulations of uNK cells, this will also begin to tease out if uNK subpopulations explain variation seen in the endometrium from women with recurrent pregnancy loss. The variation identified in the results between recurrent pregnancy loss and control could also be analysed by stratifying the data by the number of pregnancy losses. This could determine if there is an association between the number of pregnancy losses and endometrial stromal cell 3D spatial relationships. These methods can also be applied to study wider reproductive phenotypes such as infertility and recurrent implantation failure.

This study has shown the stromal – glands 3D spatial relationships are altered in the endometrium of women with recurrent pregnancy loss. This difference could have been due to altered endometrial gland morphology or altered endometrial gland distribution (Kara et al., 2007). Therefore endometrial gland volumes and gland distribution should be

taken into consideration in future studies. The 3D imaging techniques used in this study can be applied to lightsheet microscopy techniques, which will allow multiple gland sections to be imaged per tissue volume while keeping image resolution. This will provide a more representative investigation into stromal cell to glandular relationships and address sampling variation. Going forward, it should be kept in mind that faster and automated image segmentation such as artificial intelligence could help prepare stromal cell measurements for clinical applications (Lewis & Pearson-Farr, 2020). By taking endometrial glands into account in 3D analyses will provide insight into endometrial gland structure and function during the window of implantation which is currently very limited. Further investigations into this structure may facilitate better understanding of the uNK and gland interactions.

3.8 Conclusions

In conclusion, this study demonstrates for the first time that the 3D spatial relationships of endometrial stromal cells and glands can be quantified. This study has gone beyond cell density quantification and shown that the 3D spatial relationships of uNK cells and stromal cells are altered in the endometrium from women with recurrent pregnancy loss. This could have been otherwise under-represented or missed in 2D tissue sectioning. Developing faster and accurate automated image analysis methods could allow these methods to identify endometrial markers which can be used in the clinic or suggest possible new avenues of diagnostics

Chapter 4   Investigating the 3D architecture and function of endometrial glands during the window of implantation in healthy women, recurrent pregnancy loss and subfertility

4.1 Introduction

The window of implantation encompasses a receptive endometrium, which is defined as a physiological and molecular endometrial profile, ready to receive an implanting blastocyst. It has been suggested that there is a trade off during implantation, between a receptive endometrium and embryo quality, where an imbalance of these factors could lead to recurrent implantation failure or recurrent pregnancy loss (Macklon & Brosens, 2014). Endometrial glands are invaginations of the luminal epithelium, that secrete factors important for endometrial-trophoblast communication, consisting of secretory cells and ciliated epithelial cells (Filant & Spencer, 2013; Wang et al., 2018). Little is known about the 3D ultrastructure of endometrial glands, nor the role of ciliated cells inside endometrial glands. In this chapter, I use a multi-scale and 3D imaging approach to investigate endometrial glands during the window of implantation.

The endometrial epithelium demonstrates morphological changes during the window of implantation, characterised by increased coverage of microvilli and pinopode protrusions from the epithelial apical surface. The glandular epithelium consists of four cell types, these include microvillus rich, pinopode, vesiculated and ciliated cells (Bartosch et al., 2011). The luminal epithelial pinopode number has been suggested as an endometrial receptivity marker as it is associated with pregnancy rate and embryo implantation rate following IVF procedures (Jin et al., 2017). The number of pinopodes has been reported to decrease in recurrent implantation failure endometrium showing a menstrual cycle phase delay in glandular morphology in patients of a poor IVF outcome (Aunapuu et al., 2018; Bahar et al., 2015). No change in pinopode coverage, however was reported in recurrent pregnancy loss endometrium (Xu et al., 2012). The role of increased extracellular protrusions during the window of implantation is yet to be determined.

Maternal extracellular vesicles have been found in the uterus of fertile women (Simon et al., 2018). These microvesicles are thought to play a role in transporting miRNA cargo from the endometrium to the invading trophoblast, therefore playing a role in endometrial–trophoblast communication (Evans et al., 2019; O'Neil et al., 2020). Endometrial microvesicles have been observed in the endometrium, however, less

understood are the physiological mechanisms by which glandular microvesicles are produced.

Endometrial cilia are present on the lumen of the endometrium and within glands. Glandular ciliated cells could facilitate the movement of glandular products into the uterine cavity, however the role of glandular cilia are largely unexplored (Perry & Crombie, 1982). Ultrastructural abnormalities have been reported in the glandular epithelium from women with recurrent implantation failure, endometriosis and miscarriage (Bahar et al., 2015; Kara et al., 2007; Roshangar et al., 2013). Atypical cilia from the endometrial epithelium include ciliary axoneme defects, such as impaired microtubule arrangement in the ciliary shafts, and deletion of central tubules, associated to a disturbed steroid hormone milieu (Denholm & More, 1980; Fedele et al., 1996; More & Masterton, 1976). The health of a ciliated epithelial cell has been reported as an all of nothing concept, however, thin sectioning electron microscopy would have limited the cilia which could be analysed (Denholm & More, 1980). 3D imaging techniques such as serial block face scanning electron microscopy (SBFSEM) overcome limitations of traditional electron microscopy techniques, allowing whole cellular structures to be characterised (Lewis & Pearson-Farr, 2020).

The role of endometrial gland cilia during implantation is not understood. This study aims to use a multiscale 3D imaging approach to characterise 3D glandular cilia architecture in healthy women, providing a platform for future work on unsuccessful pregnancy phenotypes. Secondly, this chapter aims to investigate the association between recurrent pregnancy loss and glandular cilia during the window of implantation by applying a multi-modal imaging approach.

4.2 Aims

1. To develop a 3D image analysis approach to characterise the 3D architecture of endometrial gland cilia during the implantation window in healthy women.
2. To investigate endometrial gland cilia ultrastructure and function during the window of implantation in women with recurrent pregnancy loss and subfertility versus controls.

4.3 Methods

The 3D architecture of healthy endometrial gland cilia were characterised during the window of implantation by a multiscale imaging approach. Endometrial gland cilia from a cohort of egg donor control participants were imaged by SBFSEM, transmission electron microscopy (TEM) and high-speed video of freshly isolated endometrial glands. To quantify 3D ciliary parameters, novel 3D image analysis workflows were developed.

To investigate endometrial gland cilia ultrastructure and function during the window of implantation in women with recurrent pregnancy loss and subfertility versus controls, endometrial gland cilia were compared by TEM and high-speed video respectively.

4.3.1 Endometrial biopsy collection

Endometrial pipelle biopsies were collected from egg donor controls (n = 11), recurrent pregnancy loss participants (n = 7) and subfertility participants (n = 3) across the window of implantation (LH + 4 - 10), as described in *General methods* section 2.2. Briefly, endometrial biopsies were collected by Pipelle catheter (Stocker et al., 2017), rapidly split and placed in 3% glutaraldehyde in 0.1 M cacodylate buffer at pH 7.4 for SBFSEM and TEM, or into 50:50 DMEM and Ham's F12 nutrient media, 5% streptomycin without serum for endometrial gland isolation.

Control participants met criteria for egg donation under Complete Fertility Centre Southampton. Recurrent pregnancy loss participants had a history of three or more miscarriages, while subfertility participants had a history of more than one year of infertility.

4.3.2 Serial block face scanning electron microscopy (SBFSEM)

Egg donor control endometrium were processed for SBFSEM and embedded in resin blocks, as described in *General methods* section 2.7. Once embedded, individual endometrial glands, of a transverse orientation, were identified close to the luminal

epithelial surface by thick sectioning (0.5 µm, Figure 4.1). Thick tissue sectioning, however, did not confirm if the endometrial glands were connected to the luminal epithelium.

Once an endometrial gland was identified, the resin block was trimmed to a 1 mm^3 block, mounted onto a pin and splutter coated with gold/palladium. The endometrial gland was imaged by Gatan 3View inside a FEI Quanta 250 FEGSEM microscope at 3.0 kV accelerating voltage and a vacuum of 40 Pa. A stack of consecutive images were generated at a constant voxel size of 0.01 x 0.01 x 0.05 µm.

4.3.3   3D cilia reconstruction and dimension quantification

To characterise the healthy 3D architecture of endometrial gland cilia, a 3D image analysis workflow was developed in Avizo (version 9.5.0), and applied to SBFSEM stacks of healthy endometrial gland cilia, all work carried out using the IRIDIS 5 High Performance Computing Facility. This workflow aimed to isolate and quantify the 3D dimensions of individual cilia of a multi-ciliated cell. To apply 3D workflows to raw data SBFSEM stacks, grey scale images first had to be converted to binary images via segmentation. Cilia segmentation was carried out on a semi-automated platform ITK snap (version 3.6.0), via seeded segmentation. Once complete, the seeded segmentations were tidied manually to ensure that individual cilia of a multi-ciliated cell were separated. A 3D workflow including the skeletonization module, listed in Appendix A, was applied to the segmented cilia in Avizo (version 9.5.0) to characterise endometrial gland cilia 3D parameters. 3D parameters included number of cilia per ciliated cell and the length of cilia from basal body to tip. This workflow took the curvature of cilia into account, thus allowing for cilia in different phases of a stroke pattern.

4.3.4   Transmission electron microscopy (TEM)

Endometrial tissue pieces were processed for TEM, as described in *General methods* section 2.6. Tissue quality was first checked with toluidine blue stained thick sections (0.5 µm), followed by the preparation of ultra-thin sections (90 nm) for imaging on the TEM Hitachi HT7700 with the titled stage.
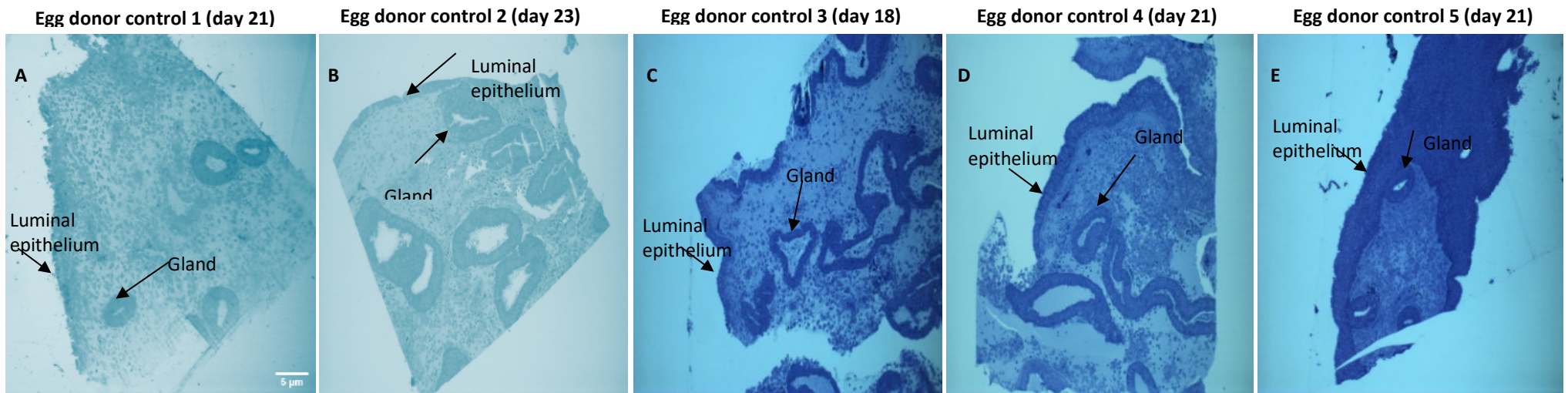
Figure 4.1 *Endometrial glands chosen for imaging were those that were close to the luminal epithelium.* ***A - E)*** *Light microscopy images of endometrial tissue sections (0.5 µm) taken from the top of each block of endometrial tissue prior to imaging on the SBFSEM.*

4.3.5 Endometrial gland isolation

Endometrial tissue pieces were processed for endometrial gland isolation by enzyme digestion, as described in *General methods* section 2.8. Briefly, whole endometrial glands were separated out from endometrial tissue pieces by digestion with 0.7 mg/ml type 1A collagenase in 50:50 DMEM and Ham's F12 nutrient media, 5% streptomycin without serum with gentle agitation. The solution was then sieved to isolate endometrial glands from the rest of the endometrial tissue. 1.5 ml isolated endometrial gland suspension in complete culture media was plated on a corning 12-well plate and kept at 37°C until imaging on high speed video within 1 h.

4.3.6 Flow cytometry

Flow cytometry was carried out to identify the cell types present in an isolated endometrial gland cell population. Prior to flow cytometry, single cell suspensions were fixed in 2 ml 4% PFA overnight at 4°C, and then re-suspended in 2 ml sterile PBS. The cells were counted using the Coulter cell counter, and adjusted to a cell concentration of 1,000,000 cells per ml of PBS. Flow cytometry was carried out on single cell suspensions by methods described in *General methods* section 2.9.

To prepare for flow cytometry, single cell suspensions were incubated with 3 leukocyte cell markers for 20 min. These included PerCP labelled CD3 (Fisher Scientific; 1:100 dilution) to mark T-cells, CD56 (Fisher Scientific; 1:20 dilution) to mark uNK cells and CD45 (Fisher Scientific; 1:20 dilution) a pan leukocyte marker. The cell suspensions were then washed 3x PBS and run on the FACSCalibur Flow cytometer.

4.3.7 High speed live imaging

Isolated endometrial glands in complete media were imaged by high-speed video microscopy as described in *General methods* section 2.8.4, no longer than 3.5 h after tissue collection. 100 µl of gland suspension was mounted into a cover well, that was then attached to a slide. The slide was inserted onto the microscope, and then the cilia were left to acclimatize for 30 min. The cilia beat frequency was then determined via an inverted

microscope Olympus 1 X 71 with Photron fastcam MC2 high speed video, at 37°C in a custom built environmental chamber. The glandular cilia beat frequency was calculated by counting how many frames it took for the cilia to make 10 full beats, to get a parameter of beats per second (Hz).

4.3.8   Data analysis

Motile glandular cilia beat function data is presented as mean and standard deviation. Data management was carried out in Microsoft excel 2016.

To investigate the association of recurrent pregnancy loss and subfertility on glandular cilia ultrastructure and function, TEM data and high-speed video data were compared. TEM descriptive data was compared between patient groups.

To compare cilia beat frequency was compared between patient groups. Data were tested for a normal distribution by the Shapiro-Wilk normality test before further statistical analysis was carried out. Data that were not normally distributed are presented as median and statistically analysed by a non-parametric Mann Whitney U test.

4.4 Results

No significant differences were observed in clinical characteristics, apart from a significantly higher number of pregnancies and miscarriages in recurrent pregnancy loss participants compared to controls (p < 0.01, Table 4.1).

Table 4.1 *Demographics, menstrual cycle characteristics and fertility history of participants.*

Characteristic	Aim 1	Aim 2		
	Controls (n = 5) mean (SD)	Controls (n = 6) mean (SD)	RPL (n = 7) mean (SD)	Subfertility (n = 3) mean (SD)
Demographic characteristics				
Age	28.6 (2.4)	29.5 (5.0)	33.3 (3.3)	33.0 (2.0)
BMI	26.6 (5.0)	25.0 (0.70)	23.8 (3.5)	22.3 (1.3)
Menstrual cycle characteristics				
Day of menstrual cycle	20.8 (1.6)	20.5 (1.5)	21.6 (1.7)	21.3 (2.4)
Length of menstrual cycle	28.4 (0.6)	28.6 (0.8)	27.5 (0.5)	Insufficient data
Fertility history				
Contraceptive use in last year (months)	none	none	none	none
Number of pregnancies	0.8 (0.4)	0.5 (0.5)	6.5 (2.9) *	1.0 (0.0)
Number of miscarriages	0.0 (0.0)	0.0 (0.0)	5.8 (3.1) *	0.0 (0.0)
Met criteria for egg donation	Yes	Yes	n/a	n/a

* = p < 0.01 indicates significantly different from control group, AMH = anti-mullerian hormone, n/a = not applicable. RPL = recurrent pregnancy loss. Aim 1: Characterising 3D endometrial gland cilia in healthy women. Aim 2: Comparing endometrial gland cilia in RPL and subfertility versus controls

4.4.1 Isolated endometrial gland optimisation

Endometrial gland isolation was achieved in the Southampton Placenta lab, using a 50 μm cell sieve to get rid of any unwanted endometrial stromal cells. Sieved glands contained less stromal cell contamination (Figure 4.2B), compared to non-sieved glands (Figure 4.2A). Long isolated glands (Figure 4.2C) are comparable to those in whole

endometrial tissue (Figure 4.2D), including distinct epithelial cell structures and a glandular lumen. Flow cytometry reinforced low stromal cell contamination, by a low presence of stromal leukocytes (Figure 4.2).
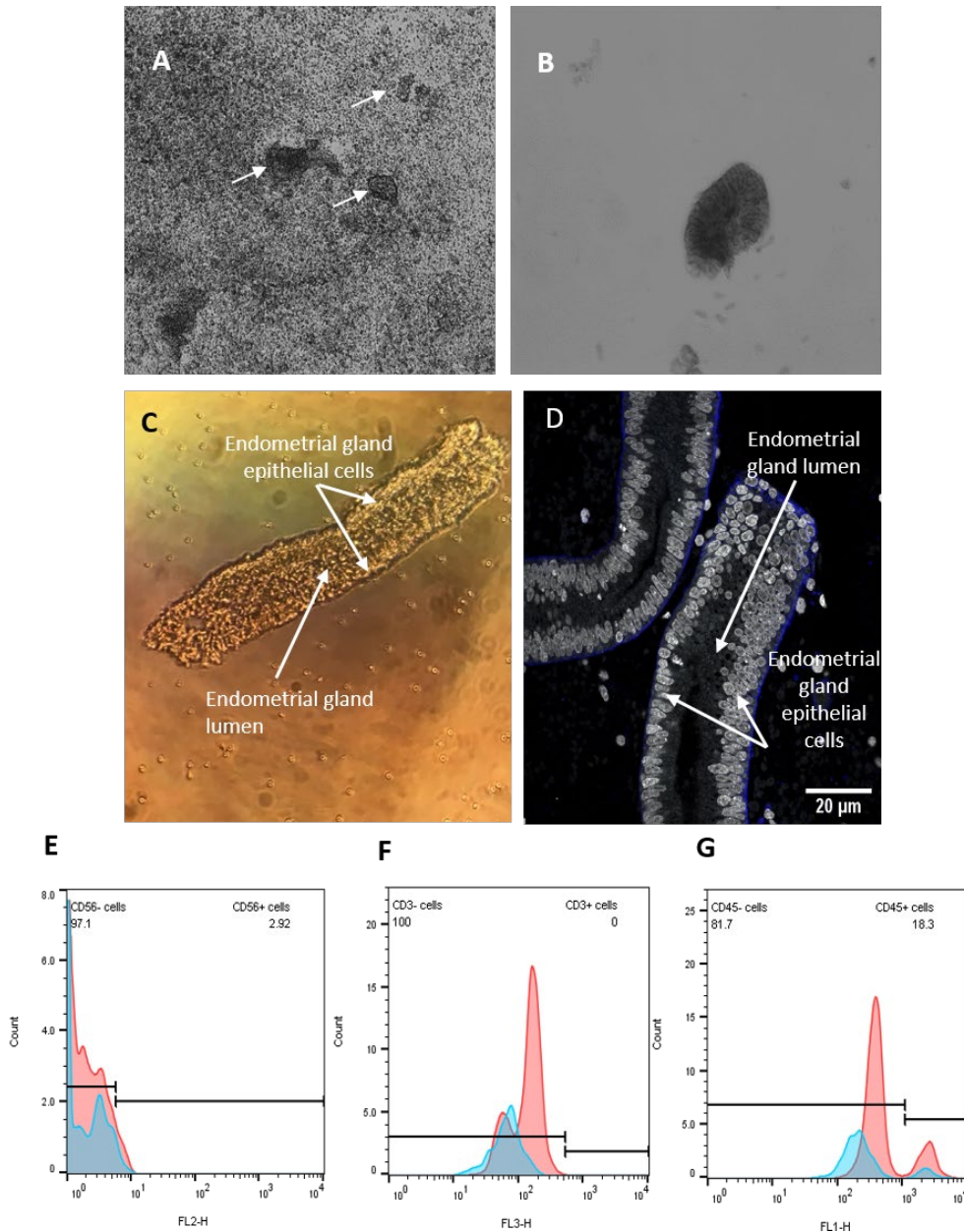
Figure 4.2 *Endometrial gland isolation achieved.* ***A)*** *Pre cell sieving endometrial glands (white arrows) stromal cells and red blood cells.* ***B and C)*** *Post cell sieving endometrial glands only.* ***D)*** *Confocal image of endometrial glands in endometrial tissue.* ***E)*** *Flow cytometry of disaggregated cells from isolated endometrial glands with a uterine natural killer cells CD56 marker,* ***F)*** *T- cells CD3 marker and* ***G)*** *pan leukocyte marker CD45.*

4.4.2   Glandular 3D architecture of healthy women during the window of implantation

SBFSEM and 3D image reconstruction have provided new insights into the receptive glandular epithelium, including the production of microvesicles by microvilli and the presence of intercellular sacs separate from the glandular lumen.

3D reconstruction of the glandular luminal epithelium, highlights the vast contribution of cellular projections, including a microvilli forest, cilia (Figure 4.3, Video 4.1: https://youtu.be/IGO8GrcQS7Y) and pinopodes (Figure 4.4). 3D measurements were made on a non-ciliated glandular luminal surface (15.0 µm length by 13.1 µm maximum diameter), giving a glandular luminal surface area of 19409.9 µm^2 and a glandular lumen volume 2403.0 µm^3.

Microvesicles forming on glandular microvilli

SBFSEM of the glandular lumen epithelium have demonstrated that glandular microvilli form microvesicles (Figure 4.4). This event was seen in all five egg donor control samples.

Intercellular sacs in the glandular epithelium

Intercellular sacs were observed within glandular epithelial cells (Figure 4.5A) in two out of five egg donor control samples. These intracellular sacs were not connected to the glandular lumen, appeared to be formed by invagination of the apical microvillus membrane. An intracellular sac of a subfertility sample (maximum diameter 4.82 µm) contained an unidentified structure which had some similarity to electron microscopy images of bacteria (Figure 4.5 B to D, Video 4.2: https://youtu.be/GmeepETM8Wk). The unidentified structure consisted of two components, an outer membrane (maximum diameter 1.94 µm, 4.49 µm^3) and an inner triplet structure (average diameter 0.96 µm, 2.39 µm^3). The unidentified structure differs from granular secretory material, which bulbs above the microvillus surface (Figure 4.6).
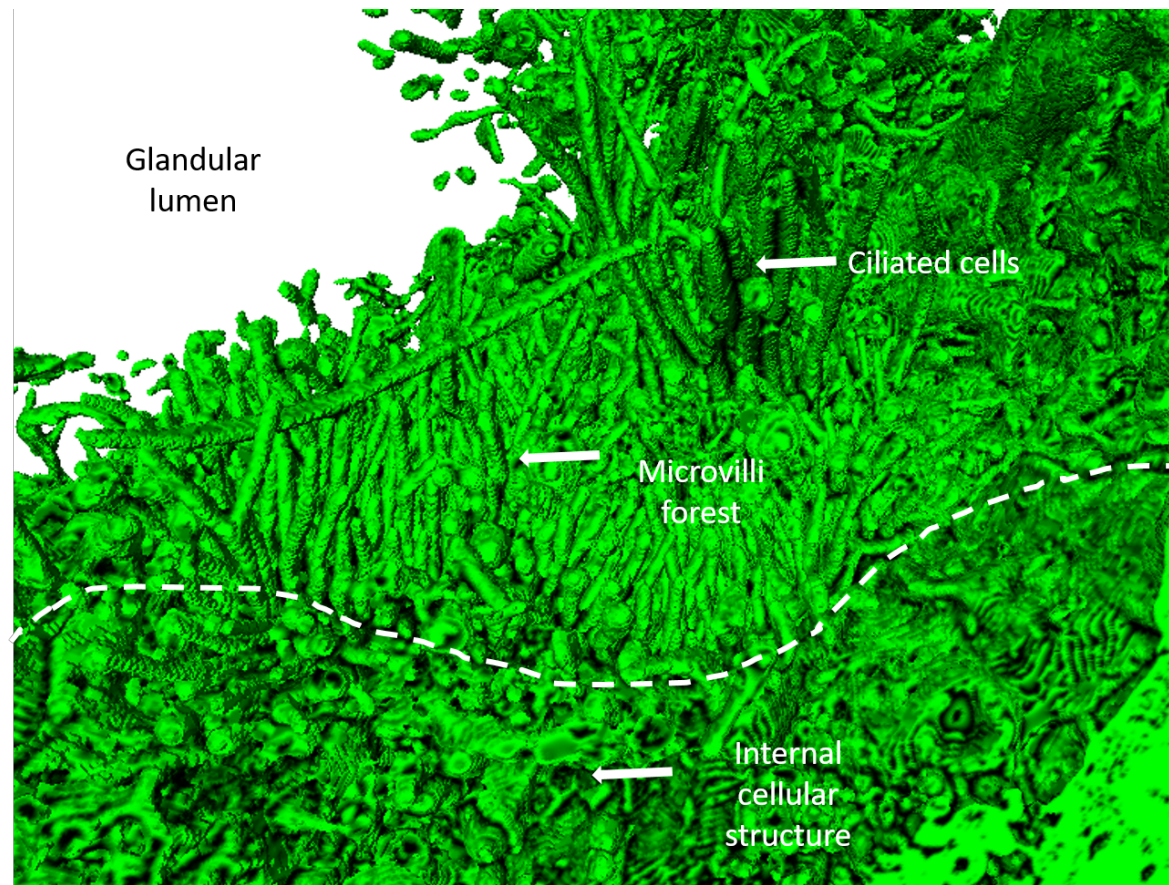
Figure 4.3 *3D reconstruction of glandular epithelium generated from SBFSEM stack of images by semi-automated image segmentation. Dense microvilli coverage, and ciliated cells protruding out into the glandular lumen.*
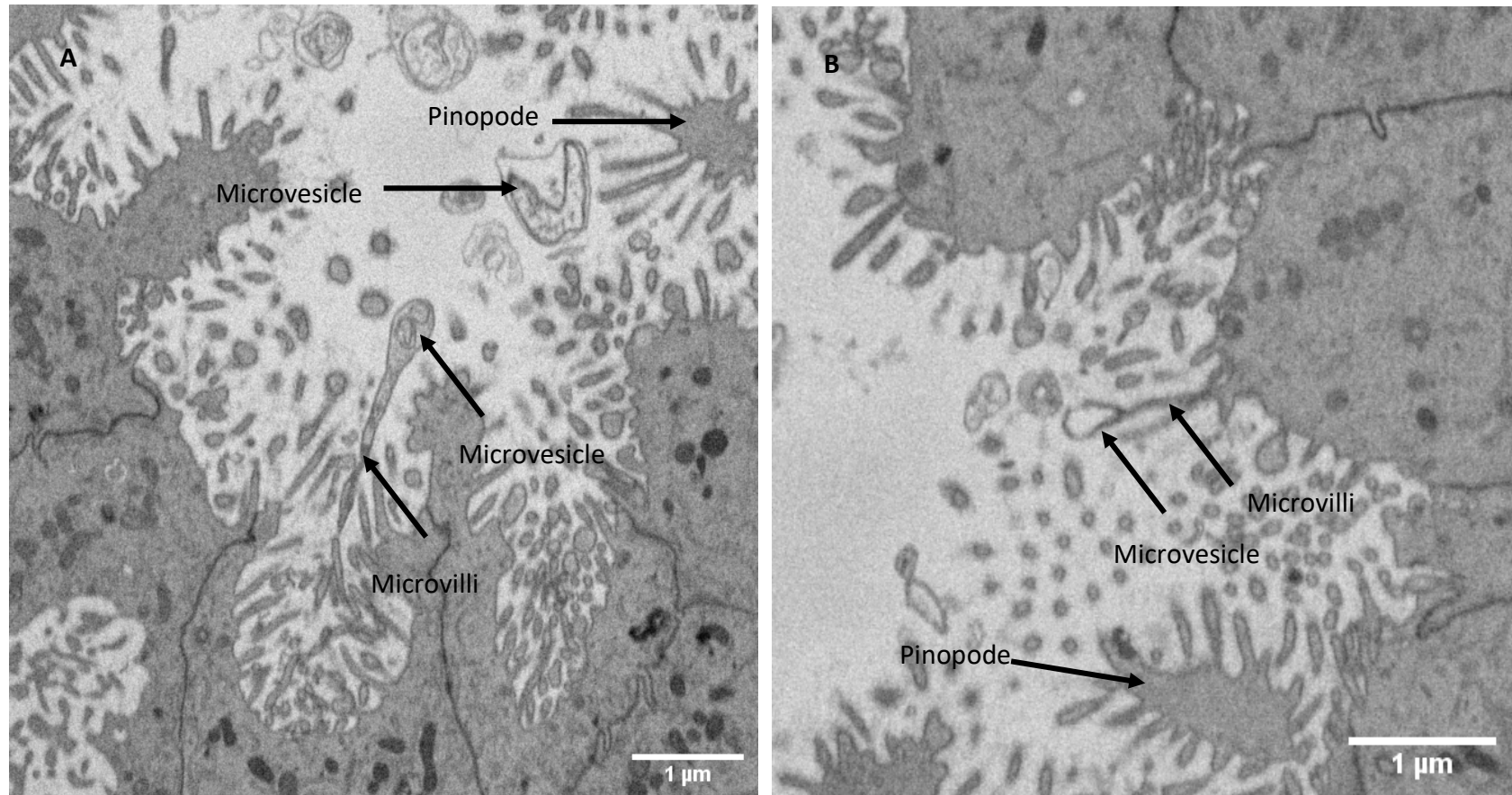
Figure 4.4 *Representative SBFSEM images showing microvesicles forming on the tips of microvilli at the endometrial gland luminal surface. Pinopodes were also present on the apical surface of glandular epithelial cells.*
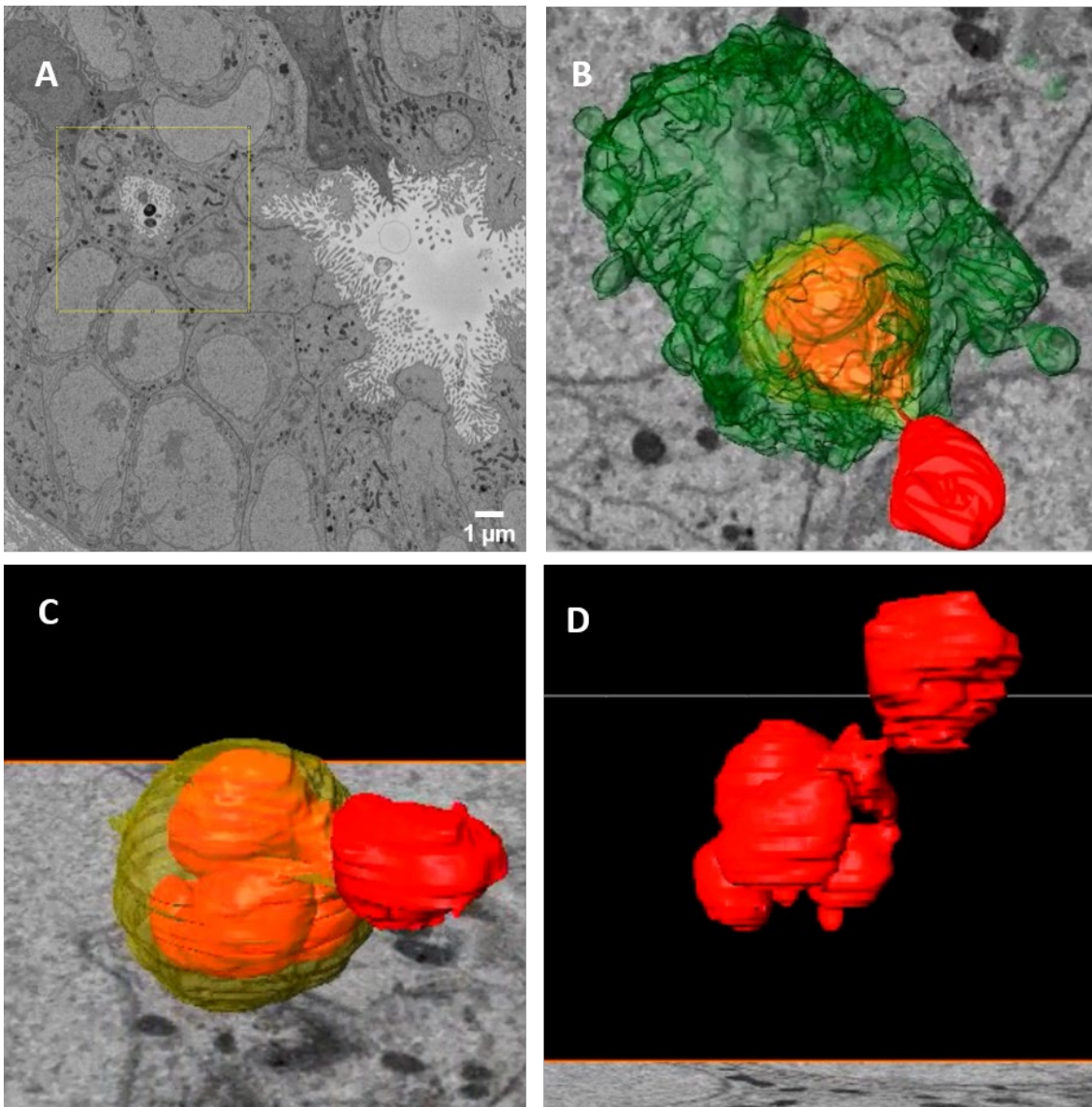
Figure 4.5 *Intracellular microvillus structure inside the glandular epithelium separated from the glandular lumen.* ***A)*** *SBFSEM image of an endometrial gland in transverse section, yellow box highlights the intracellular microvillus structure.* ***B)*** *3D reconstruction of the intracellular microvillus sac (green) of a glandular epithelial cell,* ***C)*** *containing an unidentified structure inside (yellow outer membrane) and* ***D)*** *red internal structure*
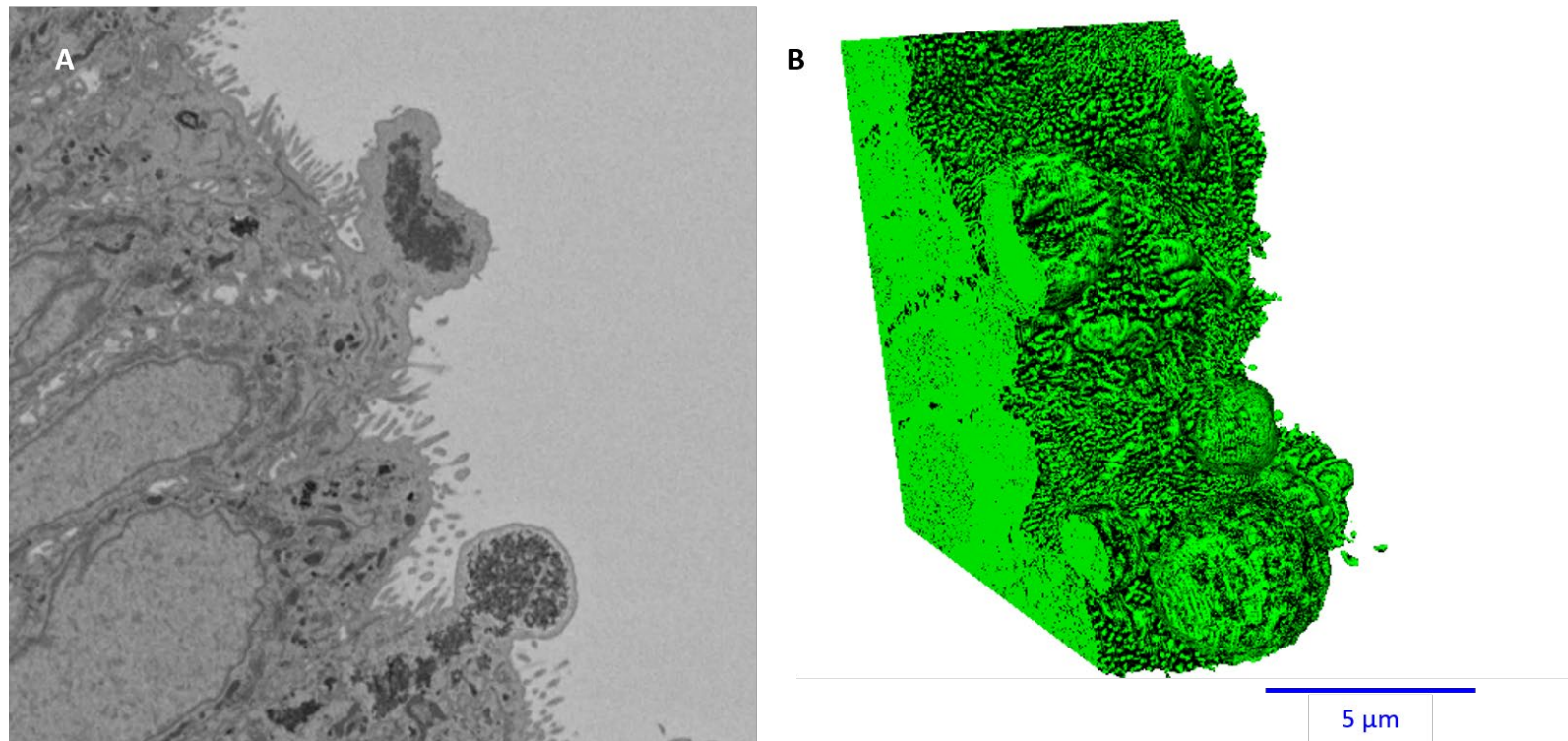
Figure 4.6 *Granular secretory material forming on the apical surface of glandular epithelial cells.* **A)** *Representative SBFSEM image and* **B)** *3D reconstruction of the secretory material by semi-automated image segmentation.*

4.4.3 Characterising motile glandular cilia 3D architecture and beat function during the window of implantation in healthy women

Motile glandular cilia 3D architecture

To characterise the 3D architecture of motile glandular cilia, multi-ciliated cells were identified in egg donor control SBFSEM gland portions, 3D reconstructed and quantified. Eleven multi-ciliated cells were identified in four out of five egg donor control gland portions, of which seven multi-ciliated cells had complete cilia from root to tip (Figure 4.7A). Glandular cilia protrude into the glandular lumen, above the forest of microvilli (Figure 4.7B) and are distinguished from microvilli and pinopode cellular projections, by an internal striated protein structure (Figure 4.8A and B) and cilia basal bodies which root in glandular epithelial cells (Figure 4.9, Video 4.3: https://youtu.be/4NMWunVLyRM). The same egg donor samples were processed for TEM, whereby high resolution images of multi-ciliated glandular epithelial cells confirmed healthy motile axoneme structure, including a close-fitting 9 + 2 arrangement of microtubules, visible dynein arms and a central pair (Figure 4.8C).

Five multi-ciliated glandular epithelial cells from two egg donor controls were 3D reconstructed, separated into their individual cilia (Figure 4.10A) by skeletonization (Figure 4.10B) and quantified. The average number of cilia per multi-ciliated glandular cell was approximately 100 cilia per cell and the average length of cilia per multi-ciliated glandular cell was approximately 5 µm.
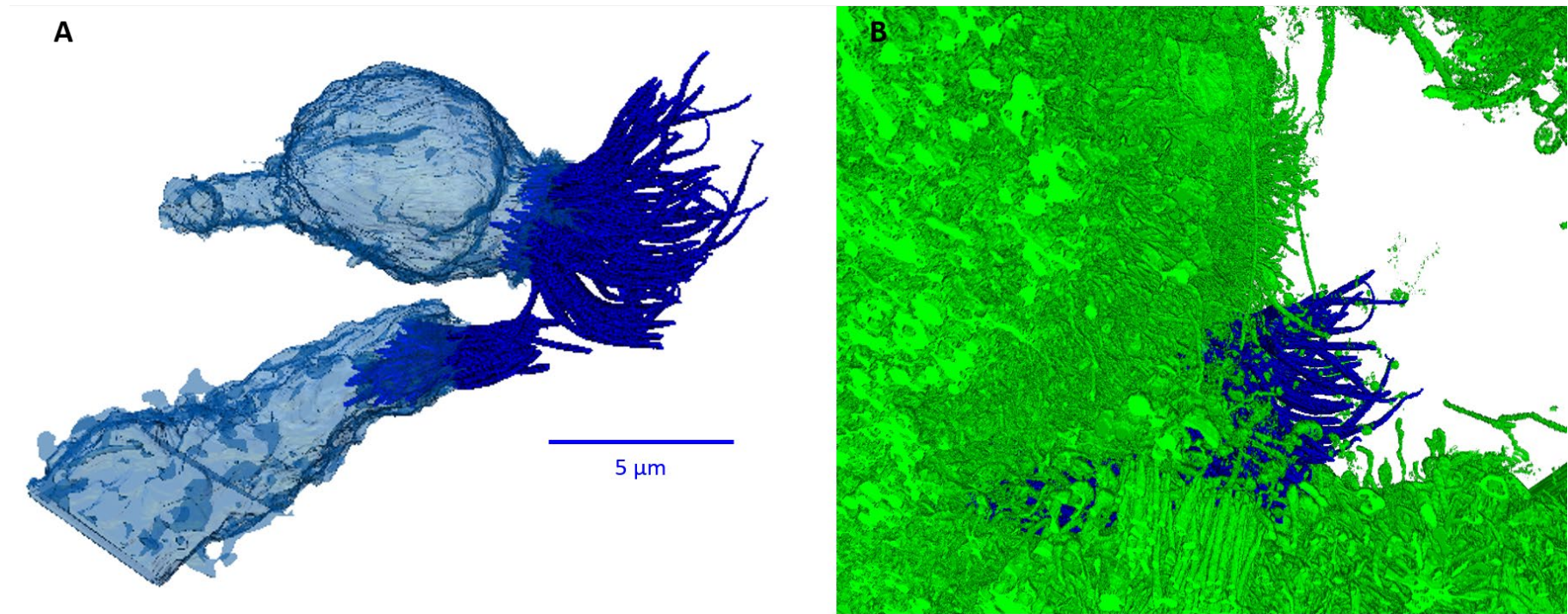
Figure 4.7 *3D reconstructions of glandular multi-ciliated epithelial cells.* ***A)*** *Cilia (dark blue) and ciliated epithelial cell (light blue). The flat edges of the epithelial cell are where the tissue volume ended.* ***B)*** *3D reconstruction of glandular cilia (dark blue) protruding into the glandular lumen amongst cellular protrusions microvilli and pinopodes (green).*
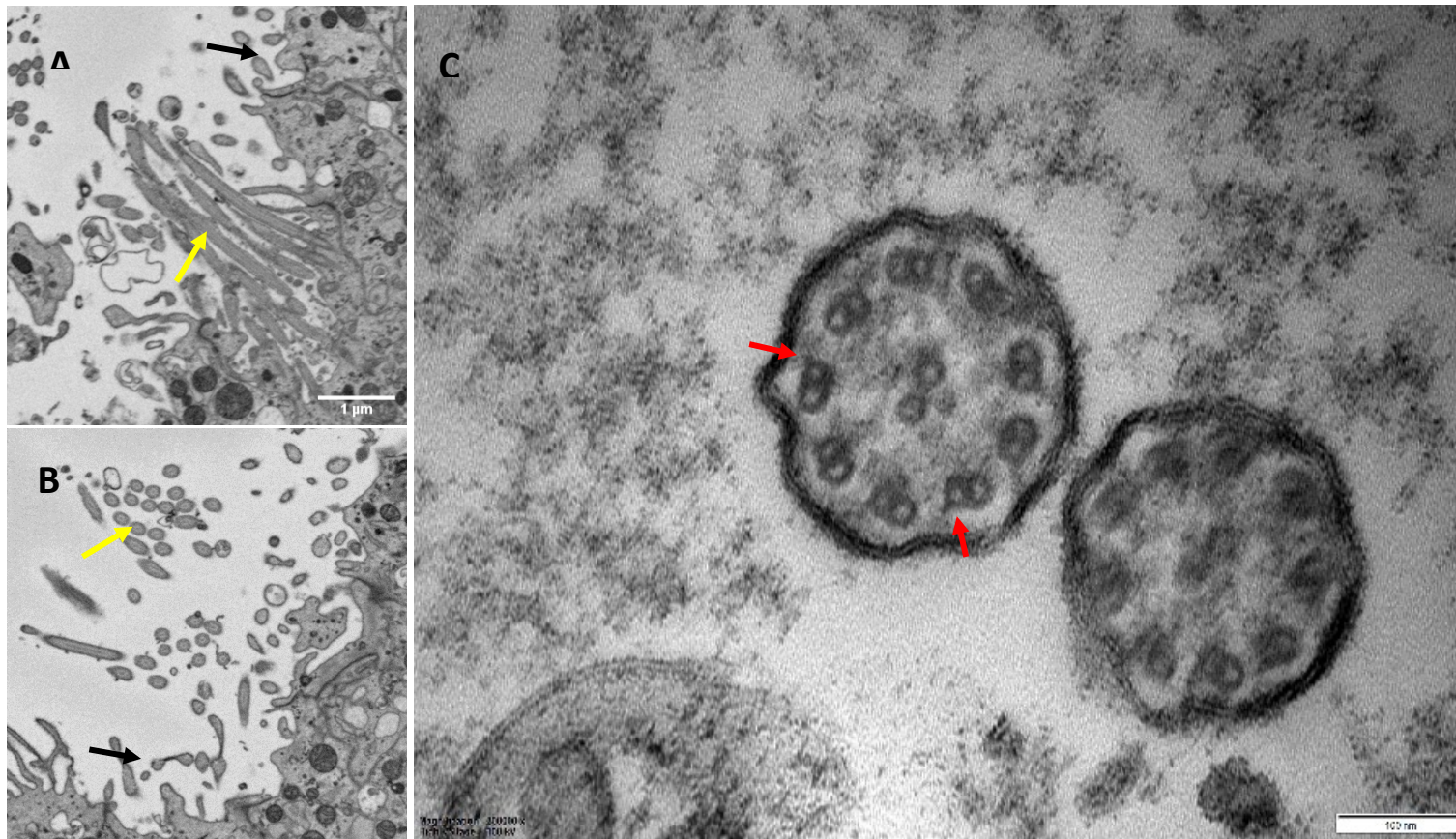
Figure 4.8 *Representative electron microscopy images of glandular cilia. **A)** Endometrial gland cilia (yellow arrow) in longitudinal section **B)** and transverse section showing an internal striated protein structure compared to microvilli (black arrow). **C)** TEM images of control glandular motile cilia 9 + 2 axoneme ultrastructure, dynein arm motor proteins (red arrow) and a central pair surrounded by a lipid bilayer membrane.*
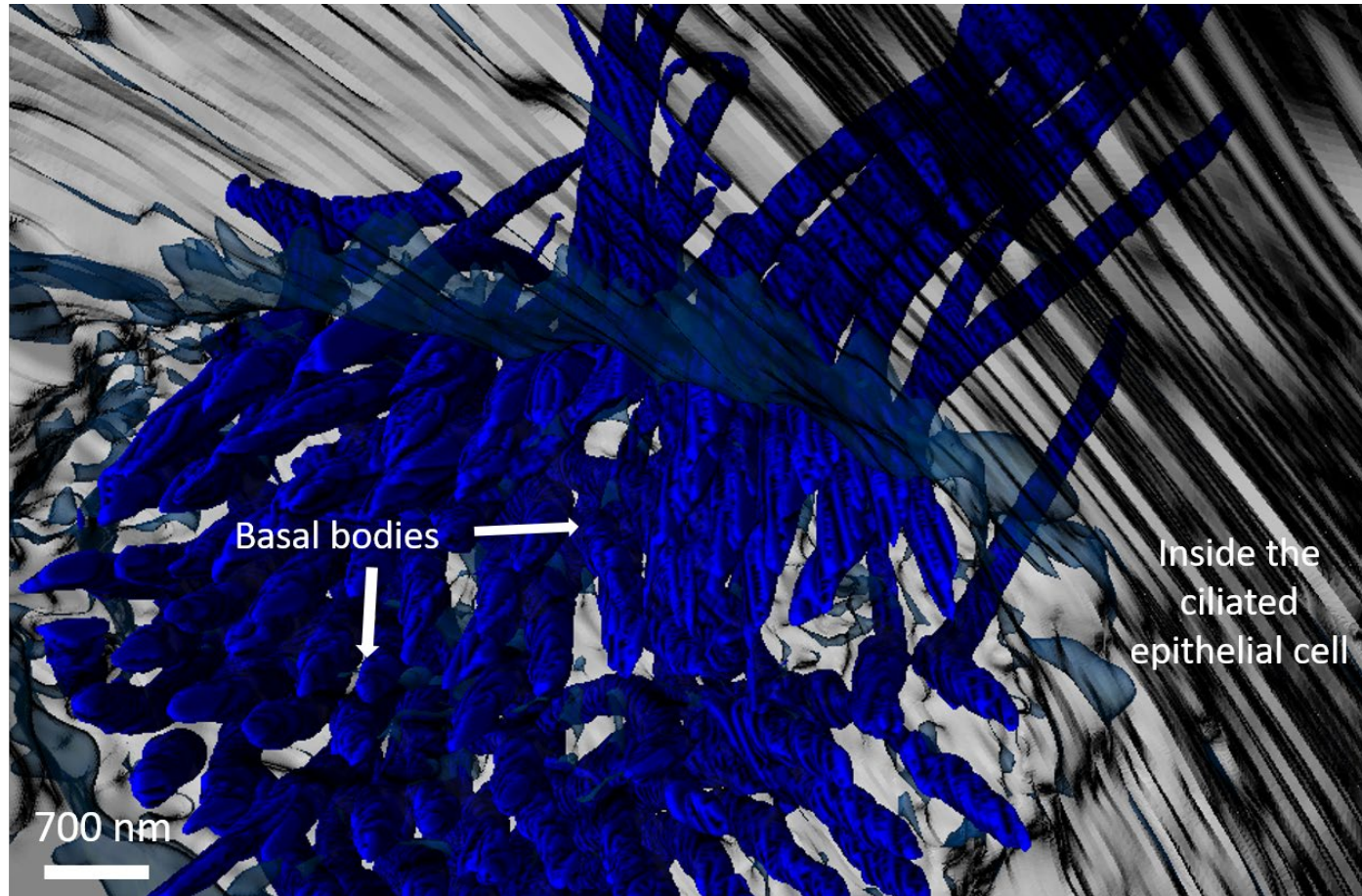
Figure 4.9 *3D reconstruction of motile cilia basal bodies inside the glandular ciliated epithelial cell. The transparent ciliated epithelial cell (grey) and basal bodies anchored inside the ciliated epithelial cell (blue).*

A

B

5 um
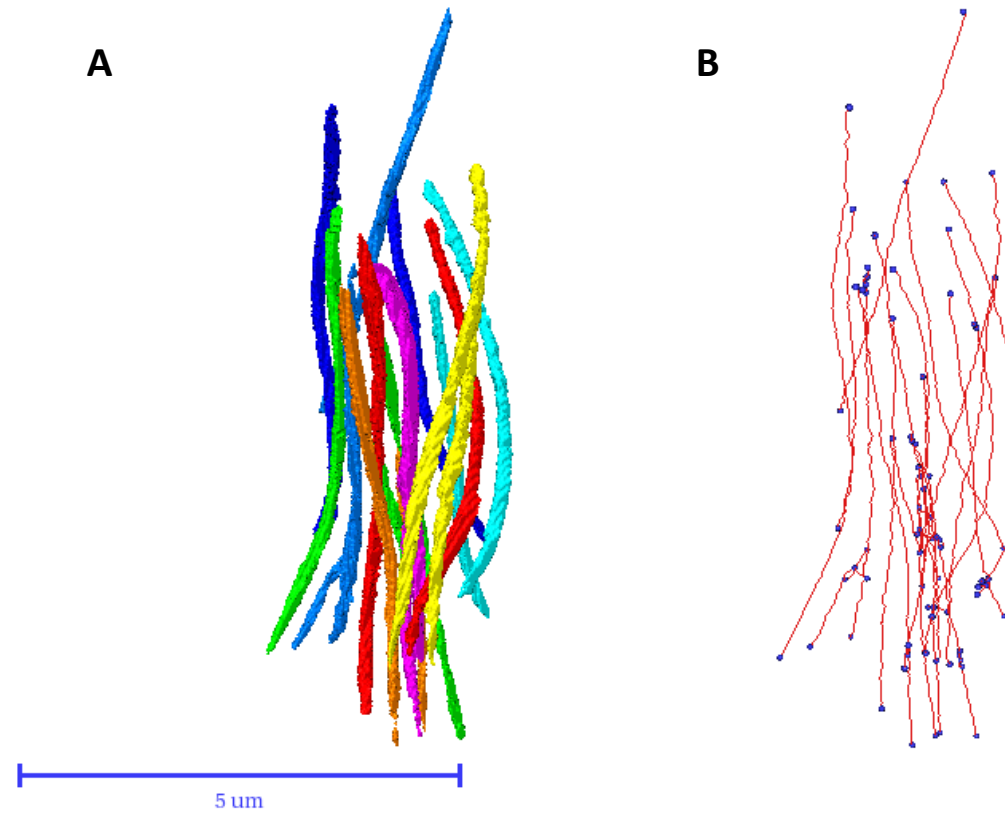
*Figure 4.10 Representative 3D reconstruction and separation of individual cilia from a multi-ciliated glandular epithelial cell. **A)** Individual cilia are separated into separate labels and therefore separate colours. **B)** Individual cilia are then eroded down to their skeleton allow length calculations. The skeleton is in red and the end point/branching nodes are in blue. This process ensures individual cilia are not touching each other.*

Motile glandular cilia beat function

To characterise the beat function of motile glandular cilia in healthy women, egg donor control endometrial glands were isolated from fresh tissue biopsies during the window of implantation. The cilia beat frequency of multi-ciliated cells was determined by high-speed video, no longer than 3.5 h after sample collection (Video 4.4: https://youtu.be/ggf1aNXNZDI, Video 4.5: https://youtu.be/cMLHr3W9RSE).

The average cilia beat frequency of control motile glandular cells was 13.85 ± 1.59 Hz (n = 3), which is within the normal range for airway cilia (11 − 20 Hz). Motile glandular cilia demonstrated an uncoordinated cilia beat. Cilia of the same multi-ciliated cell were beating forward and backwards, however at different times and not in a mixing manner. The uncoordinated beat was further confirmed at the ultrastructural level by the non-uniform direction of glandular cilia central pairs (Figure 4.11).

The gland isolation procedure uses enzymatic digestion, so could be unsettling for cells. To establish glandular cells were alive post high-speed video, a live-dead stain Propidium Iodide was applied and detected by confocal microscopy. Propidium iodide is a nuclei stain, not permeant to viable cells, demonstrating positive staining (red) if cell membranes are compromised (Figure 4.12B). The live-dead stain was not detected post high-speed video, confirming glandular cells were alive throughout live imaging (Figure 4.12A).
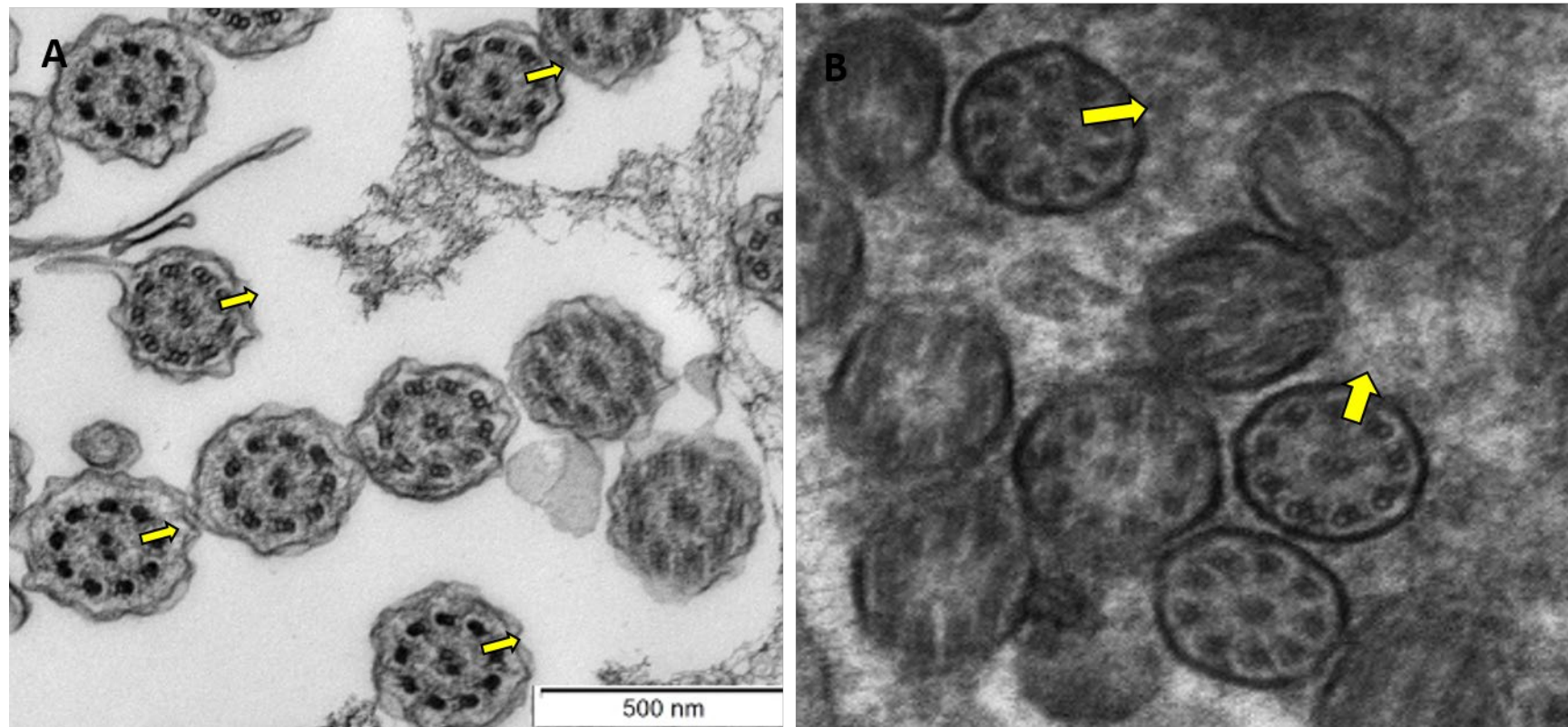
Figure 4.11 *Ultrastructural comparison of cilia from the airways and cilia inside endometrial glands.* ***A)*** *TEM image showing uniform central pair direction amongst cilia from the human airway, TEM image provided by primary cilia dyskinesia team Professor Lucas Southampton.* ***B)*** *Central pairs in different directions in motile cilia from glandular ciliated epithelial cells. Yellow arrows show the cilia beat direction.*
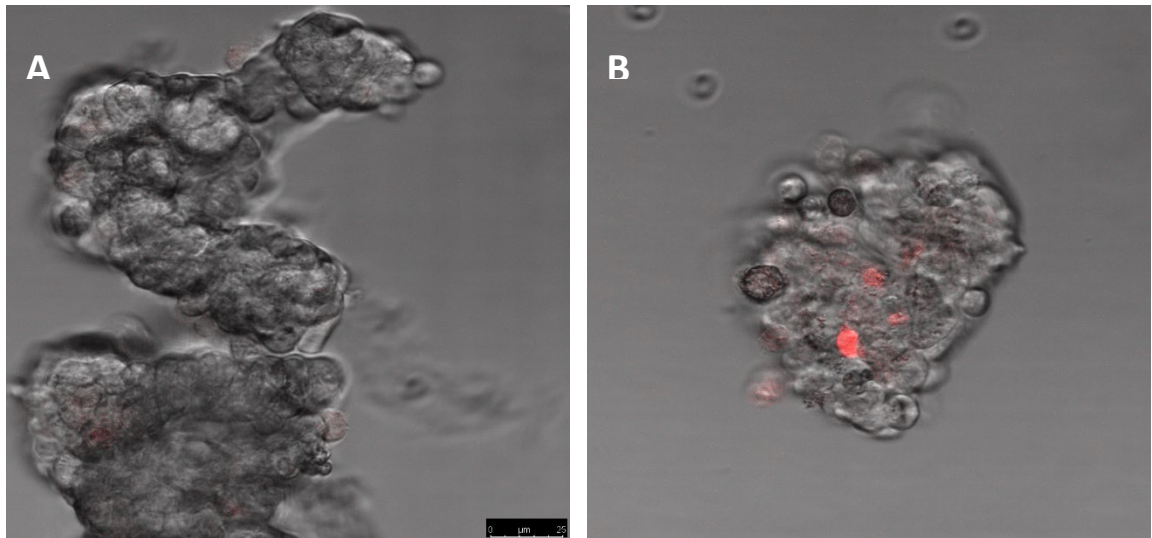
Figure 4.12 *Endometrial glands were alive post high-speed video live imaging. **A)** The absence of red staining (Propidium Iodide) indicates that the cell membranes were not compromised and therefore the cells were alive compared to **B)** glandular cells that were no longer viable.*

4.4.4 The axoneme ultrastructure and cilia beat function of motile cilia in endometrial glands from women with recurrent pregnancy loss and subfertility during the window of implantation

To investigate the axoneme ultrastructure of motile cilia in endometrial glands from women with recurrent pregnancy loss and subfertility samples were studied by TEM. Axoneme defects were observed in endometrial gland motile cilia from one recurrent pregnancy loss participant and one subfertility participant compared to three controls. The axoneme of egg donor controls demonstrated a close-fitting 9 + 2 axoneme arrangement (Figure 4.13A). In contrast, recurrent pregnancy loss cilia show microtubule disarrangement, whereby outer microtubules sit at obscure angles relative to the central pair (Figure 4.13B), and loss of central tubules (Figure 4.13C). Recurrent pregnancy loss cilia did not present any healthy ciliary axoneme structure; however, there was no evidence of secondary defects, such as unwell cells. In comparison, subfertility cilia demonstrated 'spikey' cilia (Figure 4.13D), suggestive of unhealthy cells.
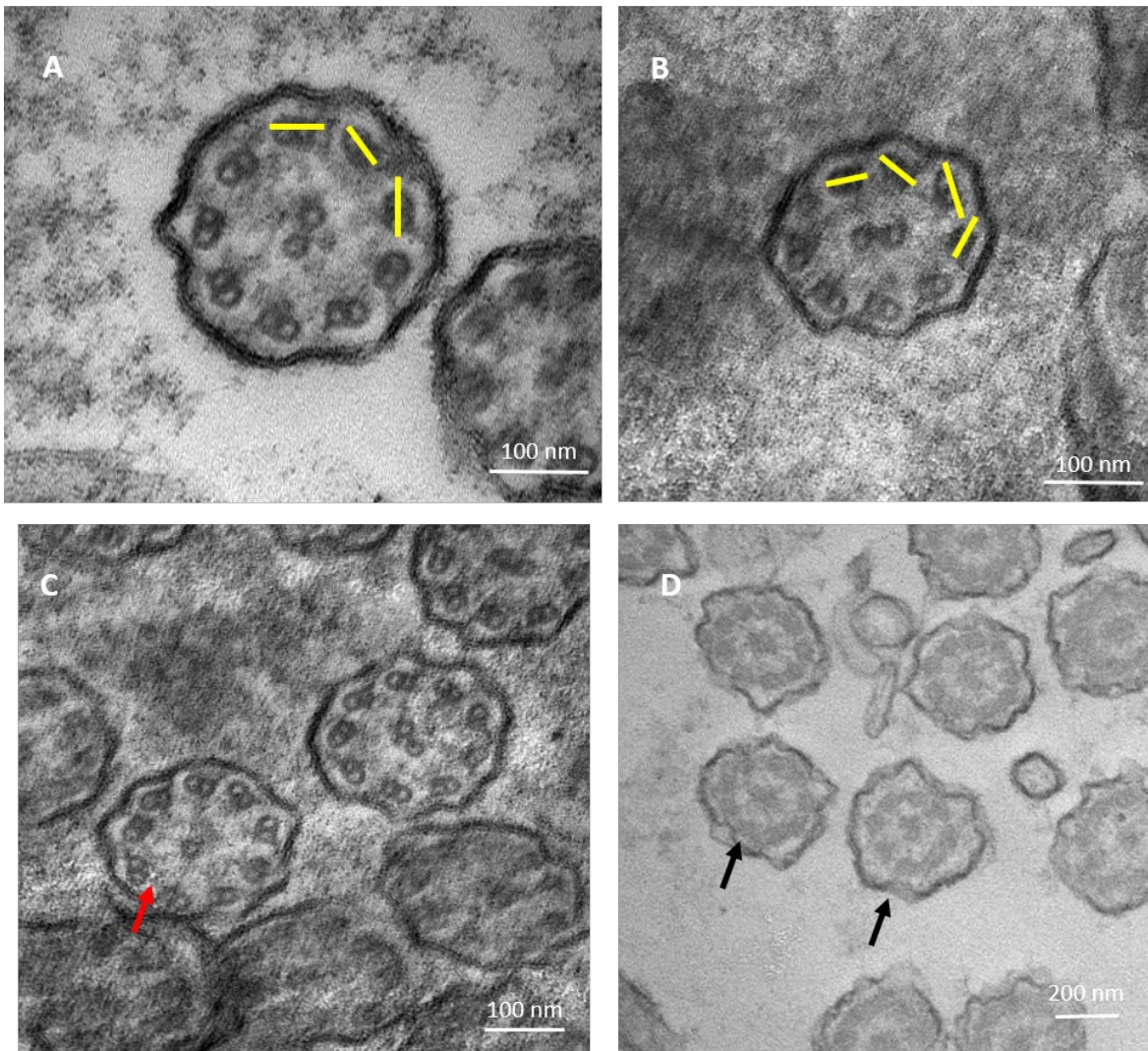
Figure 4.13 *Representative images of motile cilia axoneme structure in endometrial glands from controls, women with recurrent pregnancy loss and subfertility. **A)** Egg donor controls demonstrate a close-fitting 9 + 2 microtubule arrangement. **B)** Motile glandular cilia from women with recurrent pregnancy loss demonstrate axonemal defects including micro tubule disarrangement (yellow bands mark the angle of outer microtubule doublets) and **C)** loss of central pair microtubules (red arrow). **D)** Motile cilia axoneme structure in endometrial glands from women with subfertility demonstrate secondary defects such as spikey unhealthy cells (black arrows).*

To investigate the association of recurrent pregnancy loss and subfertility on motile glandular cilia function, the cilia beat frequency was compared between control, recurrent pregnancy loss and subfertility participants during the window of implantation (Figure 4.14). One subfertility participant was diagnosed with primary cilia dyskinesia (PCD), therefore cilia dysfunction in the airways. Recurrent pregnancy loss participants (n = 5) demonstrated an overall decrease in glandular cilia beat frequency compared to egg donor controls (n = 3), however, were not significantly altered when analysed by Mann Whitney U test (p = 0.14). PCD and subfertility groups also demonstrated a decrease in glandular cilia beat frequency compared to egg donor controls, however were not statistically analysed due to low sample size (Video 4.6: https://youtu.be/Gv1GHwnSstw).
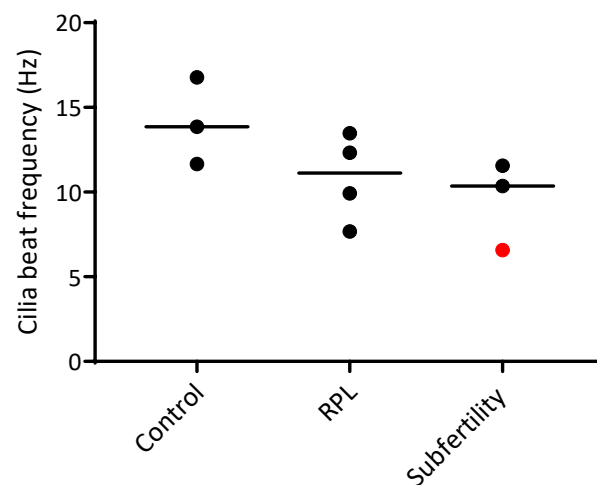
Figure 4.14 *Comparing the cilia beat frequency in endometrial glands between controls, women with recurrent pregnancy loss and subfertility. Red subfertility participant diagnosed with primary cilia dyskinesia. No significant differences were observed. The median for each group is indicated by the line. RPL = recurrent pregnancy loss.*

4.5 Discussion

This study has applied a multi-scale and multi-modal 3D imaging approach to investigating endometrial glands during the window of implantation, providing new insights into endometrial gland cilia structure and function.

Glandular 3D architecture

Investigating endometrial gland portions with SBFSEM has provided novel insights into the function of the glandular epithelium. This 3D SBFSEM data demonstrate microvilli cover the entire apical glandular surface of the endometrium, which is inconsistent with inferences from 2D TEM studies that suggest the glandular epithelium is made up of four separate epithelial cell types, including microvillus rich, pinopode, vesiculated and ciliated cells (Bartosch et al., 2011). Glandular ciliated epithelial cells and those with pinopodes are also microvillus rich. Vesiculated cells also have a microvillus apical surface which was reported by other researchers as rare (Bartosch et al., 2011). The appearance of pseudostratification is a characteristic of glandular epithelial cells in the luteal phase endometrium (Noyes et al., 1975). The glandular epithelial cells in this 3D SBFSEM data appear to be layered in 2D, but in 3D it is apparent they all connect to the underlying basement membrane. High resolution SBFSEM allows structures of interest to be extracted and quantified in 3D, compared to traditional scanning electron microscopy methods that only give surface topography information.

Endometrial glands are understood to have a secretory function, therefore a high coverage of microvilli during the window of implantation is a surprise, as microvillus surfaces are traditionally absorbing not secretory. The glandular microvillus surface, similar to the microvillus brush border of the gastrointestinal glands, suggests a large surface area for glandular absorption (Gelberg, 2014). The proportion of glandular microvilli may vary dependent upon the stage of the menstrual cycle (Bartosch et al., 2011). A 3D spatial analysis could be performed on microvillus and non-microvillus cell types using the methods described in chapter 3 to establish if the microvillus coverage changes in endometrial gland portions in women with recurrent pregnancy loss or subfertility. The presence of invaginated microvillus structures inside the glandular epithelium, separate

from the glandular lumen, pose questions to the turnover of the apical glandular surface. The similarity between the isolated microvillus surface and that of the glandular lumen, suggest they were connected at one point in time, and have been separated by a phagocytosis or pinocytosis mechanism.

It has been proposed that endometrial extracellular vesicles mediate endometrial-conceptus communication (O'Neil et al., 2020). This study shows for the first time that glandular microvesicles form on the tips of microvilli, a physiological mechanism similar to that seen on the maternal villous membrane of the placenta (personal communication, Rohan Lewis). Endometrial glands may have a microvillus rich apical surface during the window of implantation to enable the production of microvesicles and miRNA cargo transport to the conceptus. Microvesicles being produced on the tips of microvilli is also seen in T-cell interactions, where T-cell receptors cluster on the microvillus tips (Kim & Jun, 2019).

Ciliated cells may help in the directional movement of microvesicles out of the endometrial glands, where they have been found in the uterus of healthy women (Simon et al., 2018). The beating pattern of the cilia may facilitate this movement of microvesicles. The physiological mechanisms at play here are yet to be established. To analyse the cilia beat pattern of glandular ciliated epithelial cells fluorescent beads could be introduced to live endometrial glands and detected by confocal laser scanning microscopy to detect the direction of the glandular luminal fluid. Alternatively, fluorescent beads could be attached to the tips of cilia to determine the cilia stroke pattern (Katoh et al., 2018).

Characterising glandular cilia 3D structure and function in healthy women

When investigating glandular ciliated cells via traditional electron microscopy, very few cilia were found inside endometrial glands due to the limitation of thin sectioning traditional electron microscopy methods (Bartosch et al., 2011). By application of SBFSEM and 3D reconstruction, glandular cilia 3D architecture and function have been characterised in complete ciliated cells of healthy women during the window of implantation. These 3D methods provide a platform to study whole ciliated cells in unsuccessful pregnancy endometrial phenotypes.

To my knowledge this is the first study to live image cilia inside endometrial glands. In contrast to airway epithelial cilia which have a coordinated unidirectional beat, glandular cilia were observed to have a non-synchronous beating pattern. This suggests that endometrial cilia are more likely to be involved in creating circulation of glandular secretions rather than any sort of directional movement. However, this theory would not provide a dominant direction of flow which would transport microvesicles into the uterine lumen. Impaired synchronicity in cilia beating from women with recurrent pregnancy loss may result in an abnormal uterine environment of the implanting embryo or may disrupt signal transduction by hindered microvesicle transport. This could result in reduced glandular secretions (Dalton et al., 1998; Mikołajczyk et al., 2003).

Endometrial gland mucus production increases during the progesterone dominant luteal phase (Kelleher et al., 2016). This suggests that glandular cilia may act as a muco-ciliary elevator, similar to that of airway cilia. A muco-ciliary elevator could be compromised in the endometrial glands from women with recurrent pregnancy loss or subfertility if cilia beating pattern is abnormal. Further studies into the coordination of multiple cilia of one gland portion, would help decipher the role cilia impose on the glandular milieu during the window of implantation.

Glandular cilia structure and function in recurrent pregnancy loss and subfertility

Ciliary axonemal defects found in endometrial glands from women with recurrent pregnancy loss and subfertility reflect those earlier observed by Denholm & More (1980) and Fedele et al., (1996). Ciliary axonemal defects include microtubule disarrangement, suggested to be a loss of hydin linkages that hold the outer microtubule lattice in a neat arrangement, and a loss of central pair tubules. For the first time, this study demonstrates impaired ciliary beat function in cilia from recurrent pregnancy loss participants and subfertility participants; an abnormal phenotype shared with glandular cilia from a PCD case study of known ciliary defects. Previous literature has reported that ciliary beat is the production of dynein arm activation (Satir et al., 2014). Lack of ciliary axoneme structures could be in part responsible for abnormal cilia function. These provisional findings require

further investigation of paired ultrastructural and cilia beat frequency analysis to better understand the association between suboptimal receptivity phenotype and ciliary function.

Ciliary function in the airways is regulated by both genetic and environmental factors, where PCD provides a well-studied reference point for associated genetic and structural ciliary impairments. Environmental stimuli such as air pollutants and smoking have been reported to associate to ciliary impairments (Cao, et al., 2020; Shah et al., 2009). Women who smoke have an increased risk of ectopic pregnancy and increased incidence of tubal infertility (Bouyer et al., 2003). This suggests that glandular cilia could be influenced on a genetic and an environmental level, influencing the regrowth of cilia at every menstrual cycle.

4.6 Limitations

The ability to access reliably dated clinical samples and 3D image data sets were both limitations for this study. The sampling window (LH + 4-10) was self-reported which could have led to potential mismatches between the menstrual cycle day and glandular morphology. However, all samples showed characteristics of a luteal phase endometrium. In future studies ovulation sticks should be used to determine the LH surge, therefore improving the accuracy of the menstrual cycle day.

Glutaraldehyde fixative and heavy metal staining leads to a degree of shrinkage in the tissue which has been estimated to be approximately 10% (Kizilyaprak et al., 2015). This may mean my cilia length and cell volume measurements are underestimates. These limitations can be easily overcome by measuring a reference cell type such as red blood cells, which can be measured before and after tissue processing to estimate shrinkage factors.

The 3D data sets produced by SBFSEM microscopy and 3D reconstruction contain large amounts of data, my gland SBFSEM stacks were approximately 1 TB each. Although these data sets were time consuming to analyse, I used semi-automated segmentation methods to help speed up process. In future studies, machine learning based approaches could be developed to speed up this process (Lewis and Pearson Farr 2020).

Thick tissue sectioning (0.5 µm) was used to determine the endometrial gland of interest close to the luminal surface, however, this connection and subsequent orientation to the luminal surface could not be established. SBFSEM is a destructive process, preventing correlative imaging approaches post SBFSEM. However, future studies could assess the fixed tissue by micro CT prior to SBFSEM imaging providing context of the tissue volume and its components or orientation to regions of interest. During the live imaging of endometrial gland portions, their orientation and relationship to the luminal surface could not be established. Future work should develop a way to orientate isolated endometrial glands to the luminal surface in order to understand cilia beating direction.

4.7 Future directions

Future work aims to apply these novel methods to larger numbers of egg donor controls to establish a better understanding of glandular cilia 3D structure and function. Once healthy cilia have been characterised, larger numbers of recurrent pregnancy loss and subfertility participants can be studied. Further study design should investigate how multiple cilia of an endometrial gland coordinate in beat. This will help identify how cilia work together and if they affect the glandular secretions. Cilia coordination can be investigated by the direction of cilia basal bodies, by cilia alignment analysis by super resolution imaging techniques such as STORM microscopy (Liu et al., 2020).

My SBFSEM datasets can be used to study microvesicles forming on the tips of microvilli. 3D reconstruction of this process in gland portions will provide insight into how they are formed, how often they occur, and if there is a spatial relationship between ciliated cells and sites of microvesicle production. SBFSEM data sets can also be used to 3D reconstruct glandular epithelial cells, to study the degree of pseudostratification to the glandular basal membrane, and 3D quantify pinopode coverage which has been suggested as an endometrial receptivity marker (Jin et al., 2017).

4.8 Conclusions

In conclusion, I have characterised endometrial gland cilia 3D ultrastructure and provided the first live cell imaging of cilia inside endometrial glands. These results provide new insights into glandular function during the window of implantation in healthy women, which can be applied to the study of unsuccessful pregnancy phenotypes. Paired ultrastructural and live cell cilia imaging will provide a better understanding of glandular ciliary biology and pathophysiology.

Chapter 5   Analysis of the endometrial gland transcriptome and beta-tubulin during the window of implantation in recurrent pregnancy loss and subfertility

5.1 Introduction

Recurrent pregnancy loss is a problem for approximately 2% of women (Ford & Schust, 2009). We need to understand why recurrent pregnancy loss occurs in order to develop clinical treatments. For days 21-24 of the menstrual cycle the endometrium undergoes hormonally regulated cellular changes into a receptive state, in which it can receive an implanting embryo, termed the window of implantation. Recurrent pregnancy loss and implantation failure are thought to be governed by altered endometrial receptivity states such as an over or under receptive endometrium (Huang et al., 2017; Macklon & Brosens, 2014). Researchers have attempted to identify genes associated with a receptive endometrium, yet a consistent pattern of receptivity associated gene expression has not been established (Hu et al., 2014). One reason for this may be that the endometrium is a heterogeneous tissue consisting of different epithelial and stromal cell types. The gene expression profiles do not take into account the cell specific expression patterns associated with receptivity or differences in the cell populations that can influence overall gene expression. In this chapter, I apply RNA sequencing to isolated glandular epithelium to determine a gene expression pattern of endometrial glands in recurrent pregnancy loss during the window of implantation.

Microarray and RNA sequencing studies have attempted to identify a pattern of endometrial gene expression associated with recurrent pregnancy loss (Huang et al., 2017; Othman et al., 2012). Studies on whole endometrium however, do not account for different endometrial cell types or structures including the glandular epithelium and the luminal epithelium. Candidate gene and microarray studies have been performed on whole endometrium to identify a potential gene expression profile associated with endometrial receptivity which they called 'the endometrial receptivity array' (ERA) (Díaz-Gimeno et al., 2011). The ERA however, could not identify a non-receptive endometrium or implantation failures (Ruiz-Alonso et al., 2013). Microarray and RNA sequencing studies have since associated a pattern of endometrial gene expression with implantation failure (Chen et al., 2018; Koot et al., 2016). Studies on whole endometrium have not provided a consistent pattern of gene expression that relates to unsuccessful pregnancy, potentially due to the

heterogeneity of endometrium not being taken into account and differences in methodology (Table 5.1).

To overcome endometrial heterogeneity, single cell RNA sequencing has been used to identify individual endometrial cell type gene expression profiles during the window of implantation in control women. This does not however, establish whether different epithelial cell populations are from glandular or luminal epithelial regions (Lucas et al., 2020). Epithelial and stromal cell gene expression profiles have also been established by isolating epithelial and stromal cell types prior to RNA sequencing by enzymatic digestion or FACS sorting (Krjutškov et al., 2016; Wang et al., 2018). A meta-analysis utilized microarray studies and one RNA sequencing study to establish a consistent gene expression pattern in the pre-receptive and receptive endometrium (Altmäe et al., 2017). RNA sequencing validation of pre-receptive and receptive endometrium also highlighted specific gene expression patterns associated with FACS sorted epithelial and stromal cells (Altmäe et al., 2017). No studies to date however, have measured the gene expression profile of endometrial glands only, allowing the endometrial gland epithelium to be clearly distinguished from other epithelial populations.

Endometrial glands are invaginations in the luminal epithelium, secreting essential factors during the window of implantation. Gene knock-out studies show that endometrial glands are important for successful embryo implantation and for histotrophic nutrition in early pregnancy (Burton et al., 2002; Filant & Spencer, 2013). Within endometrial glands there are four different epithelial cell types including secretory cells and ciliated cells (Lucas et al., 2020). The beating of ciliated epithelial cells within the gland may be involved in mixing glandular secretions or moving these towards the uterine lumen, however their role is not well understood.

Cilia contain microtubules that are polymers of tubulin. Tubulin are dimers of α-tubulin and β-tubulin 55 kDa subunits. β-tubulin proteins are encoded by nine genes (*TUBB1-9*) and different isoforms are more or less prone to post translational modifications at the C-terminus tail regions that decorate the outside of the microtubule lattice. Different tissue types demonstrate specificity to certain β-tubulin isoforms, known as isoform

enrichment (Girotra et al., 2017). This suggests that different β-tubulin isoforms have different functions specific to cell types. Different tubulin isoforms and their respective post-translational modification have been reported to affect cilia beat function (Kubo et al., 2010; Vent et al., 2005). The entry of post-translational modification glutamylases are controlled at the base of the cilium. Regulation in and out of the cilium may also impact upon β-tubulin isoform post-translational modification (He et al., 2018). The β-tubulin isoform enrichment of endometrial gland ciliated cells is not understood.

This study uses RNA sequencing analysis to compare the gene expression profile of isolated endometrial glands in recurrent pregnancy loss participants compared to healthy controls during the window of implantation. This chapter also aims to investigate β-tubulin enrichment in glandular ciliated epithelial cells and determine whether there is an association between β-tubulin gene or protein expression and recurrent pregnancy loss.

5.2 Aims

1. To investigate the gene expression profile of isolated endometrial glands during the window of implantation in women with recurrent pregnancy loss versus controls.
2. To investigate β-tubulin in isolated endometrial glands during the window of implantation from women with recurrent pregnancy loss versus controls.

Table 5.1 *Summary of gene expression studies in unsuccessful pregnancy.*

Reference	Method and model	Endometrium sample	Menstrual cycle day/ study group	Finding	Strengths	Weaknesses
(Brooks et al.,2016)	Microdissection and RNA-sequencing Sheep	Luminal epithelium, glandular epithelium, the conceptus and endometrial luminal fluid	Peri-implantation period of pregnancy	Genes expressed in luminal epithelium and glandular epithelium involved in cell survival and growth	Endometrial epithelium split into glandular and luminal epithelium	Translation of sheep model to human endometrium
(Chen et al., 2018)	RNA-sequencing Human	Whole endometrium	Women with RIF vs control (LH+ 3 - 7 days)	Differentially expressed genes: 460 mRNA and 742 long noncoding RNA clustered into TNF and toll-like receptor signalling pathway	Pre-implantation period of menstrual cycle	Whole endometrium
(Krjutškov et al., 2016)	FACS cell sorting and RNA-sequencing Human	CD39 stroma and CD9 epithelium	2 samples 1) LH + 8 days and 2) day 25 late secretory with known endometriosis.	Genes more active in cultured stromal cells vs biopsy. Low RNA yield from cultured epithelium	Endometrium split into epithelial and stromal cells	No comparison of RIF or RM patient groups to controls
(Hu et al., 2014)	RNA-sequencing Human	Whole endometrium	Pre-receptive (LH + 2 days) versus receptive endometrium (LH + 7 days)	2372 differentially expressed genes in LH + 7 vs LH + 2. Pathways: mineral absorption and cell cycle	LH + 2 and 7 timed samples	No comparison of patient groups/ whole endometrium
(Koot et al., 2016)	Microarray Human	Whole endometrium	RIF vs controls (LH + 6 - 7 days)	303 genes predictive of RIF, suggesting RIF is associated with reduced cellular proliferation	LH + 6 - 7 timed samples	Whole endometrium
(Huang et al., 2017)	RNA-sequencing Human	Whole endometrium	RIF/RM vs controls (LH + 7 days)	Complementary and coagulation cascades pathway was up-regulated in RIF, while down regulated in RM	LH + 7 timed samples	Gene expression analysis not compared to control cohort/ whole endometrium
(Kosova et al., 2015)	Microarray Human	Whole endometrium	Recurrent early pregnancy loss < 10 weeks (LH + 9 - 11 days)	Differentially expressed genes: 58 genes associated with out of phase endometrium; 81 genes associated with elevated glandular cyclin E levels	Compares gene expression profile to endometrial abnormalities	Lack of control cohort/ whole endometrium
(Othman et al., 2012)	Microarray Human	Whole endometrium	RM vs controls (days 21 - 24 of the menstrual cycle)	346 differentially expressed genes in RM vs controls. Associated pathways included cell differentiation and angiogenesis.	Compared to fertile controls	Whole endometrium

RM = recurrent miscarriage, RIF = recurrent implantation failure, LH = luteinising hormone

5.3   Methods

In this chapter I compare the transcriptome in isolated endometrial glands between women with recurrent pregnancy loss and egg donor controls using RNA sequencing. I also perform a targeted analysis of β-tubulin gene isoforms in endometrial glands using qPCR and wholemount immunohistochemistry in women with recurrent pregnancy loss and subfertility versus controls.

5.3.1   Endometrial biopsy collection

Endometrial biopsies (approximately 1.5 cm x 0.5 cm x 0.3 cm) were collected using a Pipelle catheter (Stocker et al., 2017), from egg donor control (total, n = 11), recurrent pregnancy loss (total, n = 20) and subfertility (total, n = 9) participants during the window of implantation (LH + 4 - 10), as described in *General methods* section 2.2. One of the subfertility participants was also diagnosed with PCD. PCD is a genetic defect which causes reduced or completely non-functioning cilia in the airways, with the main consequence being frequent respiratory infections (Gravesande & Omran, 2005).

Half of each endometrial biopsy was placed into 50:50 DMEM/ Ham's F12 nutrient mixture containing 5% streptomycin for endometrial gland isolation, and the other half was immediately fixed in 4% paraformaldehyde for 2 h for wholemount immunohistochemistry. Samples were then stored in 0.1% sodium azide in PBS until image processing.

5.3.2   Endometrial gland isolation

Whole endometrial tissue biopsies were processed for endometrial gland isolation from egg donor control (n = 6) control and recurrent pregnancy loss participants (n = 9), plus one from a PCD patient case study. Endometrial gland isolation was performed by enzyme digestion within 1 h of tissue collection, as described in *General methods* section 2.8. Tissue samples were kept on ice prior to endometrial gland isolation to reduce metabolic activity. Endometrial tissue pieces were digested with 0.7 mg/ml type 1A collagenase in 50:50 DMEM/ Ham's F12 nutrient mixture, containing 5% streptomycin at 37°C for 2 x 15 min intervals with gentle agitation. The solution was then passed through a

50 µm sieve to isolate endometrial glands from other endometrial cell types. Endometrial glands were then stored in 700 µl QIAol lysis reagent at -80°C until RNA extraction.

5.3.3 RNA extraction

RNA extraction was carried out on isolated endometrial glands, as described in *General methods* section 2.10. Isolated endometrial glands were homogenised by gentle agitation in 700 µl QIAol lysis reagent, before the Qiagen miRNeasy extraction kit protocol was followed to elute RNA into ddH$_2$0. The RNA yield was quantified by Thermos Scientific Nanodrop 1000 Spectrophotometer and RNA quality was analysed using an Agilent 2100 bioanalyser.

5.3.4 RNA sequencing

The gene expression profile was compared between five pairs of endometrial glands from participants with recurrent pregnancy loss and egg donor controls, matched by the day of the menstrual cycle. Total RNA extraction, cDNA library preparation, RNA sequencing and bioinformatics data analysis was carried out by Dr Sybil Jongen, as described in *General methods* section 2.11. Library preparation was carried out (TruSeq; Illumina) to convert RNA to cDNA, add index adapters and flow cell adapters, to allow sample quantification and sequencing on the flow cell respectively. The cDNA library was quantified by a Roche KAPA library quantification kit (Illumina). Paired end RNA sequencing (2 x 150 bp) was carried out on Illumina NextSeq 550 which provided an average of 24.7 million reads.

Gene count data were normalised, and differential expression analysis was carried out in RStudio R-3.6.2 package DESeq2. The Empirical Bayes approach to false discovery rate (FDR) was applied to correct for multiple testing at 5%. Significance was determined by a Wald test and accepted as $p \leq 0.05$. To increase stringency, a further log fold change threshold of 1.25 was applied.

Genes which were significantly expressed in recurrent pregnancy loss endometrial glands compared to egg donor controls (no log fold change threshold), were mapped to

pathways using the publically available software Toppgene (Division of Bioinformatics, Cincinnati Children's Hospital Medical Centre). A Benjamini & Hochberg (B&H) FDR was used to correct findings p ≤ 0.05.

Secondary targeted analyses included the identification of genes associated with PCD (Lucas et al., 2017) and β-tubulin. Data are presented as log (base2) of count data.

5.3.5   Quantitative PCR analysis of β-tubulin genes

Egg donor control (n = 6) control, recurrent pregnancy loss participants (n = 9), and one PCD participant gland RNA was first converted to cDNA by reverse transcription, as described in *General methods* section 2.12. Gland RNA samples were prepared to a final concentration of 0.25 μg in 13 μl final volume using ddH$_2$O. In addition to RNA samples, six coefficients of variation (CV) controls (C1 – C6) were prepared to a final concentration of 0.05 μg/μl and no enzyme controls (NECs) were prepared with ddH$_2$O in the place of the reverse transcriptase enzyme. Samples were incubated with random primers (C1181, Promega UK, 250 ng per reaction) in the PCR cycler (Verti 96 well thermal cycler, Applied Biosystems) at 70°C for 5 min to allow primers to anneal. Samples were then run on the PCR cycler, to perform reverse transcription by heating at 37°C for 60 min to allow reverse transcriptase (Moloney Murine Leukaemia Virus Reverse Transcriptase MMLV RT, M1701, Promega UK) to elongate the annealed primers and 95°C for 10 min to inactive the reverse transcriptase enzyme. Samples were then kept at 4°C continuously until samples were collected. cDNA samples were centrifuged and stored at -20°C.

Gene expression of β-tubulin genes *TUBB1, TUBB5V4* and *TUBB4B* were measured in endometrial gland cDNA from women egg donor controls women with recurrent pregnancy loss using qPCR, as described in *General methods* section 2.13. Genes of interest were measured using a Roche Universal Probe library assay on the Roche 480 Lightcycler, primer sequences listed in Table 5.2. cDNA was heated to 95°C for 10 min to activate the 'hot start' polymerase, followed by 40X cycles of 95°C 15 sec to denature cDNA and 60°C 60 sec for annealing and elongation.

Housekeeping genes *UBC* and *UBE4A*, previously validated by (Stocker et al., 2017)*,* were measured using a Primer Design Double Dye assay on the Roche 480 Lightcycler. cDNA was heated to 95°C for 2 min to activate the 'hot start' polymerase, followed by 40X cycles of 95°C 15 sec to denature cDNA and 60°C 60 sec for annealing and elongation. For all qPCR assays, samples were run in triplicate alongside a standard curve, controls, NECs and NTCs. Cp values were determined by the second derivate method and were converted to DNA concentration using a standard curve.

The relative expression of genes *TUBB1, TUBB5V4* and *TUBB4B* were normalised to the geometric mean of two selected housekeeping genes (*UBC* and *UBE4A*).

Table 5.2 *Primers designed for β-tubulin genes.*

Gene	Position	Tm	%GC	Primer sequence (5'-3')	Probe UPL #
TUBB1	1646-1666	59	52	F cggagtcgcttacagaacagt	#2
	1695 -1714	60	55	R cagagtgggtttggagtgc	
TUBB5V4	19	60	47	F accttgaggcgagcaaaaa	#64
	20	60	50	R aggatggcacgaggaacata	
TUBB4B	51-72	59	50	F ctgctgctgtttgtctacttcc	#38
	156-176	59	48	R ctgatcacctcccaaaacttg	

Tm = melting temperature, F = forward, R = reverse, %GC = guanine-cytosine, UPL # = Roche Universal Probe Library number.

5.3.6   Whole-mount immunohistochemistry

Endometrial samples were collected and fixed into 4% PFA for 2 h and then stored in 0.1% sodium azide in PBS until tissue processing as described in *General methods* section 2.2.2. At the time of tissue processing a wholemount immunohistochemistry protocol was carried out on egg donor control (n = 11), recurrent pregnancy loss (n = 18) and subfertility (n = 9) endometrial samples to identify ciliated epithelial cells in endometrial glands, as described in *General methods* section 2.4. The assessor was blinded to patient group throughout the endometrial sample tissue processing, confocal imaging and image analysis to avoid sample bias. In short, endometrial samples were permeabilised in 0.5% Titron X-100 in PBS for 1.5 h, washed in 1x PBS and then blocked with 2% BSA for 1 h.

Two wholemount immunohistochemistry experiments were carried out on endometrial samples with different β-tubulin antibodies. Primary antibody incubation was carried out in 75 μl droplets overnight at 4°C. Rabbit anti-radial spoke head 4 homolog A (RSPH4A) antibody (polyclonal, Sigma Aldrich, 1:100 dilution) was used as a cilia marker while, mouse anti-human general β-tubulin antibody (clone 2-28-33, Sigma Aldrich SAB4200715, 1:500 dilution), of unknown isoform specificity, and a specific mouse anti-human TUBB5 antibody (clone AA2, Abcam ab231082, 1:500) marked ciliated cells positive for β-tubulin. To ensure consistency, master mix solutions were made up for all primary and secondary antibody incubations.

Following 3 x PBS wash, secondary antibody incubation was carried out at room temperature for 2 h in 50 μl per endometrial sample. Secondary antibodies were donkey anti-mouse IgG 550 (Thermo fisher #SA5-10167, 1:200), Goat anti-rabbit CF^{TM}633 conjugate (Sigma-Aldrich #SAB4600140, 1:200) and DAPI nuclear stain (Sigma-Aldrich #D9542, 1:250). Finally, samples were cleared using TDE and stored at 4°C ready for imaging.

Both wholemount immunohistochemistry experiments included a no-primary antibody control experiment to check for non-specific secondary antibody binding and a positive β-tubulin control to check for positive β-tubulin staining. Positive β-tubulin controls were healthy human airway nasal brushing slide preparations, donated by Southampton PCD team Professor Lucas. Traditional immunohistochemistry was carried out on the nasal brushing slides as described in *General methods* section 2.3.

5.3.7 Confocal image analysis of endometrial gland portions

Five endometrial gland portions per participant were imaged on the SP8 confocal laser-scanning microscope. The confocal laser scanning microscope settings were applied as described in *General methods* section 2.5. The first gland portion was selected by exciting only the DAPI channel, using a x 40 oil emersion objective. Endometrial glands were identified by their tube-like and columnar cell structure. Subsequent endometrial glands

two to five were chosen using a random method involving tossing a coin, whereby a head or a tail dictated if the field of view was moved in the X or Y direction respectively.

Image analysis was acquired in real time as the field of view was manually moved through the gland portion. The number of ciliated epithelial cells were counted through a 3D gland portion (Figure 5.1), identified by radial spoke head staining. Ciliated cells also positive for β-tubulin staining were also recorded. The outcome measurement was the percentage of cilia per gland portion positive for β-tubulin protein expression. The depth of the gland portion (μm) was consistent throughout participant groups, and image analysis acquisition was stopped if the laser intensity changed and made cilia identification unclear. Videos of all image analysis were taken but to save time image stacks were not acquired.
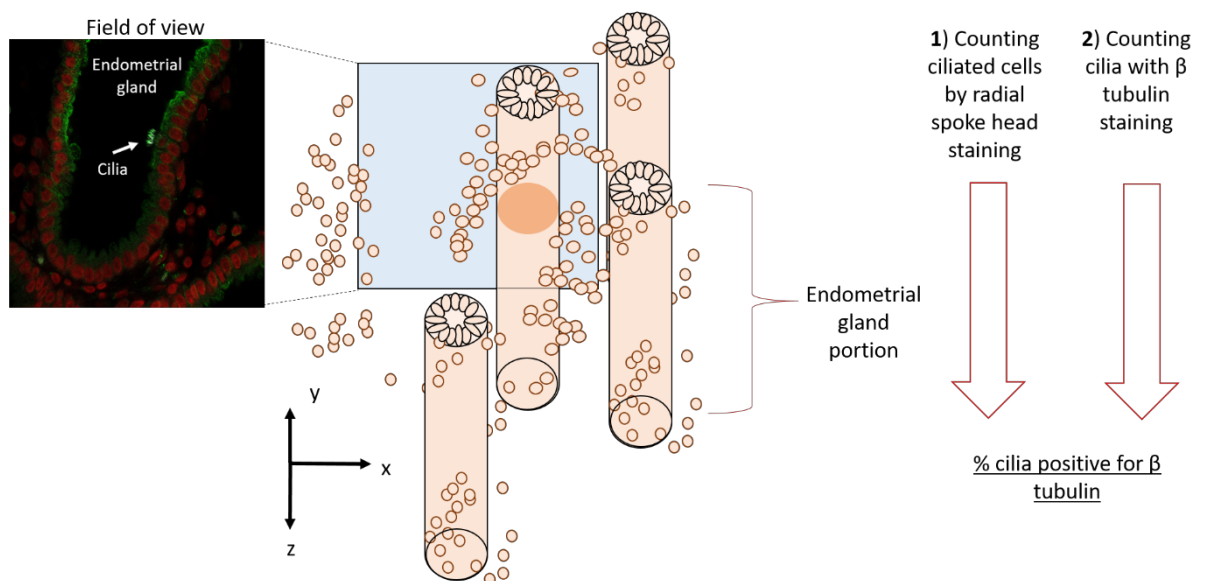
Figure 5.1 *Confocal laser scanning microscopy methods for beta-tubulin protein expression quantification. A field of view is selected at the top of the gland portion, the field of view is then moved down the gland portion and the number of cilia are counted (identified by radial spoke head protein) and those positive for beta-tubulin staining to give an outcome = % cilia positive for beta-tubulin staining in a gland portion.*

5.3.8   Protein extraction and quantification

Western blotting was carried out to validate the presence of general tubulin and TUBB5 protein isoforms in endometrial tissue and endometrial glands.

The protein fraction was extracted from matched whole endometrial tissue pieces in RNAlater® and isolated endometrial glands in Qiazol lysis buffer from the same patient, as described in *General methods* section 2.14. All steps were undertaken at 4°C. Briefly, endometrium in RNAlater® were incubated in 1x RIPA buffer with 1:100 proteinase inhibitors for 2 h on ice with gentle agitation. Cells were then centrifuged at 12000 rpm for 20 min at 4°C to remove insoluble material and the lysate was stored at -20°C. Meanwhile the Endometrial glands in 700 µl Qiazol lysis buffer were split into its aqueous phases by the addition of 400 µl chloroform. The protein fraction was isolated from the organic phase and stored at -20°C.

Human embryonic kidney 293 cells (HEK293) were used as a positive control for β-tubulin, while bacteria cells (XL-1- Blue competent cells LOT# 0540286) were used as a negative control for β-tubulin. Both cell types were centrifuged at 10000 rpm at 4°C and re-suspended in 100 µl PBS to wash the cells. The centrifuge step was repeated and cells re-suspended in 50 µl 1 x RIPA buffer with 1:100 proteinase inhibitors. The suspension was gently homogenised for 15 min, and then centrifuged at 12000 rpm. The lysate was stored at -20°C.

Protein quantification was carried out via the BCA assay according to manufacturer's instructions, as described in General methods section 2.14.1. A BSA standard curve was used in the same RIPA dilution as that of the samples. The sample protein concentration was acquired from a BSA standard curve.

5.3.9   Western blotting and chemiluminescence detection

Protein analysis of all samples were run in accordance with *General methods* section 2.14. In short, whole endometrium (30 µg), endometrial gland protein lysate (15 µg) and positive control HEK293 (30 µg) were denatured by heating at 95°C for 4-10 min in sample

reducing buffer. Samples and Precision Plus Western C standard (Bio Rad #161-0376) were run in reducing conditions via SDS-PAGE, on a 10% separating gel. SDS-PAGE was run at 200 V for until the dye front ran off the gel, typically just under 1 h.

Protein blotting was carried out onto methanol activated PVDF membranes by semi-dry transfer (Bio Rad), for 1.5 h at a 25 V limit and constant 75 mA. Membranes were blocked in 2% BSA to prevent non-specific binding, and then Western blotting primary antibody incubation was carried out overnight at 4°C with gentle agitation. The primary antibodies used were mouse anti-human general β-tubulin antibody (clone 2-28-33, Sigma Aldrich SAB4200715, 1:500 dilution, 50 kDa) and mouse anti-human TUBB5 antibody (clone AA2, Abcam ab231082, 1:2000, 49 kDa). All following Western blotting steps were carried out at room temperature with gentle agitation and 3 x 1 x TBST washes in-between steps. PVDF membranes were incubated with horseradish peroxidase (HRP) – bound anti-mouse secondary antibody (cell signalling #7076) for 1 h, a Precision Protein™ Strep-Tactin-HRP conjugate (Bio Rad #161-0380) for 1 h and a HRP- conjugated β-actin antibody loading control (Sigma A3854, 1:10000, 45 kDa) for 1 h.

Chemiluminescence detection was carried out using the Amersham ECL Western Blotting Detection Kit (Cytiva, #RNP2108) on the Ingenius Gel Doc. The outcome of Western blotting was the presence or absence of the protein. Exposure times for general β-tubulin antibody were 1 min for whole endometrium protein and 5 min for isolated endometrial gland protein. While for the TUBB5 antibody, 2 min for whole endometrium protein and 6 min for isolated endometrial gland protein. Higher exposure times were required for 15 μg of glandular protein compared to 30 μg whole endometrium. The presence of β-tubulin staining was compared to a ladder standard to determine protein size.

5.3.10 Data analysis

Data analysis and management was carried out in Prism 8 (GraphPad Software Inc., California, USA) and Microsoft excel 2016. All data were tested for a normal distribution by the Shapiro-Wilk normality test before further statistical analysis was carried out.

To investigate the association of recurrent pregnancy loss on glandular β-tubulin gene expression, the relative expression of *TUBB1, TUBB5V4* and *TUBB4B* were compared between egg donor controls and recurrent pregnancy loss participants. Data were normally distributed, therefore presented as the mean and analysed by a t-test with Welch's correction which does not assume equal variance. This assumes that the standard deviations are different between patient groups.

To investigate the association of recurrent pregnancy loss and subfertility on β-tubulin protein expression, the proportion of cilia with β-tubulin was compared between groups. Samples were removed if there were less than three gland portion replicates per participant, if there were no cilia in the gland portions or if there were no glands in the endometrial tissue sample. Data were presented as the percentage of cilia in the gland portion positive for β-tubulin. Data were normally distributed, therefore presented as the mean and analysed by a t-test with Welch's correction.

5.4 Results

No significant differences were observed in clinical characteristics between participant groups investigating gene expression in endometrial glands, other than a significant increase in pregnancies and miscarriages in recurrent pregnancy loss participants versus controls (p < 0.01, Table 5.3).

No significant differences were observed in clinical characteristics between participant groups investigating protein expression in endometrial glands, other than a significant increase in pregnancies and miscarriages and age in recurrent pregnancy loss participants versus controls and age was significantly increased in recurrent pregnancy loss and subfertility participants versus controls (p < 0.01, Table 5.4).

Table 5.3 *Participant clinical characteristics (investigating gene expression in endometrial glands: RNA sequencing and targeted qPCR).*

Characteristic	Controls (n = 6) mean (SD)	RPL (n = 9) mean (SD)	PCD (n = 1)
Demographic characteristics			
Age	29.8 (5.2)	33.1 (3.5)	35.0
BMI	22.0 (2.2)	24.6 (2.7)	21.0
Menstrual cycle characteristics			
Day of menstrual cycle	20.8 (2.0)	23.0 (2.6)	23.0
Length of menstrual cycle	28.7 (0.9)	28.4 (1.5)	24.0
Fertility history			
Contraceptive use in last year	none	none	none
Number of pregnancies	0.5 (0.5)	6.3 (2.3) *	1.0
Number of miscarriages	0.0 (0.0)	5.3 (2.3) *	0.0
Met AMH criteria for egg donation	Yes	n/a	n/a

* = p < 0.01 indicates significantly different from control group, AMH = anti-mullerian hormone, n/a = not applicable.

Table 5.4 *Participant clinical characteristics (investigating protein expression in endometrial glands: wholemount immunohistochemistry).*

Characteristic	Controls (n = 11) mean (SD)	RPL (n = 18) mean (SD)	Subfertility (n = 9) mean (SD)
Demographic characteristics			
Age	29.3 (4.2)	33.6 (3.9) *	34.7 (4.8) *
BMI	23.7 (4.2)	25.6 (3.2)	25.8 (3.4)
Menstrual cycle characteristics			
Day of menstrual cycle	20.2 (1.8)	20.7 (2.0)	20.0 (2.9)
Length of menstrual cycle	28.5 (0.8)	27.8 (1.2)	26.5 (2.9)
Fertility history			
Contraceptive use in last year	none	none	none
Number of pregnancies	0.5 (0.5)	5.4 (1.9) *	1.4 (1.3)
Number of miscarriages	0.1 (0.3)	4.3 (2.0) *	0.1 (0.3)
Met AMH criteria for egg donation	Yes	n/a	n/a

* = $p < 0.01$ indicates significantly different from control group, AMH = anti-mullerian hormone, n/a = not applicable.

5.4.1 Gene expression (RNA-Seq) of endometrial glands in recurrent pregnancy loss

To determine whether the gene expression profile of isolated endometrial glands was altered in women with recurrent pregnancy loss, paired end RNA sequencing was carried out on five pairs of control vs recurrent pregnancy loss samples. Principle component analyses of paired samples and dispersion plot of normalised counts are shown in Appendix B. 19 genes were differentially expressed using a 5% FDR (Figure 5.2). Of these, 18 genes were upregulated and 1 gene was down regulated. Three of these genes also met a more stringent 1.25 log fold change threshold: *AKR1B10*, *SYT13* and *DPP4*.

Pathways containing genes that were significantly altered were identified via pathway analysis (Figure 5.3) and a full list of identified pathways, molecular functions and biological processes are listed in Appendix C.

The expression levels of known PCD genes, understood to associate to ciliary axonemal ultrastructure defects, in endometrial glands were compared between groups

(Figure 5.4). These results identify genes which could be targeted in future ciliary axonemal investigations.
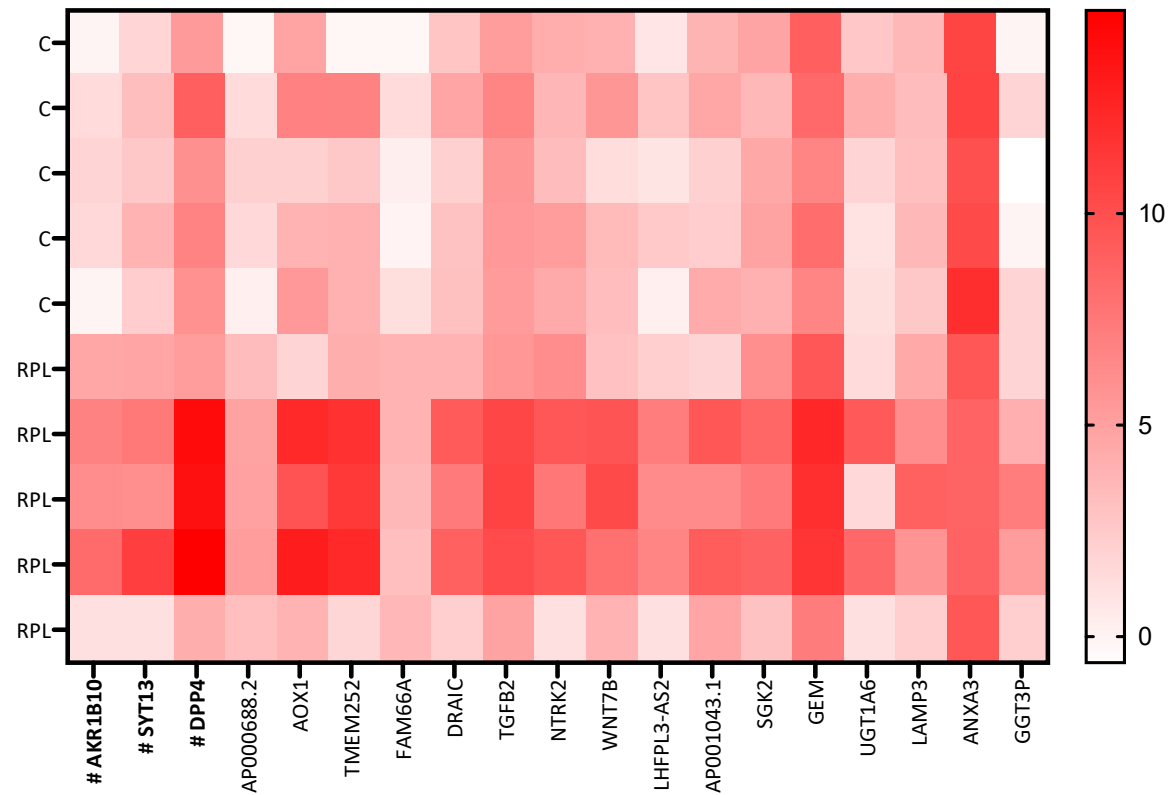
Figure 5.2 *Differentially expressed genes (p ≤ 0.05) in endometrial glands from women with recurrent pregnancy loss (RPL) versus controls (C). RNA-seq data presented as log base 2 normalised gene expression # indicate 1.25 log fold change threshold. Genes arranged by p value, lowest p value on the left.*
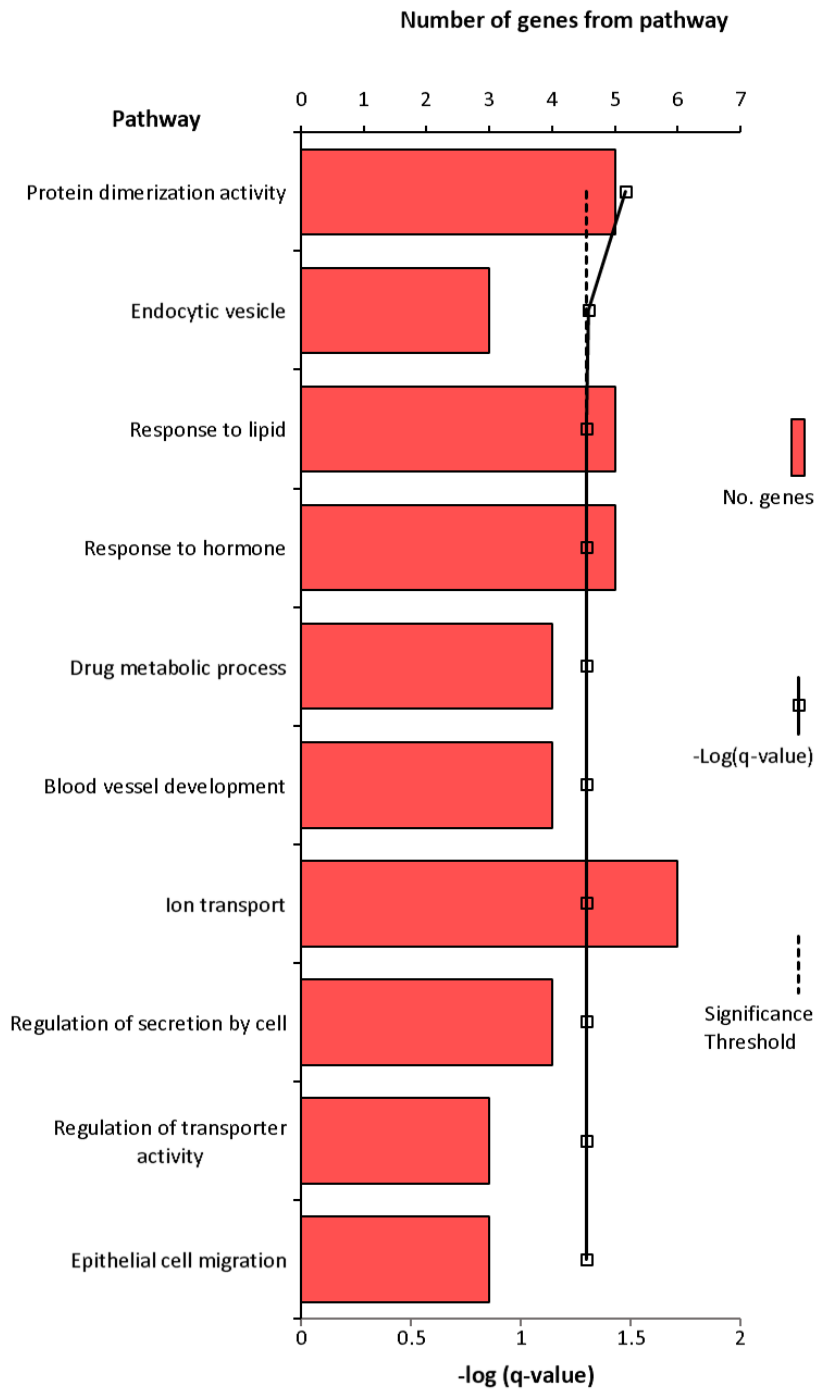
Figure 5.3 *Biological processes containing differentially expressed genes in endometrial glands from women with recurrent pregnancy loss. Data displayed as -log (FDR B&H corrected q value). Protein dimerization molecular function, endocytic vesicle cellular component, other pathways biological processes.*
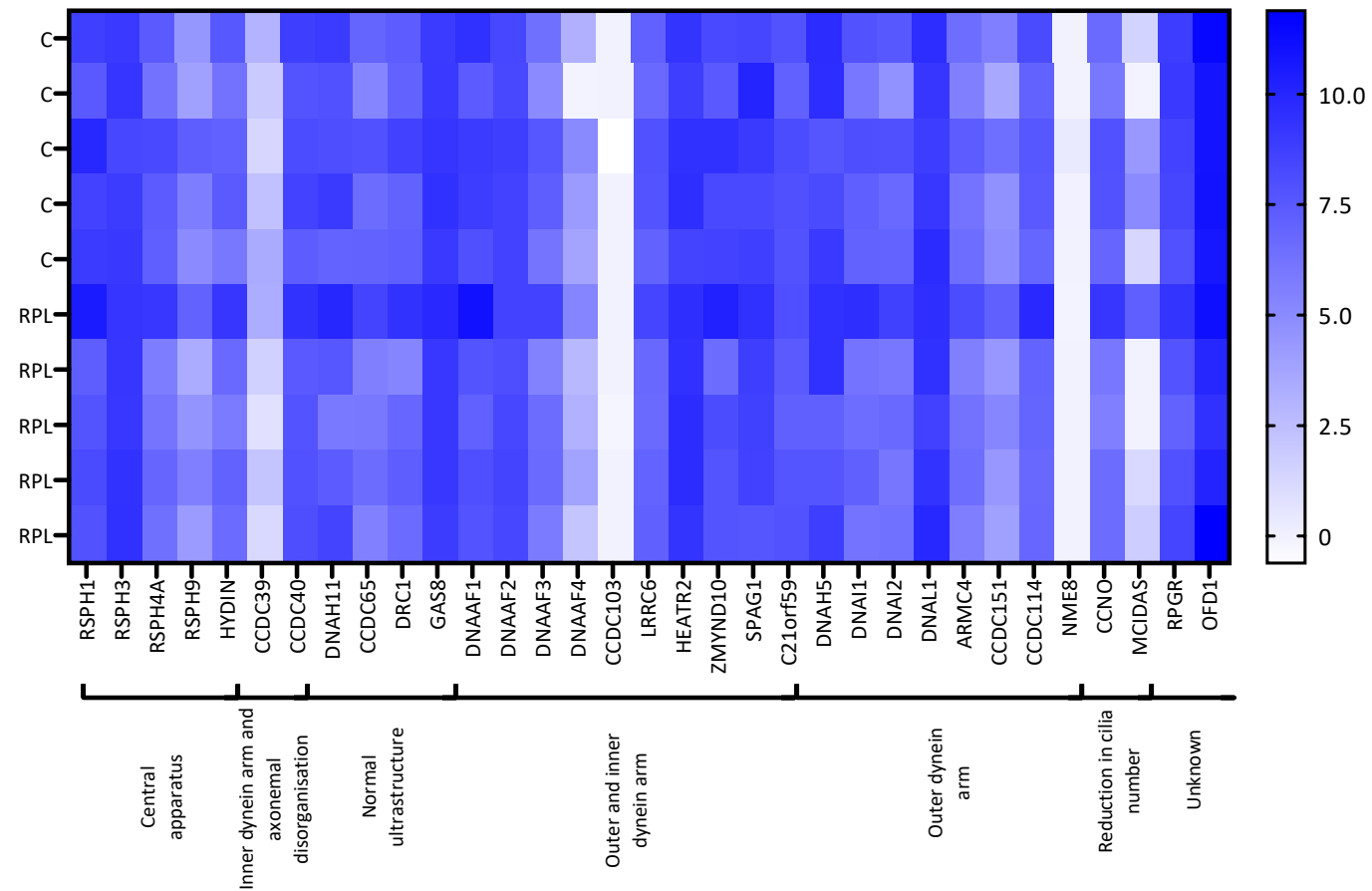
Figure 5.4 *Targeted analysis of known PCD genes associated with ciliary axonemal defects in endometrial glands. No significant differences were observed between control and recurrent pregnancy loss (RPL). RNA-seq data presented as log base 2 normalised gene expression.*

5.4.2 Endometrial gland β-tubulin in recurrent pregnancy loss and subfertility

B-tubulin protein expression

Wholemount immunohistochemistry and confocal fluorescence microscopy was applied to endometrial tissue biopsies, so as to investigate the association between β-tubulin in endometrial gland cilia and recurrent pregnancy loss and subfertility.

The proportion of cilia positive for TUBB5 protein, showed a decreasing trend in endometrial glands from women with recurrent pregnancy loss (n = 15) compared to controls (n = 9, p = 0.08, Figure 5.5A). Representative images of positive and absent TUBB5 ciliary staining inside endometrial glands (Figure 5.6, Video 5.1: https://youtu.be/3yWLBziNG6U, Video 5.2: https://youtu.be/lqhPW6uTmQs). Participants with a history of more than four prior miscarriages (n = 3) had a significant decrease in the proportion of cilia with positive TUBB5 expression compared to controls (n = 9, p = 0.02, Figure 5.5B). The proportion of β-tubulin expression in the endometrial glands of women with recurrent pregnancy loss showed a decreasing trend with menstrual cycle day for the general β-tubulin antibody (Figure 5.5C) and a bimodal population for TUBB5 antibody (Figure 5.5D). There was no association between the proportion of β-tubulin and cycle day, however the cycle length of non-control participants demonstrated a greater spread (Figure 5.5E and F).

In endometrial tissue where less β-tubulin staining was observed, β-tubulin staining was still present on the luminal epithelium (Figure 5.7). Paired whole endometrial tissue and isolated endometrial gland lysate were analysed by Western blotting. This demonstrated positive staining for the general β-tubulin antibody (clone 2-28-33, Sigma Aldrich SAB4200715) of unknown isoform specificity, and the specific mouse anti-human TUBB5 antibody (clone AA2, Abcam ab231082) marked ciliated cells positive for β-tubulin in whole endometrium and isolated endometrial glands. Further work is required to make study group comparisons. Western blotting optimisation, including the establishment of positive and negative controls, lysate extraction medium comparison and antibody dilutions are summarised in Appendix D.
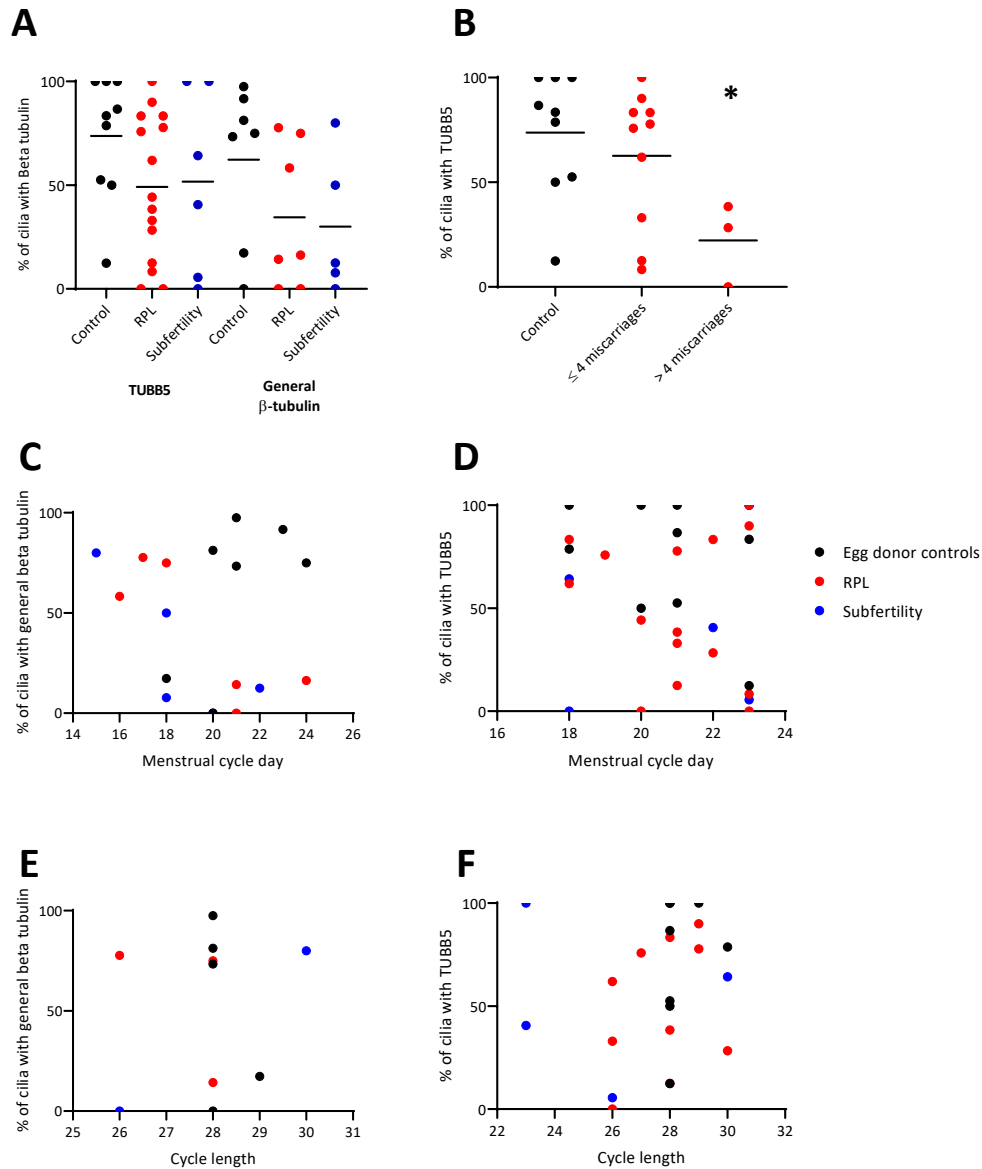
Figure 5.5 *Decreasing trends in beta-tubulin protein expression in endometrial gland portions between controls and women with recurrent pregnancy loss (RPL). Two beta-tubulin antibodies used, a TUBB5 antibody and a general TUBB antibody. A) The percentage of cilia positive for beta-tubulin and B) RPL group sub-divided by the number of miscarriages, data presented as the mean * p ≤ 0.05 indicates RPL different from control. C) The percentage of cilia with positive staining for general beta-tubulin antibody by menstrual cycle day and D) the percentage of cilia with positive staining for TUBB5 antibody by menstrual cycle day. E) The percentage of cilia with positive staining for general beta-tubulin antibody by cycle length and F) the percentage of cilia with positive staining for TUBB5 antibody by cycle length, all participants with irregular cycles are not included.*
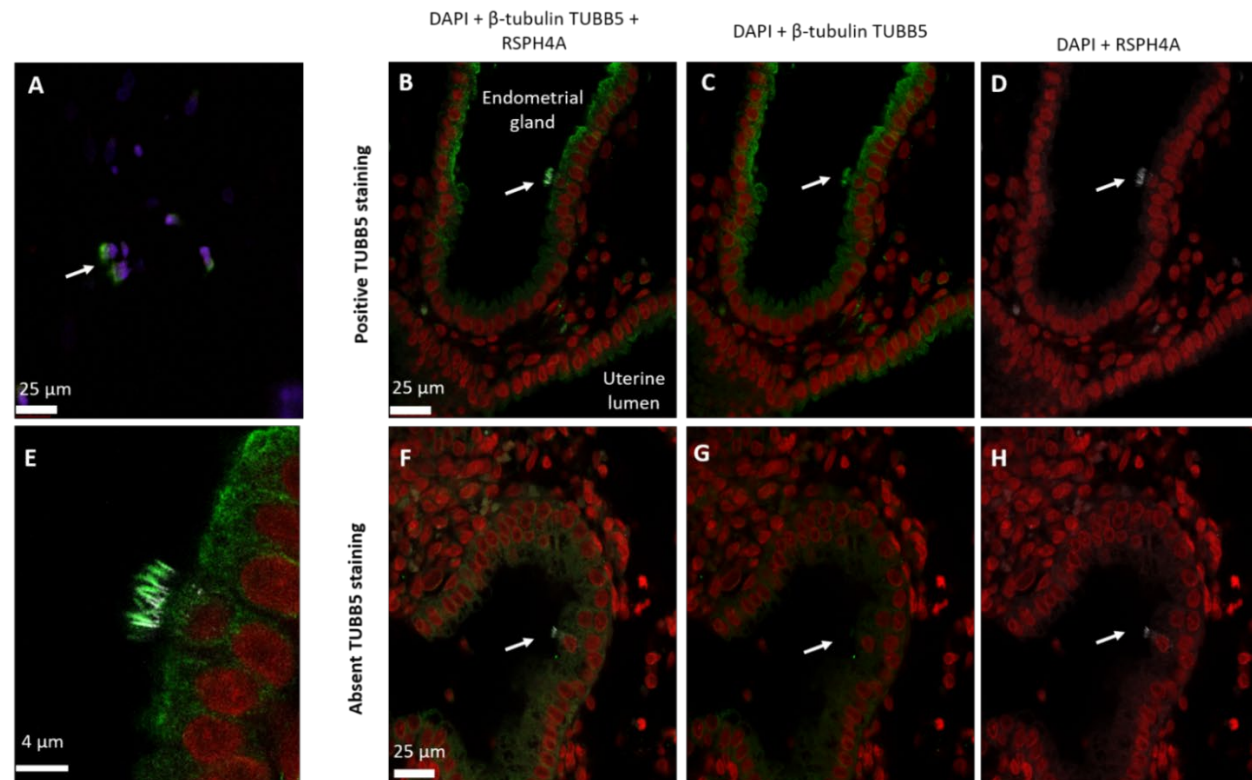
Figure 5.6 Representative images of positive or absent TUBB5 staining of glandular ciliated epithelial cells. A) Positive control nasal brushing ciliated epithelial cells (white arrow), cilia (green) and DAPI nuclei staining (blue). B C and D) Positive TUBB5 staining, DAPI nuclei staining (red), glandular ciliated epithelial cell (white arrow) cilia identified by the radial spoke head 4 homolog A (RSPH4A, white) and positive TUBB5 staining (green). E) A higher magnification image of ciliated epithelial cell with positive TUBB5 staining (green) and radial spoke head protein (white). F G and H) Absent TUBB5 staining from cilia.
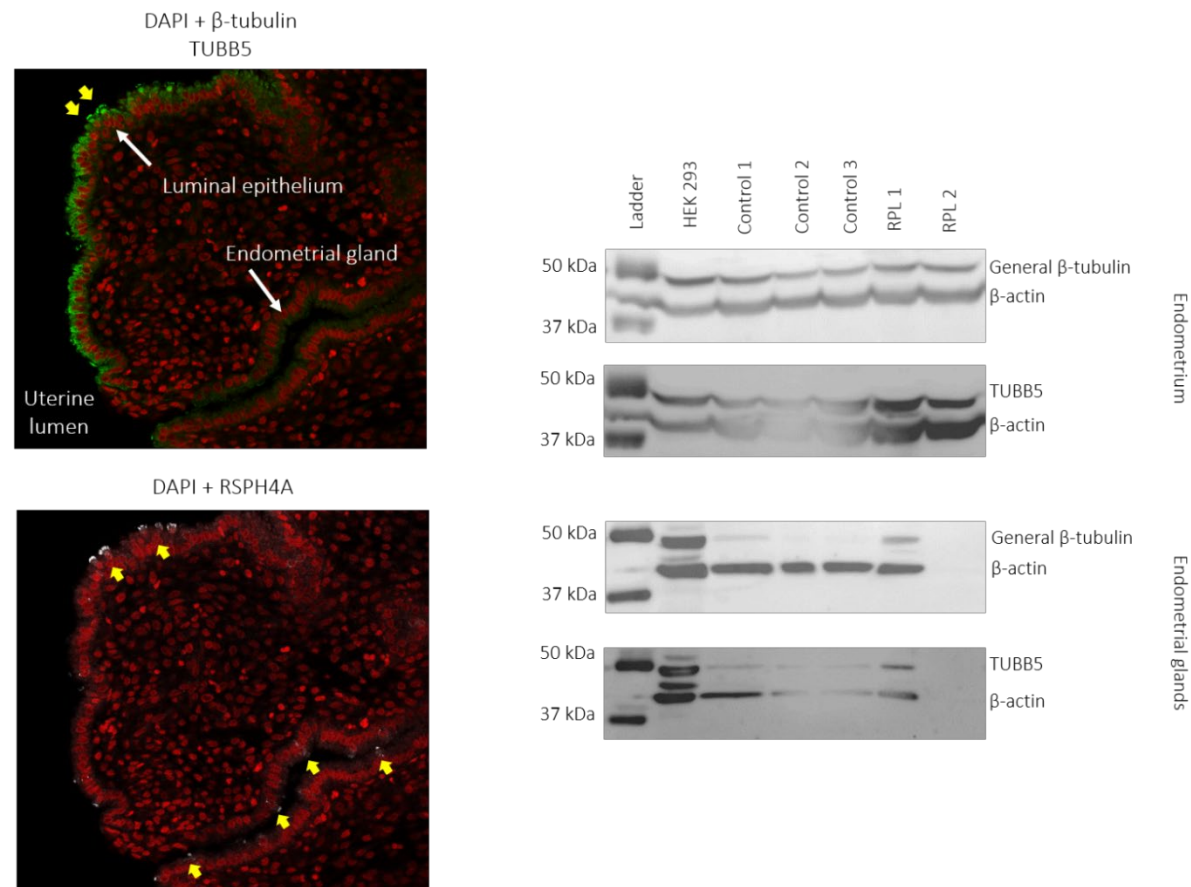
Figure 5.7 *Representative images of the luminal epithelium positive for beta-tubulin TUBB5 (green), compared to endometrial gland cilia (white) negative for beta-tubulin TUBB5. Provisional western blot of paired endometrium and isolated endometrial glands, of general beta-tubulin antibody (50 kDa) and TUBB5 (49 kDa). Loading control beta-actin (45 kDa).*

B-tubulin gene expression

The RNA sequencing data was used to identify β-tubulin genes present in endometrial glands during the implantation window of the menstrual cycle. When comparing the gene expression of nine known β-tubulin genes, *TUBB5* and *TUBB4B* were the two highest expressed β-tubulin genes in endometrial glands (Figure 5.8). There was no difference observed in endometrial gland β-tubulin gene expression between women with recurrent pregnancy loss and controls (Figure 5.8).

qPCR was carried out to compare β-tubulin gene expression and β-tubulin gene transcript variants expression in endometrial glands from women with recurrent pregnancy loss compared to controls. *TUBB5* has 6 known transcript variants, where *TUBB5V4* was investigated. *TUBB5V4* mRNA expression was significantly increased in endometrial glands from women with recurrent pregnancy loss (n = 9) compared to controls (n = 5, p = 0.03, Figure 5.9) There was no significant alteration in *TUBB4B* and *TUBB1* mRNA expression in endometrial glands from women with recurrent pregnancy loss compared to controls. These results, however, confirm these β-tubulin isoforms are present inside endometrial glands. There was no association between the relative mRNA expression of *TUBB5V4*, *TUBB1* and *TUBB4B* and menstrual cycle day (Figure 5.10). There was also no association between the relative mRNA expression of TUBB5V4 and TUBB1 and cycle length, however there was a decreasing trend between the relative mRNA expression of TUBB4B and cycle length (Figure 5.10).
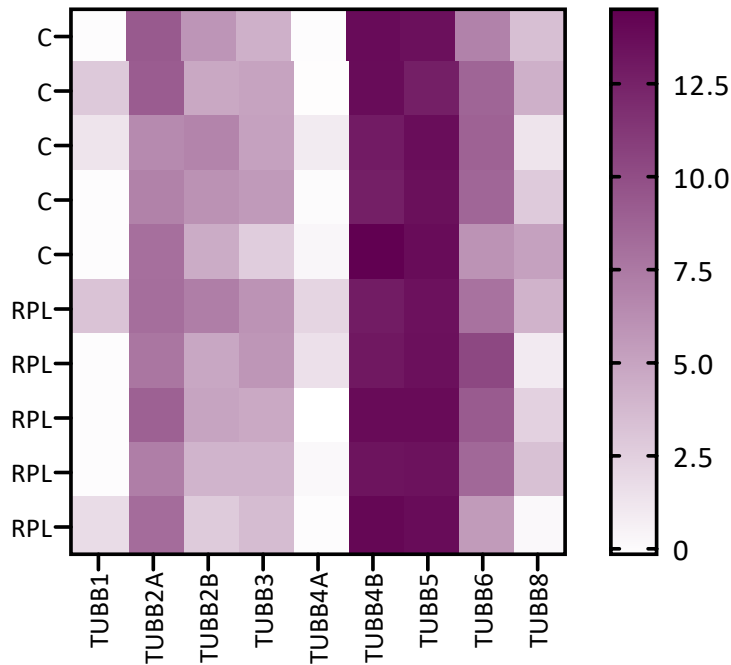
Figure 5.8 *Targeted analysis of beta-tubulin gene expression in endometrial glands. No differences were observed between control and recurrent pregnancy loss (RPL). RNA-seq data presented as log base 2 normalised gene expression.*
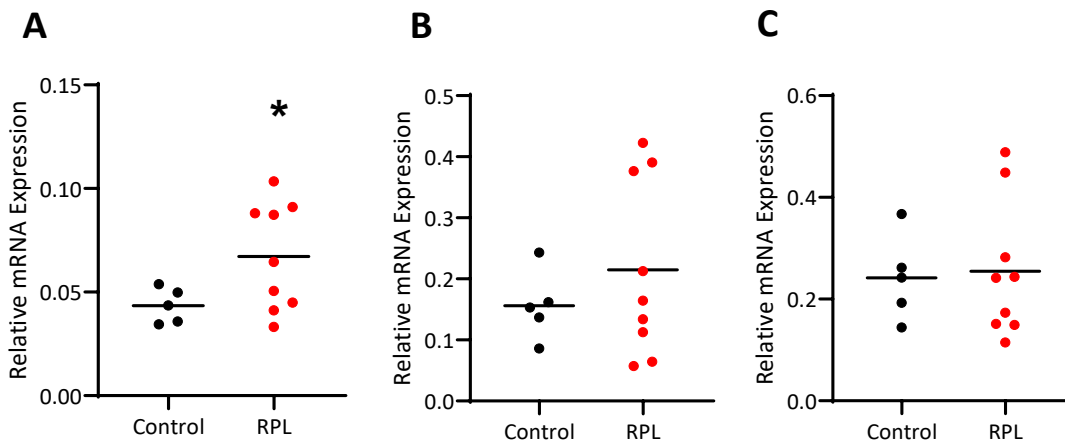
Figure 5.9 *Relative mRNA expression of beta-tubulin genes **A)** TUBB5V4, **B)** TUBB1 and **C)** TUBB4B in endometrial gland samples from control and recurrent pregnancy loss (RPL) participants. Lines indicate the mean of each group, * p ≤ 0.05 indicates a significant difference from control.*
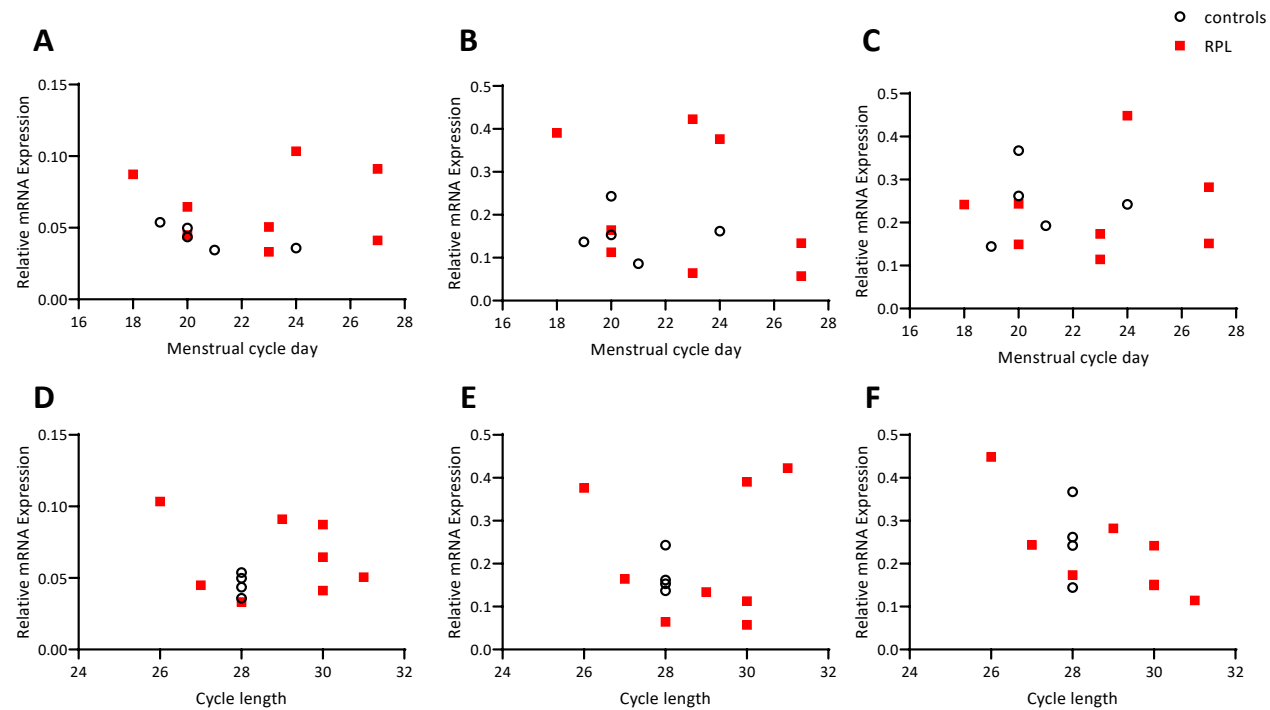
Figure 5.10 *No associations were observed between relative mRNA expression of glandular ciliated epithelial TUBB54V and TUBB1 and menstrual cycle characteristics between controls and women with recurrent pregnancy loss (RPL).* ***A and D)*** *TUBB5V4,* ***B and E)*** *TUBB1.* ***C)*** *No association between relative mRNA expression of TUBB4B and menstrual cycle day.* ***F)*** *A decreasing trend between the relative mRNA expression of TUBB4B and cycle length.*

5.5 Discussion

This chapter has described the gene expression profile of the glandular epithelium from controls and women with recurrent pregnancy loss during the window of implantation (LH + 7 - 10 days). Glandular ciliated epithelial cell β-tubulin isoform enrichment was established and shown to be altered in women with recurrent pregnancy loss.

Endometrial gland transcriptome in recurrent pregnancy loss

This study has established a differential gene expression profile of isolated endometrial glands from women with recurrent pregnancy loss compared to controls. Freshly isolating endometrial glands allowed the glandular epithelium to be investigated separately from the luminal epithelium, therefore overcoming previous study limitations of FACS sorting the endometrium into the total epithelial cells and total stromal cells (Krjutškov et al., 2016).

The differentially expressed genes identified in our study show similarities to genes identified in the receptive endometrium compared to the non-receptive endometrium. However there are no similarities between our study and previous microarray studies comparing whole endometrium between recurrent pregnancy loss and fertile controls (Othman et al., 2012). This could be that glandular epithelium gene expression changes could have been obscured by other endometrial cell types. Stromal specific upregulated genes, *APOD*, *CFD*, *C1R* and *DKK1*, were present in our endometrial gland RNA sequencing data set. These genes, however are highly expressed in the epithelium as well (Altmäe et al., 2017).

Our study identified that *DPP4* and *LAMB3* are upregulated in the glandular epithelium of women with recurrent pregnancy loss. These findings align with previous studies reporting that *DPP4* and *LAMB3* are upregulated in epithelial cells rather than the stromal cells (Altmäe et al., 2017). *DPP4* and *LAMB3* were also on the gene panel of the endometrial receptivity array (Díaz-Gimeno et al., 2010). Comparison to previous studies suggests these genes are associated with a receptive endometrium. Our study, however,

focuses on endometrial glands, providing a more accurate account of where gene expression changes are occurring.

DPP4 has previously been associated with one of four endometrial epithelial cell subsets identified in control endometrium who were awaiting IVF procedures with good prognosis (Lucas et al., 2020). An increase in *DPP4* gene expression in endometrial glands from women with recurrent pregnancy loss could be due to an increase or proportional change in endometrial epithelial cell subtypes. Endometrial glands could have a higher proportion of the epithelial cell subtype enriched in *DPP4* than the luminal epithelium. Droplet generating single cell sequencing (Drop-seq) could be performed on isolated endometrial glands, comparing the glandular epithelium from women with recurrent pregnancy loss and controls. This would help establish if the proportion of epithelial cell types was altered in the glandular epithelium of recurrent pregnancy loss. Again this would give locational information, and demonstrate where gene expression changes are occurring compared to performing Drop-seq on whole endometrium.

In our study, the upregulation of *DPP4* and *WNT7B* in the glandular epithelium of women with recurrent pregnancy loss were associated with epithelial cell migration and endocytic vesicles. Exosomes may fuse with the plasma membrane of the target cell or they may be endocytosed. Previous research has associated DPP4 and LAMB3 proteins with exosomes (Altmäe et al., 2017). This could suggest increased production of exosomes during the window of implantation in women with recurrent pregnancy loss. This study observed a down regulation of *ANXA3* in the glandular epithelium from women with recurrent pregnancy loss. Down regulation of *ANXA3* could impact on epithelial function by altered cellular signal transduction. Other annexin family members identified in the mid-secretory endometrium, *ANXA2* and *ANXA4*, are associated with exosomes and upregulated in epithelial cell types during mid-secretory phase endometrium in healthy women (Altmäe et al., 2017). To investigate if *DPP4*, *WNT7B* and *ANXA3* are differentially expressed in glandular exosomes or other extracellular vesicles, endometrial gland extracellular vesicles could be extracted from glands by aspirating the fluid from the glandular lumen by microinjection.

The Wnt/β-catenin pathway has been reported to facilitate endometrial gland formation. *WNT7B* upregulation observed in our study could be an overcompensation for impaired glandular function, as a depletion of β-catenin has been associated to fertility defects in mice (Jeong et al., 2009). Altered gene expression in the Wnt signalling pathway may also influence glandular ciliated epithelial cell ion signalling and cilia beat function (Sreekumar & Norris, 2019; Wheway et al., 2018).

TGFB2 is associated with hormone response cell secretion regulation and epithelial migration. Endometrial hormonal profiles regulate the menstrual cycle and ovulation, defining the start of the luteal phase. Changes to hormonal responses by the glandular epithelium such as progesterone receptors could be influenced by an increase in *TGFB2* expression (Snijders et al., 1992). This could be one factor that accounts for cycle length variation seen in the RNA-sequencing data. The genotype *TGFB1* has previously been associated with recurrent pregnancy loss (Magdoud et al., 2013).

Our study provides, for the first time, a gene expression profile of the endometrial gland epithelium from controls and women with recurrent pregnancy loss. This work takes the first steps to identifying a gene expression profile of the glandular epithelium separate from the luminal epithelium. qPCR could be performed to validate the list of differentially expressed genes. To relate gene expression changes to endometrial gland 3D structural changes, proteins could be quantified by the 3D imaging methods described in this chapter.

Endometrial gland β-tubulin in recurrent pregnancy loss and subfertility

Our study demonstrates β-tubulin gene enrichment in glandular ciliated epithelial cells. Glandular ciliated epithelial cells have a preference for *TUBB5* and *TUBB4B* isoforms, both of which are associated with motile cilia beat function (Vent et al., 2005). Imaging of endometrial tissue pieces confirmed glandular β-tubulin was localised to ciliated epithelial cells. However, glandular ciliated epithelial cells β-tubulin isoform enrichment would have also taken into account other cellular compartments such as mitotic spindles for DNA segregation. General β-tubulin protein expression reflected the RNA-sequencing data showing no change between clinical groups. However when individual β-tubulin isoforms and gene transcript variants were investigated, differences were observed in endometrial

glands from women with recurrent pregnancy loss glands on a gene expression level and a protein expression level.

In our study, not all cases of recurrent pregnancy loss demonstrate increased *TUBB5V4* expression, and decreased TUBB5 protein expression. One suggestion is that different β-tubulin isoforms were present in the ciliary microtubule lattice and therefore not detected. This suggests that recurrent pregnancy loss could be associated with a different proportion of β-tubulin isoforms compared to egg donor controls, associated with an altered β-tubulin enrichment (Girotra et al., 2017). Alternatively, β-tubulin isoforms in the glandular epithelium from women with recurrent pregnancy loss could be more or less prone to post translational modifications preventing the antibody from binding to the β-tubulin epitope (Kubo et al., 2010; Vent et al., 2005).

In our study decreased TUBB5 protein expression was not observed on the luminal ciliated epithelial cells. This suggests that the luminal epithelial ciliated cells and glandular ciliated epithelial cells could have different β-tubulin enrichments or they are more or less prone to post-translational modifications. A lack of tubulin post-translational modifications have been associated with an altered ciliary beat (Kubo et al., 2010), which could have a direct impact upon the movement of glandular products. This is supported by altered glandular secretions in recurrent pregnancy loss (Dalton et al., 1998; Mikołajczyk, et al., 2003). Western blotting analysis of isolated glandular epithelium protein could be performed to identify which β-tubulin isoforms are present from women with recurrent pregnancy loss compared to controls. Antibody probes raised specifically to post-translational proteins such as glutamylases could also be applied to isolated endometrial gland protein lysates (Pathak et al., 2011). Methods to perform Western blotting on isolated endometrial gland lysate have been established in this thesis.

Other ciliopathies are prone to a set of gene mutations which alter the spliceosome machinery dictating mRNA transcripts understood to differ between tissue types (Wheway et al., 2015). Differential expression of β-tubulin gene transcripts may be due to mutations to spliceosome machinery causing changes in alternative splicing in recurrent pregnancy loss. Alternatively, placenta from women with recurrent pregnancy loss has been

associated with downregulation of genes involves in the spliceosome (Sõber et al., 2016). Changes to spliceosome gene expression could be pre-established in the decidualised endometrium. Performing a transcript differential expression analysis on β-tubulin between glandular epithelium in recurrent pregnancy loss compared to controls will help identify how β-tubulin isoforms are changing in recurrent pregnancy loss. RNA immuno-precipitation experiments could also be performed on the glandular epithelium to identify RNAs associated with spliceosome proteins. RNA identified could then be quantified by RNA sequencing or qPCR (Wu et al., 2020).

Altered tubulin function could be the primary cause of ciliary dysfunction. It might be expected however that people with reduced ciliary function to also experience the symptoms of PCD, however this is not observed. Environmental factors impacting on ciliary function may not be present in the airways, and the airways do not undergo cyclic and receptivity changes like that of the endometrium. Pairing these samples with live cilia beat analysis will also allow an association to be made between glandular ciliated epithelial β-tubulin and glandular ciliated epithelial beating. Progress in this work would establish biomarkers that predispose recurrent pregnancy loss or potential therapeutic targets.

5.6 Limitations

There were limitations to what could be achieved in this study, due to the same clinical sample restraints described in chapter 3 and chapter 4. For this study, egg donor control and recurrent pregnancy loss paired samples were matched for RNA-sequencing by the day of the menstrual cycle. The day of the menstrual cycle was self-reported, therefore would have been less accurate than if the LH surge was timed by using ovulation sticks. The window of implantation is typically considered to be LH +7 - 10 but because of sample availability this study used samples from LH + 4 - 10. The results in this study were not changed if samples from only the standard implantation window were considered (LH + 7 – 10).

The R package DESeq2 is a differential expression analysis based on the negative binomial modal. DESeq2 demonstrated a high dispersion variability for low and high gene

counts and high within group variability. This could be due to the small sample size or the outlier cut off point dictated by the model. qPCR experiments could be performed to validate differentially expressed genes and gene targets associated with an underlying biology.

This study identified which β-tubulin genes were expressed in the glandular epithelium by RNA-sequencing, however it did not identify all β-tubulin isoforms that were expressed at a protein level. Antibodies raised specifically to other β-tubulin isoforms could be applied to gland portions as described in this study to quantify the protein expression of all β-tubulin isoforms. Alternatively, proteomics could be carried out on the glandular epithelium.

This study did not identify if glandular cilia β-tubulin isoforms are associated with post-translational modifications. Post translational modifications could be identified using proteomics or alternatively Western blotting could be performed on glandular epithelial lysate with antibodies raised to post-translational modification proteins.

5.7 Future work

Future work aims to investigate other *TUBB5* gene transcript variants by qPCR and immunohistochemistry analysis, to decipher their contribution towards overall *TUBB5* gene expression, and subsequent β-tubulin isoform enrichment. The results of which can be correlated to cilia function, by the recording of cilia beat function in freshly prepared samples.

RNA sequencing could be carried out on a cellular level by droplet generation single cell RNA sequencing. Sequencing isolated endometrial glands by single cell sequencing will allow glandular sub cell signatures to be established, and how this is changing in endometrial glands from women with recurrent pregnancy loss and subfertility. Glandular cell signatures, β-tubulin isoform enrichment, 3D image analysis and live cell imaging together will allow us to determine how molecular changes relate to the 3D glandular epithelium and cilia beat function.

5.8 Conclusion

This study has paired 3D image analysis of endometrial gland portions with RNA sequencing and targeted qPCR to investigate glandular ciliated epithelial β-tubulin. Uncovering changes to the glandular epithelium only, alternatively to all endometrial epithelium, provides a more targeted data set which can be related to glandular function. These findings demonstrate for this first time that changes to mRNA expression and semi-quantitate protein expression of TUBB5 in the glandular ciliated epithelium may associate with recurrent pregnancy loss. A paired 3D imaging and differential gene expression analysis can be applied to other β-tubulin isoforms to build a picture of all β-tubulins

Chapter 6   General discussion

The underlying causes of recurrent pregnancy loss are not fully understood. Endometrial gland structure and function during the window of implantation have been associated with recurrent pregnancy loss and infertility, however limitations in 2D imaging have meant endometrial structures have been under-represented.

Using a stepwise multi-modal and multi-scale approach, I have shown that 3D quantitative image analysis can be applied to glandular structures from a tissue level down to glandular sub-cellular components. I have characterised glandular 3D structures and identified a glandular gene expression pattern that would have otherwise been obscured by other endometrial cell types. Combining 3D imaging of endometrial glands with their cilia beat function provides a 4-dimensional approach. In this chapter, I will summarise my findings and discuss the implications pertaining to future work.

6.1   Endometrial 3D architecture in health and disease

By quantifying the endometrial architecture in 3D I have provided a new, informative perspective on stromal-epithelial spatial relationships in pieces of endometrial tissue. Two key findings of chapter 3 were clustered uNK cells and stromal cells and an altered spatial relationship between uNK cells and endometrial glands in the endometrium from women with recurrent pregnancy loss endometrium compared to controls. Analysing endometrial tissue volumes provides a more representative uNK cell measurement compared to 2D tissue sectioning. This study does not only demonstrate it is possible to quantify 3D spatial relationships between endometrial stroma and epithelial cells but reinforces an increase in uNK cell density in recurrent pregnancy loss endometrium reported in previous studies (Chen et al., 2017; Kuon et al., 2017; Quenby et al., 1999).

The 3D spatial arrangements of uNK cells and stromal cells provides insight into the underlying biology. An increased uNK cell density and clustering in recurrent pregnancy loss endometrium may be associated with uNK cell clearance of heightened senescent decidualised cells, regulating endometrial homeostasis during the window of implantation (Brighton et al., 2017; Lucas et al., 2020). Alternatively, altered 3D spatial cell arrangements in recurrent pregnancy loss endometrium could be associated with an altered signal

propagation from the decidualised stroma essential to tissue remodelling and the activation of uNK cells (Faridi & Agrawal, 2011).

For the first time, this thesis quantifies endometrial stromal cell to glandular 3D spatial relationships, however further work is required to understand stromal – epithelial function. This could be performed by investigating other endometrial cell types such as macrophages, dendritic cells and T-cells. uNK cell subpopulations are characterised by different KIR receptor regions. The bi-modal recurrent pregnancy loss population observed in the stromal-epithelial spatial relationships could be due to changes in uNK subtypes characterised by different KIR receptor regions. This could be investigated further by performing the spatial relationship methodology applied in this thesis on antibodies raised to specific uNK subtypes. Different uNK cell subtypes could differentially impact on uNK KIR receptor to trophoblast HLA interactions during embryo implantation (Faridi & Agrawal, 2011).

Manual labelling of uNK cell and stromal cell nuclei in endometrial tissue volumes was a time-consuming process. Fast and accurate automated image segmentation with machine learning techniques coupled with artificial intelligence could help prepare samples for 3D image analysis (Lewis and Pearson Farr 2020). The resolution used in this study was a compromise between cellular detail and tissue volume. If these methods were to be repeated on other endometrial cell types more advanced lightsheet microscopy could be used which images large tissue volumes while maintaining high cellular resolution (L. A. Chu et al., 2019). If automated endometrial stromal-epithelial spatial relationship analysis could be achieved, these methods could be adopted clinically and incorporated into routine uNK clinical measurements and thus modernise endometrial dating (Liu et al., 2014; Chiokadze et al., 2019).

By quantifying 3D endometrial architecture and stromal-epithelial spatial relationships, I have not only highlighted a spatial arrangement for endometrial cell types but also shown that these spatial arrangements change in recurrent pregnancy loss endometrium. This has implications for clinical biopsy testing and endometrial dating.

6.2 Endometrial gland 3D architecture in health and disease

By applying a multi-modal 3D imaging approach to endometrial gland cell types, I have characterised glandular ciliated epithelium structure and function. Two key findings of chapter 4 were beat function of glandular ciliated epithelial cells and the production of microvesicles on microvillus tips. These findings highlight the potential of 3D imaging in studying and quantifying complete endometrial structures. SBFSEM microscopy and 3D reconstruction contain large datasets which were time consuming to analyse. I used semi-automated segmentation methods to help speed up this process, which could be developed further to include artificial intelligence processes (Lewis and Pearson Farr 2020).

For the first time, I used live imaging approaches of freshly isolated endometrial glands to study glandular ciliated epithelial cell function. Although live cell preparations are short lived, this approach provided a more physiologically representative model for studying the function of glandular ciliated epithelial cells compared to current organoid culture models (Turco et al., 2017). A limitation of live imaging freshly isolated endometrial gland portions however, is that they cannot be orientated to the luminal surface. Live imaging ciliated epithelial cells form current diagnostic approaches in respiratory ciliopathies such as PCD. Following further investigation with larger sample numbers this quick technique has the potential to be a clinical tool providing fast results for the patient. Future research can pair live cilia beating with 2D and 3D ultrastructural analysis, providing a multi-modal 4-dimensional approach to studying endometrial glands.

The observation made that microvesicles are formed on the tips of glandular epithelial microvilli identifies one mechanism by which microvesicles are produced in the uterus. This is a novel form of microvesicle production which has only been observed previously on placental microvilli (personal communication, Rohan Lewis). Microvesicles found in the uterus of health women (Simon et al., 2018) could be an ad hoc mixture of glandular and luminal epithelial origin. Endometrial gland microvesicles and protein secretions are understood to target an implanting trophoblast (O'Neil et al., 2020). These microvesicles may be part of the signalling pathway for the embryo and the luminal

epithelium to facilitate the creation of the optimal endometrial environment for successful implantation and pregnancy development.

It is unclear regarding the fate of the microvesicles observed, and their transport from the endometrial gland to the endometrial surface. Although my observation of cilia within the gland described in this thesis suggests that the movement of microvesicle is likely to be cilia-facilitated, the role of synchronous versus nonsynchronous cilia beating pattern still needs to be determined. One possible hypothesis is that the beating cilia creates a fluid circulation, and serves to equilibrate glandular contents, and where necessary, the outward transport of microvesicles and other glandular products. Impaired synchronicity in cilia beat may result in an abnormal uterine environment for an implanting embryo or may disrupt signal transduction by way of hindered microvesicle transport (summarised in Figure 6.1). This theory is supported in part by the observed reduction in glandular secretions of MUC-1, LIF and Glycodelin, in the uterine flushing's of women with recurrent pregnancy loss (Dalton et al., 1998; Mikołajczyk, et al., 2003).

The simultaneous presence of cell types specialising in secretory and absorption functions within the endometrial glands is an interesting observation. It is plausible that the proportion of glandular microvillus and ciliated cells vary depending on the stage of the menstrual cycle, reflecting endometrial receptivity. Performing 3D imaging and the spatial relationship analysis methods I describe in chapter 3 on different glandular cell types during the window of implantation may help to determine the relationship between ciliated and microvillus glandular cell types.

Using 3D imaging, I described the observation that microvesicles are formed on the apical aspects of the glandular epithelial microvilli, in addition to demonstrating nonsynchronous cilia beat within the glandular ciliated epithelial cells during the window of implantation. These findings may have implications on how the endometrial glands create a favourable environment for an implanting embryo.
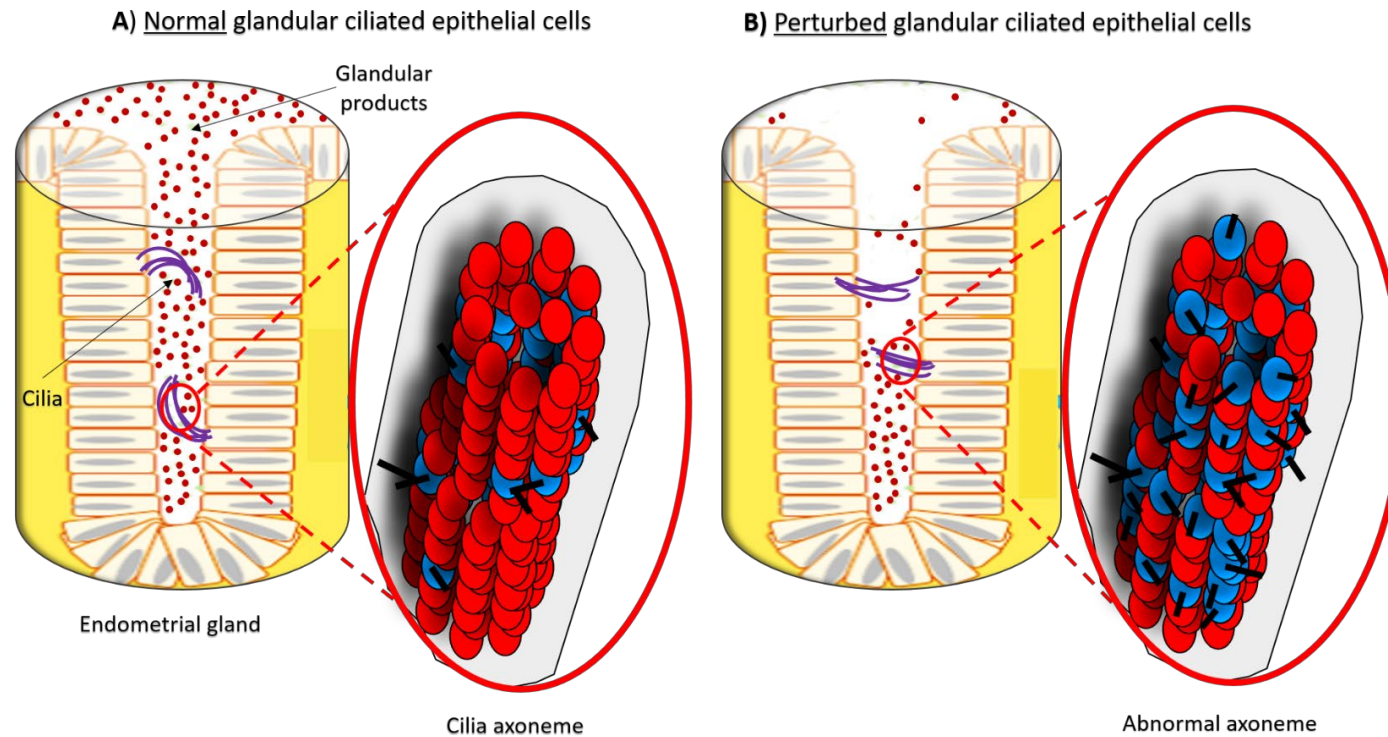
Figure 6.1 *Proposed implications of thesis findings. **A)** Normal glandular ciliated epithelial cells, the cilia beats effectively to maintain a homeostatic fluid circulation of glandular secretions and microvesicles, promoting a favourable environment for embryo implantation. The cilia axoneme is made up of different beta-tubulin isoforms (blue and red). One beta-tubulin isoform is more prone to post translational modifications (black line). **B)** In the perturbed glandular ciliated epithelial cells, the cilia beat mechanics are altered resulting in a potential non-favourable environment for embryo implantation. Cilia axoneme β-tubulin isoform proportions may be altered, leading to more post translational modifications known to impair cilia function.*

6.3   Endometrial gland transcriptome in recurrent pregnancy loss

Previously, I have focused on novel 3D architectural findings of the endometrium and endometrial glands during the window of implantation. By isolating endometrial glands from a fresh endometrial biopsy, I was also able to determine the glandular transcriptome in isolation from other endometrial cell types. By comparing the transcriptome of endometrial glands between control and recurrent pregnancy loss, I have made the first steps to identify a set of genes in the endometrial glands of women with recurrent pregnancy loss.

Differentially expressed genes in the glandular epithelium from women with recurrent pregnancy loss were associated with cell secretion regulation and epithelial migration pathways. Changes to cell secretion and epithelial migration could have implications on the glandular function globally. For example, increased gene expression of cell secretion regulation could be an over compensation for reduction of glandular secretions seen in recurrent pregnancy loss groups (Dalton et al., 1998; Mikołajczyk, et al., 2003). Alterations to genes in the Wnt/β-catenin pathway could alter glandular epithelium regeneration impairing glandular function, shown previously by fertility defects in β-catenin mutant mice (Jeong et al., 2009). Finally ciliated epithelial cells are understood to sense environmental cues via ion signalling. Changes to ion signalling could impact on cilia beat function and in turn movement or mixing of glandular secretory products (Sreekumar & Norris, 2019). The extent to which glandular ciliated cells are impacted by their environment, stem cell epigenetics and gene mutations is not established and could be investigated in the future.

Future studies could be performed on a larger sample size and validated by qPCR. Different glandular subtypes will have specific gene expression signatures relevant to their role. Droplet generation single-cell RNA sequencing could be performed on isolated endometrial glands as previously carried out on whole endometrium (Lucas et al., 2020). This would enable glandular cell signatures to be identified alone, unobscured by luminal epithelial cell types. Future work could also pair single cell RNA sequencing to targeted 3D image analysis in participant samples, to relate the relevant gene expression changes to

glandular cell type and location. Finally, alternation in cilia gene expression can also be related to glandular cilia beat function.

By applying RNA sequencing to endometrial glands, I was able to determine the glandular transcriptome in isolation from other endometrial cell types. I also identified differentially expressed genes in endometrial glands from women with recurrent pregnancy loss associated with cell secretion and epithelial migration. Differentially expressed genes in the endometrial glands of women with recurrent pregnancy loss can further supplement the current literature on useful biomarkers in endometrial receptivity.

6.4 Glandular ciliated epithelial cell β-tubulin in recurrent pregnancy loss

Previously, I have shown that my 3D imaging data characterises complete glandular ciliated epithelial cells, and I have shown that my glandular gene expression data identifies potential biomarker gene targets. In chapter 5, I combined quantitative 3D analysis with differential gene expression analysis of endometrial glands to investigate glandular ciliated epithelial β-tubulin and its association with recurrent pregnancy loss.

Two key findings of chapter 5 were identifying β-tubulin gene enrichment in endometrial glands and reporting altered relative gene expression and protein expression of β-tubulin isoform TUBB5 in endometrial glands from women with recurrent pregnancy loss compared to controls.

My work on β-tubulin gene enrichment identifies which β-tubulin isoforms are present in endometrial glands, highlighting possible mechanistic targets for future work. Post translational modifications of the tubulin C' terminus tail of the heterogeneous family of β-tubulin isoforms could in turn influence the efficacy of ciliary beat mechanics and therefore a favourable environment for embryo implantation (summarised in Figure 6.1) (Kubo et al., 2010). Alternatively, the endometrium of women with recurrent pregnancy loss may favour alternative splicing of particular tubulin transcript variants (Wheway et al., 2015). This may explain the increased gene expression of TUBB5 transcript variant 4 and the overall decrease in TUBB5 protein expression in recurrent pregnancy loss. The bi-modal

recurrent pregnancy loss population observed in β-tubulin gene expression and protein expression may also be a result of altered β-tubulin gene transcript variants.

More work needs to be performed on β-tubulin isoforms and their gene transcript variants identified by β-tubulin enrichment to delineate the role of β-tubulin isoform on endometrial gland biology, and its possible pathophysiology in women with recurrent pregnancy loss. Collating the live analysis of cilia beat function with the gene expression and 3D architectural analysis of glandular cilia β-tubulin will undoubtedly provide significant insight not only into the pathophysiology but also into the potential therapeutics of recurrent pregnancy loss.

Glandular ciliated epithelial cell β-tubulin is altered in recurrent pregnancy loss endometrium at the protein and the gene expression level. Future work to identify the associative β-tubulin isoforms and transcript variants in recurrent pregnancy loss phenotype is now needed.

6.5 Linking physiological understanding to clinical implication and future direction

Environmental influences

The variation in results in this thesis in women with recurrent pregnancy loss leads to questions regarding a woman's environment, and if this had an influence on endometrial gland architecture and function. Cilia function in the airways has been demonstrated to be regulated by environmental factors such as air pollution and smoking (Cao et al., 2020; Shah et al., 2009). Long term air pollution or obesity could impact on the menstrual cycle and therefore gland function. Future work could perform an additional data analysis to associate endometrial gland structure and function with clinical characteristics, such as BMI and smoking status, to determine if there are any correlations.

Translating uNK spatial relationships into standardised uNK measurements

My findings in chapter 3 highlight that the spatial distribution of stromal cells may not be uniform and could relate to endometrial gland distribution. Endometrial 3D architecture could help clinical endometrial biopsy sampling and 2D tissue sectioning

analysis by overcoming limitations of endometrial tissue sectioning. Applying 3D spatial relationship analysis to larger tissue volumes or a higher number of replicate tissue volumes per participant could be more representative of the endometrium as a whole and reflect different regions of the endometrium. These could include stroma cells close to the luminal surface and stroma cells close to the endometrial glands. Advanced lightsheet microscopy allows larger tissue volumes to be imaged while maintaining cellular resolution (L. A. Chu et al., 2019). Progress in this area could be applied to endometrial dating and standardising uNK cell results between clinical centres (Chiokadze and Kristesashvili 2019).

Glandular ciliated epithelial cell function

In this thesis, I have established a pipeline to isolate and assess cilia beat function inside intact endometrial gland portions, within 3.5 h of endometrial biopsy collection. Analysing glandular ciliated epithelial cells by high-speed video could be a quick method of testing cilia beat function in a clinical setting. High-speed video is already used in the clinical diagnostics of PCD (Lucas et al., 2017). To develop this work further, high-speed video analysis could first be performed on a larger number of isolated endometrial gland samples and compared between egg donor controls, recurrent pregnancy loss and recurrent implantation failure. Parameters that could be quantified include the average cilia beat frequency and the number of motile cilia in the gland portion. These results would help us understand if there is an association between cilia beat function, recurrent implantation failure and recurrent pregnancy loss.

Further work could also investigate glandular ciliated epithelial cell beat synchronicity. Fluorescent beads could be introduced to isolated endometrial glands and detected under the confocal laser scanning microscope to detect the directional movement of glandular products. Alternatively, fluorescent beads could be attached to the tips of cilia and detected via the confocal microscope to determine cilia beat coordination within one multi-ciliated cell and between multiple multi-ciliated cells in a gland portion (Katoh et al., 2018). Performing these experiments could not only provide insight into glandular ciliated epithelial cell beat mechanics, but also take steps to designing a potential diagnostic tool that could analyse endometrial cilia beat coordination, not just inside the endometrial glands but also on luminal ciliated epithelial cells.

Glandular biomarkers of a receptive endometrium

Differential gene expression patterns of isolated endometrial glands joint with altered glandular 3D architectural findings may provide biomarkers of a receptive endometrium during the window of implantation that predispose recurrent pregnancy loss. My findings in chapter 5 demonstrate that β-tubulin isoform TUBB5 gene and protein expression are altered in endometrial glands from women with recurrent pregnancy loss. Future work could apply these methods to other β-tubulin isoforms and their respective transcript variants to understand how all β-tubulin isoforms are functioning in endometrial glands. However these methods do not target glandular ciliated epithelial cells. The axoneme could be isolated from ciliated cells and analysed by mass spectrometry to identify which β-tubulin isoforms are present (Blackburn et al., 2017). A more targeted approach to investigating β-tubulin isoforms in glandular ciliated epithelial cells would confirm the changes to β-tubulin observed in clinical groups are of cilia origin.

From the glandular epithelium to the luminal epithelium

In this thesis, I have applied multi-modal 3D imaging alone and in combination with RNA sequencing and targeted qPCR to establish the structure, function and gene expression profile of endometrial glands during the window of implantation. These findings provide more representative results of endometrial glands as they are not obscured by luminal epithelial cells. Future work could apply the techniques describe in this thesis to the luminal epithelium. This would allow both structural and functional comparisons to be made between the glandular and luminal epithelium during the window of implantation, when the endometrium is potentially receptive to an implanting blastocyst.

Droplet generation single cell RNA sequencing could also be carried out to identify gene signatures for glandular and luminal subtypes. Performing gene expression analysis on a single cell level will provide context to epithelial subtypes and generate insight into their contribution to the endometrial phenotype as a whole, both in healthy endometrium and in recurrent pregnancy loss.

6.6 Summary

In summary, the aims of this thesis were addressed by investigating the association between glandular structure and function and recurrent pregnancy loss during the window of implantation using a multi-scale approach. My findings suggest that the 3D spatial relationship between stromal cells and endometrial glands was altered in recurrent pregnancy loss endometrium. Complete 3D glandular ciliated cells were constructed and quantified in a control cohort. A differential gene expression profile was determined in recurrent pregnancy loss endometrial glands. Finally, β-tubulin expression was altered in recurrent pregnancy loss glandular epithelium on both a gene level and a protein level. My stepwise multi-scale and multi-modal 3D imaging approach have identified that glandular ciliated cell can be impaired; such findings cannot be observe with the traditional 2D diagnostic techniques. The endometrium with perturbed glandular ciliated cells may be non-conducive to embryo implantation and development (summarised in Figure 6.1). This work proposes new avenues for future diagnostics and therapeutics

Appendix A   Image analysis details

Fiji Image J macro batch processing cell count and cell-cell distances:

```
dirIn = getDirectory("Choose the folder with the 3D stacks");

dirOut = getDirectory("Select a folder for the distance txt files");

list = getFileList(dirIn);

Array.sort(list);

setBatchMode(true);

for(i=0; i<list.length; i++){

        open(dirIn+list[i]);

        Title = getTitle();

        stackName = File.nameWithoutExtension;

        selectWindow(Title);

        run("Properties...", "channels=1 slices=47 frames=1 unit=pixel pixel_width=0.24
pixel_height=0.24 voxel_depth=1.807 global");

        run("3D Manager");

        Ext.Manager3D_Segment(1, 255);

        Ext.Manager3D_AddImage();

        Ext.Manager3D_Distance();

        Ext.Manager3D_SaveResult("D", dirOut + stackName + "_distance.csv");

        Ext.Manager3D_SelectAll();

        Ext.Manager3D_Delete();

        run("Close All");

}

        exit("END OF MACRO");
```

Fiji Image J macro batch processing cell clustering:

```
dirIn = getDirectory("Choose the folder with the 3D stacks");
dirOut = getDirectory("Select a folder for the SDI log files");
list = getFileList(dirIn);
Array.sort(list);
setBatchMode(true);
for(i=0; i<list.length; i++){
            open(dirIn+list[i]);
            Title = getTitle();
            stackName = File.nameWithoutExtension;
            selectWindow(Title);
            run("Duplicate...", "duplicate");
            makeRectangle(10, 4, 1002, 1010);
            setForegroundColor(223, 0, 0);
            run("Fill", "stack");
            selectWindow(Title);
            run("Restore Selection");
            run("Spatial Analysis 2D/3D", "g nb_points=10000 samples=100
            distance=0.000 error=5 spots=sample mask=sample multithread=10
            draw_color=Red show save");
            selectWindow("Log");
            saveAs("Text", dirOut + stackName + "_log.txt");
            close();
            close();
            close();
            selectWindow(Title);
            close();
            close();
}
            exit("END OF MACRO");
```

Fiji Image J macro batch processing 3D distance mapping:

```
dirIn = getDirectory("Choose the folder with the 3D stacks");

dirOut = getDirectory("Select a folder for the binary centroid stack");

list = getFileList(dirIn);

Array.sort(list);

setBatchMode(true);

for(i=0; i<list.length; i++){

        open(dirIn+list[i]);

        Title = getTitle();

        stackName = File.nameWithoutExtension;

        run("8-bit");

        run("Multiply...", "value=255.000 stack");

        run("3D OC Options", "centroid dots_size=1 font_size=10
store_results_within_a_table_named_after_the_image_(macro_friendly)
redirect_to=none");

        run("3D Objects Counter", "threshold=128 slice=23 min.=1 max.=49283072
centroids summary");

        selectWindow(Title);

        close();

        selectWindow("Log");

        saveAs("Text", dirOut + stackName + "_log.txt");

        run("Close");

        saveAs("Tiff", dirOut + stackName + "_CentroidMap.tif");

        run("8-bit");

        setAutoThreshold("Default dark");

        //run("Threshold...");

        setThreshold(1, 255);

        //setThreshold(1, 255);

        setOption("BlackBackground", false);

        run("Convert to Mask", "method=Default background=Dark");

        run("Invert LUT");

        run("Divide...", "value=255 stack");

        saveAs("Tiff", dirOut + stackName + "_CentroidMap_Binary.tif");

        close();

}exit("END OF MACRO");
```

Cilia isolation and quantification workflow in Avizo:

1) Import binary stack (correct voxel size)

2) Import grey scale stack (for reference)

3) Reslice at a 45 degree angle

4) Convert your image type to 8 bit label

5) In segmentation tab double check your binary segmentation against your grey scale images, and check cilia are not joined

6) Erosion module in the x/y plane

7) Label analysis, select 3D parameters

8) 2) label module convert image type to 8 bit unsigned

9) Auto-skeleton module

10) Spatial graph statistics module

11) Spatial graph view

Appendix B   RNA sequencing of endometrial glands
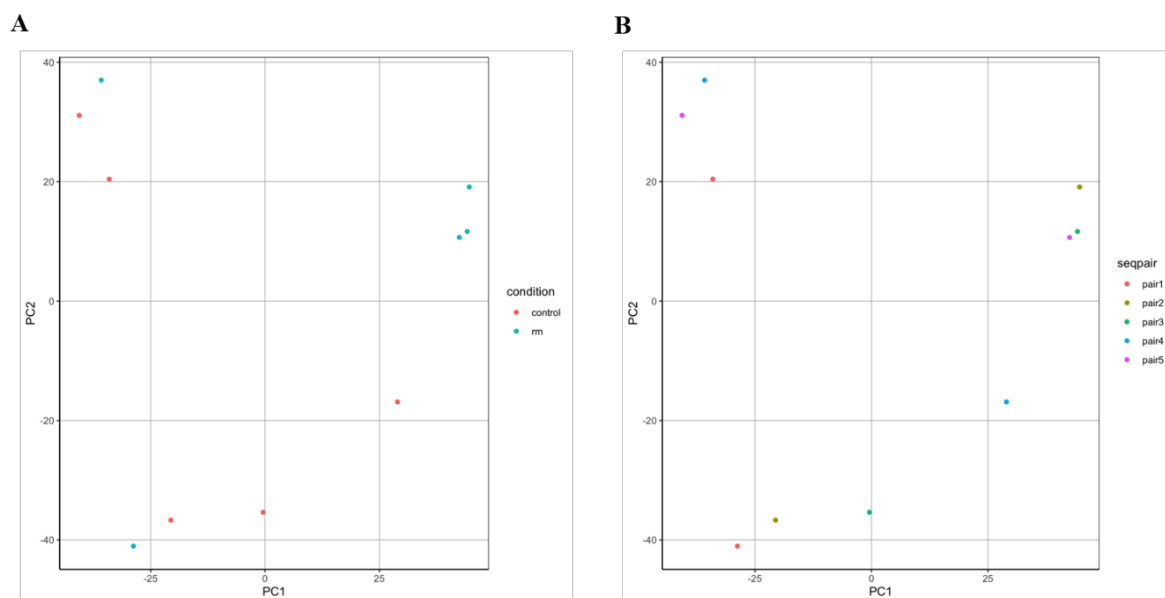
Figure 6.2 *Principle component analysis results of endometrial gland RNA sequencing dataset.* **A)** *Comparing recurrent pregnancy loss (rm) to egg donor controls and* **B)** *samples represented by their pairs matched by the day of the menstrual cycle.*
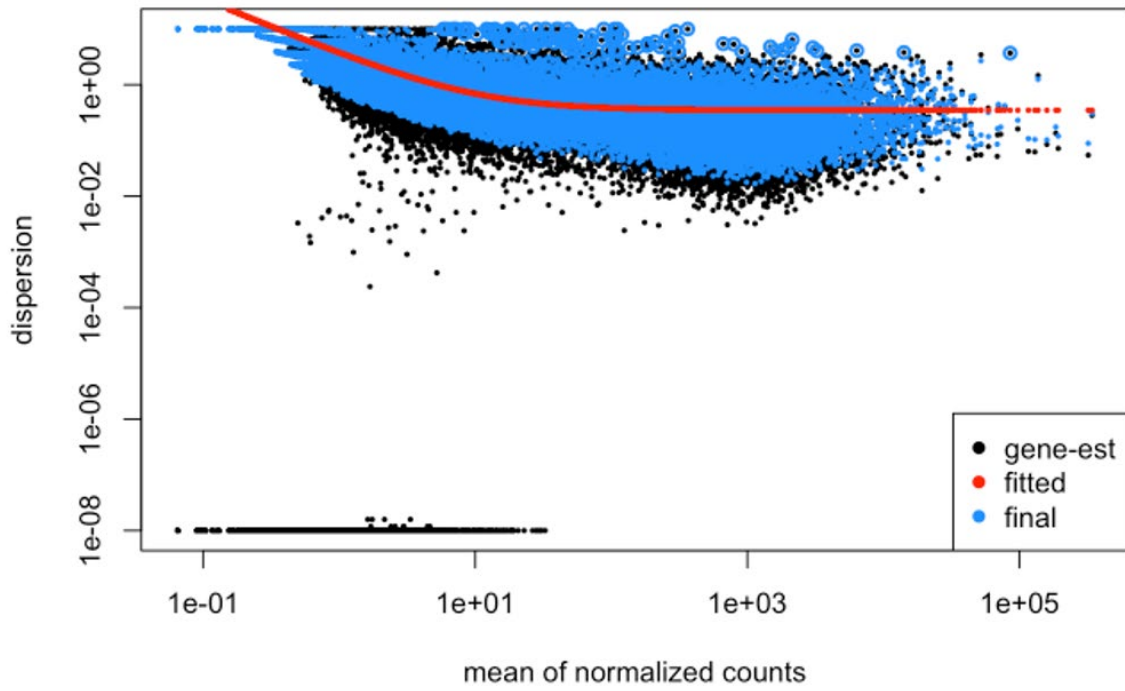
Figure 6.3 *Dispersion plot of normalised gene counts from RNA sequencing dataset of endometrial glands.*

Appendix C Pathway analysis

Table 6.1 *All pathways with altered gene expression in endometrial glands from women with recurrent pregnancy loss compared to egg donor controls. Data displayed as FDR B&H corrected q-value.*

Category	Name	q-value	Gene(s)
Molecular function	protein homodimerization activity	0.0272	TGFB2,DPP4,UGT1A6,NTRK2,AOX1
	geranial:oxygen oxidoreductase activity	0.0272	AOX1
	heptaldehyde:oxygen oxidoreductase activity	0.0272	AOX1
	retinal oxidase activity	0.0272	AOX1
	calcium-dependent phospholipid binding	0.0272	SYT13,ANXA3
	oxidoreductase activity, acting on CH or CH2 groups, NAD or NADP as acceptor	0.0272	AOX1
	aldehyde oxidase activity	0.0272	AOX1
	geranylgeranyl reductase activity	0.0272	AKR1B10
	brain-derived neurotrophic factor-activated receptor activity	0.0272	NTRK2
	oxidoreductase activity, acting on the aldehyde or oxo group of donors, oxygen as acceptor	0.0272	AOX1
	xanthine dehydrogenase activity	0.0272	AOX1
	indanol dehydrogenase activity	0.0331	AKR1B10
	chemoattractant activity involved in axon guidance	0.0331	WNT7B
	brain-derived neurotrophic factor binding	0.0331	NTRK2
	type III transforming growth factor beta receptor binding	0.0331	TGFB2
	allyl-alcohol dehydrogenase activity	0.0331	AKR1B10
	exopeptidase activity	0.0331	DPP4,GGT3P
	hypoglycin A gamma-glutamyl transpeptidase activity	0.0331	GGT3P
	leukotriene C4 gamma-glutamyl transferase activity	0.0331	GGT3P
	phospholipase A2 inhibitor activity	0.0331	ANXA3
	peptidyltransferase activity	0.0331	GGT3P
	ion channel regulator activity	0.0331	GEM,SGK2

	protein dimerization activity	0.0331	TGFB2,DPP4,UGT1A6,NTRK2,AOX1
	molybdopterin cofactor binding	0.0374	AOX1
	neurotrophin receptor activity	0.0419	NTRK2
	channel regulator activity	0.0424	GEM,SGK2
	retinal dehydrogenase activity	0.0424	AKR1B10
	type II transforming growth factor beta receptor binding	0.0424	TGFB2
	cation channel activity	0.0424	GEM,ANXA3,SGK2
	glutathione hydrolase activity	0.0438	GGT3P
	oxidoreductase activity, acting on the aldehyde or oxo group of donors	0.0438	AKR1B10,AOX1
Biological Process	regulation of extracellular matrix disassembly	0.05	TGFB2,DPP4
	response to steroid hormone	0.05	TGFB2,ANXA3,NTRK2,WNT7B
	apoptotic process involved in morphogenesis	0.05	TGFB2,WNT7B
	response to lipid	0.05	TGFB2,ANXA3,NTRK2,WNT7B,GGT3P
	regulation of extracellular matrix organization	0.05	TGFB2,DPP4
	apoptotic process involved in development	0.05	TGFB2,WNT7B
	regulation of cell adhesion mediated by integrin	0.05	TGFB2,DPP4
	response to hormone	0.05	TGFB2,ANXA3,NTRK2,WNT7B,GGT3P
	response to organic cyclic compound	0.05	TGFB2,ANXA3,NTRK2,WNT7B,GGT3P
	negative regulation of calcium ion transmembrane transport	0.05	TGFB2,GEM
	positive regulation of activation-induced cell death of T cells	0.05	TGFB2
	substantia propria of cornea development	0.05	TGFB2
	outer medullary collecting duct development	0.05	WNT7B
	chemoattraction of dopaminergic neuron axon	0.05	WNT7B
	cell adhesion mediated by integrin	0.05	TGFB2,DPP4
	ion transport	0.05	TGFB2,GEM,SYT13,ANXA3,NTRK2,SGK2
	regulation of transporter activity	0.05	GEM,ANXA3,SGK2
	xanthine catabolic process	0.05	AOX1
	farnesol catabolic process	0.05	AKR1B10
	farnesol metabolic process	0.05	AKR1B10
	sesquiterpenoid catabolic process	0.05	AKR1B10
	uterine wall breakdown	0.05	TGFB2

renal outer medulla development	0.05	WNT7B
establishment or maintenance of polarity of embryonic epithelium	0.05	WNT7B
negative regulation of cardiac epithelial to mesenchymal transition	0.05	TGFB2
renal inner medulla development	0.05	WNT7B
trans-synaptic signaling by neuropeptide, modulating synaptic transmission	0.05	NTRK2
negative regulation of epithelial to mesenchymal transition involved in endocardial cushion formation	0.05	TGFB2
sesquiterpenoid metabolic process	0.05	AKR1B10
menstruation	0.05	TGFB2
negative regulation of calcium ion transport	0.05	TGFB2,GEM
blood vessel morphogenesis	0.05	TGFB2,ANXA3,NTRK2,WNT7B
drug metabolic process	0.05	TGFB2,GGT3P,AKR1B10,AOX1
extracellular matrix disassembly	0.05	TGFB2,DPP4
camera-type eye development	0.05	TGFB2,NTRK2,WNT7B
positive regulation of phosphatidylinositol 3-kinase signaling	0.05	TGFB2,NTRK2
regulation of ion transport	0.05	TGFB2,GEM,SYT13,ANXA3
epithelial cell migration	0.05	TGFB2,DPP4,ANXA3
epithelium migration	0.05	TGFB2,DPP4,ANXA3
cation transport	0.05	TGFB2,GEM,SYT13,ANXA3,SGK2
apoptotic process involved in outflow tract morphogenesis	0.05	TGFB2
inner medullary collecting duct development	0.05	WNT7B
positive regulation of timing of catagen	0.05	TGFB2
regulation of apoptotic process involved in outflow tract morphogenesis	0.05	TGFB2
positive regulation of integrin biosynthetic process	0.05	TGFB2
polyprenol catabolic process	0.05	AKR1B10
trans-synaptic signaling by neuropeptide	0.05	NTRK2
xanthine metabolic process	0.05	AOX1
tissue migration	0.05	TGFB2,DPP4,ANXA3
vasculogenesis	0.05	NTRK2,WNT7B

	blood vessel development	0.05	TGFB2,ANXA3,NTRK2,WNT7B
	regulation of cation transmembrane transport	0.05	TGFB2,GEM,ANXA3
	negative regulation of cation transmembrane transport	0.05	TGFB2,GEM
	positive regulation of ossification	0.05	TGFB2,WNT7B
	vasculature development	0.05	TGFB2,ANXA3,NTRK2,WNT7B
	head development	0.05	TGFB2,ANXA3,NTRK2,WNT7B
	eye development	0.05	TGFB2,NTRK2,WNT7B
	cardiovascular system development	0.05	TGFB2,ANXA3,NTRK2,WNT7B
	regulation of secretion by cell	0.05	TGFB2,DPP4,SYT13,NTRK2
	positive regulation of GTP binding	0.05	TGFB2
	purine nucleobase catabolic process	0.05	AOX1
	synaptic signaling via neuropeptide	0.05	NTRK2
	psychomotor behavior	0.05	DPP4
	ascending aorta morphogenesis	0.05	TGFB2
	trans-synaptic signaling by BDNF, modulating synaptic transmission	0.05	NTRK2
	regulation of timing of catagen	0.05	TGFB2
	trachea cartilage morphogenesis	0.05	WNT7B
	endocardial cushion fusion	0.05	TGFB2
	trans-synaptic signaling by BDNF	0.05	NTRK2
	menstrual cycle phase	0.05	TGFB2
	visual system development	0.05	TGFB2,NTRK2,WNT7B
Cellular Component	endocytic vesicle	0.049	DPP4,ANXA3,WNT7B
	lamellar body membrane	0.049	LAMP3
	alveolar lamellar body membrane	0.049	LAMP3
Pathway	Nicotine degradation	0.0138	UGT1A6,AOX1
	Pentose and glucuronate interconversions	0.0282	UGT1A6,AKR1B10
	Vitamin B6 metabolic	0.0424	AOX1
	Retinol metabolism	0.0478	UGT1A6,AOX1
	Drug metabolism - cytochrome P450	0.0478	UGT1A6,AOX1

Appendix D   Western blotting optimisation
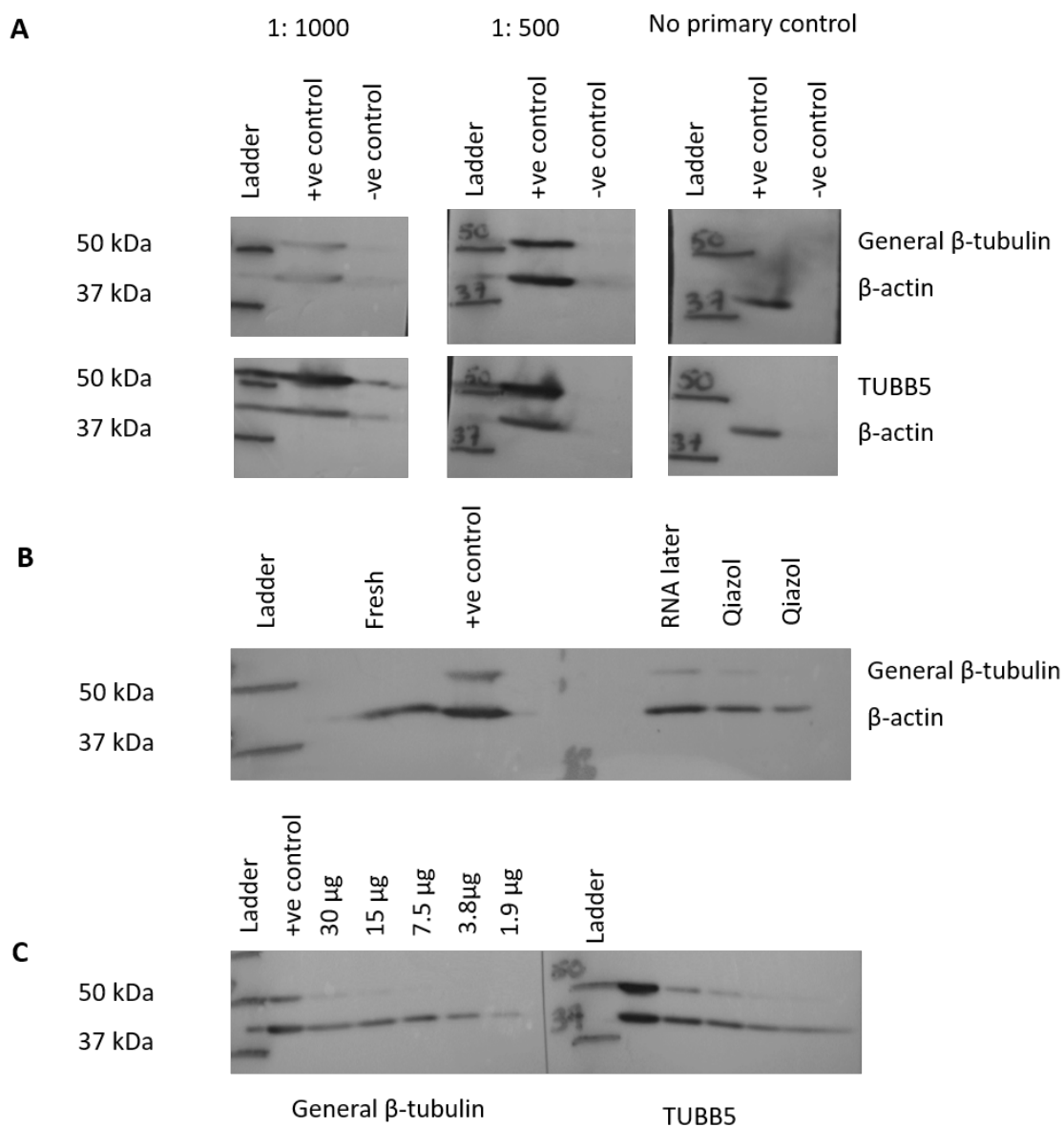
Figure 6.4 *Optimisation of the Western blotting protocol for β-tubulin antibodies in whole endometrium and isolated endometrial glands.* **A)** *Positive HEK 293 and negative bacteria β-tubulin controls were established, optimal 1:500 dilution for general β-tubulin antibody and further dilution of TUBB5 antibody, as 1:1000 demonstrated anti-bands,* **B)** *Qiazol extracted protein fraction gave a positive result similar to RNAlater® extracted samples.* **C)** *Double dilution demonstrated 15 μg was the lowest protein concentration to provide an antibody signal.*

Appendix E Abstracts

- Novel insights into 3D endometrial tissue and cellular architecture during preimplantation, in women with recurrent miscarriage. Pearson-Farr. J.E., Lewis. R., Cheong. Y. (ESHRE, 2018)
- Novel insights into 3D endometrial tissue and cellular architecture during implantation, in women with recurrent miscarriage. Pearson-Farr. J.E., Lewis. R., Cheong. Y. (Centre for Trophblast Research Annual Meeting, 2018)
- Multiscale imaging of cilia in endometrial glands. Pearson-Farr, J, Chatelet, D, Goggin, P, Page, A., Lewis, R.M., Cheong, Y. (Society of Electron Microscopy Technology Annual Meeting, 2018)
- Multiscale 3D imaging: a useful approach for the study of endometrial glandular architecture in healthy women. Pearson-Farr. J.E., Lewis. R., Cheong. Y. (ESHRE, 2019)
- Multiscale 3D imaging approach to study endometrial gland architecture in healthy women. Pearson-Farr. J.E., Lewis. R., Cheong. Y. (Centre for Trophblast Research Annual Meeting, 2019)

List of References

Alcázar, J. L. (2006). Three-dimensional ultrasound assessment of endometrial receptivity: A review. *Reproductive Biology and Endocrinology, 4*(56).

Altmäe, S., Koel, M., Võsa, U., Adler, P., Suhorutšenko, M., Laisk-Podar, T., … Salumets, A. (2017). Meta-signature of human endometrial receptivity: A meta-analysis and validation study of transcriptomic biomarkers. *Scientific Reports, 7*(1).

Andrey, P., Kiêu, K., Kress, C., Lehmann, G., Tirichine, L., Liu, Z., … Debey, P. (2010). Statistical analysis of 3D images detects regular spatial distributions of centromeres and chromocenters in animal and plant nuclei. *PLoS Computational Biology, 6*(7).

Arce, C. A., Rodriguez, J. A., Barra, H. S., & Caputto, R. (1975). Incorporation of l-Tyrosine, l-Phenylalanine and l-3,4-Dihydroxyphenylalanine as Single Units into Rat Brain Tubulin. *European Journal of Biochemistry, 59*(1), 145–149.

Arora, R., Fries, A., Oelerich, K., Marchuk, K., Sabeur, K., Giudice, L. C., & Laird, D. J. (2016). Insights from imaging the implanting embryo and the uterine environment in three dimensions. *Development, 143*, 4749-4754.

Artis, D., & Spits, H. (2015). The biology of innate lymphoid cells. *Nature, 517*(7534), 293–301.

Ashkar, A. A., Di Santo, J. P., & Croy, B. A. (2000). Interferon γ Contributes to Initiation of Uterine Vascular Modification, Decidual Integrity, and Uterine Natural Killer Cell Maturation during Normal Murine Pregnancy. *The Journal of Experimental Medicine*, *192*(2), 259–270.

Aunapuu, M., Kibur, P., Järveots, T., & Arend, A. (2018). Changes in Morphology and Presence of Pinopodes in Endometrial Cells during the Luteal Phase in Women with Infertility Problems: A Pilot Study. *Medicina, 54*(5).

Bahar, L., Kahraman, S., Eras, N., & Pirkevi, C. (2015). Comparison of endometrial biopsies

of fertile women and women with repeated implantation failure at the ultrastructural level. *Turkish Journal of Medical Sciences, 45*(3), 706–713.

Barker, N., van Es, J. H., Kuipers, J., Kujala, P., van den Born, M., Cozijnsen, M., … Clevers, H. (2007). Identification of stem cells in small intestine and colon by marker gene Lgr5. *Nature, 449*(7165), 1003–1007.

Bartosch, C., Lopes, J. M., Beires, J., & Sousa, M. (2011). Human Endometrium Ultrastructure During the Implantation Window. *Reproductive Sciences, 18*(6), 525–539.

Bastide, P., Darido, C., Pannequin, J., Kist, R., Robine, S., Marty-Double, C., … Jay, P. (2007). Sox9 regulates cell proliferation and is required for Paneth cell differentiation in the intestinal epithelium. *The Journal of Cell Biology, 178*(4), 635–648.

Bazer, F. W. (2010). Uterine Adenogenesis and Pregnancy: Multiple Roles for Foxa2 in Mice. *Biology of Reproduction, 83*(3), 319–321.

Besnard, V., Wert, S. E., Hull, W. M., & Whitsett, J. A. (2004). Immunohistochemical localization of Foxa1 and Foxa2 in mouse embryos and adult tissues. *Gene Expression Patterns, 5*(2), 193–208.

Bidarimath, M., Khalaj, K., Kridli, R. T., Kan, F. W. K., Koti, M., & Tayade, C. (2017). Extracellular vesicle mediated intercellular communication at the porcine maternal-fetal interface: A new paradigm for conceptus-endometrial cross-talk. *Scientific Reports, 7*, 1–14.

Bielas, S. L., Silhavy, J. L., Brancati, F., Kisseleva, M. V., Al-Gazali, L., Sztriha, L., … Gleeson, J. G. (2009). Mutations in INPP5E, encoding inositol polyphosphate-5-phosphatase E, link phosphatidyl inositol signaling to the ciliopathies. *Nature Genetics, 41*(9), 1032–1036.

Binder, N. K., Evans, J., Salamonsen, L. A., Gardner, D. K., Kaitu'u-Lino, T. J., & Hannan, N. J. (2016). Placental growth factor is secreted by the human endometrium and has potential important functions during embryo development and implantation. *PLoS ONE, 11(*10), 1–15.

Blackburn, K., Bustamante-Marin, X., Yin, W., Goshe, M. B., & Ostrowski, L. E. (2017). Quantitative Proteomic Analysis of Human Airway Cilia Identifies Previously Uncharacterized Proteins of High Abundance. *Journal of Proteome Research, 16*(4), 1579–1592.

Blois, S. M., Freitag, N., Tirado-González, I., Cheng, S.-B., Heimesaat, M. M., Bereswill, S., … Sharma, S. (2017). NK cell-derived IL-10 is critical for DC-NK cell dialogue at the maternal-fetal interface. *Scientific Reports, 7*(1), 2189.

Boggavarapu, N. R., Lalitkumar, S., Joshua, V., Kasvandik, S., Salumets, A., Lalitkumar, P. G., & Gemzell-Danielsson, K. (2016). Compartmentalized gene expression profiling of receptive endometrium reveals progesterone regulated ENPP3 is differentially expressed and secreted in glycosylated form. *Scientific Reports, 6,* 1–13.

Boretto, M., Cox, B., Noben, M., Hendriks, N., Fassbender, A., Roose, H., … Vankelecom, H. (2017). Development of organoids from mouse and human endometrium showing endometrial epithelium physiology and long-term expandability. *Development, 144*(10), 1775–1786.

Boulenouar, S., Doisne, J.-M., Sferruzzi-Perri, A., Gaynor, L. M., Kieckbusch, J., Balmas, E., … Colucci, F. (2016). The Residual Innate Lymphoid Cells in NFIL3-Deficient Mice Support Suboptimal Maternal Adaptations to Pregnancy. *Frontiers in Immunology, 7,* 43.

Boutin, C., & Kodjabachian, L. (2019). Biology of multiciliated cells. *Current Opinion in Genetics and Development, 56,* 1-7.

Bouyer. J., Coste. J., Shojaei. T., Pouly. J.L., Fernandez. H., Gerbaud. L., J.-S. N. (2003). Risk Factors for Ectopic Pregnancy: A Comprehensive Analysis Based on a Large Case-Control, Population-based Study in France. *American Journal of Epidemiology*, *157*(3):185-94.

Braud, V. M., Allan, D. S. J., O'Callaghan, C. A., Soderstrom, K., D'Andrea, A., Ogg, G. S., … McMichael, A. J. (1998). HLA-E binds to natural killer cell receptors CD94/NKG2A, B and C. *Nature, 391*(6669), 795–799.

Braundmeier, A. G., Dayger, C. A., Mehrotra, P., Belton, R. J., & Nowak, R. A. (2012). EMMPRIN is secreted by human uterine epithelial cells in microvesicles and stimulates metalloproteinase production by human uterine fibroblast cells. *Reproductive Sciences, 19*(12), 1292–1301.

Brighton, P. J., Maruyama, Y., Fishwick, K., Vrljicak, P., Tewary, S., Fujihara, R., … Brosens, J. J. (2017). Clearance of senescent decidual cells by uterine natural killer cells in cycling human endometrium. *ELife*, 6:e31274.

Brooks, K., Burns, G. W., Moraes, J. G. N., & Spencer, T. E. (2016). Analysis of the Uterine Epithelial and Conceptus Transcriptome and Luminal Fluid Proteome During the Peri-Implantation Period of Pregnancy in Sheep. *Biology of Reproduction, 95*(4), 88–88.

Bulmer, J. N., & Lash, G. E. (2005). Human uterine natural killer cells: a reappraisal. *Molecular Immunology*, *42*(4), 511–521.

Burghoorn, J., Piasecki, B. P., Crona, F., Phirke, P., Jeppsson, K. E., & Swoboda, P. (2012). The in vivo dissection of direct RFX-target gene promoters in C. elegans reveals a novel cis-regulatory element, the C-box. *Developmental Biology*, *368*(2), 415–426.

Burton, G. J., Scioscia, M., & Rademacher, T. W. (2011). Endometrial secretions: Creating a stimulatory microenvironment within the human early placenta and implications for the aetiopathogenesis of preeclampsia. *Journal of Reproductive Immunology*, *89*(2), 118–125.

Burton, G.J., Woods, A. W., Jauniaux, E., & Kingdom, J. C. P. (2009). Rheological and Physiological Consequences of Conversion of the Maternal Spiral Arteries for Uteroplacental Blood Flow during Human Pregnancy. *Placenta*, *30*(6), 473–482.

Burton, Graham J., Watson, A. L., Hempstock, J., Skepper, J. N., & Jauniaux, E. (2002). Uterine Glands Provide Histiotrophic Nutrition for the Human Fetus during the First Trimester of Pregnancy. *The Journal of Clinical Endocrinology & Metabolism*, *87*(6), 2954–2959.

Cao, Y., Chen, M., Dong, D., Xie, S., & Liu, M. (2020). Environmental pollutants damage airway epithelial cell cilia: Implications for the prevention of obstructive lung

diseases. *Thoracic Cancer*, 11, 505-510.

Chaen, T., Konno, T., Egashira, M., Bai, R., Nomura, N., Nomura, S., … Imakawa, K. (2012). Estrogen-Dependent Uterine Secretion of Osteopontin Activates Blastocyst Adhesion Competence. *PLoS ONE*, *7*(11), 1–12.

Chan, R. W. S., Schwab, K. E., & Gargett, C. E. (2004). Clonogenicity of Human Endometrial Epithelial and Stromal Cells. *Biology of Reproduction*, *70*(6), 1738–1750.

Chang, R. Q., Zhou, W. J., Li, D. J., & Li, M. Q. (2020). Innate lymphoid cells at the maternal-fetal interface in human pregnancy. *International Journal of Biological Sciences, 16*(6), 957-969.

Chen, J. C., Erikson, D. W., Piltonen, T. T., Meyer, M. R., Barragan, F., McIntire, R. H., … Irwin, J. C. (2013). Coculturing human endometrial epithelial cells and stromal fibroblasts alters cell-specific gene expression and cytokine production. *Fertility and Sterility*, *100*(4), 1132–1143.

Chen, M.-Y., Liao, G.-D., Zhou, B., Kang, L.-N., He, Y.-M., & Li, S.-W. (2018). Genome-Wide Profiling of Long Noncoding RNA Expression Patterns in Women With Repeated Implantation Failure by RNA Sequencing. *Reproductive Sciences*, 26(1):18-25.

Chen, X., Mariee, N., Jiang, L., Liu, Y., Wang, C. C., Li, T. C., & Laird, S. (2017). Measurement of uterine natural killer cell percentage in the periimplantation endometrium from fertile women and women with recurrent reproductive failure: establishment of a reference range. *American Journal of Obstetrics and Gynecology*, *217*(6), 680.e1-680.e6.

Cheong, Y., Boomsma, C., Heijnen, C., & MacKlon, N. (2013). Uterine secretomics: A window on the maternal-embryo interface. *Fertility and Sterility*, *99*(4), 1093–1099.

Chiokadze, M & Kristesashvili, J. (2019). On the issue of standardization of uterine natural killer cell measurement in patients with recurrent pregnancy loss. *Georgian Medical News*, 294, 31-36.

Chu, C. W., Hou, F., Zhang, J., Phu, L., Loktev, A. V., Kirkpatrick, D. S., … Zou, H. (2011). A novel acetylation of β-tubulin by San modulates microtubule polymerization via

down-regulating tubulin incorporation. *Molecular Biology of the Cell*, *22*(4), 448–456.

Chu, L. A., Lu, C. H., Yang, S. M., Liu, Y. T., Feng, K. L., Tsai, Y. C., … Chen, B. C. (2019). Rapid single-wavelength lightsheet localization microscopy for clarified tissue. *Nature Communications*, *10*(1), 4762.

Chung, M. I., Peyrot, S. M., LeBoeuf, S., Park, T. J., McGary, K. L., Marcotte, E. M., & Wallingford, J. B. (2012). RFX2 is broadly required for ciliogenesis during vertebrate development. *Developmental Biology*, *363*(1), 155–165.

Clifford, K., Flanagan, A. M., & Regan, L. (1999). Endometrial CD56+ natural killer cells in women with recurrent miscarriage: a histomorphometric study. *Human Reproduction*, *14*(11), 2727–2730.

Cockburn, K., & Rossant, J. (2010). Making the blastocyst: lessons from the mouse. *The Journal of Clinical Investigation*, *120*(4), 995–1003.

Colucci, F., & Gaynor, L. M. (2017). Uterine Natural Killer Cells: Functional Distinctions and Influence on Pregnancy in Humans and Mice. *Frontiers in Immunology*, *8*, 467.

Coombes, C., Yamamoto, A., McClellan, M., Reid, T. A., Plooster, M., Luxton, G. W. G., … Gardner, M. K. (2016). Mechanism of microtubule lumen entry for the α-tubulin acetyltransferase enzyme αTAT1. *Proceedings of the National Academy of Sciences of the United States of America*, *113*(46), E7176–E7184.

Coons, A. H., Creech, H. J., & Jones, R. N. (1941). Immunological Properties of an Antibody Containing a Fluorescent Group. *Experimental Biology and Medicine*, *47*(2), 200–202.

Coutifaris, C., Myers, E. R., Guzick, D. S., Diamond, M. P., Carson, S. A., Legro, R. S., … NICHD National Cooperative Reproductive Medicine Network. (2004). Histological dating of timed endometrial biopsy tissue is not related to fertility status. *Fertility and Sterility*, *82*(5), 1264–1272.

Critoph, F. N., & Dennis, K. J. (1977). The cellular composition of the human oviduct epithelium. *BJOG: An International Journal of Obstetrics & Gynaecology*, *84*(3), 219–221.

Croy, B., He, H., Esadeg, S., Wei, Q., McCartney, D., Zhang, J., … Yamada, A. (2003). Uterine natural killer cells: insights into their cellular and molecular biology from mouse modelling. *Reproduction*, *126*(2), 149–160.

Cuevas, C. A., Tapia-Pizarro, A., Salvatierra, A. M., Munroe, D. J., Velasquez, L., & Croxatto, H. B. (2016). Effect of single post-ovulatory administration of mifepristone (RU486) on transcript profile during the receptive period in human endometrium. *Reproduction*, *151*(4), 331–349.

D'Aurora, M., Romani, F., Franchi, S., Diomede, F., Merciaro, I., Impicciatore, G. G., … Gatta, V. (2019). MRAP2 regulates endometrial receptivity and function. *Gene*, *703*, 7–12.

Dalton, C. K., Laird, S. M., Estdale, S. E., Saravelos, H. G., & Li, T. C. (1998). Endometrial protein PP14 and CA-125 in recurrent miscarriage patients; Correlation with pregnancy outcome. *Human Reproduction*, *13*(11), 3197–3202.

Denholm, R. B., & More, I. A. (1980). Atypical cilia of the human endometrial epithelium. *Journal of Anatomy*, *131*(Pt 2), 309–315.

Díaz-Gimeno, P., Horcajadas, J. A., Martinez-Conejero, J. A., Esteban, F. J., Alama, P., Pellicer, A., & Simon, C. (2010). A genomic diagnostic tool for human endometrial receptivity based on the transcriptomic signature. *Revista Iberoamericana de Fertilidad y Reproduccion Humana*, *27*(4), 337–351.

Díaz-Gimeno, P., Horcajadas, J. A., Martínez-Conejero, J. A., Esteban, F. J., Alamá, P., Pellicer, A., & Simón, C. (2011). A genomic diagnostic tool for human endometrial receptivity based on the transcriptomic signature. *Fertility and Sterility*, *95*(1), 50-60.e15.

Díaz-Gimeno, P., Ruiz-Alonso, M., Blesa, D., Bosch, N., Martínez-Conejero, J. A., Alamá, P., … Simón, C. (2013). The accuracy and reproducibility of the endometrial receptivity array is superior to histology as a diagnostic method for endometrial receptivity. *Fertility and Sterility*, *99*(2), 508–517.

Doisne, J.-M., Balmas, E., Boulenouar, S., Gaynor, L. M., Kieckbusch, J., Gardner, L., …

Colucci, F. (2015). Composition, Development, and Function of Uterine Innate Lymphoid Cells. *The Journal of Immunology*, *195*(8), 3937-45.

Downing, M. J., Papke, D. J., Tyekucheva, S., & Mutter, G. L. (2019). A New Classification of Benign, Premalignant, and Malignant Endometrial Tissues Using Machine Learning Applied to 1413 Candidate Variables. *International Journal of Gynecological Pathology, 39*(4):333-343.

Dunlap, K. A., Erikson, D. W., Burghardt, R. C., White, F. J., Reed, K. M., Farmer, J. L., … Johnson, G. A. (2008). Progesterone and Placentation Increase Secreted Phosphoprotein One (SPP1 or Osteopontin) in Uterine Glands and Stroma for Histotrophic and Hematotrophic Support of Ovine Pregnancy1. *Biology of Reproduction*, *79*(5), 983–990.

Eddé, B., Rossier, J., Le Caer, J. P., Desbruyères, E., Gros, F., & Denoulet, P. (1990). Posttranslational glutamylation of α-tubulin. *Science*, *247*(4938), 83–85.

El Zein, L., Ait-Lounis, A., Morlé, L., Thomas, J., Chhin, B., Spassky, N., Durand, B. (2009). RFX3 governs growth and beating efficiency of motile cilia in mouse and controls the expression of genes involved in human ciliopathies. *Journal of Cell Science*, *122*(17), 3180–3189.

Enciso, M., Carrascosa, J. P., Sarasa, J., Martínez-Ortiz, P. A., Munné, S., Horcajadas, J. A., & Aizpurua, J. (2018). Development of a new comprehensive and reliable endometrial receptivity map (ER Map/ER Grade) based on RT-qPCR gene expression analysis. *Human Reproduction*, *33*(2), 220–228.

ESHRE Early Pregnancy Guideline Development Group. (2017). Recurrent pregnancy loss. Guideline of the European Society of Human Reproduction and Embryology. *European Society of Human Reproduction and Embryology*, *20,* 0–153.

Evans, J., Rai, A., Nguyen, H. P. T., Poh, Q. H., Elglass, K., Simpson, R. J., … Greening, D. W. (2019). Human Endometrial Extracellular Vesicles Functionally Prepare Human Trophectoderm Model for Implantation: Understanding Bidirectional Maternal-Embryo Communication. *Proteomics*, *19*(23), e1800423.

Faridi, R.M., Agrawal, S. (2011). Killer immunoglobulin-like receptors (KIRs) and HLA-C allorecognition patterns implicative of dominant activation of natural killer cells contribute to recurrent miscarriages. Human Reproductio*n, 26*(2):491-7.

Fedele, L., Bianchi, S., Marchini, M., Franchi, D., Tozzi, L., & Dorta, M. (1996). Ultrastructural aspects of endometrium in infertile women with septate uterus. *Fertility and Sterility*, *65*(4), 750–752.

Fevr, T., Robine, S., Louvard, D., & Huelsken, J. (2007). Wnt/beta-catenin is essential for intestinal homeostasis and maintenance of intestinal stem cells. *Molecular and Cellular Biology*, *27*(21), 7551–7559.

Filant, J., & Spencer, T. E. (2013). Endometrial Glands Are Essential for Blastocyst Implantation and Decidualization in the Mouse Uterus. *Biology of Reproduction*, *88*(4), 93.

Filant, J., & Spencer, T. E. (2014). Uterine glands: Biological roles in conceptus implantation, uterine receptivity and decidualization. *International Journal of Developmental Biology*, *58*(2–4), 107–116.

Fiore, M., Goulas, C., & Pillois, X. (2017). A new mutation in TUBB1 associated with thrombocytopenia confirms that C-terminal part of β1-tubulin plays a role in microtubule assembly. *Clinical Genetics, 91*(6):924-926.

Fitzgerald, H. C., Dhakal, P., Behura, S. K., Schust, D. J., & Spencer, T. E. (2019). Self-renewing endometrial epithelial organoids of the human uterus. *Proceedings of the National Academy of Sciences of the United States of America*, *116*(46), 23132–23142.

Ford, H. B., & Schust, D. J. (2009). Recurrent pregnancy loss: etiology, diagnosis, and therapy. *Reviews in Obstetrics & Gynecology*, *2*(2), 76–83.

Gargett, C. E. (2007). Uterine stem cells : What is the evidence ?. *Human Reproduction Update, 13*(1), 87–101.

Gargett, C. E. (2004). Stem cells in gynaecology. *The Australian and New Zealand Journal of Obstetrics and Gynaecology*, *44*(5), 380–386.

Gargett, C. E. (2006). Identification and characterisation of human endometrial stem/progenitor cells. *The Australian and New Zealand Journal of Obstetrics and Gynaecology*, *46*(3), 250–253.

Gargett, C. E., Zillwood, R. M., Schwab, K. E., & Naqvi, S. Z. (2005). 236. Characterising the stem cell activity of human endometrial epithelial and stromal cells. *Reproduction, Fertility and Development*, *17*(9), 93.

Garry, R., Hart, R., Karthigasu, K. A., & Burke, C. (2010). Structural changes in endometrial basal glands during menstruation. *BJOG: An International Journal of Obstetrics and Gynaecology*, *117*(10), 1175–1185.

Gaynor, L. M., & Colucci, F. (2017, April 24). Uterine natural killer cells: Functional distinctions and influence on pregnancy in humans and mice. *Frontiers in Immunology, 8*, 467.

Gelberg, H. B. (2014). Comparative anatomy, physiology, and mechanisms of disease production of the esophagus, stomach, and small intestine. *Toxicologic Pathology*, *42*(1), 54–66.

Gellersen, B., & Brosens, J. J. (2014). Cyclic Decidualization of the Human Endometrium in Reproductive Health and Failure. *Endocrine Reviews*, *35*(6), 851–905.

Georgiades, P., Ferguson-Smith, A. C., & Burton, G. J. (2002). Comparative Developmental Anatomy of the Murine and Human Definitive Placentae. *Placenta*, *23*(1), 3–19.

Gerdes, J. M., Davis, E. E., & Katsanis, N. (2009). The Vertebrate Primary Cilium in Development, Homeostasis, and Disease. *Cell, 137*(1):32-45.

Gibson, D.A., Greaves, E., Critchlet, H.O.D., Saunders, P. T. (2015). Estrogen-dependent regulation of human uterine natural killer cells promotes vascular remodelling via secretion of CCL2. *Human Reproduction, 30*(6):1290-301.

Girotra, M., Srivastava, S., Kulkarni, A., Barbora, A., Bobra, K., Ghosal, D., … Ray, K. (2017). The C-terminal tails of heterotrimeric kinesin-2 motor subunits directly bind to α-tubulin1: Possible implications for cilia-specific tubulin entry. *Traffic*, *18*(2), 123–133.

Glatstein, I. Z., Harlow, B.L., & Hornstein, D.M. (1997). Practice patterns among reproductive endocrinologists : the infertility evaluation. *Fertility and Sterility, 67*(3), 443–451.

Gonçalves, J., & Pelletier, L. (2017). The ciliary transition zone: Finding the pieces and assembling the gate. *Molecules and Cells*, *40*(4):243-253.

Gray, C. A., Burghardt, R. C., Johnson, G. A., Bazer, F. W., & Spencer, T. E. (2002). Evidence that absence of endometrial gland secretions in uterine gland knockout ewes compromises conceptus survival and elongation. *Reproduction*, *124*(2), 289–300.

Guirao, B., Meunier, A., Mortaud, S., Aguilar, A., Corsi, J. M., Strehl, L., … Spassky, N. (2010). Coupling between hydrodynamic forces and planar cell polarity orients mammalian motile cilia. *Nature Cell Biology*, *12*(4), 341–350.

Guo, W., Li, P., Zhao, G., Fan, H., Hu, Y., & Hou, Y. (2012). Glucocorticoid Receptor Mediates the Effect of Progesterone on Uterine Natural Killer Cells. *American Journal of Reproductive Immunology*, *67*(6), 463–473.

Hannan, N. J., Jones, R. L., Critchley, H. O. D., Kovacs, G. J., Rogers, P. A. W., Affandi, B., & Salamonsen, L. A. (2004). Coexpression of fractalkine and its receptor in normal human endometrium and in endometrium from users of progestin-only contraception supports a role for fractalkine in leukocyte recruitment and endometrial remodeling. *Journal of Clinical Endocrinology and Metabolism*, *89*(12), 6119–6129.

Hantak, A. M., Bagchi, I. C., & Bagchi, M. K. (2014). Role of uterine stromal-epithelial crosstalk in embryo implantation. *International Journal of Developmental Biology*, *58*(2-3–4), 139–146.

Hatta, K., Chen, Z., Carter, A.L., Leno-Duran, E., Zhang, J.,… Croy, B.A. (2010). Orphan Receptor Kinase ROR2 Is Expressed in the Mouse Uterus. *Placenta, 31*(4) 327-33.

Hazan, A. D., Smith, S. D., Jones, R. L., Whittle, W., Lye, S. J., & Dunk, C. E. (2010). Vascular-Leukocyte Interactions: Mechanisms of Human Decidual Spiral Artery Remodeling in Vitro. *The American Journal of Pathology*, *177*(2), 1017–1030.

He, K., Ma, X., Xu, T., Li, Y., Hodge, A., Zhang, Q., … Hu, J. (2018). Axoneme polyglutamylation regulated by Joubert syndrome protein ARL13B controls ciliary targeting of signaling molecules. *Nature Communications*, *9*(1), 1–14.

Helige, C., Ahammer, H., Moser, G., Hammer, A., Dohr, G., Huppertz, B., & Sedlmayr, P. (2014). Distribution of decidual natural killer cells and macrophages in the neighbourhood of the trophoblast invasion front: a quantitative evaluation. *Human Reproduction*, *29*(1), 8–17.

Hempstock, J., Cindrova-Davies, T., Jauniaux, E., & Burton, G. J. (2004a). Endometrial glands as a source of nutrients, growth factors and cytokines during the first trimester of human pregnancy: a morphological and immunohistochemical study. *Reproductive Biology and Endocrinology, 2*(1), 58.

Hey, N. A., Li, T. C., Devine, P. L., Graham, R. A., Saravelos, H., & Aplin, J. D. (1995). MUC1 in secretory phase endometrium: expression in precisely dated biopsies and flushings from normal and recurrent miscarriage patients. *Human Reproduction*, *10*(10), 2655–2662.

Hiby, S. E., Regan, L., Lo, W., Farrell, L., Carrington, M., & Moffett, A. (2009). Association of maternal killer-cell immunoglobulin-like receptors and parental HLA-C genotypes with recurrent miscarriage. *Human Reproduction, 23*(4):972-6.

Hilton, H. G., Guethlein, L. A., Goyos, A., Nemat-Gorgani, N., Bushnell, D. A., Norman, P. J., & Parham, P. (2015). Polymorphic HLA-C Receptors Balance the Functional Characteristics of KIR Haplotypes . *The Journal of Immunology*, *195*(7), 3160–3170.

Hondo, E., Phichitrasilp, T., Kokubu, K., Kusakabe, K., Nakamuta, N., Oniki, H., & Kiso, Y. (2007). Distribution patterns of uterine glands and embryo spacing in the mouse. *Journal of Veterinary Medicine Series C: Anatomia Histologia Embryologia*, *36*(2), 157–159.

Horani, A., Ferkol, T. W., Dutcher, S. K., & Brody, S. L. (2016). Genetics and biology of primary ciliary dyskinesia. *Paediatric Respiratory Review*s, 18:18-24.

Horcajadas, J. A., Minguez, P., Dopazo, J., Esteban, F. J., Pellicer, A., & Simon, C. (2007).

Gene expression analysis of the endometrium reveals that controlled ovarian stimulation induces a genomic delay with potential clinical implications. *Fertility and Sterility*, *88*, S43–S44.

Hornung, D., Lebovic, D. I., Shifren, J. L., Vigne, J. L., & Taylor, R. N. (1998). Vectorial secretion of vascular endothelial growth factor by polarized human endometrial epithelial cells. *Fertility and Sterilityl*, *69*(5), 909–915.

Hu, S., Yao, G., Wang, Y., Xu, H., Ji, X., He, Y., … Sun, Y. (2014). Transcriptomic changes during the pre-receptive to receptive transition in human endometrium detected by RNA-Seq. *Journal of Clinical Endocrinology and Metabolism*, *99*(12), E2744–E2753.

Huang, J., Qin, H., Yang, Y., Chen, X., Zhang, J., Laird, S., … Li, T. C. (2017). A comparison of transcriptomic profiles in endometrium during window of implantation between women with unexplained recurrent implantation failure and recurrent miscarriage. *Reproduction*, *153*(6), 749–758.

Ishikawa, H., & Marshall, W. F. (2011). Ciliogenesis: Building the cell's antenna. *Nature Reviews Molecular Cell Biolog*y, 12(4):222-34.

Jablonski, A. (1933) 'Efficiency of Anti-Stokes Fluorescence in Dyes', *Nature, 131*(3319), pp. 839–840.

Jacoby, M., Cox, J. J., Gayral, S., Hampshire, D. J., Ayub, M., Blockmans, M., … Schurmans, S. (2009). INPP5E mutations cause primary cilium signaling defects, ciliary instability and ciliopathies in human and mouse. *Nature Genetics*, *41*(9), 1027–1031.

Jeong, J-W, Lee, H. S., Franco, H. L., Broaddus, R. R., Taketo, M. M., Tsai, S. Y., … DeMayo, F. J. (2009). Beta-catenin mediates glandular formation and dysregulation of beta-catenin induces hyperplasia formation in the murine uterus. *Oncogene*, *28*(1), 31–40.

Jeong, Jae-Wook, Kwak, I., Lee, K. Y., Kim, T. H., Large, M. J., Stewart, C. L., … DeMayo, F. J. (2010). Foxa2 Is Essential for Mouse Endometrial Gland Development and Fertility. *Biology of Reproduction*, *83*(3), 396–403.

Jin, X.Y., Zhao, L.J., Luo, D.H., Liu , L., Dai, Y.D., Hu, X.X., Wang, Y.Y., Lin, X., Hong, F, Li, T.C., Zhang, S. Y. (2017). Pinopode score around the time of implantation is predictive of

successful implantation following frozen embryo transfer in hormone replacement cycles. *Human Reproduction, 32*(12):2394-2403.

Joshi, H. C., & Cleveland, D. W. (1989). Differential utilization of β-tubulin isotypes in differentiating neurites. *Journal of Cell Biology*, *109*(2), 663–673.

Jovanovic, M., Stefanoska, I., Radojcic, L., & Vicovac, L. (2010). Interleukin-8 (CXCL8) stimulates trophoblast cell migration and invasion by increasing levels of matrix metalloproteinase (MMP)2 and MMP9 and integrins 5 and 1. *Reproduction*, *139*(4), 789–798.

Kam, E. P. Y., Gardner, L., Loke, Y. W., & King, A. (1999). The role of trophoblast in the physiological change in decidual spiral arteries. *Human Reproduction*, *14*(8), 2131–2138.

Kann, A. P., & Krauss, R. S. (2019). Multiplexed RNAscope and immunofluorescence on whole-mount skeletal myofibers and their associated stem cells. *Development*, *146*(20).

Kara, F., Cinar, O., Erdemli-Atabenli, E., Tavil-Sabuncuoglu, B., & Can, A. (2007). Ultrastructural alterations in human decidua in miscarriages compared to normal pregnancy decidua. *Acta Obstetricia et Gynecologica Scandinavica*, *86*(9), 1079–1086.

Katoh, T. A., Ikegami, K., Uchida, N., Iwase, T., Nakane, D., Masaike, T., … Nishizaka, T. (2018). Three-dimensional tracking of microbeads attached to the tip of single isolated tracheal cilia beating under external load. *Scientific Reports*, *8*(1), 1–9.

Kelleher, A. M., Burns, G. W., Behura, S., Wu, G., & Spencer, T. E. (2016). Uterine glands impact uterine receptivity, luminal fluid homeostasis and blastocyst implantation. *Scientific Reports*, *6*, 1–18.

Kennedy, P. R., Chazara, O., Gardner, L., Ivarsson, M. A., Farrell, L. E., Xiong, S., … Moffett, A. (2016). Activating KIR2DS4 Is Expressed by Uterine NK Cells and Contributes to Successful Pregnancy. *The Journal of Immunology*, *197*(11).

Keskin, D. B., Allan, D. S. J., Rybalov, B., Andzelm, M. M., Stern, J. N. H., Kopcow, H. D., …

Strominger, J. L. (2007). TGFβ promotes conversion of CD16+ peripheral blood NK cells into CD16- NK cells with similarities to decidual NK cells. *Proceedings of the National Academy of Sciences of the United States of America*, *104*(9), 3378–3383.

Kieckbusch, J., Gaynor, L. M., Moffett, A., & Colucci, F. (2014). MHC-dependent inhibition of uterine NK cells impedes fetal growth and decidual vascular remodelling. *Nature Communication*s, 28; 5, 3359.

Kim, H. R., & Jun, C. D. (2019). T Cell Microvilli: Sensors or Senders? *Frontiers in Immunolo*gy, 10, 1753.

King, A., Wellings, V., Gardner, L., & Loke, Y. W. (1989). Immunocytochemical characterization of the unusual large granular lymphocytes in human endometrium throughout the menstrual cycle. *Human Immunology*, *24*(3), 195–205.

Kitaya, K., Yamaguchi, T., Yasuo, T., Okubo, T., & Honjo, H. (2007). Post-ovulatory rise of endometrial CD16(−) natural killer cells: in situ proliferation of residual cells or selective recruitment from circulating peripheral blood? *Journal of Reproductive Immunology*, *76*(1–2), 45–53.

Kizilyaprak, C., Longo, G., Daraspe, J., & Humbel, B. M. (2015). Investigation of resins suitable for the preparation of biological sample for 3-D electron microscopy. *Journal of Structural Biology*, *189*(2), 135–146.

Kolte, A. M., Bernardi, L. A., Christiansen, O. B., Quenby, S., Farquharson, R. G., Goddijn, M., & Stephenson, M. D. (2015). Terminology for pregnancy loss prior to viability: a consensus statement from the ESHRE early pregnancy special interest group. *Human Reproduction*, *30*(3), 495–498.

Koopman, L. A., Kopcow, H. D., Rybalov, B., Boyson, J. E., Orange, J. S., Schatz, F., … Strominger, J. L. (2003). Human Decidual Natural Killer Cells Are a Unique NK Cell Subset with Immunomodulatory Potential. *The Journal of Experimental Medicine, 101200*(8), 1201–1212.

Koot, Y. E.M., Teklenburg, G., Salker, M. S., Brosens, J. J., & Macklon, N. S. (2012). Molecular aspects of implantation failure. *Molecular Basis of Disease*, *1822*(12),

1943–1950.

Koot, Yvonne E.M., Van Hooff, S. R., Boomsma, C. M., Van Leenen, D., Koerkamp, M. J. A. G., Goddijn, M., … Macklon, N. S. (2016). An endometrial gene expression signature accurately predicts recurrent implantation failure after IVF. *Scientific Reports*, *6*(2015), 1–12.

Korekane, H., Park, J. Y., Matsumoto, A., Nakajima, K., Takamatsu, S., Ohtsubo, K., … Taniguchi, N. (2013). Identification of ectonucleotide pyrophosphatase/phosphodiesterase 3 (ENPP3) as a regulator of N-acetylglucosaminyltransferase GnT-IX (GnT-Vb). *Journal of Biological Chemistry*, *288*(39), 27912–27926.

Kosova, G., Stephenson, M. D., Lynch, V. J., & Ober, C. (2015). Evolutionary forward genomics reveals novel insights into the genes and pathways dysregulated in recurrent early pregnancy loss. *Human Reproduction*, *30*(3), 519–529.

Krjutškov, K., Katayama, S., Saare, M., Vera-Rodriguez, M., Lubenets, D., Samuel, K., … Kere, J. (2016). Single-cell transcriptome analysis of endometrial tissue. *Human Reproduction*, *31*(4), 844–853.

Krusche, C. A., Kroll, T., Beier, H. M., & Classen-Linke, I. (2007). Expression of leucine-rich repeat-containing G-protein-coupled receptors in the human cyclic endometrium. *Fertility and Sterility*, *87*(6), 1428–1437.

Kubo, T., Yanagisawa, H. aki, Yagi, T., Hirono, M., & Kamiya, R. (2010). Tubulin Polyglutamylation Regulates Axonemal Motility by Modulating Activities of Inner-Arm Dyneins. *Current Biology*, *20*(5), 441–445.

Kuon, R.-J., Weber, M., Heger, J., Santillán, I., Vomstein, K., Bär, C., … Toth, B. (2017). Uterine natural killer cells in patients with idiopathic recurrent miscarriage. *American Journal of Reproductive Immunology*, *78*(4), e12721.

Kutteh, W. (2015). Novel Strategies for the Management of Recurrent Pregnancy Loss. *Seminars in Reproductive Medicine*, *33*(03), 161–168.

Kwak-Kim, J., & Gilman-Sachs, A. (2008). REVIEW ARTICLE: Clinical Implication of Natural

Killer Cells and Reproduction. *American Journal of Reproductive Immunology*, *59*(5), 388–400.

Lachapelle, M. H., Miron, P., Hemmings, R., & Roy, D. C. (1996). Endometrial T, B, and NK cells in patients with recurrent spontaneous abortion. Altered profile and pregnancy outcome. *Journal of Immunology*, *156*(10), 4027–4034.

Lash, G. E., Bulmer, J. N., Li, T. C., Innes, B. A., Mariee, N., Patel, G., … Laird, S. M. (2016). Standardisation of uterine natural killer (uNK) cell measurements in the endometrium of women with recurrent reproductive failure. *Journal of Reproductive Immunology*, *116*, 50–59.

Lash, G. E., Otun, H. A., Innes, B. A., Bulmer, J. N., Searle, R. F., & Robson, S. C. (2005). Inhibition of Trophoblast Cell Invasion by TGFB1, 2, and 3 Is Associated with a Decrease in Active Proteases1. *Biology of Reproduction*, *73*(2), 374–381.

Leigh, M. W., Pittman, J. E., Carson, J. L., Ferkol, T. W., Dell, S. D., Davis, S. D., … Zariwala, M. A. (2009). Clinical and genetic aspects of primary ciliary dyskinesia/kartagener syndrome. *Genetics in Medicin*e, 11(7):473-87.

Lewis, R. M., & Pearson-Farr, J. E. (2020). Multiscale three-dimensional imaging of the placenta. *Placenta*.

Lewis, S. A., Gu, W., & Cowan, N. J. (1987). Free intermingling of mammalian β-tubulin isotypes among functionally distinct microtubules. *Cell*, *49*(4), 539–548.

Li, Q., Kannan, A., DeMayo, F. J., Lydon, J. P., Cooke, P. S., Yamagishi, H., … Bagchi, I. C. (2011). The antiproliferative action of progesterone in uterine epithelium is mediated by Hand2. *Science, 331*(6019), 912.

Li, T. C., & Cooke, I. D. (1991). Review: Evaluation of the luteal phase. *Human Reproduction*, *6*(4), 484–499.

Li, T. C., Rogers, A. W., Dockery, P., Lenton, E. A., & Cooke, I. D. (1988). A new method of histologic dating of human endometrium in the luteal phase. *Fertility and Sterility*, *50*(1), 52–60.

Liu, B., Mariee, N., Laird, S., Smith, J., Li, J., & Li, T. C. (2014). The prognostic value of uNK cell count and histological dating in the mid-luteal phase of women with reproductive failure. *European Journal of Obstetrics & Gynecology and Reproductive Biology*, *181*, 171–175.

Liu, Z., Nguyen, Q. P. H., Guan, Q., Albulescu, A., Erdman, L., Mahdaviyeh, Y., … Mennella, V. (2020). A quantitative super-resolution imaging toolbox for diagnosis of motile ciliopathies. *Science Translational Medicine*, *12*(535).

Lleres, D., Swift, S., & Lamond, A. I. (2007). Detecting Protein-Protein Interactions In Vivo with FRET using Multiphoton Fluorescence Lifetime Imaging Microscopy (FLIM). In *Current Protocols in Cytometry*, Chapter 12, Unit12.10.

Lo, W., Rai, R., Hameed, A., Brailsford, S., Al-Ghamdi, A., & Regan, L. (2012). The effect of body mass index on the outcome of pregnancy in women with recurrent miscarriage. *Journal of Family and Community Medicine*, *19*(3), 167.

Lucas, E. S., Dyer, N. P., Murakami, K., Hou Lee, Y., Chan, Y.-W., Grimaldi, G., … Brosens, J. J. (2016). Loss of Endometrial Plasticity in Recurrent Pregnancy Loss. *STEM CELLS*, *34*(2), 346–356.

Lucas, E. S., Vrljicak, P., Muter, J., Diniz-da-Costa, M. M., Brighton, P. J., Kong, C. S., … Brosens, J. J. (2020). Recurrent pregnancy loss is associated with a pro-senescent decidual response during the peri-implantation window. *Communications Biology*, *3*(1), 1–14.

Lucas, J. S., Barbato, A., Collins, S. A., Goutaki, M., Behan, L., Caudri, D., … Kuehni, C. E. (2017). European Respiratory Society guidelines for the diagnosis of primary ciliary dyskinesia. The *European Respiratory Journa*l, 49(1):1601090.

Luddi, A., Pavone, V., Semplici, B., Governini, L., Criscuoli, M., Paccagnini, E., … Piomboni, P. (2020). Organoids of Human Endometrium: A Powerful In Vitro Model for the Endometrium-Embryo Cross-Talk at the Implantation Site. *Cells*, *9*(5).

Lund, M., Kamper-Jørgensen, M., Nielsen, H. S., Lidegaard, Ø., Andersen, A. M. N., & Christiansen, O. B. (2012). Prognosis for live birth in women with recurrent

miscarriage: What is the best measure of success? *Obstetrics and Gynecology*, *119*(1), 37–43.

Lyons, R. A., Saridogan, E., & Djahanbakhch, O. (2006). The reproductive significance of human Fallopian tube cilia. *Human Reproduction Update*, *12*(4), 363–372.

Lyzikova, Y. A., Zinovkin, D. A., & Pranjol, M. Z. I. (2020). Increase in FoxP3, CD56 immune cells and decrease in glands PGRMC1 expression in the endometrium are associated with recurrent miscarriages. *European Journal of Obstetrics and Gynecology and Reproductive Biology*, *245*, 121–126.

Macklon, N. (2017). Recurrent implantation failure is a pathology with a specific transcriptomic signature. *Fertility and Sterility*, *108*(1), 9–14.

Macklon, N. S., & Brosens, J. J. (2014). The Human Endometrium as a Sensor of Embryo Quality. *Biology of Reproduction*, *91*(4), 98.

Magdoud, K., Granados Herbepin, V., Messaoudi, S., Hizem, S., Bouafia, N., Almawi, W. Y., … Touraine, R. (2013). Genetic variation in TGFB1 gene and risk of idiopathic recurrent pregnancy loss. *Molecular Human Reproduction*, *19*(7), 438–443.

Manaster, I., & Mandelboim, O. (2010). The Unique Properties of Uterine NK Cells. *American Journal of Reproductive Immunology*, *63*(6), 434–444.

Mariee, N., Tuckerman, E., Ali, A., Li, W., Laird, S., & Li, T. C. (2012). The observer and cycle-to-cycle variability in the measurement of uterine natural killer cells by immunohistochemistry. *Journal of Reproductive Immunology*, *95*(1–2), 93–100.

Masterton, R., Armstrong, E. M., & More, I. A. R. (1975). The cyclical variation in the percentage of ciliated cells in the normal human endometrium. *Journal of Reproduction and Fertility*, *42*(3), 537–540.

Matsuura-Sawada, R., Murakami, T., Ozawa, Y., Nabeshima, H., Akahira, J., Sato, Y., … Okamura, K. (2005). Reproduction of menstrual changes in transplanted human endometrial tissue in immunodeficient mice. *Human Reproduction*, *20*(6), 1477–1484.

McLennan, C. E., & Rydell, A. H. (1965). Extent of endometrial shedding during normal menstruation. *Obstetrics and Gynecology*, *26*(5), 605–621.

Michimata, T., Ogasawara, M. S., Tsuda, H., Suzumori, K., Aoki, K., Sakai, M., … Saito, S. (2002). Distributions of endometrial NK cells, B cells, T cells, and Th2/Tc2 cells fail to predict pregnancy outcome following recurrent abortion. *American Journal of Reproductive Immunology*, *47*(4), 196–202.

Mikołajczyk, M., Skrzypczak, J., Szymanowski, K., & Wirstlein, P. (2003). The assessment of LIF in uterine flushing--a possible new diagnostic tool in states of impaired fertility. *Reproductive Biology*, *3*(3), 259–270.

Moffett-King, A. (2002). Natural killer cells and pregnancy. *Nature Reviews Immunology*, *2*(9), 656–663.

Moffett, A., & Shreeve, N. (2015). First do no harm: uterine natural killer (NK) cells in assisted reproduction. *Human Reproduction*, *30*(7), 1519–1525.

Moffett, A., & Colucci, F. (2014). Uterine NK cells: active regulators at the maternal-fetal interface. *Journal of Clinical Investigation*, *124*(5), 1872–1879.

Monici, M. (2005). Cell and tissue autofluorescence research and diagnostic applications. In *Biotechnology annual review, 11*, 227–256.

More, I. A. R., & Masterton, R. G. (1976). The role of oestrogen in the control of ciliated cells of the human endometrium. *Journal of Reproduction and Fertility*, *47*(1), 19–24.

Murray, M. J., Meyer, W. R., Zaino, R. J., Lessey, B. A., Novotny, D. B., Ireland, K., … Fritz, M. A. (2004). A critical analysis of the accuracy, reproducibility, and clinical utility of histologic endometrial dating in fertile women. *Fertility and Sterility*, *81*(5), 1333–1343.

Mylonas, I., Jeschke, U., Winkler, L., Makovitzky, J., Richter, D. U., Briese, V., & Friese, K. (2003). Immunohistochemical expression of inhibin-alpha in human endometrium and the in vitro secretion of inhibin, estradiol and cortisol in cultured human endometrial glandular cells. *Archives of Gynecology and Obstetrics*, *268*(3), 142–150.

Mylonas, I., Speer, R., Makovitzky, J., Richter, D. U., Briese, V., Jeschke, U., & Friese, K. (2000). Immunohistochemical analysis of steroid receptors and glycodelin A (PP14) in isolated glandular epithelial cells of normal human endometrium. *Histochem Cell Biol*, *114*(5), 405–411.

Naftalin, R. J., Thiagarajah, J. R., Pedley, K. C., Pocock, V. J., & Milligan, S. R. (2002). Progesterone stimulation of fluid absorption by the rat uterine gland. *Reproduction*, *123*(5), 633–638.

Newton, F. G., zur Lage, P. I., Karak, S., Moore, D. J., Göpfert, M. C., & Jarman, A. P. (2012). Forkhead Transcription Factor Fd3F Cooperates with Rfx to Regulate a Gene Expression Program for Mechanosensory Cilia Specialization. *Developmental Cell*, *22*(6), 1221–1233.

Nguyen, H. P. T., Sprung, C. N., & Gargett, C. E. (2012). Differential expression of Wnt signaling molecules between pre- and postmenopausal endometrial epithelial cells suggests a population of putative epithelial stem/progenitor cells reside in the basalis layer. *Endocrinology*, *153*(6), 2870–2883.

Noyes, R. W., Hertig, A. T., & Rock, J. (1975). Dating the endometrial biopsy. *American Journal of Obstetrics and Gynecology*, *122*(2), 262–263.

Odendaal, J., Quenby, S., Sammaritano, L, Macklon, N., Branch, D.W. & Rosenwaks, Z. (2019). Immunologic and rheumatollgic causes and treatment of recurrent pregnancy loss: what is the evidence? *Fertility and Sterility, 112*(6):1002-1012.

O'Neil, E. V., Burns, G. W., & Spencer, T. E. (2020). Extracellular vesicles: Novel regulators of conceptus-uterine interactions? *Theriogenology*, *150*, 106–112.

O'Sullivan, C. M., Liu, S. Y., Karpinka, J. B., & Rancourt, D. E. (2002). Embryonic hatching enzyme strypsin/ISP1 is expressed with ISP2 in endometrial glands during implantation. *Molecular Reproduction and Development*, *62*(3), 328–334.

O'Sullivan, C. M., Ungarian, J. L. R., Singh, K., Liu, S., Hance, J., & Rancourt, D. E. (2004). Uterine secretion of ISP1 & 2 tryptases is regulated by progesterone and estrogen during pregnancy and the endometrial cycle. *Molecular Reproduction and*

Development, *69*(3), 252–259.

Olmos-Ortiz, A., Flores-Espinosa, P., Mancilla-Herrera, I., Vega-Sánchez, R., Díaz, L., & Zaga-Clavellina, V. (2019). Innate immune cells and toll-like receptor–dependent responses at the maternal–fetal interface. *International Journal of Molecular Sciences*, 20(15), 3654.

Omoto, C. K., Gibbons, I. R., Kamiya, R., Shingyoji, C., Takahashi, K., & Witman, G. B. (1999). Rotation of the central pair microtubules in eukaryotic flagella. *Molecular Biology of the Cell*, *10*(1), 1–4.

Othman, R., Omar, M. H., Shan, L. P., Shafiee, M. N., Jamal, R., & Mokhtar, N. M. (2012). Microarray profiling of secretoryphase endometrium from patients with recurrent miscarriage. *Reproductive Biology*, *12*(2), 183–199.

Padykula, H. A. (1991). Regeneration in the Primate Uterus: The Role of Stem Cells. *Annals of the New York Academy of Sciences*, *622*, 47–56.

Padykula, H. A., Coles, L. G., Okulicz, W. C., Rapaport, S. I., McCracken, J. A., King, N. W., … Kaiserman-Abramof, I. R. (1989). The Basalis of the Primate Endometrium: A Bifunctional Germinal Compartment1. *Biology of Reproduction*, *40*(3), 681–690.

Palaiologou, E., Goggin, P., Chatelet, D. S., Lofthouse, E. M., Torrens, C., Sengers, B. G., … Lewis, R. M. (2017). Serial block-face scanning electron microscopy of erythrocytes protruding through the human placental syncytiotrophoblast. *Journal of Anatomy*, *231*(4), 634–637.

Pathak, N., Austin, C. A., & Drummond, I. A. (2011). Tubulin tyrosine ligase-like genes ttll3 and ttll6 maintain zebrafish cilia structure and motility. *Journal of Biological Chemistry*, *286*(13), 11685–11695.

Peel, S., & Stewart, I. (1984). The differentiation of granulated metrial gland cells in chimeric mice and the effect of uterine shielding during irradiation. *Journal of Anatomy*, 593–598.

Perry, J.S., Crombie, P. R. (1982). Ultrastructure of the uterine glands of the pig. *Journal of Anatomy*, *134*(2), 339–350.

Prota, A. E., Magiera, M. M., Kuijpers, M., Bargsten, K., Frey, D., Wieser, M., … Steinmetz, M. O. (2013). Structural basis of tubulin tyrosination by tubulin tyrosine ligase. *Journal of Cell Biology*, *200*(3), 259–270.

Qiong, Z., Jie, H., Yonggang, W., Bin, X., Jing, Z., & Yanping, L. (2017). Clinical validation of pinopode as a marker of endometrial receptivity: a randomized controlled trial. *Fertility and Sterility*, *108*(3), 513-517.e2.

Quayle, A. J., Porter, E. M., Nussbaum, A. A., Wang, Y. M., Brabec, C., Yip, K. P., & Mok, S. C. (1998). Gene expression, immunolocalization, and secretion of human defensin-5 in human female reproductive tract. *American Journal of Pathology*, *152*(5), 1247–1258.

Quenby, S., Bates, M., Doig, T., Brewster, J., Lewis-Jones, D. I., Johnson, P. M., & Vince, G. (1999). Pre-implantation endometrial leukocytes in women with recurrent miscarriage. *Human Reproduction*, *14*(9), 2386–2391.

Reardon, S. N., King, M. L., MacLean, J. A., Mann, J. L., DeMayo, F. J., Lydon, J. P., & Hayashi, K. (2012). Cdh1 Is Essential for Endometrial Differentiation, Gland Development, and Adult Function in the Mouse Uterus1. *Biology of Reproduction*, *86*(5), 141, 1–10.

Redeker, V., Levilliers, N., Schmitter, J. M., Le Caer, J. P., Rossier, J., Adoutte, A., & Bré, M. H. (1994). Polyglycylation of tubulin: A posttranslational modification in axonemal microtubules. *Science*, *266*(5191), 1688–1691.

Richardson, D. S., & Lichtman, J. W. (2017). SnapShot: Tissue Clearing. *Cell*, *171*(2), 496-496.e1.

Rock, J. R., Gao, X., Xue, Y., Randell, S. H., Kong, Y. Y., & Hogan, B. L. M. (2011). Notch-dependent differentiation of adult airway basal stem cells. *Cell Stem Cell*, *8*(6), 639–648.

Roshangar, L., Abdollahifard, S., Majdi, A., Zarrintan, A., Ghasemzade, A., Farzadi, L., … Soleimani Rad, J. (2013). Study of ultrastructure and apoptosis in the endometrium of women with or without endometriosis. *Iranian Journal of Reproductive Medicine*,

11(5), 399–404.

Royal College Obstetricians and Gynaecologists (RCOG). (2011). The Investigation and Treatment of Couples with Reccurent First-trimester and Second-trimester Miscarriage, *22*(2), 0–2.

Ruiz-Alonso, M., Blesa, D., Díaz-Gimeno, P., Gómez, E., Fernández-Sánchez, M., Carranza, F., … Simón, C. (2013). The endometrial receptivity array for diagnosis and personalized embryo transfer as a treatment for patients with repeated implantation failure. *Fertility and Sterility*, *100*(3), 818–824.

Russell, P., Anderson, L., Lieberman, D., Tremellen, K., Yilmaz, H., Cheerala, B., & Sacks, G. (2011). The distribution of immune cells and macrophages in the endometrium of women with recurrent reproductive failure. *Journal of Reproductive Immunology*, *91*(1–2), 90–102.

Salker, M. S., Nautiyal, J., Steel, J. H., Webster, Z., Šućurović, S., Nicou, M., Brosens, J. J. (2012). Disordered IL-33/ST2 Activation in Decidualizing Stromal Cells Prolongs Uterine Receptivity in Women with Recurrent Pregnancy Loss. *PLoS ONE*, *7*(12), e52252.

Satir, P., Heuser, T., Sale, W. (2014). A Structural Basis for How Motile Cilia Beat. *Bioscience 64*(12), 1073–1083.

Sawin, K. E., Mitchison, T. J., & Wordeman, L. G. (1992). Evidence for kinesin-related proteins in the mitotic apparatus using peptide antibodies. *Journal of Cell Science*, *101*(2), 303–313.

Schaefer, T. M., Fahey, J. V., Wright, J. A., & Wira, C. R. (2005). Migration inhibitory factor secretion by polarized uterine epithelial cells is enhanced in response to the TLR3 agonist poly (I:C). *American Journal of Reproductive Immunology*, *54*(4), 193–202.

Schwab, K. E., Chan, R. W. S., & Gargett, C. E. (2005). Putative stem cell activity of human endometrial epithelial and stromal cells during the menstrual cycle. *Fertility and Sterility*, *84*, 1124–1130.

Seshadri, S., & Sunkara, S. K. (2014). Natural killer cells in female infertility and recurrent

miscarriage: a systematic review and meta-analysis. *Human Reproduction Update*, *20*(3), 429–438.

Shah, A. S., Yehuda, B. S., Moninger, T. O., Kline, J. N., & Welsh, M. J. (2009). Motile cilia of human airway epithelia are chemosensory. *Science*, *325*(5944), 1131–1134.

Sharkey, A. M., Gardner, L., Hiby, S., Farrell, L., Apps, R., Masters, L., … Moffett, A. (2008). Killer Ig-Like Receptor Expression in Uterine NK Cells Is Biased toward Recognition of HLA-C and Alters with Gestational Age. *The Journal of Immunology*, *181*(1), 39–46.

Shelton, D. N., Fornalik, H., Neff, T., Park, S. Y., Bender, D., DeGeest, K., … Goodheart, M. J. (2012). The role of LEF1 in endometrial gland formation and carcinogenesis. *PloS One*, *7*(7), e40312.

Shimada, S., Kato, E. H., Morikawa, M., Iwabuchi, K., Nishida, R., Kishi, R., … Yamada, H. (2004). No difference in natural killer or natural killer T-cell population, but aberrant T-helper cell population in the endometrium of women with repeated miscarriage. *Human Reproduction*, *19*(4), 1018–1024.

Simon, C., Greening, D. W., Bolumar, D., Balaguer, N., Salamonsen, L. A., & Vilella, F. (2018). Extracellular vesicles in human reproduction in health and disease. *Endocrine Reviews*, *39*(3), 292–332.

Simpson, J. L. (2007). Causes of Fetal Wastage. *Clinical Obstetrics and Gynecology*, *50*(1), 10–30.

Smith, E. F., & Yang, P. (2004). The Radial Spokes and Central Apparatus: Mechano-Chemical Transducers That Regulate Flagellar Motility. *Cell Motility and the Cytoskeleton, 57*(1), 8–17.

Snijders, M. P., de Goeij, A. F., Debets-Te Baerts, M. J., Rousch, M. J., Koudstaal, J., & Bosman, F. T. (1992). Immunocytochemical analysis of oestrogen receptors and progesterone receptors in the human uterus throughout the menstrual cycle and after the menopause. *Journal of Reproduction and Fertility*, *94*(2), 363–371.

Sõber, S., Rull, K., Reiman, M., Ilisson, P., Mattila, P., & Laan, M. (2016). RNA sequencing of chorionic villi from recurrent pregnancy loss patients reveals impaired function of

basic nuclear and cellular machinery. *Scientific Reports, 6*, 38439.

Southcombe, J.H., Mounce, G., McGee, K., Elghajiji, A., Brosens, J., Quenby, S., Child, T., & Granne, I. (2017). An altered endometrial CD8 tissue resident memory T cell population in recurrent pregnancy loss. *Scientific Reports*, 7, 41335.

Spassky, N., & Meunier, A. (2017). The development and functions of multiciliated epithelia. *Nature Reviews Molecular Cell Biology, 18*, 423–436.

Spencer, T. E., Dunlap, K. A., & Filant, J. (2012). Comparative developmental biology of the uterus: Insights into mechanisms and developmental disruption. *Molecular and Cellular Endocrinology*, *354*(1–2), 34–53.

Spits, H., & Di Santo, J. P. (2010). The expanding family of innate lymphoid cells: regulators and effectors of immunity and tissue remodeling. *Nature Immunology*, *12*(1), 21-27.

Sreekumar, V., & Norris, D. P. (2019). Cilia and development. *Current Opinion in Genetics and Development*, 56, 15-21.

Stewart, C. L., Kaspar, P., Brunet, L. J., Bhatt, H., Gadi, I., Köntgen, F., & Abbondanzo, S. J. (1992). Blastocyst implantation depends on maternal expression of leukaemia inhibitory factor. *Nature*, *359*(6390), 76–79.

Stocker, L., Cagampang, F., & Cheong, Y. (2017). Identifying stably expressed housekeeping genes in the endometrium of fertile women, women with recurrent implantation failure and recurrent miscarriages. Scientific Reports.

Stokes, G. G. (1852). On the Change of Refrangibility of Light. *Philosophical Transactions of the Royal Society of London*, *142*(0), 463–562.

Tabibzadeh, S., & Babaknia, A. (1995). The signals and molecular pathways involved in implantation, a symbiotic interaction between blastocyst and endometrium involving adhesion and tissue invasion. *Molecular Human Reproduction*, *1*(4), 179–202.

Tempest, N., Baker, A. M., Wright, N. A., & Hapangama, D. K. (2018). Does human endometrial LGR5 gene expression suggest the existence of another hormonally

regulated epithelial stem cell niche? *Human Reproduction*, 1–11.

The Practice Committe of the American Society for Reproductive. (2012). Evaluation and treatment of recurrent pregnancy loss: A committee opinion. *Fertility and Sterility*, *98*(5), 1103–1111.

The prognostic value of uNK cell count and histological dating in the mid-luteal phase of women with reproductive failure. (2014). *European Journal of Obstetrics & Gynecology and Reproductive Biology*, *181*, 171–175.

Tischfield, M. A., Baris, H. N., Wu, C., Rudolph, G., Van Maldergem, L., He, W., … Engle, E. C. (2010). Human TUBB3 Mutations Perturb Microtubule Dynamics, Kinesin Interactions, and Axon Guidance. *Cell*, *140*(1), 74–87.

Tuckerman, E., Laird, S. M., Prakash, A., & Li, T. C. (2007). Prognostic value of the measurement of uterine natural killer cells in the endometrium of women with recurrent miscarriage. *Human Reproduction*, *22*(8), 2208–2213.

Turco, M. Y., Gardner, L., Hughes, J., Cindrova-Davies, T., Gomez, M. J., Farrell, L., … Burton, G. J. (2017). Long-term, hormone-responsive organoid cultures of human endometrium in a chemically defined medium. *Nature Cell Biology*, *19*(5), 568–577.

Vacca, P., Vitale, C., Montaldo, E., Conte, R., Cantoni, C., Fulcheri, E., … Mingari, M. C. (2011). CD34+ hematopoietic precursors are present in human decidua and differentiate into natural killer cells upon interaction with stromal cells. *Proceedings of the National Academy of Sciences of the United States of America*, *108*(6), 2402–2407.

Vacca, P., Vitale, C., Munari, E., Cassatella, M.A., Mingari, M.C., & Moretta, L. (2018). Human Innate Lymphoid Cells: Their Functional and Cellular Interactions in Decidua. *Frontiers in Immunology*, *9*, 1897.

Valentijn, A. J., Palial, K., Al-Lamee, H., Tempest, N., Drury, J., Von Zglinicki, T., … Hapangama, D. K. (2013). SSEA-1 isolates human endometrial basal glandular epithelial cells: Phenotypic and functional characterization and implications in the pathogenesis of endometriosis. *Human Reproduction*, *28*(10), 2695–2708.

Van's Gravesande, K. S., & Omran, H. (2005). Primary ciliary dyskinesia: Clinical presentation, diagnosis and genetics. *Annals of Medicine*. Ann Med.

Van de Wetering, M., Sancho, E., Verweij, C., de Lau, W., Oving, I., Hurlstone, A., … Clevers, H. (2002). The β-Catenin/TCF-4 Complex Imposes a Crypt Progenitor Phenotype on Colorectal Cancer Cells. *Cell*, *111*(2), 241–250.

Vent, J., Wyatt, T. A., Smith, D. D., Banerjee, A., Ludueña, R. F., Sisson, J. H., & Hallworth, R. (2005). Direct involvemnet of the isotype- specific C- terminus of β tubulin in ciliary beating. *Journal of Cell Science*, *118*(19), 4333–4341.

Vento-Tormo, R., Efremova, M., Botting, R. A., Turco, M. Y., Vento-Tormo, M., Meyer, K. B., … Teichmann, S. A. (2018). Single-cell reconstruction of the early maternal–fetal interface in humans. *Nature*, *563*(7731), 347–353.

Verma, S., Hiby, S. E., Loke, Y. W., & King, A. (2000). Human Decidual Natural Killer Cells Express the Receptor for and Respond to the Cytokine Interleukin 151. *Biology of Reproduction*, *62*(4), 959–968.

Von Wolff, M., Thaler, C. J., Zepf, C., Becker, V., Beier, H. M., & Strowitzki, T. (2002). Endometrial expression and secretion of interleukin-6 throughout the menstrual cycle. *Gynecological Endocrinology*, *16*(2), 121–129.

Vujaklija, D. V., Gulic, T., Sucic, S., Nagata, K., Ogawa, K., Laskarin, G., Rukavina, D. (2011). First trimester pregnancy decidual natural killer cells contain and spontaneously release high quantities of granulysin. *American Journal of Reproductive Immunology*, *66*(5), 363–372.

Wagner, M. K., & Yost, H. J. (2000). Left-right development: The roles of nodal cilia. *Current Biology*, *10*(4), R149-R151.

Wang, D., Villasante, A., Lewis, S. A., & Cowan, N. J. (1986). The mammalian β-tubulin repertoire: Hematopoietic expression of a novel, heterologous β-tubulin isotype. *Journal of Cell Biology*, *103*(5), 1903–1910.

Wang, H., Zhang, S., Lin, H., Kong, S., Wang, S., Wang, H., & Armant, D. R. (2013). Physiological and molecular determinants of embryo implantation. *Molecular*

Aspects of Medicine, *34*(5), 939–980.

Wang, W., Vilella, F., Moreno, I., Pan, W., Quake, S., & Simon, C. (2018). Single cell RNAseq provides a molecular and cellular cartography of changes to the human endometrium through the menstrual cycle. *Fertility and Sterility*, *110*(4), e2.

Watson, E. D., Cross, J. C., Liu, S., Wiggins, J. F., Sreenath, T., Kulkarni, A. B., … Leppla, S. H. (2005). Mouse Placenta Development of Structures and Transport Functions in the Dph3, a Small Protein Required for Diphthamide Biosynthesis, Is Essential in Mouse Development. *Mol. Cell. Biol*, *20*, 180–193.

Weintraub, J., Bischof, P., Tseng, L., Redard, M., & Vassilakos, P. (1990). CA 125 is an excretory product of human endometrial glands. *Biology of Reproduction*, *42*(4), 721–726.

Wheway, G., Nazlamova, L., & Hancock, J. T. (2018). Signaling through the primary cilium. *Frontiers in Cell and Developmental Biology*, 6, 8.

Wheway, G., Schmidts, M., Mans, D. A., Szymanska, K., Nguyen, T. M. T., Racher, H., Johnson, C. A. (2015). An siRNA-based functional genomics screen for the identification of regulators of ciliogenesis and ciliopathy genes. *Nature Cell Biology*, *17*(8), 1074–1087.

Whitsett, J. A., & Kalinichenko, V. V. (2011). Notch and basal cells take center stage during airway epithelial regeneration, 8(6), 597-8.

Willem Borst, J., & Visser, A. J. W. G. (2010). Fluorescence lifetime imaging microscopy in life sciences. *Measurement Science and Technology*, *21*(10).

Wu, X. M., Wang, Y. H., Zhong, W. J., Cheng, H. F., & Tian, Z. F. (2020). RNA Binding Protein RNPC1 Suppresses the Stemness of Human Endometrial Cancer Cells via Stabilizing MST1/2 mRNA. *Medical Science Monitor*, *26*, e921389-1.

Xu, B., Sun, X., Li, L., Wu, L., Zhang, A., & Feng, Y. (2012). Pinopodes, leukemia inhibitory factor, integrin-β3, and mucin-1 expression in the peri-implantation endometrium of women with unexplained recurrent pregnancy loss. *Fertility and Sterility*, *98*(2), 389–395.

Xu, J.-W., Yasui, N., Ikeda, K., Pan, W.-J., Watanabe, J., Shiotani, M., … Yamori, Y. (2008). Isoflavones regulate secretion of leukemia inhibitory factor and transforming growth factor {beta} and expression of glycodelin in human endometrial epithelial cells. *The Journal of Endocrinology*, *196*(2), 425–433.

Zegers-Hochschild, F., Adamson, G. D., de Mouzon, J., Ishihara, O., Mansour, R., Nygren, K., … World Health Organization. (2009). International Committee for Monitoring Assisted Reproductive Technology (ICMART) and the World Health Organization (WHO) revised glossary of ART terminology, 2009∗. *Fertility and Sterility*, *92*(5), 1520–1524.

Zhang, S., Lin, H., Kong, S., Wang, S., Wang, H., Wang, H., & Armant, D. R. (2013). Physiological and molecular determinants of embryo implantation. *Molecular Aspects of Medicine*, *34*(5), 939–980.

Zhioua, A., Elloumi, H., Fourati, S., Merdassi, G., Ben Ammar, A., Sajia, B. S., … Jaafoura, M. H. (2012). Morphometric analysis of the human endometrium during the implantation window. Light and transmission electron microscopy study. *Journal de Gynecologie, Obstetrique et Biologie de La Reproduction*, *41*(3), 235–242.